EPFL

Limestone calcined clay cements (LC3): raw material processing, sulfate balance and hydration kinetics

Présentée le 5 juin 2020

à la Faculté des sciences et techniques de l'ingénieur
Laboratoire des matériaux de construction
Programme doctoral en science et génie des matériaux

pour l'obtention du grade de Docteur ès Sciences

par

Franco Alberto ZUNINO SOMMARIVA

Acceptée sur proposition du jury

Prof. V. Michaud, présidente du jury
Prof. K. Scrivener, directrice de thèse
Dr P. Juilland, rapporteur
Prof. T. Matschei, rapporteur
Prof. R. Flatt, rapporteur

École
polytechnique
fédérale
de Lausanne

2020

To my (grand)parents

"Truth is ever to be found in simplicity,
and not in the multiplicity and confusion of things"

Sir Isaac Newton

Acknowledgements

First of all, I have to acknowledge Karen, my thesis director, for trusting me and giving me the chance to come and become part of her amazing laboratory. Despite not knowing me personally and not having an open Ph.D. position at that moment, she believed in my intentions and walked with me the way to find a mechanism to make it happen. Four years and many conferences/trips/cultures/continents and one global pandemic later, I couldn't be happier with my decision, and I'm always grateful to her for the opportunity. You are the best.

I would also like to acknowledge my jury members for the time, effort, insightful comments, interesting discussion and positive feedback provided during the last part of this Ph.D. My acknowledgements to Prof. Robert Flatt, Prof. Thomas Matschei and Dr. Patrick Juilland for their contributions and efforts to bring this work to a good ending and for the excellent discussion during the oral exam. I also would like to acknowledge Prof. Véronique Michaud, my jury president, for being available throughout the process and managing my oral exam smoothly despite the special circumstances surrounding the examination. Finally, I'm honored and thankful to all my jury members for the nomination of this thesis to be distinguished by EPFL.

The LC^3 is a collective effort, and I'm grateful to the team members all over the world for the experiences, discussions and exchange throughout these years. My gratitude to Fernando and his nice team in Cuba, Shashank, Manu, Ravindra, Soumen and the rest of the Indian members of the LC^3 family. Special mention to the Ph.D. students in these latitudes that I had the chance to meet and enjoy with: Anuj, Yuvaraj, Vineet, Sundar, Sreejith, Arun. Of course, special mention to my LC^3 fellows at EPFL with whom I shared a workplace and experiences during this process, you are all part of this and definitely this wouldn't be the same without your contributions: Julien, π-Mink, François and Aurèlie. My gratitude also to the support staff of the project and the lab: Silas, Marie-Alix, and specially Anne-Sandra, Mirabela and Maude, you are really the ones making things possible for us. Finally, I'm grateful to Prof. Paul Bowen and Dr. Marta Palacios for their input, support and the enjoyment of collaboration in surface characterization and others!

To my LMC brothers and sisters in crime, thanks for all the years of fun and good moments. Our lab is definitely a workplace (and a very good one), but also some sort of extended family. My gratitude and appreciation to Alex, Lili, Qiao, Mahsa, Wiolleta, William (Dr. Wilson), Sarra, Andrea, Yu Yan, Yosra, Frank, Diana, Xuerun, Adrien, Elise, Maya, Gabi, Ziga, Anna (the real one), Masood, Hamed, and anybody else whose name might be skipping my mind now, thank you very much. Thanks to Emmanuelle for preparing so many lamellas for me and for the fun TEM sessions.

Special mention to Lionel, Jean and Antonio for always being happy, smiling, complaining, talking loud as hell and making the impossible a reality. Without you the lab wouldn't be the same. Thanks for always being in a

good mood even in difficult days. Last but not least, a special place in my heart goes to the ขี้เมา gang: Natechanok Chitvoranund, Fabien (the French), Ka-Hill (the fake-French), Solène (retired - honorary member) and Joseph (future member/president). To my friends and colleagues in Chile, here and there: Javier, Ricardo, Dale, Álvaro, Gavin, Euge, Sandra, thanks for being there.

I want to thank all the students that, somehow and in different contexts, contributed time, effort and ideas to this project. My gratitude goes to Ioannis, Raymond, Nicolas, Edgar, Romans, George, Philipp, Diandian and Luca (only now I realized that you're a lot!). Thanks for being there, for standing my jokes, committing to the goals of this work and ultimately contributing to the success of the project. This thesis wouldn't be the same without your involvement and contributions.

Finally, I cannot conclude without thanking my family. My mom and dad for always believe in me and allowing me to come so far away to pursue this dream, my (not so) little brother for his non-explicit support and Greta for taking care of everyone at home for so many years. This is as yours as it is mine.

Lausanne, le 24 mai 2020   FZ

Abstract

Limestone calcined clay cements (LC^3) are blended cements that combine clinker, limestone, calcined clay and gypsum. The availability of the materials required to produce LC^3 and the good performance that it achieves, makes LC^3 suitable as a sustainable replacement of Portland cement.

Significant advances have been made to assess the properties of LC^3, compare it to other common blended cements and establish benchmark characterization procedures. However, there are still open questions that are relevant for a successful adoption of this technology and consequently, to make a better use of the resources available. This research project addresses some of these questions related to processing, blend design and microstructural development of LC^3 cements.

The effect of calcite impurities in calcined clay reactivity was explored. It was found that at calcination temperatures below the recrystallization threshold, an intermediate produce was formed between kaolinite and calcite. A slight reduction in reactivity was observed, which can be mostly offset by reducing the calcination temperature of the clay and extending the residence time.

The effect of using grinding aids was studied at the grinding/classification stage and also during hydration. The use of grinding aids significantly improves the efficiency of dry classification of clay particles, which could prevent overgrinding and increase yield in closed circuit milling units. Furthermore, the use of alkanolamines was shown to be effective to enhance the formation of hemicarboaluminate and monocarboaluminate and thus increase strength.

LC^3 cements require optimization of the calcium sulfate (gypsum). There is an increase in the sulfate needed relative to the clinker content. The mechanism that explains this increased sulfate demand was found to be linked to the enhancement of alite reaction due to filler effect and the adsorption of sulfate in C-A-S-H, rather than the aluminate content of the calcined clay. In addition, the reaction rate of C_3A and the dissolution rate of the sulfate source used are also important to describe the sulfate balance of a cementitious system in general.

The effect of hemicarboaluminate and monocarboaluminate on mechanical properties of LC^3 was also studied. Metakaolin and sulfate content were found to influence significantly the kinetics of AFm formation. Furthermore, the precipitation of AFm between 2 and 3 days of hydration were directly linked to the strength increase observed. The amount of initial space in the system determines the extent to which hydration takes place at a high rate. Afterwards, the porosity refinement leads to a decrease in reaction rate. However, evidence for a continued reaction of metakaolin in the long term was found.

The insights presented in this thesis provide new knowledge that enables a better use of LC^3 in the field. Together, they also show the robustness and versatility of this technology, and deliver guidelines for future developments and field implementation of LC^3.

Keywords

Metakaolin, sulfate, kinetics, grinding aids, calcite, sustainability, hydration, microstructure, porosity, pozzolan.

Résumé

Les ciments de calcaire et argile calcinée (LC^3) sont des ciments composés qui combinent le clinker, le calcaire, l'argile calcinée et le gypse. La disponibilité des matériaux nécessaires à la production de LC^3 et ses bonnes performances font du LC^3 un remplacement durable pour le ciment Portland.

Des progrès importants ont été réalisés pour évaluer les propriétés du LC^3, le comparer à d'autres ciments composés courants et pour établir des procédures de caractérisation de référence. Cependant, il reste des questions ouvertes qui sont pertinentes pour une adoption réussie de cette technologie et, par conséquent, pour une meilleure utilisation des ressources disponibles. Ce projet de recherche aborde certaines de ces questions liées au traitement, à la conception des mélanges et au développement microstructural des ciments LC^3.

L'effet des impuretés de calcite sur la réactivité de l'argile calcinée a été étudié. Il a été constaté qu'à des températures de calcination inférieures au seuil de recristallisation, un produit intermédiaire est formé entre la kaolinite et la calcite. Une légère diminution de la réactivité a été observée, qui peut être compensée principalement en réduisant la température de calcination de l'argile et en allongeant le temps de résidence dans le four.

L'effet de l'utilisation des auxiliaires de broyage a été étudié au stade du broyage/classification et également pendant l'hydratation. L'utilisation d'adjuvants de broyage améliore considérablement l'efficacité de la classification à sec des particules d'argile, ce qui pourrait empêcher le broyage excessif et augmenter le rendement dans les unités de broyage en circuit fermé. De plus, l'utilisation d'alcanolamines s'est avérée efficace pour améliorer la formation d'hémicarboaluminate et de monocarboaluminate et ainsi augmenter la résistance de la pâte de ciment hydraté.

Les ciments LC^3 nécessitent une optimisation de la quantité de sulfate de calcium (gypse). Plus de sulfate est nécessaire par rapport à la teneur en clinker. Le mécanisme qui explique cette demande accrue de sulfate s'est révélé lié à l'amélioration de la réaction d'alite due à l'effet de remplissage et à l'adsorption de sulfate dans le C-A-S-H, plutôt qu'à la teneur en aluminate de l'argile calcinée. De plus, la vitesse de réaction du C_3A et la vitesse de dissolution de la source de sulfate utilisée sont également importantes pour décrire l'équilibre en sulfate d'un système cimentaire en général.

L'effet de l'hémicarboaluminate et du monocarboaluminate sur les propriétés mécaniques de la LC^3 a également été étudié. La teneur en métakaolin et en sulfate s'est révélée influencer de manière significative la cinétique de formation de l'AFm. De plus, la précipitation de l'AFm entre 2 et 3 jours d'hydratation était directement liée à l'augmentation de résistance observée. La quantité d'espace initial dans le système détermine l'étendue où l'hydratation a lieu à un taux élevé. Ensuite, le raffinement de la porosité entraîne une diminution de la vitesse de réaction. Cependant, des preuves d'une réaction continue du métakaolin à long terme ont été trouvées.

Les idées présentées dans cette thèse apportent de nouvelles connaissances qui permettent une meilleure utilisation de LC^3 dans le domaine. Ensemble, ils montrent également la robustesse et la polyvalence de cette technologie et fournissent des directives pour les développements futurs et la mise en œuvre sur le terrain de LC^3.

Mots-clés

Métakaolin, sulfate, cinétique, adjuvants de broyage, calcite, durabilité, hydratation, microstructure, porosité, pouzzolane.

Zusammenfassung

Kalkstein-kalzinierter-Lehm Zemente (LC^3) sind Zementmischungen die Klinker mit Kalkstein, kalziniertem Lehm und Gips vermengen. Die Verfügbarkeit der zur Herstellung von LC^3 notwendigen Materialien und ihre guten technischen Eigenschaften machen LC^3 zu einer nachhaltigen Alternative zu Portlandzement.

Erhebliche Fortschritte wurden bezüglich der Erforschung der Eigenschaften von LC^3, dem Vergleich zu anderen Mischzementen und der Schaffung von Referenzgrößen und -verfahren erreicht. Dennoch bestehen weiterhin offene Fragen für die erfolgreiche Einführung der Technologie und folglich der effizienten Ressourcennutzung. Dieses Forschungsprojekt behandelt einige dieser Fragen in Bezug auf Verarbeitung, Mischung und Mikrostrukturentwicklung.

Die Auswirkung von Kalzitunreinheiten bezüglich der Reaktivität von kalziniertem Lehm wurde erforscht. Es wurde festgestellt, dass bei Kalzinierungstemperaturen unterhalb des Rekristallisierungsschwellwertes ein Zwischenprodukt geformt wurde zwischen Kaolinit und Kalzit. Eine leichte Verringerung der Reaktivität wurde beobachtet, die weitestgehend durch eine Reduzierung der Kalzinierungstemparatur des Lehms und eine Verlängerung der Aufenthaltszeit ausgeglichen werden kann.

Die Auswirkung der Benutzung von Mahlhilfen wurde bei der Mahlungs-/Einstufungsphase sowie bei der Hydratation untersucht. Die Benutzung von Mahlhilfen verbessert die Effizienz der Trockenklassifizierung von Lehmpartikeln signifikant, welche eine Übermahlung verhindern und den Ertrag in kleinen geschlossenen Mahlanlagen erhöhen kann. Ausserdem wurde herausgefunden, dass die Benutzung von Alkanolaminen zur Erhöhung der Bildung von Hemikarboaluminat und Monokarboaluminat beiträgt und dadurch die Stärke erhöht.

LC^3-Zemente benötigen eine Optimierung des Kalziumsulfats. Eine Erhöhung von Sulfat ist notwendig im Verhältnis zum Klinkeranteil. Es wurde festgestellt, dass der Mechanismus, der diesen erhöhten Sulfatbedarf erklärt, nicht mit dem Aluminatgehalt des kalzinierten Lehms, sondern mit der Verstärkung der Alitreaktion aufgrund des Füllstoffeffekts und der Adsorption von Sulfat in C-A-S-H zusammenhängt. Darüber hinaus sind die Reaktionsgeschwindigkeit von C$_3$A und die Auflösungsgeschwindigkeit der verwendeten Sulfatquelle ebenfalls wichtig, um die Sulfatbilanz eines zementartigen Systems im Allgemeinen zu beschreiben.

Die Wirkung von Hemikarboaluminat und Monokarboaluminat auf die mechanischen Eigenschaften von LC^3 wurde untersucht. Es wurde festgestellt, dass der Metakaolin- und Sulfatgehalt signifikant die Kinetik bei der AFm-Formung beeinflussen. Des Weiteren ist der Niederschlag von AFm zwischen 2 und 3 Tagen der Hydratation direkt mit einer Erhöhung der Stärke verbunden. Die Menge von ursprünglichem Raum innerhalb des Systems bestimmt die Ausweitung wo Hydratation mehrheitlich stattfindet. Anschliessend führt die Porositätsverfeinerung zu einer reduzierten Wirkungsquote. Trotzdem wurden Nachweise für eine kontinuierliche Reaktion von Metakaolin gefunden.

Die Ergebnisse dieser Dissertation tragen zum Wissen über LC^3 bei und ermöglichen eine bessere Anwendung. Insgesamt betrachtet verdeutlichen alle Ergebnisse die Robustheit und Flexibilität dieser Technologie und offerieren Leitfäden für zukünftige Anwendungen von LC^3.

Stichwörter

Metakaolin, Sulfat, Kinetik, Mahlhilfen, Kalzit, Nachhaltigkeit, Hydratation, Mikrostruktur, Porosität, Puzzolan.

Resumen

Los cementos de caliza y arcilla calcinada (LC^3) son cementos ternarios que combinan clínker, caliza, arcilla calcinada y yeso. La disponibilidad de los materiales necesarios para producir LC^3 y el buen desempeño que alcanza hacen que LC^3 sea adecuado como un reemplazo sustentable para el cemento Portland.

Se han realizado avances significativos para evaluar las propiedades de LC^3, compararlo con otros cementos con adiciones minerales comunes y establecer procedimientos de caracterización estandarizados. Sin embargo, todavía hay preguntas abiertas que son relevantes para una adopción exitosa de esta tecnología y, en consecuencia, para hacer un mejor uso de los recursos disponibles. Este proyecto de investigación aborda algunas de estas preguntas relacionadas con el procesamiento, el diseño de mezclas y el desarrollo microestructural de los cementos LC^3.

Se exploró el efecto de las impurezas de calcita en la reactividad de la arcilla calcinada. Se observó que a temperaturas de calcinación por debajo del umbral de recristalización, se forma un producto intermedio entre caolinita y calcita. Adicionalmente, se observó una ligera reducción en la reactividad, que puede compensarse principalmente reduciendo la temperatura de calcinación de la arcilla y extendiendo el tiempo de residencia.

El efecto del uso de intensificadores de molienda se estudió en la etapa de molienda/clasificación y también durante la hidratación. El uso de intensificadores de molienda mejora significativamente la eficiencia de la clasificación en seco de las partículas de arcilla, lo que podría evitar el sobre-molido y aumentar el rendimiento en las unidades de molienda de circuito cerrado. Además, se demostró que el uso de alcanolaminas es eficaz para mejorar la formación de hemicarboaluminato y monocarboaluminato y, por lo tanto, aumentar la resistencia.

Los cementos LC^3 requieren la optimización del sulfato de calcio (yeso). Hay un aumento en el sulfato necesario en relación con el contenido de clínker. Se encontró que el mecanismo que explica esta mayor demanda de sulfato está relacionado con el aumento en la velocidad de reacción de la alita debido al efecto filler y la adsorción de sulfato en el C-A-S-H, en lugar del contenido de aluminato de la arcilla calcinada. Además, la velocidad de reacción de C_3A y la velocidad de disolución de la fuente de sulfato utilizada también son importantes para describir el equilibrio de sulfato de un sistema cementoso en general.

También se estudió el efecto del hemicarboaluminato y monocarboaluminato sobre las propiedades mecánicas de LC^3. Se encontró que el contenido de metacaolín y sulfato influye significativamente en la cinética de la formación de AFm. Además, la precipitación de AFm entre 2 y 3 días de hidratación está directamente relacionada con el aumento de la resistencia a compresión observada. La cantidad de espacio inicial en el sistema determina la duración del periodo donde la hidratación tiene lugar a una velocidad alta. Posteriormente, el refinamiento de la porosidad conduce a una disminución en la velocidad de reacción. Sin embargo, se encontró evidencia de una reacción continua de metacaolín en el largo plazo.

Las conclusiones presentadas en esta tesis proporcionan nuevos conocimientos que permiten un mejor uso de LC^3 en aplicaciones industriales. En conjunto, también muestran la robustez y versatilidad de esta tecnología, y brindan pautas para futuros desarrollos e implementación en la industria de LC^3.

Palabras clave

Metacaolín, sulfato, cinética, intensificadores de molienda, calcita, sustentabilidad, hidratación, microestructura, porosidad, puzolana.

Contents

List of Figures

List of Tables

Glossary

Cement chemistry notation

C	Calcium oxide - CaO
S	Silica - SiO_2
A	Alumina - Al_2O_3
F	Iron oxide - Fe_2O_3
H	Water - H_2O
$	Sulfur trioxide - SO_3
c	Carbonate - CO_3
C_3S	Tricalcium silicate (alite) - $3CaO \cdot SiO_2$
C_2S	Dicalcium silicate (belite) - $2CaO \cdot SiO_2$
C_3A	Tricalcium aluminate - $3CaO \cdot Al_2O_3$
C_4AF	Ferrite - $4CaO \cdot Al_2O_3 \cdot Fe_2O_3$
CH	Calcium hydroxide (portlandite) - $Ca(OH)_2$
C-(A)-S-H	Calcium (aluminum) silicate hydrates
Ett	Ettringite - $6CaO \cdot Al_2O_3 \cdot 3SO_3 \cdot 32H_2O$
AFm	$Al_2O_3 \cdot Fe_2O_3 \cdot mono$ (OH, SO_3 or CO_3)
Hc	Hemicarboaluminate - $C_4Ac_{0.5}H_{12}$
Mc	Monocarboaluminate - C_4AcH_{11}

Experimental techniques and others

PSD	Particle size distribution
XRD	X-ray diffraction
XRF	X-ray fluorescence
SEM	Scanning electron microscopy
TEM	Transmission electron microscopy
EDS	Energy dispersive spectroscopy
TGA	Thermogravimetric analysis
NMR	Nuclear magnetic resonance
GA	Grinding aids
OPC or PC	(Ordinary) Portland cement
LC^3	Limestone calcined clay cement
LC^2	Limestone calcined clay
SCM	Supplementary cementitious material
DoH / DoR	Degree of hydration / Degree of reaction

Chapter 1   Introduction

Contents

1.1 The climate emergency and the cement industry

Global warming is a current concern for governments, industry and the general society. The Paris agreement, signed by 175 parties, indicates that measures to keep the global temperature rise below 2°C above pre-industrial levels should be strengthened, and further efforts to keep the temperature rise below 1.5°C should be pursued [1].

Cement is the largest manufactured product on Earth on a mass basis. Cement is mixed with aggregates, water and chemical admixtures to produce concrete. Concrete is the second most used resource by mankind after water [2]. Due to this enormous utilization, the cement used for its production accounts for about 6% of the total anthropogenic CO_2 emissions [3]. Cement is also the largest industrial energy consumer, comprising 7% of the global industrial energy use. On the other hand, 90% of cement is and will continue to be produced in non-OECD countries [4], as these are the places where the concrete demand is highest. The environmental impact of concrete is thus associated with the large quantities that we currently use. This demand for concrete can only be expected to increase, as there is no real alternative to the use of concrete to sustain development [2].

The most effective way to reduce the CO_2 footprint of Portland cement is to reduce the clinker factor. This has oriented the industry towards an increasing adoption of blended cements, which are nowadays more common than pure Portland cements. Blended cements incorporate supplementary cementitious materials (SCMs) replacing part of the clinker. Typically used SCMs such as ground granulated blast furnace slag (GGBS) and fly ash are together available in amounts close to 15% of the total cement production [4]. Regarding fly ash, the availability is expected to go down quickly in the forthcoming years due to the adoption of cleaner technologies to produce energy in place of coal power plants [2]. This has led to a levelling off of the amount of clinker substitution after 2009, as the availability of SCMs becomes the limiting factor [5]. New sources of good quality SCMs are needed if this picture is to be changed significantly in the near future.

1.2 Why LC³?

Kaolinitic clays and limestone are unique among supplementary cementitious materials because of their worldwide availability [2]. Natural clays are mixtures of clay minerals such as kaolinite and associated minerals like quartz, iron oxide and feldspars. Calcined kaolinitic clays contain a reactive aluminosilicate phase (metakaolin) and can be produced by heat treatment of natural clays at temperatures around 800°C [6].

Limestone calcined clay cements (LC³) are a family of blended cements that incorporate these materials replacing up to 50% of the clinker. They achieve similar strength to conventional Portland cement from 7 days onwards and exhibit enhanced performance against chloride penetration and alkali-silica reaction (ASR) [7]. Overall, LC³ cements can save between 30 to 40% of the CO_2 emissions per ton of cement produced compared to Ordinary Portland Cement (OPC) or CEM I [8]. Moreover, LC³ can be produced and used with the same, equipment, tools and skills as conventional Portland cement.

1.3   Statement of the problem

Significant progress has been made at the Laboratory of Construction Materials at EPFL in recent years to understand the kinetics, microstructure and properties of limestone calcined-clay cements [9–12]. However, there are still issues that require further research.

One challenge arises from the natural variability of the mineralogy of the clays used. In some cases, kaolinite is intermixed with minerals that decompose upon heating in the same temperature range required for clay calcination such as calcium carbonate. While recrystallization phenomena between kaolinite and calcite have been described at higher temperature [13], the interaction at temperatures in the range of clay calcination (750-850°C) is unclear.

The focus of previous studies has been frequently placed on the hydration, mechanical properties development and durability of LC^3. For a successful implementation of this technology, the production process should be addressed. Grinding of blended cements is a challenging field, as usually SCMs have lower hardness than clinker grains [14]. Furthermore, agglomeration and coating of the mill media by SCMs decrease the efficiency of the process [15]. The use of grinding aids could provide a solution in this matter. Some grinding aids are known to interact with aluminate and iron phases in cement [16]. Thus, their interaction in LC^3 where other sources of aluminum and iron are introduced needs to be understood.

Proper blend design is key to achieve good properties with LC^3 cements. It has been observed that LC^3 cements required additional gypsum, relative to the clinker content, compared to Portland cement, to achieve the proper sulfate balance [17]. The reason for this observed increase in the sulfate demand in LC^3 is not well understood. The mechanism of sulfate consumption needs to be better understood for reliable field applications of LC^3 technology.

In LC^3 cements, higher amounts of CO_3-AFm (hemicarboaluminate and monocarboaluminate) are observed as compared to other blended cements due to the reaction of aluminates from metakaolin and limestone [17,18]. It has been observed that the increased amount of AFm improves the binding capacity of chloride in LC^3 [19]. However, the kinetics of this reaction have not be well established, and the role of AFm on LC^3 strength and pore refinement is unclear.

1.4   Objective of the thesis and layout

The general goal of this thesis is to understand the hydration kinetics and phase assemblage of limestone calcined-clay cements (LC^3) in realistic use scenarios, in order to acquire and develop the general knowledge framework required to make better use of the natural clays available.

This thesis is divided in 9 chapters, organized following a logic analogue to the production process of LC^3 cements. To effectively improve and extend the use of the LC^3 technology, the different stages of production should be addressed. The relationship of each of the chapters with the different production stages, is shown schematically in Figure 1-1 in bold green numbers over the different stages of the diagram.
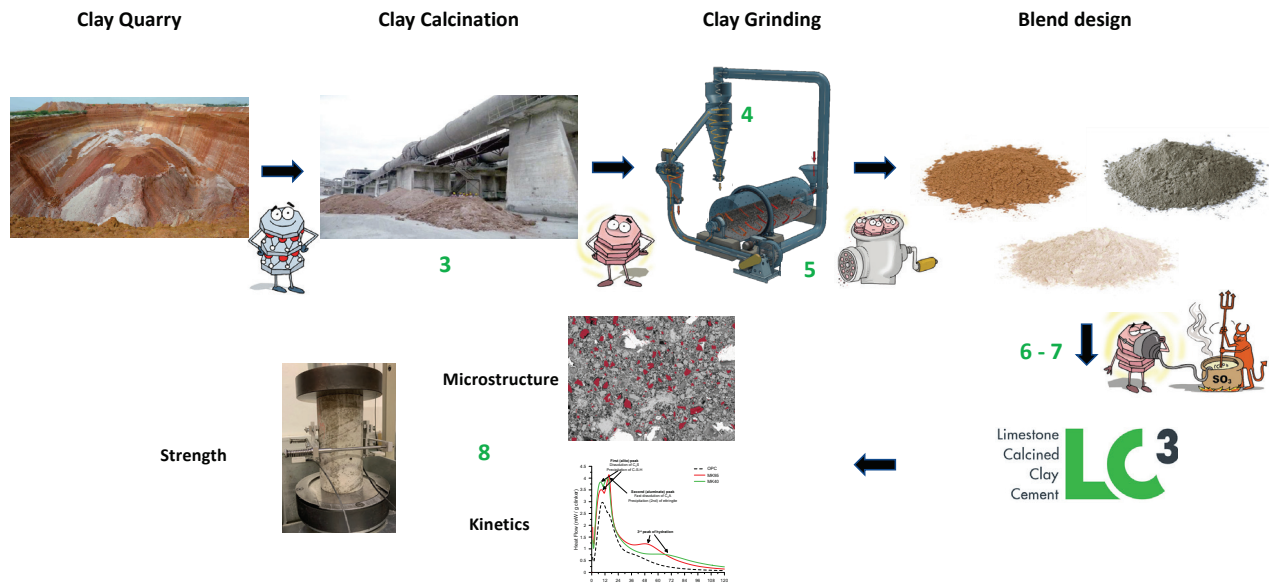
Figure 1-1: Scheme of a production process of LC³ cements, indicating the relationship of each stage with the layout of this thesis.

Chapter 2 presents a state-of-the-art review of LC³. It contains a compilation of relevant results and findings in the literature, and is complemented with some original results of this project.

Specific goals are associated with the research gaps identified in section 1.3, and are addressed in one or more chapters of the thesis. The significance of the different studies conducted in each chapter are also highlighted.

    I.   To understand the effect of calcite impurities in kaolinitic clays on the reactivity of the calcined clay produced.

        o   This is the subject of *Chapter 3*. The effect of calcination calcite content, calcination temperature and residence time was explored. New insights are provided regarding the formation of compounds between kaolinite and calcite after calcination. *These findings are relevant to extend the use of natural clays as SCMs to quarries with up to 10% calcite impurities*.

    II.   To evaluate a particle classification process as a mean to increase the kaolinite content of low-grade clays and to assess the influence of grinding aids on the efficiency of this process.

        o   This is subject of *Chapter 4*. A lab-scale air separator, with an operating principle similar to the units found in every cement plant associated to close-circuit grinding mills, was compared to traditional wet sedimentation processes. The effect of grinding aids to increase the efficiency of the dry separation process was also explored. *This study provides technical solutions to*

effectively use natural clay resources with low kaolinite content, using equipment and technology in use and known by cement producers.

III.   To assess the effect of grinding aids on hydration, phase assemblage and mechanical properties of LC^3 systems.

     o   This is subject of *Chapter 5*. A study focused on the effect of alkanolamine-based grinding aids on LC^3 hydration kinetics, porosity refinement and strength is presented. These grinding aids are compared to other common molecules used in the cement industry such as glycols and polycarboxylate ether. *The potential of alkanolamines to improve the production process and the mechanical properties of LC^3-based materials is described*.

IV.   To understand the mechanism behind the increased sulfate demand of LC^3 systems and to assess the factors that influence the sulfate balance of the system.

     o   This is subject of *Chapter 6* and *Chapter 7*. *Chapter 6* presents a comprehensive study aimed to understand the mechanism behind the increased sulfate demand in LC^3 and blended cements in general. *Chapter 7* presents a second study on sulfate balance on pure phase C$_3$S/C$_3$A systems. The use of pure phases allowed exploration in more detail of additional effects that influence sulfate balance, such as rate of reaction of C$_3$A and dissolution rate of the sulfate source. *Proper sulfate balance is required to maximize the mechanical properties of LC^3. The knowledge gathered in these studies allowed to described the mechanism behind the sulfate balance in LC^3 and other blended cements, allowing to effectively address this practical issue.*

V.   To assess the role of CO$_3$-AFm (hemicarboaluminate and monocarboaluminate) in porosity refinement and mechanical properties of LC^3 systems.

     o   This is subject of *Chapter 8*. The study aimed to understand the influence of CO$_3$-AFm precipitation in LC^3 systems on compressive strength and porosity refinement is presented. The third peak of hydration commonly observed LC^3 systems is associated with the reaction between metakaolin and limestone. *Understanding the role of AFm phases in strength development of low clinker LC^3 cements and the factors that influence the reaction kinetics is required for further optimization of mechanical properties, specially at early ages.*

Chapter 9 summarizes the main findings and conclusions of this thesis. The contributions of each of the studies are highlighted, and perspectives for future work in the field are proposed.

Chapters 2 to 8 correspond to peer-reviewed journal articles derived from this project. Details on selected journal, authors and full bibliographical information is provided on the first page of each chapter, along with the status of each article at the time of printing (in preparation, submitted or published).

1.5 References

[1] United Nations - COP21, Paris agreement, 2015.

[2] K.L. Scrivener, V. John, E.M. Gartner, Eco-efficient cements: potential, economically viable solutions for a low-CO2, cement-based materials industry, in: United Nations Environmental Programme (UNEP), 2016.

[3] T. Boden, B. Andres, G. Marland, Global CO2 Emissions from Fossil-Fuel Burning, Cement Manufacture, and Gas Flaring, 2016.

[4] IEA, CSI, Technology Roadmap: Low-Carbon transition in the Cement Industry, 2018. doi:10.1007/springerreference_7300.

[5] N. Müller, J. Harnisch, A blueprint for a climate friendly cement industry, 2008.

[6] K. Scrivener, F. Martirena, S. Bishnoi, S. Maity, Calcined clay limestone cements (LC3), Cem. Concr. Res. (2017) 1–8. doi:10.1016/j.cemconres.2017.08.017.

[7] K.L. Scrivener, F. Avet, H. Maraghechi, F. Zunino, J. Ston, A. Favier, et al., Impacting factors and properties of Limestone Calcined Clay Cements (LC3), Green Mater. (2018). doi:https://doi.org/10.1680/jgrma.18.00029.

[8] S. Sánchez Berriel, A. Favier, E. Rosa Domínguez, I.R. Sánchez MacHado, U. Heierli, K. Scrivener, et al., Assessing the environmental and economic potential of Limestone Calcined Clay Cement in Cuba, J. Clean. Prod. 124 (2016) 361–369. doi:10.1016/j.jclepro.2016.02.125.

[9] M. Antoni, Investigation of cement substitution by combined addition of calcined clays and limestone, École Polytechnique Fédérale de Lausanne, 2011.

[10] F. Avet, Investigation of the grade of calcined clays used as clinker substitute in Limestone Calcined Clay Cement (LC3), École Polytechnique Fédérale de Lausanne, 2017.

[11] J. Ston, Basic creep and autogenous shrinkage of Limestone Calcined Clay Cement (LC3), École Polytechnique Fédérale de Lausanne, 2019.

[12] W. Hanpongpan, Investigation of the use of Limestone Calcined Clay Cement (LC3) applied to Thailand, École Polytechnique Fédérale de Lausanne, 2019.

[13] H. El-Didamony, K.A. Khalil, M.S. El-Attar, Physicochemical characteristics of fired clay-limestone mixes, Cem. Concr. Res. 30 (2000) 7–11. doi:10.1016/S0008-8846(99)00181-7.

[14] K. De Weerdt, Separate grinding versus intergrinding, SINTEF Rep. SBF BK A. 7022 (2007).

[15] S. Sohoni, R. Sridhar, G. Mandal, The effect of grinding aids on the fine grinding of limestone, quartz and Portland cement clinker, Powder Technol. 67 (1991) 277–286. doi:10.1016/0032-5910(91)80109-V.

[16] E. Gartner, D. Myers, Influence of Tertiary Alkanolamines on Portland Cement Hydration, J. Am. Ceram. Soc. 76 (1993) 1521–1530. doi:10.1111/j.1151-2916.1993.tb03934.x.

[17] M. Antoni, J. Rossen, F. Martirena, K. Scrivener, Cement substitution by a combination of metakaolin and limestone, Cem. Concr. Res. 42 (2012) 1579–1589. doi:10.1016/j.cemconres.2012.09.006.

[18] F. Avet, K. Scrivener, Investigation of the calcined kaolinite content on the hydration of Limestone Calcined Clay Cement (LC3), Cem. Concr. Res. 107 (2018) 124–135. doi:10.1016/j.cemconres.2018.02.016.

[19] S. Sui, F. Georget, H. Maraghechi, W. Sun, K. Scrivener, Towards a generic approach to durability: Factors affecting chloride transport in binary and ternary cementitious materials, Cem. Concr. Res. 124 (2019). doi:10.1016/j.cemconres.2019.105783.

Chapter 2   Limestone calcined clay cements

Note: This chapter is based on an article submitted for publication in a peer reviewed journal. The results presented are a combination of literature review (indicated) and original work.

Submission title: Limestone Calcined Clay Cements (LC^3)

Franco Zunino, Fernando Martirena, Karen Scrivener

Submitted to ACI Materials Journal

Contribution of the doctoral candidate: Writing of the first manuscript draft, conduction of the original experiments shown in the manuscript, editing and compilation of input from the other authors.

The climate emergency requires the adoption of strategies and technologies that can effectively reduce the CO_2 emissions in the short-midterm. Portland cement is the material most consumed by humanity. The adoption of blended cements in many countries address this issue. However, the amount of SCMs available is limited and therefore it is the potential of clinker factor reduction. LC^3, blended cement produced by the combination of limestone, calcined clays and Portland cement provides a solution that achieves equivalent mechanical performance to OPC, better durability against chloride and ASR and a reduction of CO_2 emissions of about 40%. Furthermore, it is cost effective compared to OPC currently in the market, and due to the similarities with OPC it is a material that can be adopted today using the same construction equipment and workforce worldwide.

Contents

2.1   Introduction

As the impacts of global warming start to become apparent the spotlight is on cement and concrete which contribute around 8% to man-made CO_2 emissions. LC^3: limestone calcined clay cements are a technology which can substantially reduce this environmental impact, while giving similar of better performance to existing cements. In this feature article we explain the scientific basis of the LC^3 technology and illustrate some of its properties and performance.

2.2   Why LC^3 is a good cement for the future

Cementitious materials make up about 50% of everything we produce as civilization. If we look at the composition of the Earth's crust, only 8 elements (namely O, Si, Al, Fe, Ca, Na, K and Mg) constitute 98% of it. This means that the amount of options for a material used in this quantity are limited. Alkalis (Na and K) are too soluble, while iron and magnesium have too low mobility in alkaline solutions. Thus, any feasible material will be based on the SiO_2-CaO-Al_2O_3 ternary diagram. In this regard, materials that require higher aluminum content for production such as calcium (sulfo)aluminate cements are limited due to cost and availability of aluminum ore. Therefore, Portland cement-based materials will continue to be dominant due to their economy of scale, raw material availability, ease of manipulation and robustness.

The most effective way to reduce the CO_2 footprint of Portland cement is to reduce the clinker factor. This has oriented the industry towards an increasing adoption of blended cements. They incorporate supplementary cementitious materials (SCMs) replacing part of the clinker. Typically used SCMs such as ground granulated blast furnace slag (GGBS) and fly ash are together available in amounts close to 15% of the total cement production [1]. In the case of fly ash, the availability is expected to go down quickly in the forthcoming years due to the adoption of cleaner technologies to produce energy in place of coal power plants [2]. This situation compromises the suitability of these materials for a significant reduction of the clinker factor on a worldwide scale.

Calcined clays and limestone are the only SCMs available in the quantities and locations to make a difference in this matter. Furthermore, several deposits of waste kaolin from other industries are available, being suitable for use in cement. In addition to availability, the high reactivity of calcined clay and the synergy between calcined clay and limestone allow high levels of substitution (50%) while achieving similar mechanical performance to Portland cement. The technical aspects behind LC^3 cements will be discussed in detail in the next sections.

2.3   What is LC^3

LC^3 is family of cements containing a combination of calcined clay and limestone as a partial substitution of the clinker. In the designation LC^3-X: X is the clinker content in % by mass. For example LC^3-50, which is the most widely investigated formulation contains 50% clinker and typically 30% calcined clay and 15% limestone. However, the ratio of calcined clay to limestone may be varied as discussed below. The remaining 5% is gypsum although the precise sulfate content should be optimized for each combination as also discussed later.

2.3.1 What type of clays are we looking for?

After calcination, Kaolinitic clays are the most reactive [3]. Clays with different amounts of kaolinite can be found in different regions of the world, intermixed with associated minerals such as quartz, limestone, iron bearing phases and other rock forming minerals.

Clay particles are made up of tens to hundreds of layers, structured as a combination of alternating silica tetrahedral and alumina octahedral sheets [4,5]. The three most abundant clay types are kaolinite, illite and montmorillonite (smectite). Kaolinite (a so called 1:1 clay) has a layer structure of one silica and one alumina layer (Figure 2-1), while in illite and montmorillonite the layers are composed of two silica layers sandwiching an alumina layer (2:1 clays) [6]. In the case of kaolinite, two distinct interlayer surfaces coexist, one with aluminate groups and one with silicate groups. Thus, both aluminum and silica are exposed to the interlayer space and available to react after calcination.

Octahedral Al layer

Tetrahedral Si layer

Interlayer space

Octahedral Al layer

Tetrahedral Si layer
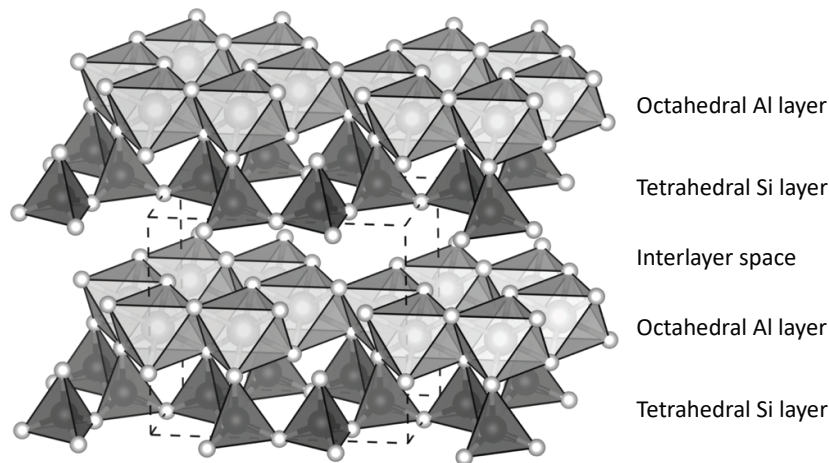
Figure 2-1: Crystal structure of kaolinite, showing a layer of octahedral aluminum sites with a layer of tetrahedral silicate sites in a 1:1 structure. Generated using VESTA [7].

2.3.2 LC^3 formulations and mixture design

LC^3-50, which contains 50% replacement of clinker by a combination of limestone and calcined clay, is the best formulation approach in terms of CO$_2$ savings while achieving the same strength as OPC. However, LC^3 type cements comprise a whole family of different formulations that can be tailored for specific applications and regulatory environments.

The main parameter influencing the strength of LC^3 cements is the metakaolin content of the calcined clay used [8]. Thus, associated minerals commonly found in natural kaolinitic clays do not play a major role in strength. Figure 2-2 shows the compressive strength of LC^3-50 systems (50% clinker factor), with a 2:1 clay to limestone ratio, incorporating different grades of clay. At 1 d, only a small contribution of the metakaolin content to the strength is observed, as it is mainly influenced by the reaction of clinker. At 2 and 3 d, a clear relationship between metakaolin content and strength is seen, due to the contribution of the synergic reaction between metakaolin and limestone during this period. From 7 d and onwards, all the systems with at

least 40% metakaolin content reach comparable strengths to OPC. In addition to a proper selection of the clay to use, the sulfate balance of the system requires adjustment as it will be discussed later.

There is no big improvement observed by using higher grade clays, this is because even with lower grade clays, unreacted clinker and metakaolin both remain due to lack of space for the hydration products [8,9]. Thus, the ideal range in terms of cost/performance effectiveness is between 40 to 60% metakaolin content. For clays with higher kaolin contents the ratio of calcined clay to limestone can be reduced, with additional benefits in CO_2 savings, cost and workability. Clays with lower kaolin contents may often be enriched by air separation of the finer fraction, as it is discussed in Chapter 4.
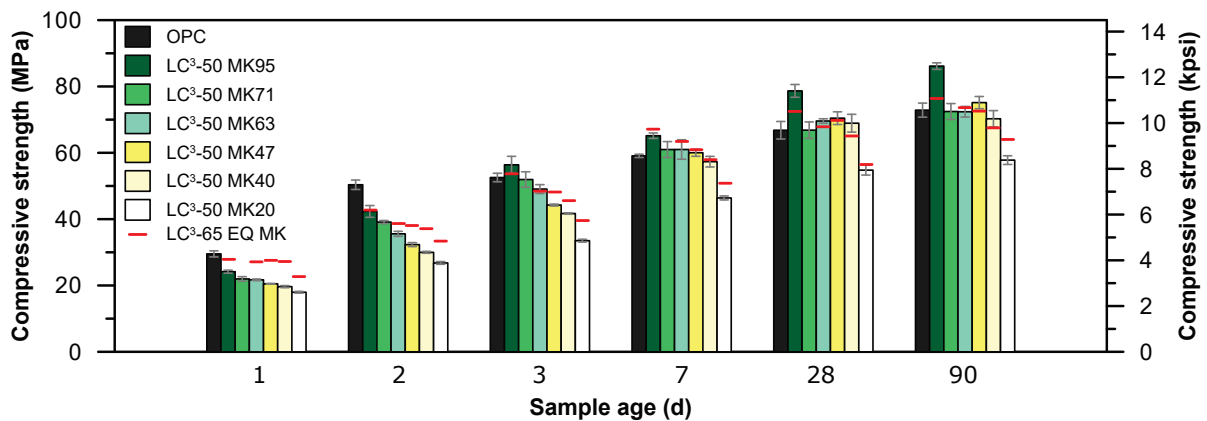
Figure 2-2: Compressive strength of LC³-50 mortars compared with OPC. The strength of LC³-65 mortars with equivalent grade clays are shown as line above (or below) the corresponding LC³-50 bars.

In the US, the ASTM C595 standard for blended cements [10] allows the use of LC³-50. For example, an LC³-50 formulation with 2:1 clay to limestone ratio would be denoted as type IT(P30)(L15). In Europe, the situation is different, as the EN 197-1 [11] standard at present only allows the replacement of 35% of the clinker. Under this standard, an LC³-65 formulation would be denoted as CEM II/B-Q-L. However, moves are underway to introduce a CEM II/C category in EN 197 which would allow commercialization of LC³-50. Figure 2-2 includes the strengths obtained for LC³-65 mortars with the same grades of clays as the LC³-50 systems. They are shown as lines over the corresponding bars for each LC³-50. As seen, there is only a difference in strength between LC³-65 and LC³-50 for the first 3 days of hydration. Afterwards, the performance of both type of formulations is equivalent.

It should also be stressed that the strength data shown here is for lab blends with no optimization of grinding of the different components. In an industrial situation it is possible to improve early strengths through the fineness of the clinker fraction. If this is done very LC³ systems will show very similar strength development to pure Portland cements.

2.3.3 LC³ compared to other common SCMs

In some places, OPC is currently blended with natural pozzolans to reduce the clinker factor. However, the reactivity of natural pozzolans is significantly lower compared to calcined clays. Consequently, the performance of these cements is lower in contrast to LC³ for the same clinker factor. Figure 2-3 compares LC³ mortars (clay grade 63% metakaolin content) with different clinker factors (2:1 clay to limestone ratio in all cases) with OPC and a general use pozzolanic cement with 65% clinker. As seen, an LC³ with a clinker factor as low as 20% yields similar performance to the commercial general use pozzolanic cement in the long term, and 35% can be used if higher strengths at 1 and 2 day are required.
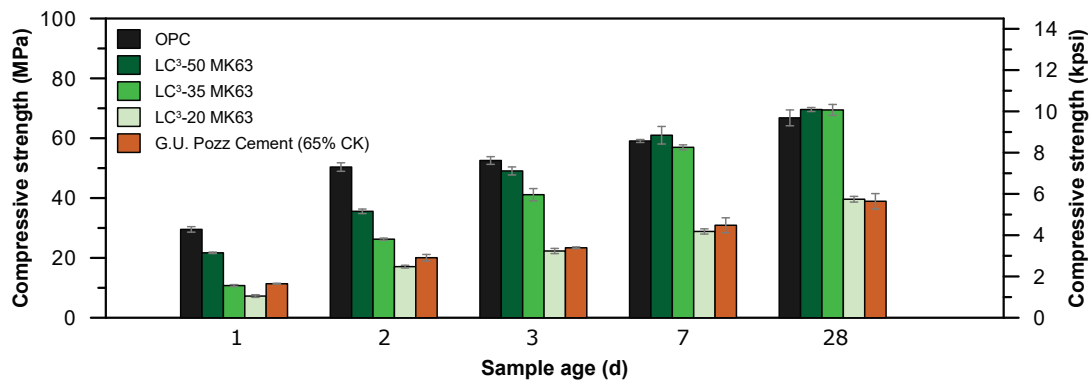
Figure 2-3: Compressive strength of LC³ mortars with a 63% metakaolin content clay, with clinker factors of 50, 35 and 20%. Results are compared with a commercial general use pozzolanic cement (clinker factor 65%).

Figure 2-4 shows a comparison of common SCMs such as slag and fly ash with calcined clays, both in binary formulations (65% clinker, 30% SCM, 5% gypsum) and also combined with limestone [12] (50% clinker, 30% SCM, 15% limestone, 5% gypsum). As seen, the systems with calcined clay outperform the other SCMs at early ages. At later ages, slag (28 d) and fly ash (180 d) reach the same strength as OPC. The strength of the system with calcined clay and limestone (LC³-50) has similar strength to the mixture incorporating only 30% calcined clay, except at 24 h. Thus, the combination of limestone and calcined clays allows further reduction of the clinker factor without a compromise of mechanical properties of the material.
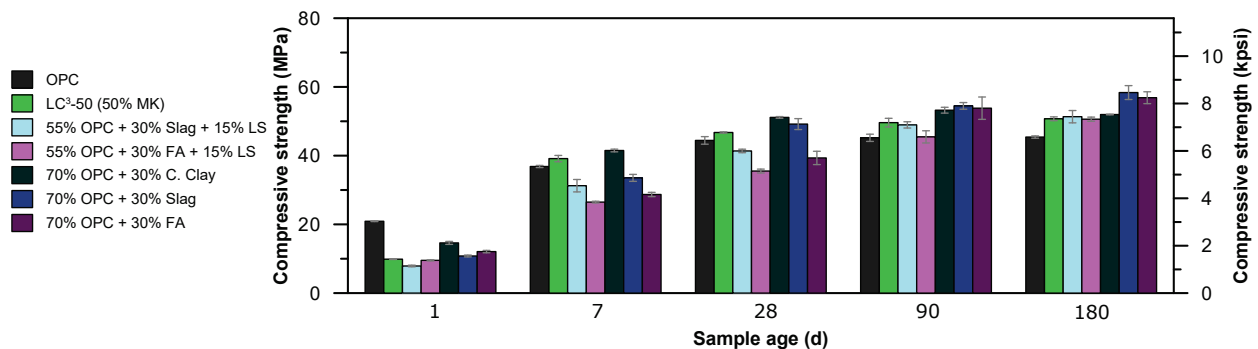
Figure 2-4: Compressive strength of mortars prepared by blending OPC with common SCMs and limestone and with the SCMs alone (30% replacement). Reproduced with data from [12].

2.3.4   Additional LC^3 formulation considerations

While the metakaolin content of the calcined clay is the main factor influencing strength of LC^3, other parameters such as the fineness of the limestone fraction can be engineered to achieve specific strength requirements. Figure 2-5 shows a comparison of LC^3-50 mortars with clay containing 63 and 40% of kaolin, incorporating coarse (cLS, SSA = 1.13 m^2/g), medium (SSA = 3.60 m^2/g) or fine (fLS, SSA = 8.96 m^2/g) limestone. As seen, a refinement of the limestone fraction increases strength specially at early ages due to the filler contribution of limestone to clinker hydration [13]. By using fLS, an LC^3-50 cement with 63% metakaolin achieves the same strength as OPC at 3 d.
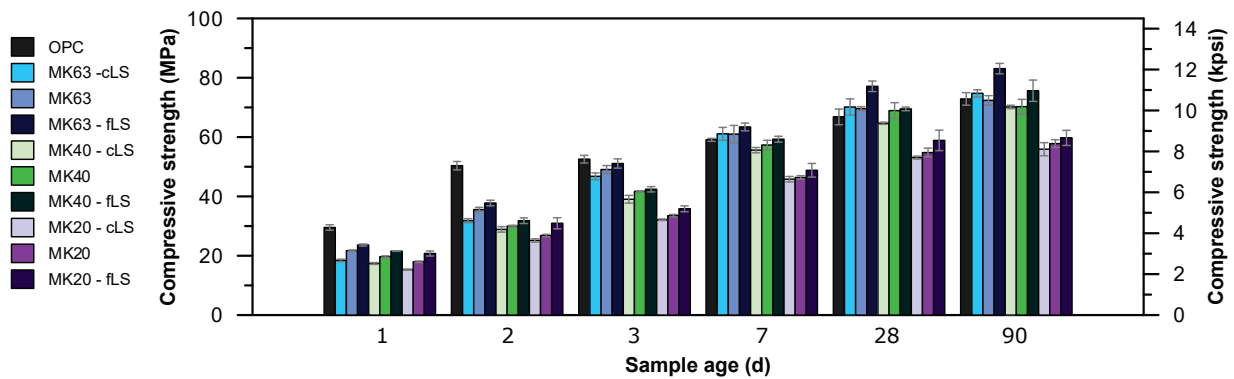
Figure 2-5: Compressive strength of LC^3-50 mortars incorporating coarse (cLS), normal or fine (fLS).

Another aspect to consider in the formulation of LC^3 is the alkali content of the system. As shown in Figure 2-6, an increase of the total alkali content can lead to an increase in the early age strength in the case of 1% Na$_2$O$_{EQ}$ systems. In this case, the alkali content was adjusted by addition of KOH to the mixing water. However, for Na$_2$O$_{EQ}$ contents beyond 1% by mass of binder it has been observed that the strength at later ages reduces significantly [14].
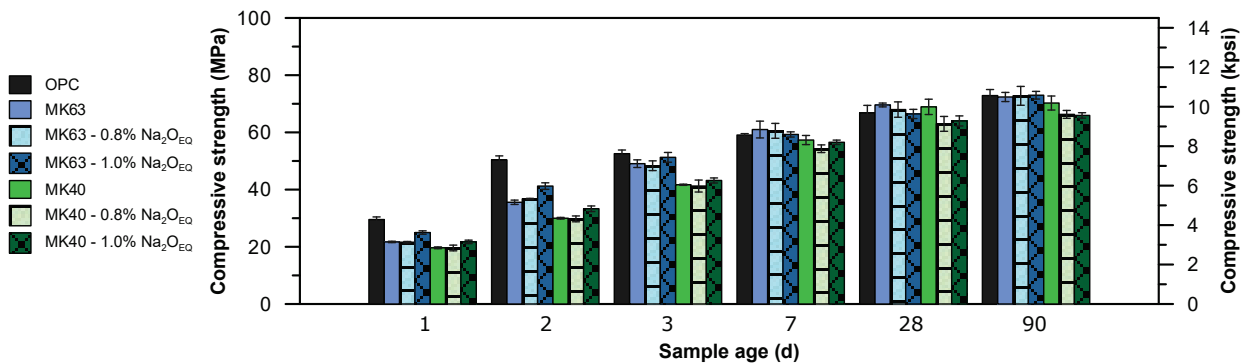
Figure 2-6: Compressive strength of LC^3-50 mortars incorporating coarse (cLS), normal or fine (fLS).

37

2.3.5   LC^3 applications in concrete

The good results achieved by LC^3 in mortar tests can also be observed at the concrete scale. A recent study [15] compared the performance of LC^3 concrete with OPC, a blend of OPC and 10% silica fume (SF) and a blend of 50% OPC and 50% slag. Figure 2-7 shows the compressive strength measured in cylindrical speci-mens at 2, 7 and 28 d. As early as 7 days, LC^3-50 reaches the same strength as OPC and the system with 10% SF. The system with the same clinker factor as LC^3 (50% slag) has lower strengths than the rest of the studied systems at all testing ages.
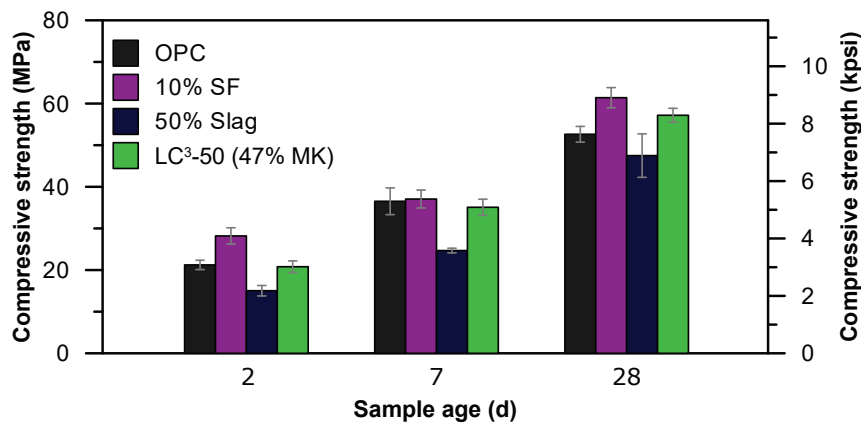
Figure 2-7: Compressive strength of concrete mixtures prepared with different blended cements (constant w/b 0.43) and compared to OPC. Reproduced with data from [15].

LC^3 can be produced as a blended cement at the level of a cement plant, but it can also be made as a mineral addition of limestone, calcined clay (LC^2) and gypsum, in order to be blended afterwards with cement at a ready-mix plant. This approach is especially suitable for markets where the incorporation of SCMs at the concrete stage is more common. Furthermore, it opens a complete variety of possibilities regarding clinker factor which can be better suited for specific applications. As it was shown in [16], the sulfate balance of LC^3 is mainly related to the amount of surface provided by the addition of calcined clay and limestone. Thus, if the LC^2 blend is correctly sulfated for its own specific surface area, it can be then used with cement at differ-ent substitution levels without risk of undersulfation.

Figure 2-8 shows the compressive strength of concrete samples made by blending a commercial pozzolanic Portland cement (PPC) with a clinker factor of 66% with LC^2. Silica fume was used as a comparison. The mix-tures were also compared with an LC^3-50 cement made with the same calcined clay and limestone as the LC^2. LC^3 outperforms the PPC concrete, even considering it has a lower clinker factor. Furthermore, LC^3 concrete exhibits higher strength than the system containing 10% silica fume. In the case of the systems made by blending PPC with LC^2, the system with 15% replacement (57% clinker factor) exhibits similar behavior as the system with 10% silica fume. Thus, LC^2 behaves as a high-performance mineral addition similar to silica fume, but at a lower cost. The system with 30% LC^2 exhibits lower strength than the LC^3 system mainly due to the low reactivity of the natural pozzolans, in agreement with the observations in mortars shown in Figure 2-3.
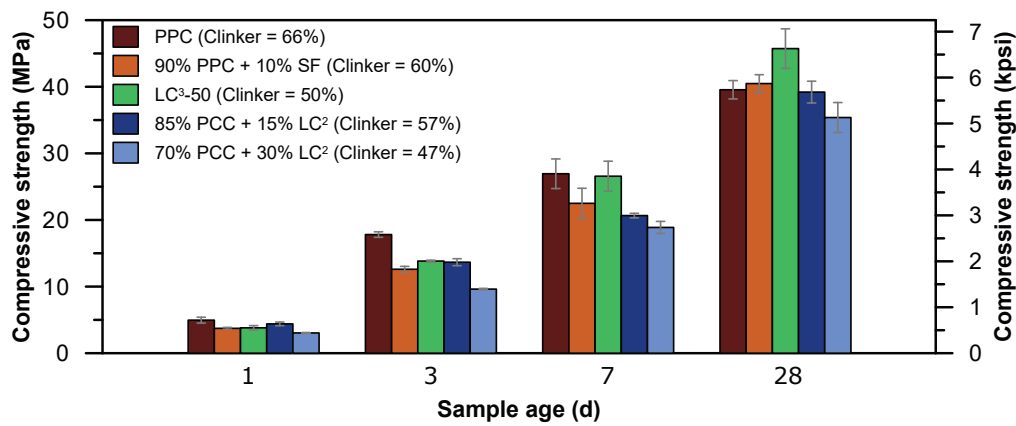
Figure 2-8: Compressive strength of concrete mixtures prepared using a commercial pozzolanic Portland cement (PPC) blended with silica fume and limestone calcined clay (LC^2). The values are also compared with an LC^3 system with the same clay and limestone.

The combination of limestone and calcined clays have the potential to reduce significantly the clinker factor in concrete mixtures, both from an LC^3 or LC^2 approach. An aspect of the technology that still requires attention is workability. The high specific surface of calcined clays has the tendency to increase the water demand of LC^3 as compared to OPC. Consequently, the amount of (super)plasticizer required to achieve a desired slump is in general higher, but well within the normal dosage ranges used with other blended cements. Dosages of PCE-based superplasticizers are increased between 25% to 50% compared to OPC, depending on the amount of kaolinite of the clay fraction.

Slump retention is another aspect to be considered, as LC^3 systems might tend to lose slump quicker than OPC based materials. While this is also a concern in the case of other SCMs, there is an opportunity to develop new technological solutions to solve this problem in a cost-effective manner. For example, the combination of two PCE molecules with different degrees of grafting allows to obtain good retention up to 3 hours as seen in Figure 2-9 compared to a commercial PCE superplasticizer, without requiring a significant increase of the total amount of admixtures that might lead to retardation.
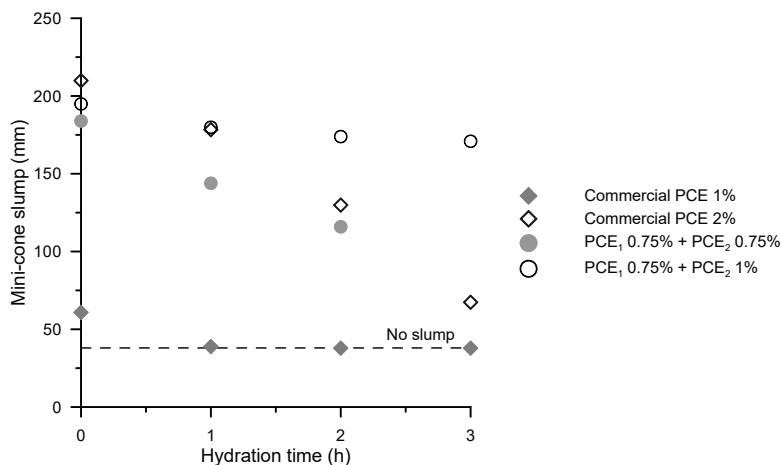
Figure 2-9: Slump retention of LC^3 using different types of PCE molecules as superplasticizer. The combination of more than one type of molecule leads to good results in terms of retention time.

2.4   Hydration reactions occurring in LC^3

Metakaolin (AS$_2$) can react with portlandite (CH) produced during cement hydration to form C–A–S–H [8,17], thus contributing to strength by space filling (Eq. 2-1).

$$AS_2 + 3CH + 6H \longrightarrow C - A - S - H + C_2ASH_8 \qquad (2\text{-}1)$$
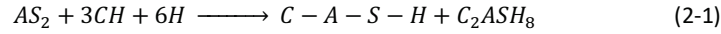
When limestone is added to an OPC system, calcium monocarboaluminate (C$_4$AcH$_{11}$, Mc) and hemicarboaluminate (C$_4$Ac$_{0.5}$H$_{12}$, Hc) are formed (Eq. 2-2) instead of monosulphoaluminate (C$_4$A\$H$_{12}$) as AFm phases, which leaves more sulfates available to form ettringite. The formation of each or both of the carbo-AFm phases has been found to be related to the bulk molar CO$_2$/Al$_2$O$_3$ and SO$_3$/Al$_2$O$_3$ ratios of the system [18].

$$C_3A + 0.5Cc + 0.5CH + 11.5H \longrightarrow C_4Ac_{0.5}H_{12} \qquad (2\text{-}2)$$

When an additional source of amorphous alumina is introduced in the system, such as metakaolin, calcite can further react with these aluminates to form more Mc and Hc phases. This so-called synergic effect of limestone/metakaolin leads to the formation of an increased amount of hydrates (Hc and Mc) which further fills in the porosity, increasing strength and reducing permeability of the material [6,9,17].

$$AS_2 + 0.5Cc + 3.5CH + 8.5H \longrightarrow C_4Ac_{0.5}H_{12} \qquad (2\text{-}3)$$

Both reaction 2-1 and 2-3 consume calcium hydroxide, but for typical clinkers with alite contents above 60% and calcined clays with kaolinite in the range 40-60% it is found that calcium hydroxide still remains unreacted in the long term. Pore solutions show pH in excess of 13 [8].

A typical calorimetry curve of and LC^3 cement is shown in Figure 2-10, compared to an OPC. The first peak associated to the alite reaction is common to both LC^3 and OPC, being enhanced in the LC^3 case due to the filler contribution of metakaolin and limestone. The second (aluminate) peak is enhanced in LC^3 due to the higher amount of sulfate adsorbed into C-S-H during the alite peak [16]. A third peak is observed both in OPC and LC^3 around 36 to 48 h of hydration, but particularly enhanced in the case of LC^3. This peak, linked to the formation of AFm, corresponds to the synergic reaction of limestone and metakaolin. Overall, the heat output of LC^3 is lower compared to OPC due to the reduction in clinker content.
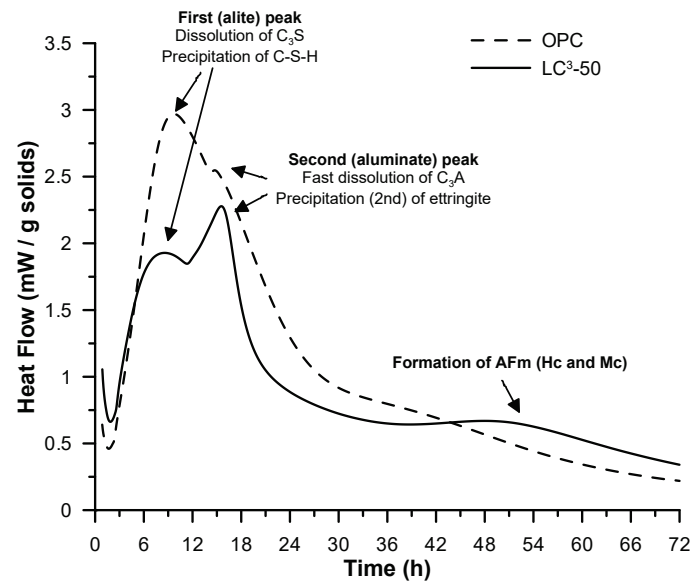
Figure 2-10: Heat flow profile of LC³ compared to a reference OPC system.

The high reactivity of metakaolin and the synergic reaction with limestone contributes to achieve a dense microstructure in LC³ systems at early ages. Figure 2-11 shows porosity profiles measured by mercury intrusion porosimetry (MIP) of LC³ (50% clinker) with different grades (metakaolin (MK) content) of clays compared to OPC. As seen, as early as 7 days the critical pore entry radius is highly refined as compared to OPC, allowing to achieve similar mechanical properties with a much lower clinker content.

a)

b)
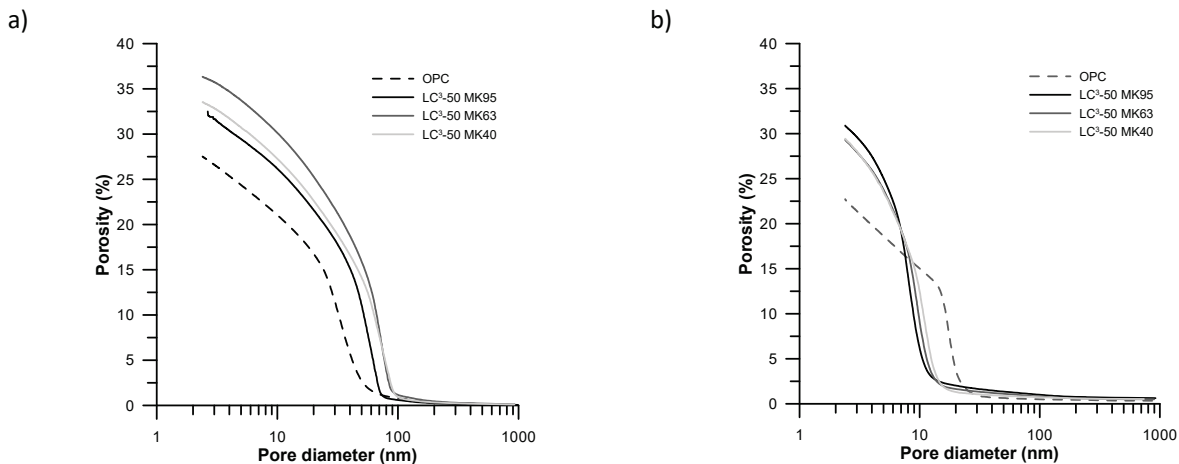
Figure 2-11: Porosity profiles of LC³-50 systems measured by MIP at 1 (a) and 7 (b) days of hydration. Assumed contact angle 120º.

To achieve the highest mechanical potential of LC³, an adjustment of the sulfate content of the formulation is required. If only the sulfate from the clinker factor is used, situations as the one shown in Figure 2-12 for 0% added gypsum can be observed, where a sharp aluminate peak precedes a lower and broader alite peak. The balance of the system can be restored by the incorporation of additional gypsum to retard the aluminate reaction. The requirement of additional gypsum in LC³ is linked to the additional surface supplied by the

addition of the SCMs, which increase the reaction rate of alite (filler effect) and consequently the precipitation rate of C-A-S-H. Sulfate is adsorbed on C-A-S-H during the acceleration period. Thus, an increased amount of C-A-S-H formed leads to an earlier depletion of solid gypsum and consequently, and earlier aluminate peak [16].
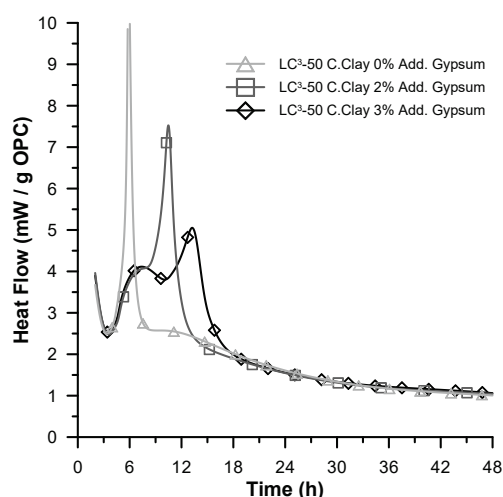
Figure 2-12: Heat flow curves of LC³-50 with different gypsum additions.

The C-A-S-H of LC³ systems shows differences in chemical composition as compared to OPC [19]. The amount of aluminium uptake by C-A-S-H is significantly higher in systems with metakaolin additions compared to pure Portland cement hydrates [8,20]. The Ca/Si is in general lower than plain OPC systems. However, the morphology of C-A-S-H is not significantly affected by the addition of limestone and calcined clay as compared to OPC. Similarly, the bulk density of C-A-S-H remains the same as OPC, around 1.9 g/cm³ at 28 days as measured by ^{1}H NMR [19].

To measure the evolution of the reaction of metakaolin, different experimental approaches have been developed. Mass balance was compared to PONCKS modeling starting from the same XRD dataset, finding similar results [21]. In the case of mass balance, the remaining amount of CH is used to compute the degree of reaction of metakaolin. ^{29}Si and ^{27}Al MAS NMR data acquired from hydrated LC³ samples have been used to assess the reaction kinetics of metakaolin over time [22] and to provide the required input for thermodynamic modelling of these systems.

2.5   Production of LC³ cements

2.5.1   Calcination process of the clay

Calcination of kaolinitic clays between 600 and 850°C leads to the removal of OH^- groups (dehydroxylation) from its crystalline structure to give a state of more structural disorder known as metakaolin [3,23], Figure 2-13. In terms of reactivity, it has been observed that between 600 and 700ºC full dehydroxylation is achieved. However, the reactivity keeps increasing with temperature [5]. The ideal range of calcination is between 700 and 850ºC, where full dehydroxylation is achieved and the maximum pozzolanic reactivity is observed. Above

this range of temperatures, a reduction in specific surface area due to sintering has a negative impact on reactivity. Beyond 1000ºC, recrystallization of non-reactive minerals takes place.
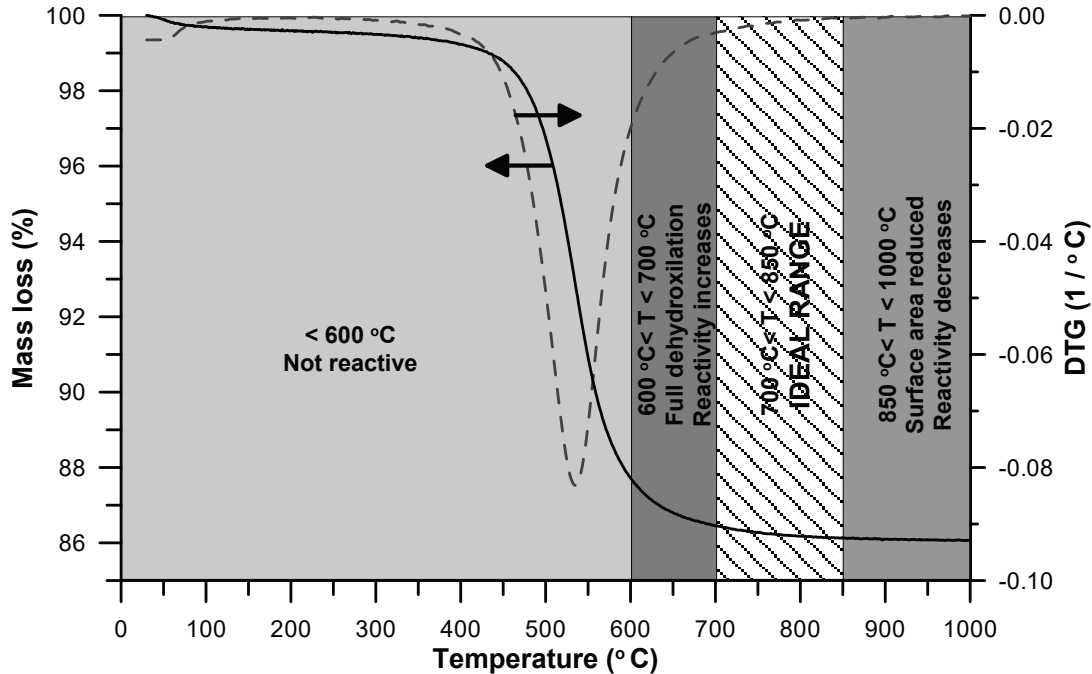
Figure 2-13: Thermal decomposition of kaolinite, showing the ideal range for calcination in terms of reactivity.

Upon dehydroxylation, nuclear magnetic resonance (NMR) tests on calcined clay samples show that aluminium in kaolinite shifts from $Al^{(VI)}$ (octahedral) in the uncalcined material structure, to $Al^{(V)}$, which is evidence of a state of more structural disorder [3]. This transition is not observed in illite and montmorillonite, where on calcination $Al^{(VI)}$ shifts to $Al^{(IV)}$ tetrahedral sites, Figure 2-14 [3].

Flash calcination exposes the material to much higher temperature gradients (10^3-10^5 ºC.s^{-1}) over short periods of time (usually 0.2-1 s) [24], leading to a higher specific surface area as compared to calcination in a rotary kiln due to the rapid release of water vapor [25]. Thus, flash calcination has been found to produce calcined clay with slightly higher reactivity as compared to static or rotary calcination [26]. However, this difference is only significant during the first hours of hydration [9] and the higher surface area may increase problems with workability.
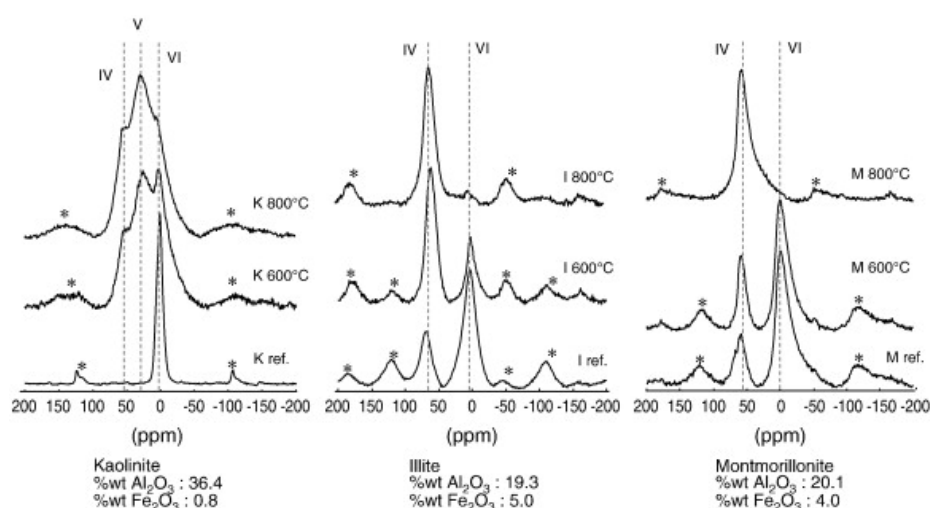
Figure 2-14: ^{27}Al NMR spectra of kaolinite, illite and montmorillonite and its calcined products at different temperatures. Reproduced from [3].

2.5.2 Calcined clay color

The intense reddish color observed in some calcined clays is explained by the oxidation of associated minerals containing iron into hematite (Fe_2O_3, red). This process takes place mainly during the cooling of the calcined clay. If, on the contrary, the cooling between 800 and 400°C takes place in a reducing atmosphere, the iron phases will stabilize as magnetite (Fe_3O_4, black). Even a small amount of iron oxides can have an important effect in color.

The control of color by managing the atmosphere during cooling is well known in the brick industry and can be easily applied in conjunction with most industrial calcination equipment. Figure 2-15 shows the results of such a procedure on a clay. For comparison purposes, the same clay was calcined with and without color control procedures upon cooling. As observed, a red material is obtained under oxidizing conditions, while a black one is obtained in the other case. In both cases, full dehydroxylation is achieved and both calcined clays exhibit equivalent reactivity.

Figure 2-15: Color appearance of raw and calcined clays obtained with and without the use of color control procedures during the cooling process.

2.5.3 Grinding

In laboratory conditions, LC^3 constituents are normally ground separately in open circuit grinding configuration. On the contrary, the most common grinding process in cement plants is based in intergrinding of cement constituents in closed circuit units. The main difference between separate and intergrinding is that during intergrinding the components interact inside the mill. These interactions are mostly due to their differences in grindability [27], which prevents harder materials from further decreasing their particle size. In LC^3, calcined clay and limestone have higher grindabilities (softer particles) as compared to clinker (harder particles). Upon intergrinding of LC^3, clinker tends to remain concentrated in the coarse fraction, which may compromise the early age strength of LC^3. Calcined clay and limestone become much finer which may have a negative effect on workability. In general, the highest reactivity is achieved when clinker is ground separately from limestone and calcined clay.

Grinding aids (GAs) incorporated during comminution of clinker reduce electrostatic forces and minimize agglomeration of clinker and SCM grains [28]. Their chemical composition mostly includes ethanol-amines such as monoethanolamine (MEA), diethanolamine (DEA), and triethanolamine (TEA) as well as glycols such as propylene glycol (PG), monoethylene glycol (MEG), and diethylene glycol (DEG). Because of their organic polar nature, GAs are preferentially adsorbed on surfaces formed by the fracture of electrovalent bonds such as Ca–O and Si–O, thus reducing surface energy forces. Such additions are commonly used to increase cement fineness and compressive strength for given specific energy consumption (Ec) of the grinding mill [28–30]. A typical GA dosage used during grinding of clinker vary from 0.01% to 0.15% of the manufactured cement (clinker + gypsum ground together) by mass.

In the case of LC^3, GAs can be used to significantly increase the yield of the grinding process of calcined clays. Clay particles tend to agglomerate due to their high surface energies, reducing the efficiency of the mill. Figure 2-16 shows a comparison of a laboratory ball mill with equal loads of grinding media and material after 45 min grinding, without (left) and with (right) the use of grinding aids. In this case, 0.015% by mass of clay of a commercial glycol-based GA was used. As observed, the use of GA is effective in avoiding the agglomeration of clay on the surface of the mill and the grinding media.

Without Grinding Aids   **With Grinding Aids**
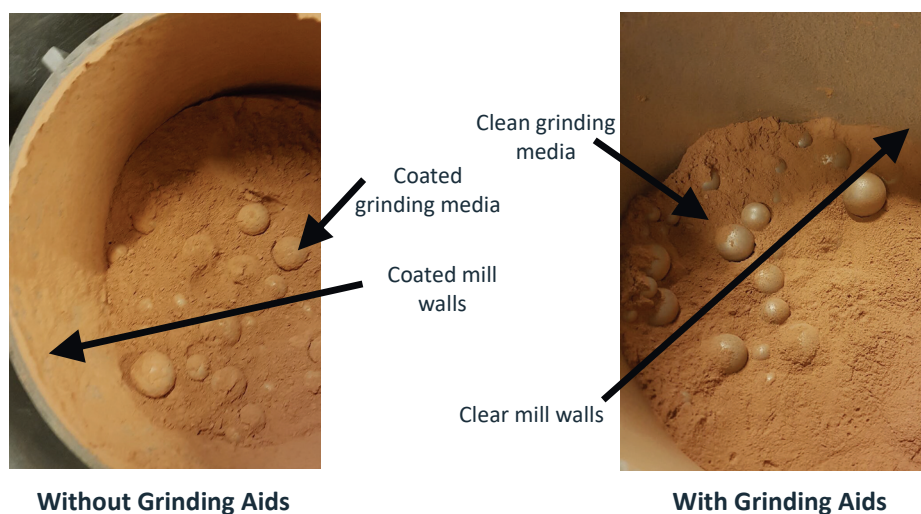
Figure 2-16: Comparison of the grinding process of clays with and without the use of grinding aids.

2.6 Durability of LC^3

2.6.1 Carbonation

The carbonation rate of concrete containing SCMs is generally known to be higher than OPC, and this is the case also for LC^3 systems [31]. The carbonation rate is mainly controlled by the calcium content of the cement paste (proportional to the clinker factor in blended cements), which is the main component binding CO_2 from the atmosphere. The carbonation resistance of LC^3, and other blended systems, can be improved by good curing of concrete prior to exposure [9].

2.6.2 Alkali silica reaction (ASR)

LC^3 is extremely promising to mitigate ASR. In general, the use of supplementary cementing materials has an effective preventive effect against alkali silica reaction in concrete [30,31] due to the reduction in alkalinity of the pore solution [34]. In addition, alumina released into the pore solution by the reaction of the calcined clay also directly inhibits the dissolution of reactive silicate minerals [35]. Figure 2-17 [9] shows the expansion of concrete bars of LC^3-65 and LC^3-50 contain 50% of metakaolin and a highly reactive aggregate. After curing in moist room condition for 28 days were soaked in 0.32 M of NaOH solutions at 38˚C. As observed, the expansion of LC^3 systems is negligible as compared to the OPC system taken as a reference.
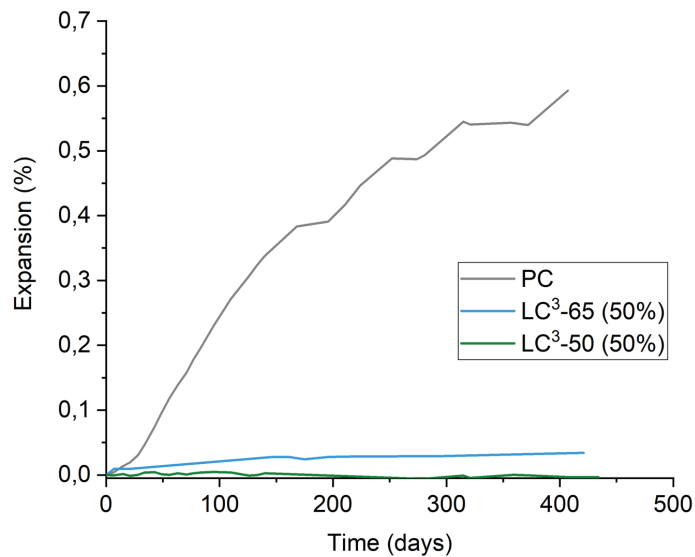
Figure 2-17: ASR expansion measured in LC^3-65 and LC^3-50 systems with metakaolin content of 50%. Reproduced from [9].

2.6.3 Chloride

Corrosion of steel reinforcement in concrete due to chemical attack of chloride ions is the most important durability concern for reinforced concrete structures worldwide. Diffusion of chloride ions through concrete is governed by the microstructural features of the cement paste. These features depend on the solid phase assemblage, the pore structure and the composition of the pore solution [12]. LC^3 exhibits an excellent resistance to chloride ion penetration, as seen in the different chloride penetration profiles after 1 year of

immersion in 0.5 M NaCl solution shown in Figure 2-18. Among the reasons for this good behavior, the alkalinity of the pore solution, the binding capacity and the porosity refinement play a role [12,36]. Recent results show that in terms of porosity, the relationship between chloride resistance and porosity refinement is more related to formation factors (tortuosity) than to a size reduction itself.
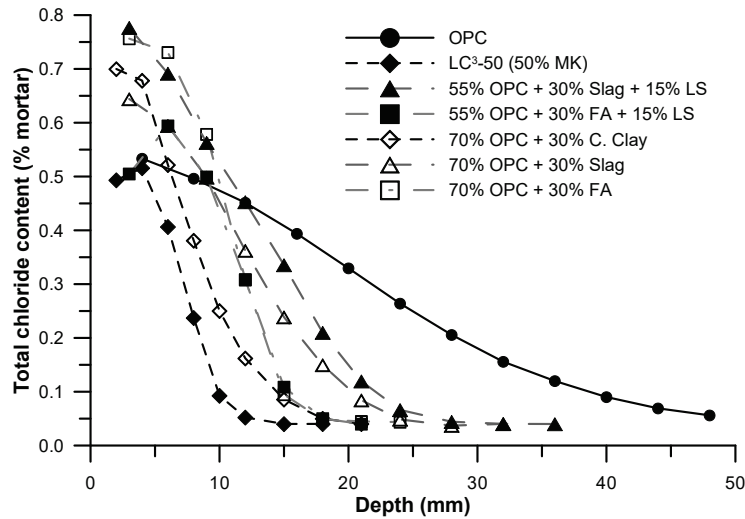
Figure 2-18: Chloride profiles of different blended cements compared to OPC after 1-year immersion in 0.5 M NaCl solution. Reproduced with data from from [12].

2.7   Environmental benefits and economic feasibility of LC^3

In addition to the technical advantages of LC^3 presented in this article, this technology also allows significant CO_2 savings as compared to OPC [37]. A detailed assessment of the environmental benefits of the LC^3-50 formulation, as compared to OPC, showed that this technology can lead to up to 40% of CO_2 savings independent of the technological process considered for the production of calcined clay and clinker [38]. Furthermore, the study shows that the environmental impact of LC^3 produced under the worst technological conditions considered by the team is still lower than the one of OPC produced using the best available technology.

LC^3 is not only technically, but also economically feasible as a cement for the future. The question is against which cement the financial benchmarking of LC^3 shall be conducted. Since the cement type having the closest performance to LC^3 is OPC, the benchmark should be done using this type of cement as a reference.

An economic feasibility study was carried out for LC^3 type cements under this assumption [39]. Flash calciner and rotary kiln were assessed as alternatives for clay calcination. It was observed that the differences between the two technologies in terms of project feasibility is very small. In addition, availability of a suitable clay close (10km) or far (200 km) from the production site was considered. This difference significantly impacts the project profitability as transport cost difference is assumed at USD 13 /T of clay. All scenarios are considered using coal, as the cost of fuels such as diesel will make LC^3 production not economically viable unless such combustible is heavily subsidized. The cost of CEM I / OPC to be benchmarked with is estimated at USD 30 /Ton cement if produced in a cement plant and USD 47/Ton if produced with imported clinker.

The results for a rotary kiln solution for a scenario of integrated plant (a cement plant willing to replace some of its CEM I / OPC production with LC^3) and a grinding unit willing to do the same with imported clinker are shown in Figure 2-19. Further details can be found in the full report [39].
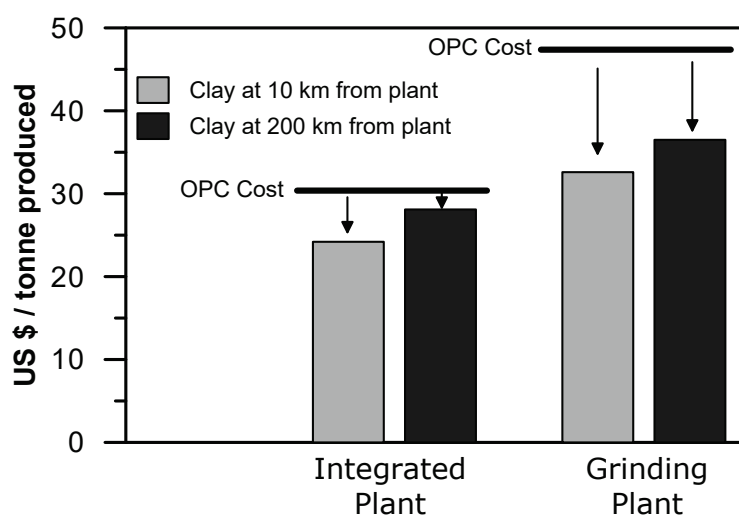
Figure 2-19: Production cost of LC^3 compared to OPC for a scenario of an integrated plant and a grinding unit, considering clay deposits close and far from the production site. Reproduced with data from [39].

2.8   Conclusions and perspectives

Limestone calcined clay cements offer a unique techno-economically feasible opportunity to reduce the clinker factor of the cement industry at a global scale, saving at least 40% CO_2 as compared to conventional Portland cement. The soundness and versatility of the limestone calcined clay combination opens possibilities of use and adoption in markets where blended cements (as LC^3) or mineral additions (as LC^2) are normally used.

Kaolinite is the main parameter determining the suitability of a natural clay for LC^3 production. Contents between 40 to 60% are ideal, and higher-grade clays can be diluted by reducing the clay to limestone ratio of the mixture design. The strength of the LC^3 systems produced with these clays is equivalent to OPC from 3 to 7 days age and onwards. To ensure proper calcination of the clay, the ideal temperature range to aim for is between 700 and 850ºC. Simple technological solutions are available to control the color of calcined clay if necessary.

In addition to the environmental benefits, some properties can be even enhanced compared to normal OPC-based concrete. Chloride penetration resistance is significantly enhanced as compared to OPC, making LC^3 suitable for applications in aggressive environments. In addition, LC^3 is able to inhibit ASR even when highly reactive aggregates are used. Some durability aspects remain open for further investigation, as it is the case of carbonation.

From an environmental perspective the potential of LC^3 technology to reduce CO_2 emissions from the construction industry is substantial. A study by the International Energy Agency (IEA) in 2009 projected that by

2050 it would only be possible to reduce the global average clinker factor for cement to 73% [40], due the limited availability of slag and fly ash. The amount of clay suitable for calcination and use as an SCM is extremely large and means that the clinker factors can be reduced much further. A global reduction to an average of 60%, would mean extra CO_2 reductions of 400 million tonnes of CO_2 per year and as discussed in this article the high performance of the combination of calcined clay and limestone means even greater reductions in clinker factors and CO_2 could be possible. This is also a technology which can be deployed immediately and which can reduce production costs. In the light of the urgency to act on climate change this is or great importance.

LC^3 has received attention from the industrial sector, especially in emerging economies, due to the high demand for buildings and infrastructure in places like Latin America, Asia and Africa. Feasibility studies has been conducted in 11 countries around the globe so far, and companies from more than 25 countries have shown high interest in LC^3 technology. Several full-scale trial productions and demonstration structures have shown the robustness and technical feasibility of LC^3. In two places, large scale LC^3 production facilities are under construction.

From a scientific point of view, 3 international conferences on calcined clays for sustainable concrete have been organized [41–43]. The topic has attracted the interest of scientists and research groups worldwide that are now collaborating in the implementation of LC^3 technology in their respective regions.

2.9 References

[1] IEA, CSI, Technology Roadmap: Low-Carbon transition in the Cement Industry, 2018. doi:10.1007/springerreference_7300.

[2] K.L. Scrivener, V. John, E.M. Gartner, Eco-efficient cements: potential, economically viable solutions for a low-CO2, cement-based materials industry, in: United Nations Environmental Programme (UNEP), 2016.

[3] R. Fernandez, F. Martirena, K.L. Scrivener, The origin of the pozzolanic activity of calcined clay minerals: A comparison between kaolinite, illite and montmorillonite, Cem. Concr. Res. 41 (2011) 113–122. doi:10.1016/j.cemconres.2010.09.013.

[4] B. Sabir, S. Wild, J. Bai, Metakaolin and calcined clays as pozzolans for concrete: A review, Cem. Concr. Compos. 23 (2001) 441–454. doi:10.1016/S0958-9465(00)00092-5.

[5] A. Alujas, R. Fernández, R. Quintana, K.L. Scrivener, F. Martirena, Pozzolanic reactivity of low grade kaolinitic clays: Influence of calcination temperature and impact of calcination products on OPC hydration, Appl. Clay Sci. 108 (2015) 94–101. doi:10.1016/j.clay.2015.01.028.

[6] M. Antoni, Investigation of cement substitution by combined addition of calcined clays and limestone, École Polytechnique Fédérale de Lausanne, 2011.

[7] K. Momma, F. Izumi, VESTA 3 for three-dimensional visualization of crystal, volumetric and morphology data, J. Appl. Crystallogr. 44 (2011) 1272–1276. doi:10.1107/S0021889811038970.

[8] F. Avet, K. Scrivener, Investigation of the calcined kaolinite content on the hydration of Limestone Calcined Clay Cement (LC3), Cem. Concr. Res. 107 (2018) 124–135. doi:10.1016/j.cemconres.2018.02.016.

[9] K.L. Scrivener, F. Avet, H. Maraghechi, F. Zunino, J. Ston, A. Favier, et al., Impacting factors and properties of Limestone Calcined Clay Cements (LC3), Green Mater. (2018). doi:https://doi.org/10.1680/jgrma.18.00029.

[10] ASTM C595/C595M, Standard Specification for Blended Hydraulic Cements, 2019. doi:10.1520/C0595.

[11] EN197-1, Cement - Part 1: Composition, specifications and conformity criteria for common cements, 2000.

[12] S. Sui, F. Georget, H. Maraghechi, W. Sun, K. Scrivener, Towards a generic approach to durability: Factors affecting chloride transport in binary and ternary cementitious materials, Cem. Concr. Res. 124 (2019). doi:10.1016/j.cemconres.2019.105783.

[13] E. Berodier, K. Scrivener, Understanding the filler effect on the nucleation and growth of C-S-H, J. Am. Ceram. Soc. 97 (2014) 3764–3773. doi:10.1111/jace.13177.

[14] W. Hanpongpan, Investigation of the use of Limestone Calcined Clay Cement (LC3) applied to Thailand, École Polytechnique Fédérale de Lausanne, 2019.

[15] F. Avet, L. Sofia, K. Scrivener, Concrete Performance of Limestone Calcined Clay Cement (LC3) Compared with Conventional Cements, Adv. Civ. Eng. Mater. 8 (2019) 20190052. doi:10.1520/acem20190052.

[16] F. Zunino, K.L. Scrivener, The influence of the filler effect in the sulfate requirement of blended cements, Cem. Concr. Res. 126 (2019). doi:10.1016/j.cemconres.2019.105918.

[17] M. Antoni, J. Rossen, F. Martirena, K. Scrivener, Cement substitution by a combination of metakaolin and limestone, Cem. Concr. Res. 42 (2012) 1579–1589. doi:10.1016/j.cemconres.2012.09.006.

[18] T. Matschei, B. Lothenbach, F.P. Glasser, The role of calcium carbonate in cement hydration, Cem. Concr. Res. 37 (2007) 551–558. doi:10.1016/j.cemconres.2006.10.013.

[19] F. Avet, E. Boehm-Courjault, K. Scrivener, Investigation of C-A-S-H composition, morphology and density in Limestone Calcined Clay Cement (LC3), Cem. Concr. Res. 115 (2019) 70–79. doi:10.1016/j.cemconres.2018.10.011.

[20] E. L'Hôpital, B. Lothenbach, G. Le Saout, D. Kulik, K. Scrivener, Incorporation of aluminium in calcium-silicate-hydrates, Cem. Concr. Res. 75 (2015) 91–103. doi:10.1016/j.cemconres.2015.04.007.

[21] F. Avet, X. Li, K. Scrivener, Determination of the amount of reacted metakaolin in calcined clay blends, Cem. Concr. Res. 106 (2018) 40–48. doi:10.1016/j.cemconres.2018.01.009.

[22] W. Kunther, Z. Dai, J. Skibsted, Thermodynamic modeling of hydrated white Portland cement-metakaolin-limestone blends utilizing hydration kinetics from 29Si MAS NMR spectroscopy, Cem. Concr. Res. 86 (2016) 29–41. doi:10.1016/j.cemconres.2016.04.012.

[23] J. Ambroise, S. Maximilien, J. Pera, Properties of Metakaolin blended cements, Adv. Cem. Based Mater. 1 (1994) 161–168. doi:10.1016/1065-7355(94)90007-8.

[24] A. Teklay, C. Yin, L. Rosendahl, Flash calcination of kaolinite rich clay and impact of process conditions on the quality of the calcines: A way to reduce CO2 footprint from cement industry, Appl. Energy. 162 (2014) 1218–1224. doi:10.1016/j.apenergy.2015.04.127.

[25] D. Bridson, T.W. Davies, D.P. Harrison, Properties of flash-calcined kaolinite, Clays Clay Miner. 33 (1985) 258–260.

[26] S. Salvador, Pozzolanic properties of flash-calcined kaolinite: A comparative study with soak-calcined products, Cem. Concr. Res. 25 (1995) 102–112. doi:10.1016/0008-8846(94)00118-I.

[27] K. De Weerdt, Separate grinding versus intergrinding, SINTEF Rep. SBF BK A. 7022 (2007).

[28] J.J. Assaad, C.A. Issa, Effect of clinker grinding aids on flow of cement-based materials, Cem. Concr. Res. 63 (2014) 1–11. doi:10.1016/j.cemconres.2014.04.006.

[29] M. Katsioti, P.E. Tsakiridis, P. Giannatos, Z. Tsibouki, J. Marinos, Characterization of various cement grinding aids and their impact on grindability and cement performance, Constr. Build. Mater. 23 (2009) 1954–1959. doi:10.1016/j.conbuildmat.2008.09.003.

[30] S. Sohoni, R. Sridhar, G. Mandal, The effect of grinding aids on the fine grinding of limestone, quartz and Portland cement clinker, Powder Technol. 67 (1991) 277–286. doi:10.1016/0032-5910(91)80109-V.

[31] A. Morandeau, M. Thiéry, P. Dangla, Impact of accelerated carbonation on OPC cement paste blended with fly ash, Cem.

Concr. Res. 67 (2015) 226–236.

[32]   M.H. Shehata, M.D.A. Thomas, The effect of fly ash composition on the expansion of concrete due to alkali–silica reaction, Cem. Concr. Res. 30 (2000) 1063–1072.

[33]   J. Duchesne, M.A. Bérubé, The effectiveness of supplementary cementing materials in suppressing expansion due to ASR: Another look at the reaction mechanisms part 1: Concrete expansion and portlandite depletion, Cem. Concr. Res. 24 (1994) 73–82.

[34]   M.H. Shehata, M.D.A. Thomas, R.F. Bleszynski, The effects of fly ash composition on the chemistry of pore solution in hydrated cement pastes, Cem. Concr. Res. 29 (1999) 1915–1920.

[35]   T. Chappex, K.L. Scrivener, The effect of aluminum in solution on the dissolution of amorphous silica and its relation to cementitious systems, J. Am. Ceram. Soc. 96 (2013) 592–597. doi:10.1111/jace.12098.

[36]   S. Sui, W. Wilson, F. Georget, H. Maraghechi, H. Kazemi-Kamyab, W. Sun, et al., Quantification methods for chloride binding in Portland cement and limestone systems, Cem. Concr. Res. 125 (2019). doi:10.1016/j.cemconres.2019.105864.

[37]   R.G. Pillai, R. Gettu, M. Santhanam, S. Rengaraju, Y. Dhandapani, S. Rathnarajan, et al., Service life and life cycle assessment of reinforced concrete systems with limestone calcined clay cement (LC3), Cem. Concr. Res. 118 (2019) 111–119. doi:10.1016/j.cemconres.2018.11.019.

[38]   S. Sánchez Berriel, A. Favier, E. Rosa Domínguez, I.R. Sánchez MacHado, U. Heierli, K. Scrivener, et al., Assessing the environmental and economic potential of Limestone Calcined Clay Cement in Cuba, J. Clean. Prod. 124 (2016) 361–369. doi:10.1016/j.jclepro.2016.02.125.

[39]   K. Scrivener, A. Dekeukeleaere, F. Avet, L. Grimmeissen, Financial Attractiveness of LC3, Lausanne, 2019.

[40]   IEA, Cement Technology Roadmap: Carbon Emissions Reductions up to 2050, Paris, 2009. doi:https://doi.org/10.1787/9789264088061-en.

[41]   K.L. Scrivener, A. Favier, eds., Proceedings of the 1st International Conference on Calcined Clays for Sustainable Concrete, in: Springer, Lausanne, 2015.

[42]   F. Martirena, A. Favier, K.L. Scrivener, eds., Proceedings of the 2nd International Conference on Calcined Clays for Sustainable Concrete, in: Springer, Havana, 2018.

[43]   S. Bishnoi, ed., Proceedings of the 3rd International Conference on Calcined Clays for Sustainable Concrete, in: Springer, New Delhi, 2020.

Chapter 3 Influence of calcite impurities on calcined clay reactivity

Note: This chapter is based on an article published in a peer reviewed journal.

The use of supplementary cementitious materials (SCM) as a partial replacement for Portland cement is the most effective way to reduce the carbon footprint of the concrete industry. Raw clays containing kaolinite (kaolin) are promising substitute materials. In the field, raw clays are often mixed with calcite and this is thought to affect their behaviour after calcination. This study explores the influence of calcite impurities on the mineralogy and reactivity a kaolinitic clay. A kaolin sample was blended with different quantities of calcite. The results show that during calcination calcite is decomposed, but no significant amount of free lime or amorphous calcium carbonate are formed. A granular deposit was observed that partially covers the kaolinite particles. The decomposition of calcite and formation of the deposit is associated with a reduction in specific surface area, which increases with the amount of calcite that is intermixed in the raw clay. TEM-EDS analysis showed that the deposit corresponds to a new phase formed from the interaction of kaolinite and calcite, with an Al/Si ratio ranging from 0.74 to 0.88 and Ca/Si ratio between 0.86 to 1.65. Reduction of the calcination temperature to 700ºC reduces the calcite decomposition and the negative impact on reactivity.

54

Contents

3.1   Introduction

Mineral additions, commonly referred as supplementary cementitious materials (SCM), are widely used either in blended cements or added to concrete separately in the mixer [1,2]. The use of SCM, leads to a reduction of CO_2 emissions per unit volume of concrete, and provides a beneficial use for wastes and by-products [3–5].

Clay minerals are unique among supplementary cementitious materials because of their abundance worldwide [6–8]. Clay mineral particles are made up of tens to hundreds of layers composed of tetrahedral silica and octahedral alumina sheets. The three most abundant clay mineral types are kaolinite, illite and montmorillonite [9]. Kaolinite is dehydroxylated in the temperature range 400-600°C. The dehydroxylation of kaolinite leads to a more disordered material known as metakaolinite [10–12]. Usually, raw clay is calcined in the range 700 and 800ºC to maximize the amount and degree of disorder of metakaolinite in the calcined clay. The reactivity of calcined clay is strongly related to its metakaolinite content [11,13]. Higher temperatures lead to reduced reactivity due to sintering and eventually recrystallization [11].

In some regions, raw clays are naturally combined with limestone (calcite). Calcite decomposes between 600ºC to 800ºC into free lime and carbon dioxide (gas), so if calcite is present some decomposition may occur during the calcination process. The interaction of calcite with clay minerals such as kaolinite has been studied for calcination temperatures above 900ºC, where the formation of metastable calcium alumino-silicate phases such as wollastonite ($CaO·SiO_2$), anhortite ($CaO·Al_2O_3·2SiO_2$) and gehlenite ($2CaO·Al_2O_3·SiO_2$) were reported [14–16]. Inclusion of calcium in an amorphous alumino-silicate phase has also been reported previously in systems with small amounts of limestone incorporation [17].

El-Didamony only observed the formation of gehlenite above 850ºC, and in increasing amounts up to 1000ºC [15]. Other studies reported the crystallization of gehlenite and anhortite in kaolinite-calcite mixes sintered at 1100ºC [14]. Snellings et al. reported incorporation of calcium into the amorphous fraction of clay-limestone residues calcined between 820 and 905ºC, indicating the formation of a Ca-aluminosilicate amorphous phase [17]. Hollanders observed positive effects on the pozzolanic reactivity of calcined clays for calcite additions above 10% and after regrinding the material [18].

Despite the abundant literature regarding the calcite-kaolinite system at higher temperatures, there is lack of systematic studies exploring these interactions at temperatures of 800ºC or lower, which is the usual range for calcined clay production for use as a substitute in blended cement. This study explores the effect of calcite impurities below 10% by mass on mineralogy, morphology and pozzolanic reactivity, calcined under typical conditions intended for metakaolinite production.

3.2   Materials and methods

3.2.1   Experimental design

A raw clay (kaolin) from China was used in this study, with 71% kaolinite content as measured by thermogravimetric analysis (TGA). The clay was selected due to its high kaolinite content and as it did not contain any limestone. The main associated minerals found in the clay are quartz and anatase. The raw clay was ground in a laboratory jar mill until a homogeneous powder was obtained with a D_{V50} below 5 μm. Different

amounts of limestone (Durcal 5; D_{V50} = 6.9 μm, 98.9% calcite by TGA) was added to the raw clay. The particle size distribution (PSD) of the raw materials was measured by laser diffractometry (Figure 1). The chemical composition determined by X-ray fluorescence (XRF), Table 1. No illite or muscovite were detected in the raw clay by XRD, so weight loss between 400C and 700ºC was only due to the dehydroxylation of kaolinite.

Table 3-1: Chemical composition of raw clay and limestone expressed as oxides mass %.

	Raw clay (kaolin)	Limestone
SiO_2	58.16	0.11
Al_2O_3	37.63	0.00
Fe_2O_3	0.79	0.04
CaO	0.17	54.96
Na_2O	0.09	0.06
K_2O	0.08	0.01
MnO	0.05	0.00
TiO_2	1.13	0.01
MgO	0.19	0.15
P_2O_5	0.41	0.00
SO_3	0.35	0.03
LOI	3.91	42.5

The raw clay and limestone powders were blended and intermixed in 150 g batches using a Turbula blender (with simultaneous shaking and rotating action) for 15 minutes, in order to obtain a homogeneous sample. The limestone content of the batches was checked by TGA after blending, it was within $\pm$ 10% of the nominal limestone content defined in the experimental design. As the limestone used was nearly pure calcite, both terms are used interchangeably in this paper to refer to the impurities incorporated in the material. The particle size distribution of the raw materials, measured by laser diffraction, are shown in Figure 3-1.
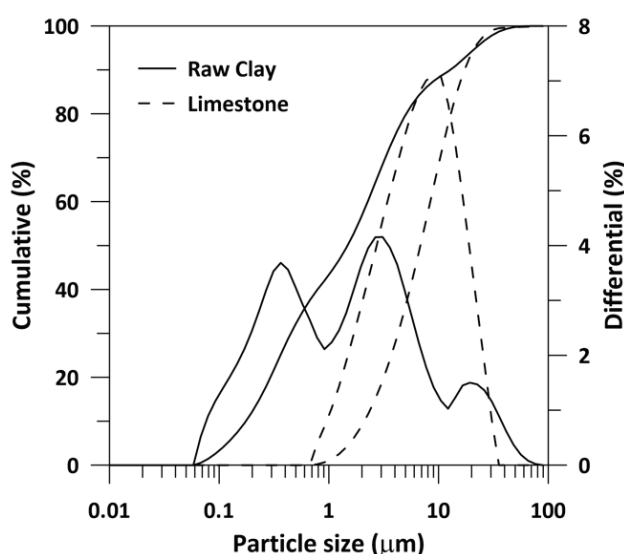
Figure 3-1: Particle size distribution of raw materials measured by laser diffractometry.

Calcination was conducted in a laboratory furnace. About 50 g of powder was placed in flat alumina crucibles to maximize the exposed surface of the material. The heating ramp was in all cases 20°C/min. After

completing the calcination process, the crucibles with the material were left inside the furnace until reaching 200°C before removing them. After calcination, the material was stored in sealed plastic containers until testing.

A composite cubic experimental design was used to select the compositions of the samples tested in two stages. The first one studied the influence of three parameters (maximum calcination temperature, limestone content and residence time) on the properties and pozzolanic reactivity of calcined clay. The range of the parameters was based on previous studies that have shown good results in terms of kaolinite dehydroxylation and pozzolanic reactivity [9,11,19], and the range of limestone impurities commonly encountered. The calcination temperature (X_1), limestone content (X_2) and residence time (X_3) were centered at 700ºC, 5% by mass and 40 minutes, respectively. A response surface methodology was used to explore the experimental region around this central point. Factor levels were defined using a central composite design (CCD) for 3 factors which produces second order response surface models [20]. Six replications of the central point allowed the experimental variance to be estimated. According to CCD each factor is applied in five levels: $-\alpha$, -1, 0, 1, α, where α ($\sqrt[4]{2^k}$, where k is the number of factors) is 1.682 in this study to obtain a rotatable design [20]. The materials and factor levels considered for the 20 experimental points (coded as M-01 to M-14 plus centerpoints Ci) of the first stage (Table 3-2).

In light of the results obtained in the first stage, a second stage was carried out to better understand the effect of calcite impurities on the reactivity of calcined clay by comparison with the behaviour of the material without calcite, and to examine the behaviour of calcite-containing materials calcined at 700ºC compared to higher temperatures. The factor levels of the 12 additional experimental points (coded M-A to M-L) of the second stage (Table 3-2 bottom part).

In order to facilitate the identification of specific experimental points in the graphs in this paper, the symbol key in Figure 2-2 is adopted. In the presentation of the results we are mainly interested in the calcite content and the calcination temperature, so the third factor (residence time) is represented by a "--", "-", "+" or "++" sign next to the experimental point.
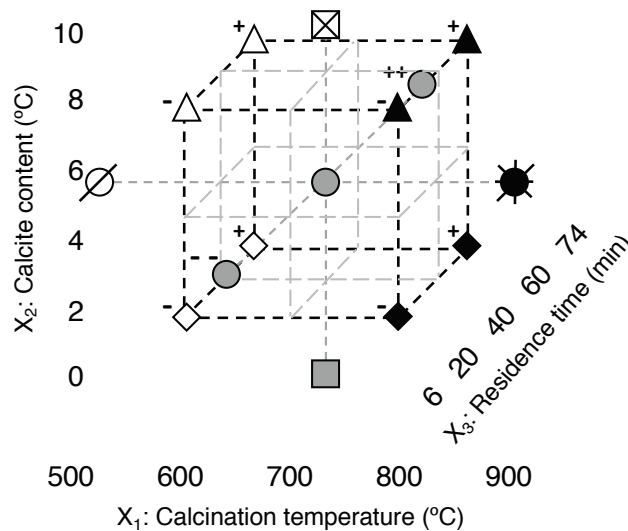
Figure 3-2: Symbol key for identification of experimental points of CCD throughout this paper.

Table 3-2: Experimental design and factor levels considered in both experimental stages of the study.

| | Material | | Factor levels | | | | | |
| | ID | Exp. | Coded | | | Experimental | | |
		block	X1: m_temp	X2: cal_cont	X3: r_time	X1: m_temp (°C)	X2: cal_cont (%)	X3: r_time (min)
FIRST STAGE	M-01	I	-1	-1	-1	600	2	20
	M-02	II	1	-1	-1	800	2	20
	M-03	II	-1	1	-1	600	8	20
	M-04	I	1	1	-1	800	8	20
	M-05	II	-1	-1	1	600	2	60
	M-06	I	1	-1	1	800	2	60
	M-07	I	-1	1	1	600	8	60
	M-08	II	1	1	1	800	8	60
	M-09	III	-1.682	0	0	532	5	40
	M-10	III	1.682	0	0	868	5	40
	M-11	III	0	-1.682	0	700	0	40
	M-12	III	0	1.682	0	700	10	40
	M-13	III	0	0	-1.682	700	5	6
	M-14	III	0	0	1.682	700	5	74
	Ci	I-II-III	0	0	0	700	5	40
SECOND STAGE	M-A	-	1	-1.682	-1	800	0	20
	M-B	-	1	-1.682	0	800	0	40
	M-C	-	1	-1.682	1	800	0	60
	M-D	-	-1	-1.682	-1	600	0	20
	M-E	-	-1	-1.682	1	600	0	60
	M-F	-	0	-1.682	-1	700	0	20
	M-G	-	0	-1.682	0	700	0	40
	M-H	-	0	-1.682	1	700	0	60
	M-I	-	0	-1	-1	700	2	20
	M-J	-	0	-1	1	700	2	60
	M-K	-	0	1	-1	700	8	20
	M-L	-	0	1	1	700	8	60

3.2.2 Material characterization

X-ray diffraction (XRD) was used to assess the mineralogical composition of the calcined materials. Measurements were made on back loaded powder samples to reduce the effects of preferred orientation. The samples were measured in Bragg–Brentano mode using a X'Pert PANalytical diffractometer with CuKα source operated at 45 kV and 40 mA with a 1/2º soller slit. Samples were scanned from 7 to 70 degrees 2θ with a step size of 0.0167 2θ using a X'Celerator detector, resulting in an equivalent time per step of 60 s. Commercial software (HighScore Plus version 4.6) coupled with the ICCD database were used for phase matching and Rietveld refinement.

Fourier transform infrared spectroscopy (FTIR) measurements were made for some of the calcined materials to complement the information obtained from XRD, using a 6700 Nicolet spectrometer by Thermo Fischer Sci. An attenuated total reflectance (ATR) accessory was used for the measurements, equipped with a diamond crystal and a potassium bromide (KBr) beam splitter. A total of 32 background and sample scans were taken each time, with a resolution of 4.0 cm^{-1}.

The specific surface area (SSA) of the materials was determined by gas adsorption using the Brunauer-Emmett-Teller (BET) method, with a Micromeritics TriStar II analyser. Nitrogen (N2) was used as analysis adsorptive gas. Samples of approximately 1 g of powder material were introduced in analysis tubes and degassed for 2 h at 200ºC under N2 flow. Subsequently, they were immersed in a liquid nitrogen bath (77.3 K) where the measurements were performed. Five measurements at different relative pressures were collected and used to calculate the specific surface area of the material.

The initial kaolinite content of the raw clay (kaolin) was determined by thermogravimetric analysis (TGA), considering the weight loss between 400-600ºC corresponding to the kaolinite dehydroxylation. A Mettler Toledo unit equipped with a rotary autosampler was used, heating from 30 to 1000ºC at 10ºC/min heating rate under a N2 30 mL/min flow as protective atmosphere. As the dehydroxylation of kaolinite and the decomposition of limestone peaks overlap, the tangent method was selected to compute both weight losses [21].

TGA was also used to assess the amount of calcined kaolinite (equivalent to the metakaolinite content) in the calcined materials. This parameter is defined as the difference on kaolinite measured on the raw clay and the calcined clay, (Eq. 3-1) to account for partial dehydroxylation.

$$\% \text{ calcined kaolinite} = \%\text{kaolinite}_{\text{raw clay}} - \%\text{kaolinite}_{\text{calcined clay}} \qquad (3\text{-}1)$$

To compare the efficiency of calcination of the kaolinite in the clay-limestone systems, the normalized calcined kaolinite content was computed according to Eq. 3-2, to account for the dilution due to the limestone additions.

$$\% \text{ normalized calcined kaolinite} = \frac{\%\text{kaolinite}_{\text{raw clay}} - \%\text{kaolinite}_{\text{calcined clay}}}{\%\text{kaolinite}_{\text{raw clay}} \cdot (1 - \%\text{limestone})} \qquad (3\text{-}2)$$

Isothermal calorimetry was used to assess the pozzolanic reactivity of calcined clays. For this purpose, the R3 test proposed by Avet et al. [13] was selected due to its reliability and ease of interpretation. In this procedure, calcined clay is mixed with portlandite, calcium carbonate, potassium sulfate, potassium hydroxide and water at 40ºC, and put into glass ampoules inside the calorimeter at 40°C. The total heat evolved after 24 h is taken as a measure of the reactivity of the clays and shows good correlation with compressive strength results obtained on blended cement-mortar bars. In this study, the heat evolved after 24 h and 72 h was analyzed. Further details can be found in [13].

In order to observe morphological changes of clays after calcination with and without limestone impurities, scanning electron microscopy (SEM) observations were conducted. A FEI XL30 series microscope equipped with a field emission gun and an in-lens SE detector was used for high resolution imaging (HR-SEM). Clay samples were dispersed in a 0.01% sodium poly-acrylic acid (PAA) solution. A few droplets of the dispersed

particles were subsequently dried on a glass plate. Afterwards, the particles were placed over carbon holders and coated with 4 nm osmium oxide (OsO_4).

Further insights into particle composition after calcination were gathered using transmission electron microscopy (TEM) analyses. A thin lamella was prepared from the calcined clay particles: the powder was first mixed with G2 resin (hard epoxy resin from Gatan®) with a high concentration of particles (approx. 50% by mass). This mix was then heated at 40°C in order to increase fluidity, and centrifuged 15 minutes at 15000 rpm. The polymerization of the resin was conducted at 80°C during 12 hours. A semi-disc of approx. 3 mm of diameter and 700 μm thick was cut from the bottom of the centrifuged cone, in order to maximize the concentration of particles. This semi-disc was then thinned down to less than 5 μm with a bevel to have a thin part at the front and a thicker part at the back, ensuring good mechanical behavior upon manipulation. The semi-disc of embedded particles was then glued on a TEM copper half-ring of 3 mm of diameter.

The sample was thinned to approx. 100-150 nm using a Gatan® Precision Ion Polishing System (PIPS, model 691), with decreasing voltages of the Argon guns from 1.5 to 0.4 kV. The TEM transparency is achieved when equal thickness fringes can be seen on the edge of the sample by optical microscopy.

The thinned lamella was then transferred into a FEI Tecnai Osiris TEM, where a voltage of 80kV and a small spot size (8, corresponding to a current of 0.15 nA) were used in order to minimize the beam damage on the sample. TEM was operating in scanning-TEM (STEM) mode and the high angular annular dark field (HAADF) detector was used. For the EDS acquisition, a set of 2 windowless FEI Super-X SDD detectors were used simultaneously and the lamella was tilted 20 degrees to face the detectors. A defocus of 200 nm was applied to minimize sample damage.

3.3   Results and discussion

3.3.1   Effect of limestone on SSA, calcined kaolinite content and reactivity

The specific surface area (SSA) results, measured using nitrogen adsorption and computed using the BET model, are shown in Figure 3-3. The repetitions of the central point give an estimation of the experimental variability. As the calcination temperature increases, the SSA is reduced. This agrees with previous studies [9,12,17]. Limestone additions lead to lower SSA at all temperatures. As the limestone is less fine than the clay (SSA of clay = 9.30 m2/g and SSA of limestone = 2.08 m^2/g) there will be some reduction of surface area just due to the incorporation of the less fine material. This can explain the reduction of SSA measured between the materials with residence times of up to 20 minutes. However, the reductions seen for the 8% limestone materials calcined for 60 min indicate another mechanism decreasing the specific surface for longer residence times.
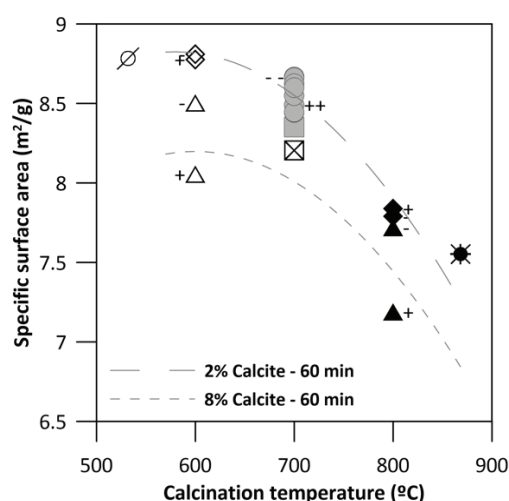
Figure 3-3: BET specific surface area versus calcination temperature for materials considered in the CCD experimental design. Contour plots of response surface for 2 and 8% materials calcined for 60 minutes are included.

XRD patterns for experimental points corresponding to the core of the experimental program (M-1 to M-8) are shown in Figure 3-4a (2% calcite materials) and Figure 4b (8% calcite materials). Calcination at 600ºC does not completely dehydroxylate kaolinite, even at high residence times (60 min), as seen by the persistence of the main kaolinite reflection at 12.36º 2θ. Furthermore, there is no change in the calcite content at this temperature. For 8% initial calcite content materials, the amount of remaining calcite after calcination at 600ºC was 7.92 and 7.85% by mass for 20 and 60 min residence time respectively, as determined by TGA.

At 800°C a higher level of dehydroxylation is measured for low residence time (20 min) materials and kaolinite became undetectable in materials calcined for 60 min (see Figure 3-4a and 3-4b). On the other hand, a reduction in the intensity of the main reflection of calcite (29.40º 2θ) is detected for the materials calcined for 20 min and, more significantly, for the material calcined for 60 min. The amount of remaining calcite determined by TGA in the material calcined for 60 minutes is 0.65% and 2.23% by mass for 2% and 8% initial calcite content, respectively. However, there was no evidence of crystalline free lime (CaO) in the 2% calcite sample and only traces in the 8% one, as seen by the lack of the main reflection at 37.30º 2θ. Therefore, there is a question of where the calcium from the calcite has gone, as XRD does not indicate any other crystalline phases containing calcium. The amount of free lime estimated from Rietveld refinement for the 8% calcite 60 m residence time clay (0.43% by mass) only accounts for a small amount of the decomposed calcite.

a)
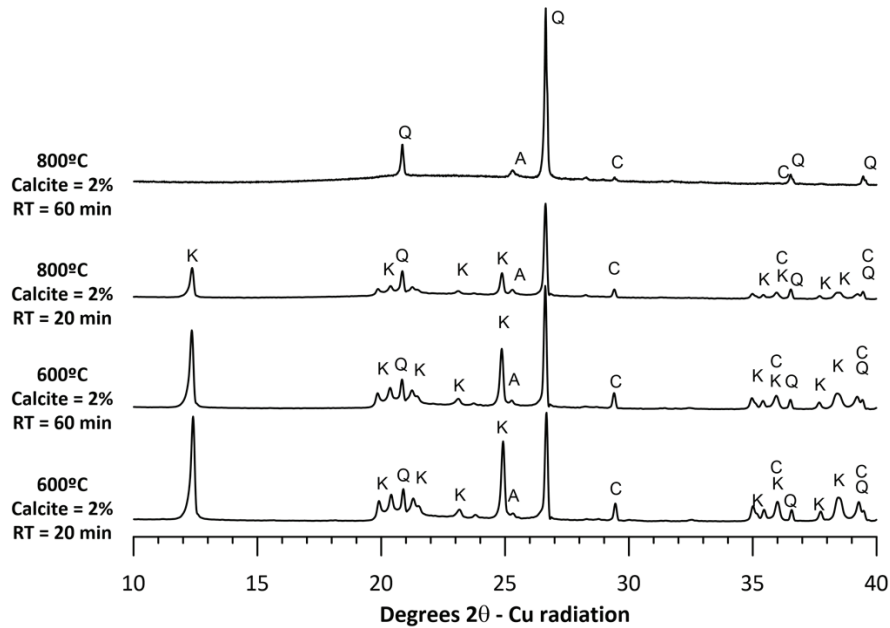
b)
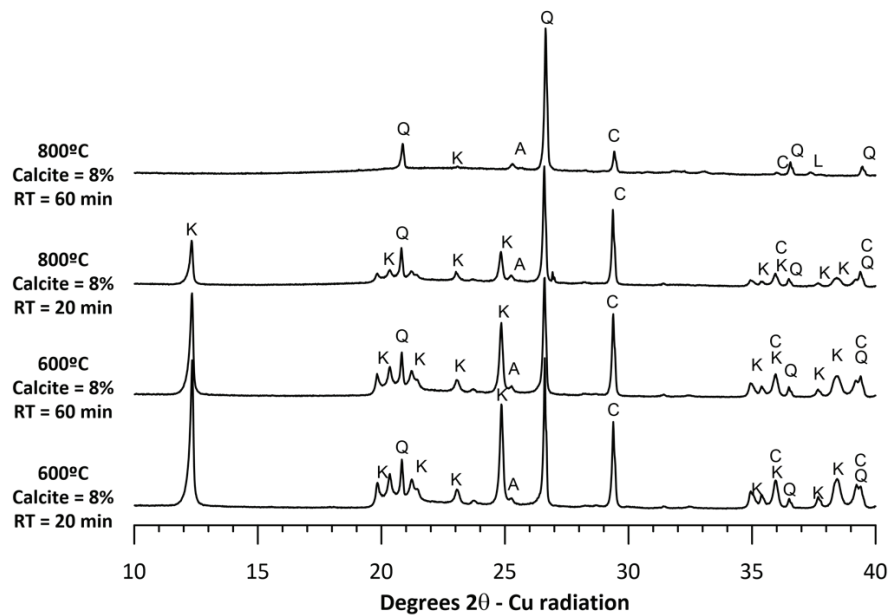
Figure 3-4: XRD patterns of a) 2% and b) 8% initial calcite content clays.

Symbol key: K = kaolinite ; Q = quartz ; A = anatase ; C = calcite ; L = lime

Figure 3-5 shows the normalized kaolinite content for blended materials with 0, 2 and 8% initial limestone contents calcined for 20 (Figure 3-5a) and 60 (Figure 3-5b) min versus calcination temperature. For 20 min residence time materials, the effect of limestone on the amount of calcined kaolinite content is detected at

700ºC and 800ºC, in comparison to the behavior of the 0% limestone clay. Extending the residence time to 60 min leads to an increased amount of calcined kaolinite. 700ºC and 800ºC for 60 min calcination conditions shows complete dehydroxylation of kaolinite.

a)

b)
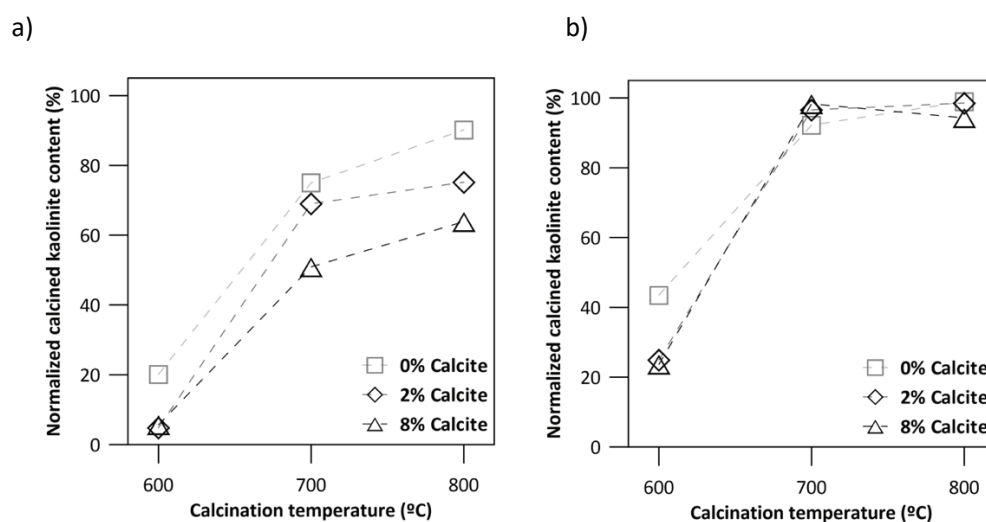
Figure 3-5: Normalized calcined kaolinite content versus calcination temperature a) materials calcined for 20 min and b) materials calcined for 60 min.

The total heat release per gram of solids obtained from the R^3 test for the samples in the first stage are shown in Figure 6a and 6b for 24 and 72 h heat release, respectively. Contour plots obtained from the regression of the experimental results are also included, corresponding to 2 and 8% limestone content clays calcined for 60 min. At 24 h (Figure 3-6a), materials calcined at 800ºC exhibit similar reactivity compared to those calcined at 700ºC. At 72 h (Figure 3-6b), there is a bigger difference between the 2 and 8% limestone materials at 800°C, as also shown by the contour plots of the response surface. These indicate that at 72 h, the heat release in the R^3 test of the high limestone content (8%) clays is slightly lower than that for the low limestone content (2%).

According to the CCD, Table 3-3 shows the regression coefficients for the effect of the different factors on kaolinite content, specific surface area and heat output, along with their respective p-values. P-values < 0.05 are statistically significant at a 95% confidence level and are indicated in bold. The maximum calcination temperature (X_1) is the dominating factor for all characteristics. Limestone content has a significant effect on specific surface area and heat release at 72 h (Figure 3 and 6b), but not on the normalized calcined kaolinite content. Residence time also appears to be a relevant factor for the kaolinite content and the heat release, but not specific surface area. The coefficients presented in Table 3 allow the reconstruction of the response surface for any given set of factor levels within the explored experimental region.

a)

b)
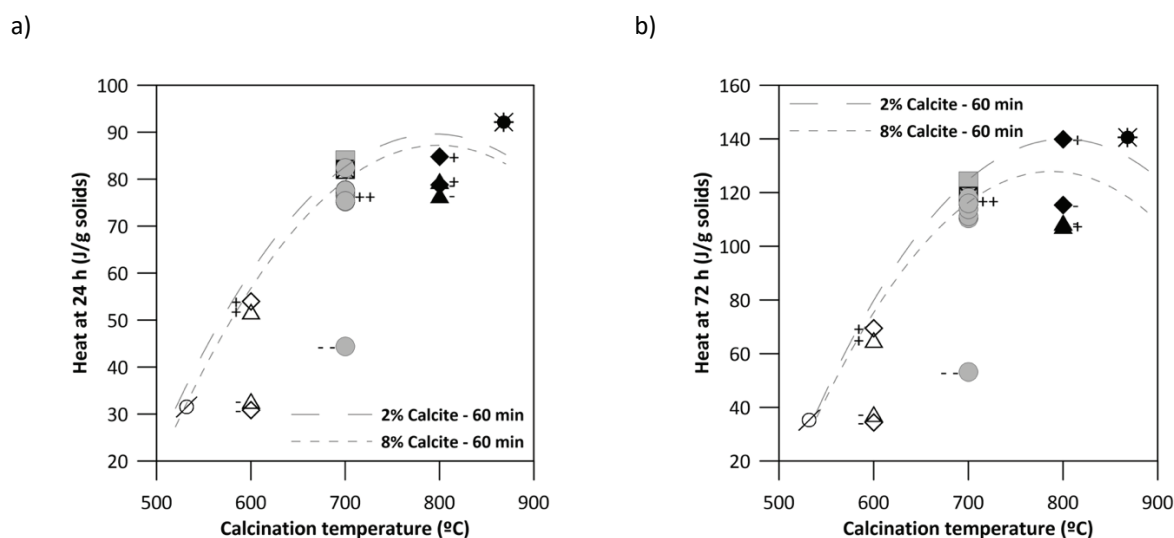
Figure 3-6: Total heat released at a) 24 h and b) 72 h, per gram of solids versus calcination temperature for materials considered in the CCD experimental design.

Table 3-3: Regression coefficients and p-values for the experimental responses analysed. Significant effects (p-value < 0.05) are shown in bold.

Factor	N. Cal. Kaolinite		SSA		Heat 24 h		Heat 72 h	
	effect (%)	p-value	effect (m^2/g)	p-value	effect (J/g)	p-value	effect (J/g)	p-value
X_0: constant	**70.08**	**0.0000**	**8.56**	**0.0000**	**78.33**	**0.0000**	**116.84**	**0.0000**
First order:								
X_1: m_temp	**30.28**	**0.0000**	**-0.42**	**0.0000**	**18.05**	**0.0000**	**31.42**	**0.0000**
X_2: ls_cont	-3.48	0.1139	**-0.15**	**0.0194**	-1.80	0.1129	**-5.37**	**0.0253**
X_3: r_time	**14.15**	**0.0000**	-0.09	0.1093	**7.58**	**0.0000**	**12.73**	**0.0000**
Interactions:								
$X_1 \cdot X_2$	-1.35	0.5829	0.04	0.5873	0.28	0.8267	-1.94	0.4561
$X_1 \cdot X_3$	-1.16	0.7004	0.00	0.9990	-3.11	0.0550	-3.29	0.3071
$X_2 \cdot X_3$	2.86	0.1805	-0.12	0.0993	0.33	0.7577	1.18	0.5965
Second order:								
$X_1 \cdot X_1$	**-11.28**	**0.0001**	**-0.19**	**0.0043**	**-7.73**	**0.0000**	**-14.87**	**0.0000**
$X_2 \cdot X_2$	3.66	0.0728	**-0.15**	**0.0155**	1.75	0.0944	2.35	0.2648
$X_3 \cdot X_3$	**-8.63**	**0.0027**	-0.04	0.4261	**-6.47**	**0.0000**	**-11.36**	**0.0004**

3.3.2 Interaction of calcite and kaolinite during calcination

As previously shown, the amount of calcium in the crystalline phases detected by XRD does not balance the initial calcium content from limestone addition. However, calcium could be included in an amorphous phase that is not detected by XRD. As the formation of metakaolinite dominates the characteristic amorphous hump of the calcined clay patterns, it is not possible to observe the possible appearance of minor amounts of other amorphous phases.

An amorphous form of calcium carbonate has been reported in the literature [22]. To explore the possibility that such phase is forming when the calcite decomposes, FTIR measurements were made of the raw materials and some calcined clays with CaO unaccounted for after calcination. These are shown in Figure 3-7. Calcite

gives two peaks at 710 and 870 cm^{-1}, corresponding to symmetric in-plane bending and asymmetric out of plane bending of CO$_3$ groups, respectively. The broad band at 1395 cm^{-1} is assigned to the asymmetric stretching of CO$_3$, while the small peak at 1795 cm^{-1} is attributed to symmetric CO$_3$ deformation and stretching [23]. In the raw clay spectra, peaks at 750 and 790 cm^{-1} are attributed to kaolinite lattice vibration, which disappear upon dehydroxylation [12,24]. The band around 910 cm^{-1} is assigned to OH$^-$ bending vibrations, while the peak at 1000 cm^{-1} is attributed to Si–O stretching vibrations of kaolinite, which broadens as the structure is distorted upon dehydroxylation [12,25]. The peak at 1115 cm^{-1} is assigned to vibration of O^{-2} atoms perpendicular to the kaolinite layers, and is also affected by stacking defects that may be introduced upon calcination of the clay [26]. The peak at 3615 cm^{-1} is assigned to inner hydroxyl groups situated at the interface of Si tetrahedral and Al octahedral layers, while the ones at 3650 and 3680 cm^{-1} are related to OH$^-$ stretching vibrations of hydroxyl groups situated at the basal surface of the Al layer of kaolinite [12]. The latter peaks are expected to disappear when dehydroxylation is complete, as they are related to the water molecules in kaolinite.

The spectra of 0% calcite material calcined at 800ºC for 60 minutes is included to give a reference for the signals from a fully dehydroxylated uncontaminated clay. The band at 1000 cm^{-1} associated to Si–O stretching vibrations of kaolinite broadens significantly as expected, and shifts to higher wavenumbers. The peaks associated with hydroxyl stretching at 3615, 3650 and 3680 cm^{-1} completely disappear. For the clay with 8% calcite addition, calcined at 800ºC for 20 min, the signals associated with hydroxyl stretching are still visible, indicating an incomplete dehydroxylation in this case. The asymmetric stretching of CO$_3$ peak at 1395 cm^{-1} is visible, suggesting the presence of remaining calcite in the calcined clay, in agreement with XRD results. Similarly, materials with 2 and 8% initial limestone contents calcined at 800ºC for 60 minutes appear both to be completely dehydroxylated. In these materials, the peak associated with calcite is barely visible. However, the characteristic peak associated with free lime around 3650 cm^{-1} is not detected in these materials, further supporting the hypothesis of the formation of a different phase upon calcination. Nevertheless, this phase does not correspond to amorphous calcium carbonate, as the peak at 870 cm^{-1} should remain visible in this case [22].
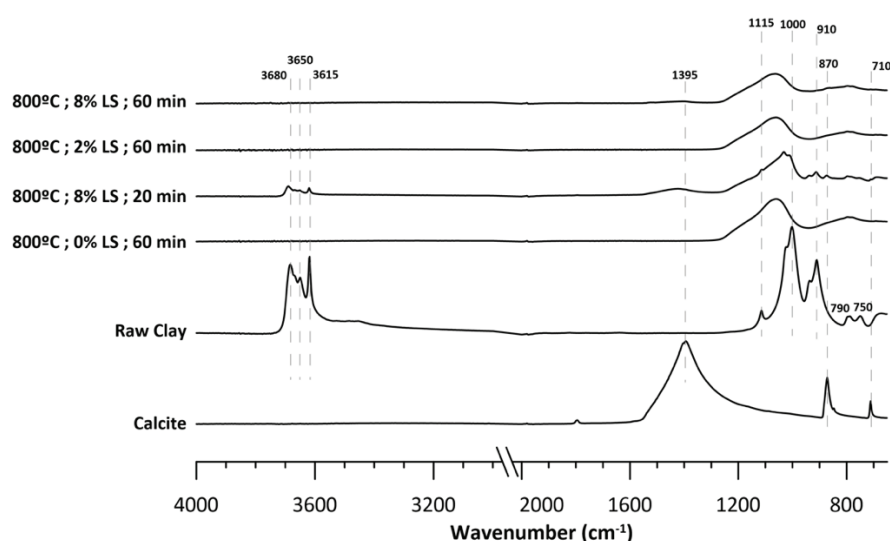
Figure 3-7: FTIR spectra of raw materials and calcined clays calcined at 800ºC with different amounts of calcite (LS).

Figure 3-8a shows a micrograph of clay mineral particles (kaolinite) contained in the raw clay. They exhibit a layered structure, with single layer thickness ranging from 30 to 50 nm.

a)

b)
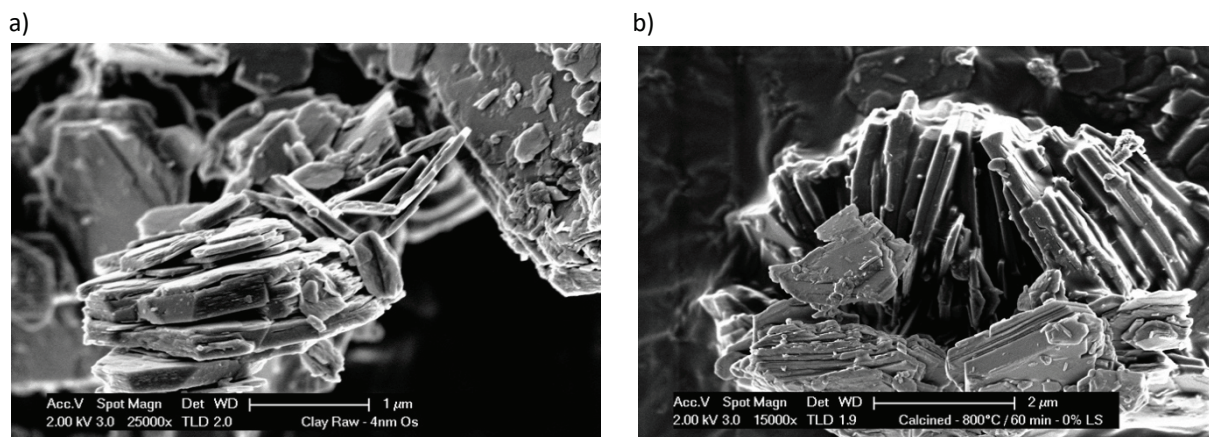
Figure 3-8: High resolution SEM micrographs of kaolinite in raw clay (a) and metakaolinite in calcined clay (b) mounted on carbon film and coated with 4 nm OsO_4.

Figure 3-8b shows a micrograph of a metakaolinite particle in calcined clay with no initial calcite addition, calcined at 800ºC for 60 min. TGA measurements confirmed complete dehydroxylation of this clay. Interestingly, the layered structure of kaolinite is persistent after complete dehydroxylation and transition into metakaolinite. The thickness of the layers remains in the same range as the ones measured for the raw clay, between 30 to 50 nm.

Figure 3-9a shows a metakaolinite particle in the material with 8% initial calcite addition and calcined at 800ºC for 60 min. While the layered structure of metakaolinite is still visible to some extent, part of the surface is covered with a granular deposit not observed in the raw materials. It consists of particles around 50 to 100 nm in size, which is a completely different size as compared to the original limestone (Figure 3-1). To study the possibility of an artefact due to sample preparation (artificial blending of raw clay and limestone powders before calcination), a raw clay naturally intermixed with calcite from the field with approximately 10% calcite (as measured by TGA) was calcined in the same conditions described above and prepared for high resolution SEM observation (Figure 3-9b). As the same morphological features were observed, the mechanism seems to be representative of the case of raw clays with limestone impurities found in quarries.

The size of the granular deposits partially covering clay particles makes EDS analysis in the SEM unsuitable for a detailed assessment due to effects of interaction volume. Therefore, a sample of the 8% calcite material calcined for 60 minutes was prepared for TEM observation.

a)

b)
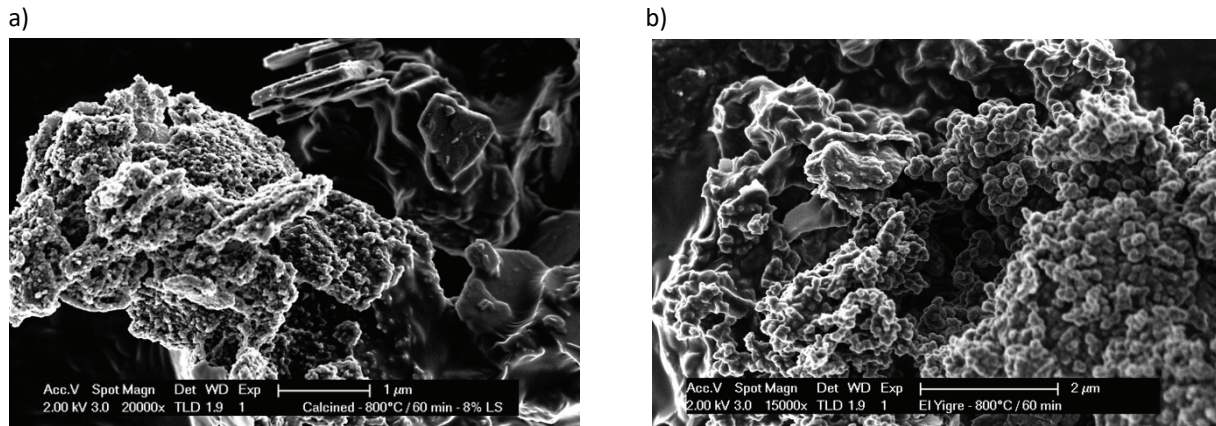
Figure 3-9: High resolution SEM micrographs of a metakaolinite particle in the material with 8% calcite addition (a) and metakaolinite particle from raw clay with approximately 10% calcite (b).

Figure 3-10a shows a HAADF image of a group of metakaolinite particles in the prepared lamella, Figure 3-10b shows the EDS map distribution of Al, Si and Ca over the same area. The calcium rich areas (1, 2 and 3 in Figure 3-10a) were analysed by EDS as well as a reference metakaolinite particle (Al/Si ratio of 1.0, corresponding to section 4 in Figure 3-10a). A summary of the values measured for Ca, Si and Al as well as computed Al/Si and Ca/Si ratios for measuring sections 1 to 4 shown in Figure 3-10 are presented in Table 3-4.

Calcium (white) is located in some of the areas containing metakaolinite particles, in general agreement with the SEM observations, where the metakaolinite particles were observed as not fully covered by the deposit (Figure 3-9). The advantage of STEM-EDS analysis is that the volume of interaction effect is restricted to the beam size and the thickness of the lamella (100-150 nm). The results show that while different amounts of calcium were detected in the different areas (between 20 to 30 at. %), the Al/Si ratio is different from 1.0 (value expected and measured for pure metakaolinite in section 4), ranging from 0.74 to 0.88 in sections 1 to 3. If the areas were solely an intermix of a free lime deposit and metakaolinite, the Al/Si should have remained equal to 1. However, results suggest that a new phase is forming, probably as an amorphous transition state between the free lime and metakaolinite and the crystalline phases expected at higher temperatures such as wollastonite, anhortite and gehlenite. The Ca/Si ratio measured ranged from 0.86 to 1.65.

a)

b)
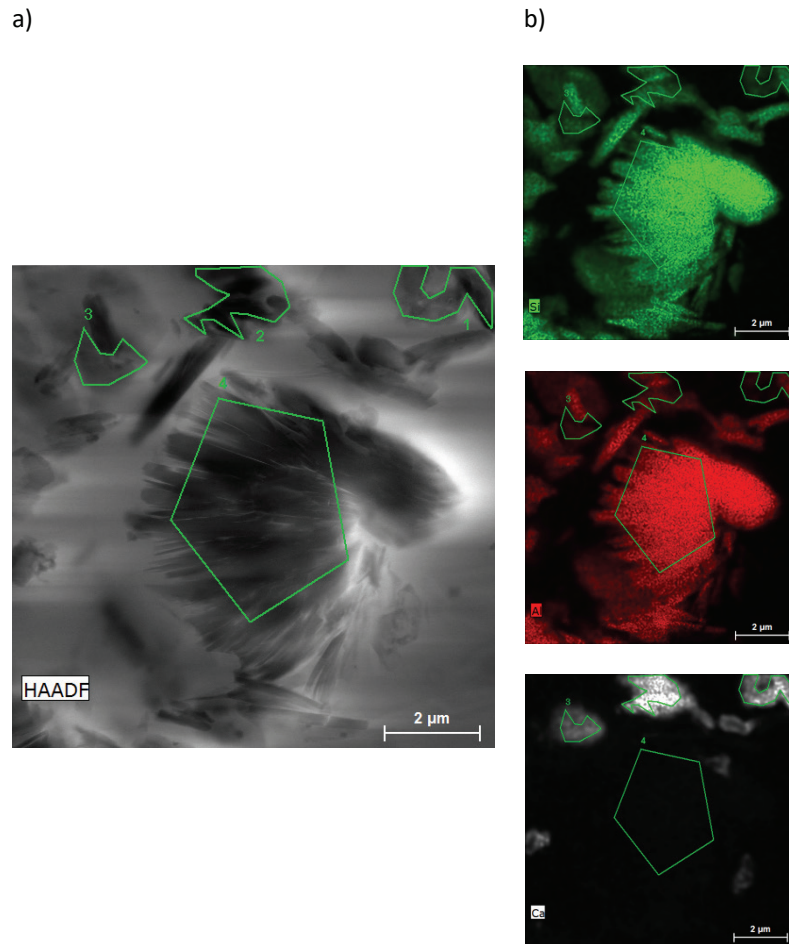
Figure 3-10: HAADF TEM micrographs of calcined clay particles with 8% calcite addition (a) and EDS map showing the distribution of silicon (green), aluminium (red) and calcium (white) (b).

Table 3-4: Summary of values measured by STEM-EDS over the observed Ca-rich phase and a clear metakaolinite particle.

Section Nº	1	2	3	4
	Ca-rich phase over MK particles			MK particle
Ca (% at.)	30.842 ± 1.932	23.393 ± 1.626	21.432 ± 1.526	0.167 ± 0.004
Si (% at.)	18.644 ± 0.402	17.951 ± 0.489	25.055 ± 0.807	30.091 ± 0.182
Al (%. at.)	16.413 ± 1.091	13.422 ± 1.005	18.775 ± 1.400	31.965 ± 1.966
Al/Si	0.88	0.75	0.74	1.06
Ca/Si	1.65	1.30	0.86	<0.01

The TEM and FTIR results show that the calcium oxide from the calcite decomposition interacts with kaolinite forming a calcium-rich phase which covers metakaolinite particles as a granular shaped deposit. This compound covers the metakaolinite particles reducing the specific surface area, but without major influence on the normalized kaolinite content of the calcined clay.

3.4   Conclusions

This study explored the effect of calcite impurities in kaolinitic clays on reactivity after calcination. Based on the results presented in this study, the following conclusions can be drawn:

1. Calcite impurities reduce the specific surface area of calcined clay as compared to clays without calcite, which explains most of the measured reduction in reactivity in the samples with calcite impurities. The decrease in specific surface area is beyond the expected reduction by the blending of limestone and the raw clay. This effect is amplified with the increase of calcination temperature, residence time and initial calcite content.

2. At calcination temperatures beyond the decarbonation threshold of calcite, a reduction in the calcite content in the calcined clay is seen compared to the uncalcined material, but this reduction does not correspond to the formation of crystalline free lime or amorphous calcium carbonate. High resolution SEM images showed a granular deposit partially covering the surface of metakaolinite particles. EDS analysis suggests that this deposit is composed of a calcium rich phase. TEM analysis showed that this deposit corresponds to a new phase formed from the interaction between calcite and kaolinite particles. This phase forms below the recrystallization temperature required to form the phases previously reported in the calcite-kaolinite system.

3. Reducing the maximum temperature to 700ºC and increasing the residence time to at least 60 min allows a significant reduction of the impact of calcite on specific surface area, while allowing a virtually complete dehydroxylation of kaolinite for the studied clay. The reduction on reactivity is minor if the dilution effect is accounted for.

Therefore, and within the experimental limits of this study, clays with calcite content up to 10% are suitable for use as SCM in cement-based materials.

3.5   References

[1]   B. Lothenbach, K. Scrivener, R.D. Hooton, Supplementary cementitious materials, Cem. Concr. Res. 41 (2011) 1244–1256. doi:10.1016/j.cemconres.2010.12.001.

[2]   P. Mehta, P. Monteiro, Concrete: Microstructure, Properties, and Materials, 3rd ed., McGraw-Hill Professional, New York, 2005.

[3]   F. Zunino, M. Lopez, A methodology for assessing the chemical and physical potential of industrially sourced rice husk ash on strength development and early-age hydration of cement paste, Constr. Build. Mater. 149 (2017) 869–881.

[4]   D.P. Bentz, C.F. Ferraris, S.Z. Jones, D. Lootens, F. Zunino, Limestone and Silica Powder Replacements for Cement: Early-Age Performance, Cem. Concr. Compos. 78 (2017) 43–56. doi:10.1016/j.cemconcomp.2017.01.001.

[5]   R. Siddique, Waste Materials and By-Products in Concrete, Springer, Berlin, 2008.

[6]   R. Fernandez Lopez, Calcined Clayey Soils as a Potential Replacement for Cement in Developing Countries, École Polytechnique Fédérale de Lausanne, 2009. doi:10.5075/epfl-thesis-4302.

[7]   A. Tironi, M. a. Trezza, A.N. Scian, E.F. Irassar, Assessment of pozzolanic activity of different calcined clays, Cem. Concr. Compos. 37 (2013) 319–327. doi:10.1016/j.cemconcomp.2013.01.002.

[8]   B. Sabir, S. Wild, J. Bai, Metakaolin and calcined clays as pozzolans for concrete: A review, Cem. Concr. Compos. 23 (2001) 441–454. doi:10.1016/S0958-9465(00)00092-5.

[9]   R. Fernandez, F. Martirena, K.L. Scrivener, The origin of the pozzolanic activity of calcined clay minerals: A comparison between kaolinite, illite and montmorillonite, Cem. Concr. Res. 41 (2011) 113–122. doi:10.1016/j.cemconres.2010.09.013.

[10]   M. Antoni, Investigation of cement substitution by combined addition of calcined clays and limestone, École Polytechnique Fédérale de Lausanne, 2011.

[11]   A. Alujas, R. Fernández, R. Quintana, K.L. Scrivener, F. Martirena, Pozzolanic reactivity of low grade kaolinitic clays: Influence of calcination temperature and impact of calcination products on OPC hydration, Appl. Clay Sci. 108 (2015) 94–101. doi:10.1016/j.clay.2015.01.028.

[12]   A. Souri, H. Kazemi-Kamyab, R. Snellings, R. Naghizadeh, F. Golestani-Fard, K. Scrivener, Pozzolanic activity of mechanochemically and thermally activated kaolins in cement, Cem. Concr. Res. 77 (2015) 47–59. doi:10.1016/j.cemconres.2015.04.017.

[13]   F. Avet, R. Snellings, A. Alujas Diaz, M. Ben Haha, K. Scrivener, Development of a new rapid, relevant and reliable (R3) test method to evaluate the pozzolanic reactivity of calcined kaolinitic clays, Cem. Concr. Res. 85 (2016) 1–11. doi:10.1016/j.cemconres.2016.02.015.

[14]   K. Traoré, T.S. Kabré, P. Blanchart, Gehlenite and anorthite crystallisation from kaolinite and calcite mix, Ceram. Int. 29 (2003) 377–383. doi:10.1016/S0272-8842(02)00148-7.

[15]   H. El-Didamony, K.A. Khalil, M.S. El-Attar, Physicochemical characteristics of fired clay-limestone mixes, Cem. Concr. Res. 30 (2000) 7–11. doi:10.1016/S0008-8846(99)00181-7.

[16]   I. Allegretta, D. Pinto, G. Eramo, Effects of grain size on the reactivity of limestone temper in a kaolinitic clay, Appl. Clay Sci. 126 (2016) 223–234. doi:10.1016/j.clay.2016.03.020.

[17]   R. Snellings, Ö. Cizer, L. Horckmans, P.T. Durdziński, P. Dierckx, P. Nielsen, et al., Properties and pozzolanic reactivity of flash calcined dredging sediments, Appl. Clay Sci. 129 (2016) 35–39. doi:10.1016/j.clay.2016.04.019.

[18]   S. Hollanders, Mineralogical study of the pozzolanic properties of calcined clays, KU Leuven, 2017. https://limo.libis.be/primo-explore/fulldisplay?docid=LIRIAS1727587&context=L&vid=Lirias&search_scope=Lirias&tab=default_tab&lang=en_US&fromSitemap=1.

[19]   M. Antoni, J. Rossen, F. Martirena, K. Scrivener, Cement substitution by a combination of metakaolin and limestone, Cem. Concr. Res. 42 (2012) 1579–1589. doi:10.1016/j.cemconres.2012.09.006.

[20]   G.E.P. Box, K.B. Wilson, On the experimental attainment of optimum conditions, J. R. Stat. Soc. Ser. B (Statistica Methodol. 13 (1951) 1–45.

[21]   K. Scrivener, R. Snellings, B. Lothenbach, A Practical Guide to Microstructural Analysis of Cementitious Materials, (2016) 540. doi:10.7693/wl20150205.

[22]   F. Andersen, L. Brecevic, Infrared spectra of amorphous and crystalline calcium carbonate, Acta Chem. Scand. 45 (1991) 1018–1024.

[23]   S. Gunasekaran, G. Anbalagan, S. Pandi, Raman and infrared spectra of carbonates of calcite structure, J. Raman Spectrosc. 37 (2006) 892–899. doi:10.1002/jrs.1518.

[24]   E. Mako, R.L. Frost, J. Kristof, E. Horvath, The Effect of Quartz Content on the Mechanochemical Activation of Kaolinite, J. Colloid Interface Sci. 244 (2001) 359–364. doi:10.1006/jcis.2001.7953.

[25]   J.G. Miller, T.D. Oulton, Prototropy in kaolinite during percussive grinding, Clays Clay Miner. 18 (1970) 313–323.

[26]   E.F. Aglietti, J.M. Porto Lopez, E. Pereira, Mechanochemical effects in kaolinite grinding. II. Structural aspects, Int. J. Miner. Process. 16 (1986) 135–146. doi:10.1016/0301-7516(86)90080-3.

Chapter 4   Particle classification of ground calcined clay

Note: This chapter is based on an article published in a peer reviewed journal.

Franco Zunino, Karen Scrivener

Contribution of the doctoral candidate: Writing of the first manuscript draft, experimental design, conduction of the experiments and supervision of semester project, reply to reviewers.

The adoption of blended cements to reduce the carbon footprint has increased significantly over the last decades. Clays containing kaolinite are a promising choice due to their widespread availability. Kaolinite content is the major factor controlling the performance of blended cements incorporating calcined clay, for example in LC^3-50 (50% clinker, 30% calcined clay, 15% limestone and 5% gypsum) clays with a kaolinite above about 40% are needed to achieve similar strength to reference OPCs at 7 days. Materials with low contents of kaolinite are often considered unsuitable. This study compares two fractionation techniques to increase the kaolinite content of a low-grade clay (30% kaolinite content). The results show that kaolinite remains concentrated in the fine particles after grinding. Both wet sedimentation and air separation were effective to increase the reactivity of the material as a combined result of increased fineness and kaolinite content. For the air separation process, it was observed that a significant amount of kaolinite remained in the rejected fraction after processing due to agglomeration of the powder. It was shown that the use of grinding aids before the separation process can further improve the results.

Contents

4.1 Introduction

The increasing concern about global warming has led to an increasing use of supplementary cementitious materials (SCMs) in the cement industry [1]. Thus, blended cements made up of clinker and SCMs are now more common than pure OPC. Among the different SCMs available, calcined clays are especially relevant as they are available in the quantities required in comparison with the worldwide cement demand [2].

Limestone calcined clay cements (LC^3) is a blended cement system combining calcined kaolin (metakaolinite) and limestone along with clinker and gypsum [3]. LC^3 offers equivalent mechanical properties as compared to Portland cement, while enhancing other aspects such as durability and decreasing the carbon footprint of concrete by at least 30% as compared to normal cement [4].

Previous studies have shown that the amount of kaolinite in the calcined clay fraction is the major factor controlling the strength of LC^3 cements. Furthermore, it has been established that about 40% of kaolinite content is required in order to achieve the same performance as normal Portland cement at 7 days [5]. In some regions, the amount of kaolinite in the clays available is generally lower and occur intermixed with other less reactive 2:1 clay (such as montmorillonite and illite) and associated minerals [6]. Therefore, their potential suitability for use in high performance blended cements is compromised.

Ground clays exhibit a characteristic bimodal particle size distribution [3,4]. This could be explained by the higher grindability of clay minerals in contrast to common associated minerals found in raw clays such as quartz, feldspars, carbonates and iron (hydr)oxides [7,8].

Fractionation techniques have been widely used for purification of clay minerals, either targeted for an application or for the analysis of the clay minerals, as some associated minerals can interfere with identification [9,10]. A common approach is fractionation by sedimentation, where the associated minerals are removed due to their difference in particle size with the clay minerals of interest. Chemical treatments can also be used to further remove these impurities. These techniques are effective, but complex and usually lack potential to be upscaled to an industrial level.

This study compares the wet sedimentation process with air classification as means to increase the reactivity of a low kaolinite content raw clay. The air classifier used was a laboratory instrument, but works in the same way as industrial classifications cyclones, which are widely available in the cement industry.

4.2 Materials and methods

4.2.1 Raw materials and characterization techniques

A kaolinitic clay from Chile was selected for this study. The material was dried at 105°C for 48 h and ground in a rotary ball mill with 20 L capacity during 2 h. The raw clay had a kaolinite content of 30% by mass as measured by thermogravimetric analysis (TGA). The TGA measurements were conducted in a Mettler Toledo TGA analyzer, between 30 and 1000°C with a heating ramp of 10°C/min. The atmosphere used was N2 at a flow rate of 30 mL/min. The raw clay also contains small amounts of 2:1 clay minerals such as illite, muscovite and montmorillonite, and therefore the tangent method was used to decouple the mass loss associated with

the dehydroxylation of kaolinite [4]. The oxide composition of the clay was determined by X-ray fluorescence (XRF), and it is shown in Table 4-1.

Table 4-1: Chemical composition of the clay used as measured by XRF.

	Kaolinitic Clay
SiO_2	63.66
Al_2O_3	24.16
Fe_2O_3	4.05
CaO	0.13
Na_2O	0.61
K_2O	2.51
TiO_2	0.72
MgO	0.49
P_2O_5	0.40
SO_3	1.31
LOI	1.75

The mineralogical composition was assessed by X-ray diffraction (XRD). Measurements were conducted on back loaded powder holders to reduce the effects of preferred orientation. The samples were measured in Bragg–Brentano mode using a X'Pert PANalytical diffractometer with CuKα source operated at 45 kV and 40 mA. Samples were scanned from 7 to 70 degrees 2θ with a step size of 0.0167 2θ using a X'Celerator detector, resulting in an equivalent time per step of 60 s. The associated minerals found in the kaolinitic clay were mainly quartz and small amounts of cristobalite and calcite. The XRD pattern of the raw clay used is shown in Figure 4-1.
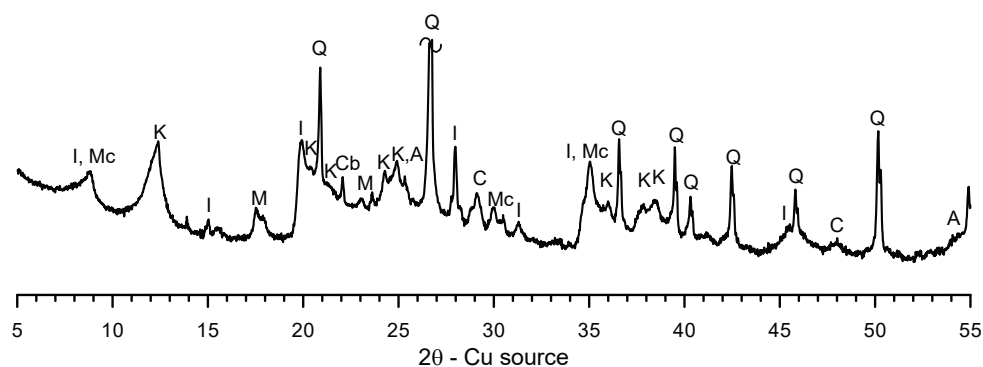
Figure 4-1: XRD pattern of natural clay used in this study, with main peaks identified.

(I: illite; Mc: muscovite; K: kaolinite; M: montmorillonite; Q: quartz; Cb: cristobalite; A: anatase; C: calcite).

The particle size distribution (PSD) was determined by laser diffraction using a Malvern S apparatus. First, a dispersion of the clay to be measured was prepared by combining approximately 0.1 g of material in 50 mL of a 0.01% solution of sodium hexametaphosphate, meant to deagglomerate and disperse kaolinite particles [11]. The suspension was placed in an ultrasonic probe for 15 minutes while stirring at the same time. Afterwards, drops of the suspension were transferred to the measuring unit filled with distilled water, until the

desired level of obscuration was reached. The optical model was set as prescribed in [12]. The PSD of the kaolinitic clay used is shown in Figure 4-2.
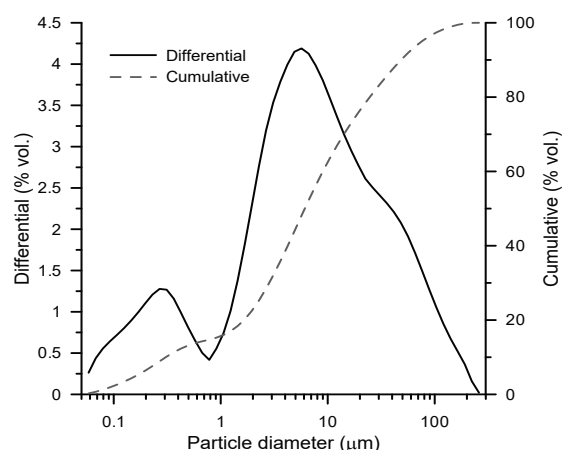
Figure 4-2: Particle size distribution of the raw clay used in this study, measured by laser diffraction.

The specific surface area (SSA) of the materials was determined by gas adsorption using the Brunauer-Emmett-Teller (BET) equation, with a Micromeritics TriStar II analyzer. Nitrogen (N_2) was used as analysis adsorptive gas. Samples of approximately 1 g of powder material were introduced in analysis tubes and degassed for 2 h at 200°C under N_2 flow. Subsequently, they were immersed in a liquid nitrogen bath (77.3 K) where the measurements were done. Five measurements at different relative pressures were collected and used to calculate the specific surface area of the material.

The clay fractions obtained after applying the separation techniques were calcined in a laboratory furnace at 800°C for 60 minutes. This set of parameters allows a complete dehydroxylation of kaolinite, while preventing the recrystallization of other high temperature minerals [13].

Isothermal calorimetry was used to assess the pozzolanic reactivity of the original calcined clay and also the materials obtained after fractionation. For this purpose, the R^3 test [14] was selected. In this procedure, calcined clay is mixed with portlandite, calcium carbonate, potassium sulphate, potassium hydroxide and water at 40°C, and put into glass ampoules inside the calorimeter at 40°C. The total heat evolved after 24 h is taken as a measure of the reactivity of the clays and shows good correlation with compressive strength results obtained on blended cement-mortar bars.

4.2.1   Particle classification techniques

In this study, accelerated sedimentation by centrifugation was used and compared with a lab-scale air classifier, which emulates the fractionation device (cyclone) found in any grinding unit of current cement plants. A suspension of raw clay and a sodium hexametaphosphate 0.1% solution was placed in a 50 mL centrifuge

tube in a mass ratio of 1:6. The tubes were homogenized for 15 min in a tube shaker. Afterwards, they were centrifuged at 1000 rpm in a programmable laboratory centrifuge for a period of time given by Eq. 1 [10],

$$T = \frac{\eta \cdot log\left(\frac{R_2}{R_1}\right)}{3.81 \cdot r^2 \cdot N^2 \cdot (\rho - \rho_0)} + \frac{2(t_a + t_d)}{3} \qquad (4\text{-}1)$$

Where T is the total time in seconds, t_a and t_d are the acceleration and deceleration times of the centrifuge, η is the viscosity in poises, R_1 and R_2 are the initial and final distance of particle from the axis of rotation, N is the angular velocity in rps, ρ and ρ_0 are the density of the particle and medium in g/cm^3 and r is the radius (in cm) of the smallest particle to be precipitated in a given separation. Based on the particle size distribution shown in Figure 4-2, centrifugations of the raw clay were conducted to obtain cut sizes of 0.8, 2, 5, 11 and 50 μm.

A lab-scale air classifier (Hosokawa Alpine 100 NZR) was used to perform fractionation tests over dry clay samples and compare the results to the ones obtained by centrifugation. First, a calibration curve was constructed to relate the selector speed with the cutting size obtained. The classifier was set at 3500, 6000, 12000, 18000 and 20500 rpm to cover a wide range of separation limits. 500 g of dry and ground clay material were passed through the classifier at each setting, and the fine and coarse (rejected) fractions were collected for analysis.

In the air classification, the impact of different grinding aids on the agglomeration of the clay particles was also investigated. Three different commercial grinding aids were assessed, each of them based on a different molecular type: diethylene glycol (DEG), poly-carboxylate ether (PCE) and triethanolamine (TEA) at the center point (12000 rpm) setting of the experimental design. The dosages used were as recommended by the manufacturer for Portland cement applications, corresponding to 0.15%, 0.45% and 0.07% by weight of material for DEG, PCE and TEA grinding aid respectively. The dosage was not corrected for the higher surface area of clay compared to cement to obtain an idea of performance under equivalent admixture consumption by unit weight of material produced. The grinding aid was sprayed over 500g of ground material in a plastic container, and then it was homogenized in a Turbula blender over 24 h. It was verified that the homogenization process did not modify the PSD of the material.

To compare the air separation process with and without the use of grinding aids (GAs), the partition (Tromp) curve was computed in each case. This allows the relevant parameters that describe the efficiency of the separation process to be obtained, such as the bypass ratio, the cut size (D_{50}), and the separation limit (D_{limit}). The bypass ratio represents the amount of material that inevitably ends up in the rejected fraction, providing an indication of the separation efficiency (the lower the bypass ratio, the higher the efficiency). The presence of bypass is associated with the presence of a superimposed splitting to the actual classification process [15]. The D_{50} represents the size at which the particle has equal probability of ending in the rejects or fine fractions. D_{limit} represents the size below which there is no more selective separation. The sharpness of the cut was computed as the ratio of the sizes at which 25% (D_{25}) and 75% (D_{75}) of the feed reports to the rejected fraction, and the imperfection factor (I) was computed as shown in Eq. 4-2 [16]. The lower the imperfection

factor, the better the separation process. An example of an ideal (sharpness equal to 1 and imperfection factor equal to 0) partition curve and a real one is shown in Figure 4-3.

$$I = \frac{D_{75} - D_{25}}{2 \cdot D_{50}} \tag{4-2}$$
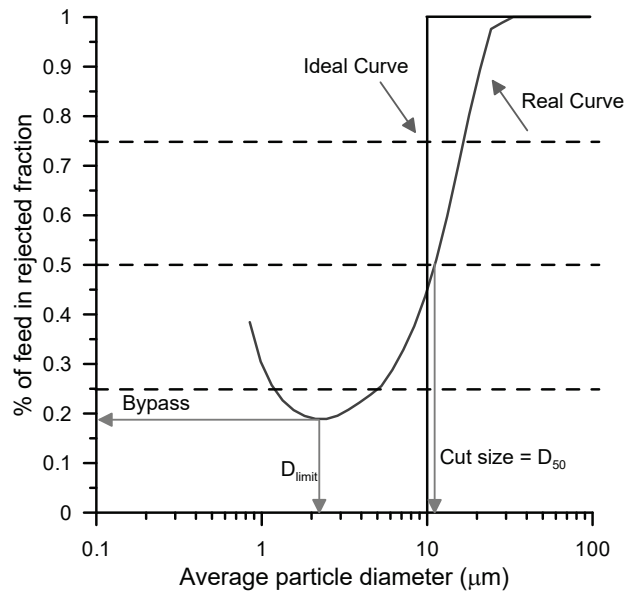
Figure 4-3: Partition (Tromp) curve (ideal and real) example and parameters that can be obtained from it.

4.3 Results and discussion

4.3.1 The relationship between particle size fraction and kaolinite content

Figure 4-4 shows the particle size distribution of the fine fractions obtained by centrifugation. As seen, there is high agreement between the nominal cut values (shown in Figure 4-4 as dashed vertical lines) used to compute the centrifugation times using Eq. 4-1 and the actual distribution sizes.
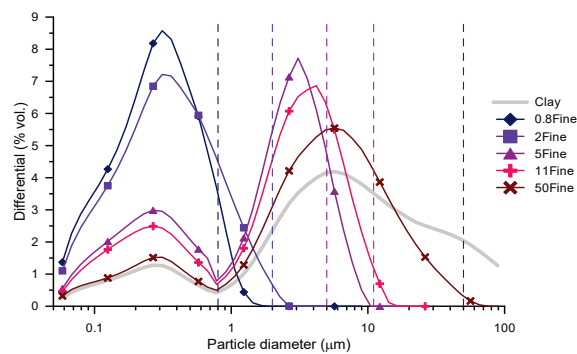
Figure 4-4: Particle size distributions of fine fractions obtained by centrifugation of a raw clay suspension.

Figure 4-5 left shows the kaolinite content measured by TGA plotted over the nominal separation limit, i.e., the kaolinite content of the fraction of particles on the left of each size limit line. As observed, the kaolinite content increases from the 30% measured in the unseparated raw clay to about 60% in the material finer than 0.8 μm. This shows that clay minerals and specifically kaolinite is indeed ground finer and therefore, remains concentrated in the smaller fraction of the size distribution of the raw clay. While there is presence of clay minerals in the coarser fraction, their amount is lower as compared to the finer one.

Figure 4-5 right provides further evidence of this observation, as the main quartz reflection detected by XRD, the main associated mineral found on the raw clay used in this study, is almost negligible in the material with a separation limit of 0.8 μm, and it increases steadily as coarser particles are incorporated to the analysis. Thus, the removal of coarser quartz particles from the fractioned material lead to the increase in the percentage of kaolinite present. It also shows that the separation process could be optimized to obtain intermediate values of kaolinite, by adjusting the amount of associated minerals to be removed, depending on the requirements of reactivity and yield of the process.
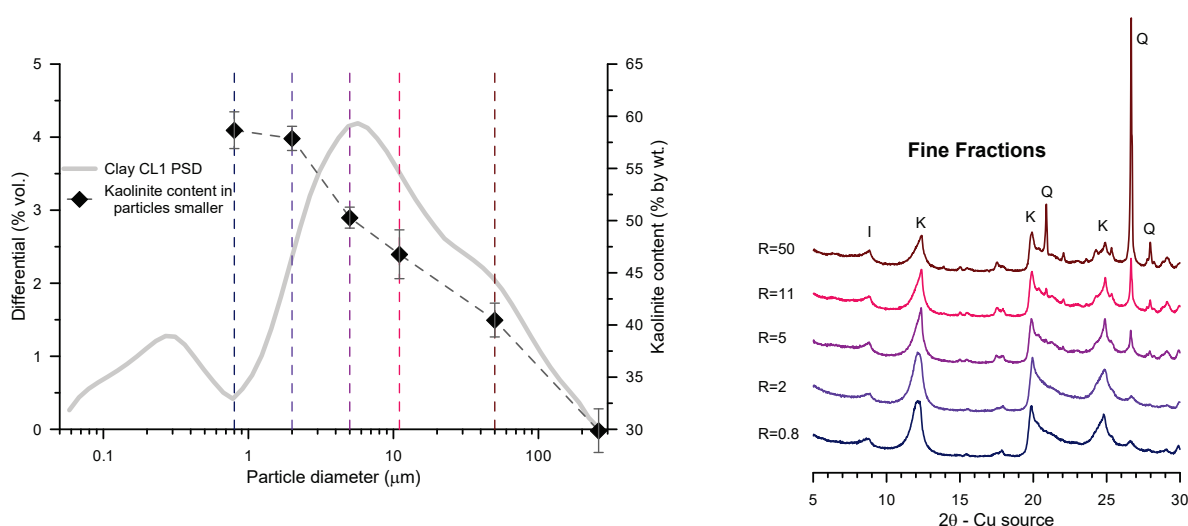
Figure 4-5: Kaolinite content versus separation limit of fine fractions separated by centrifugation (left) and XRD patterns of the corresponding fine fractions (right).

4.3.2   Application of a lab-scale air classifier to increase the kaolinite content

The lab-scale air classifier was applied to the ground raw clay using different speed settings of the selector. The separation diameter, d_S, was defined as the intersection of the differential PSD curve of the fine and rejected (coarse) fractions for each setting of the classifier (see Figure 4-6 left). In this case, it is observed that fine particles from all the range found in the raw clay are present in the rejected fraction, despite of the separation limit established. This is due to the so-called bypass of the air classifier, which is a function of the inherent efficiency of the separator and the degree of agglomeration of the particles. Using these d_S values, a calibration curve (Figure 4-6 right) was obtained. A separation diameter of 30, 12, 9, 4 and 3 μm was found for the classifier settings of 3500, 6000, 12000, 18000 and 20500 rpm respectively.
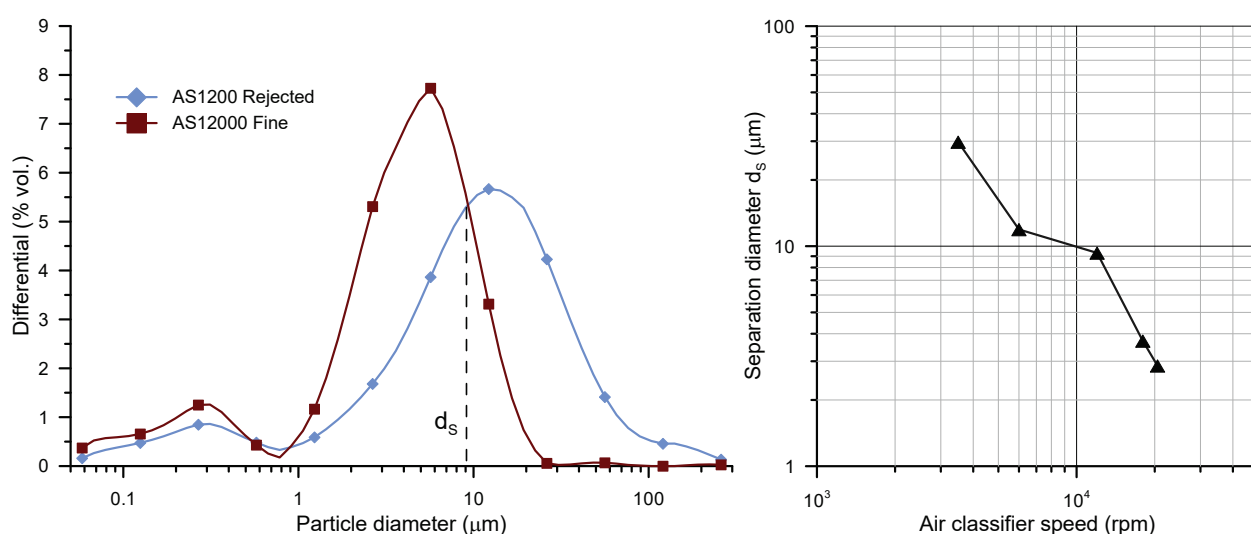
Figure 4-6: Definition of the separation diameter d_S for each setting of the air classifier (left) and calibration curve of d_S versus classifier speed (right).

The yield of the air separation process was monitored through the different air separation runs. In general, the material loss associated with the separation process is around 5%, except for the d_S=9 μm setting (see Figure 4-7 top). The fine fractions obtained for each classifier setting were characterized and the results are shown in Figure 4-7 bottom.

It can be seen that the kaolinite content increases from 37% in the d_S=30 μm setting to 48% in the d_S=3 μm one. Both values are considerably above the original 30% kaolinite of the raw clay processed. The kaolinite content of the rejected fraction increases with the reduction of d_S. As d_S is reduced in the fractionation process more fine particles are included in the rejected fraction, increasing the resulting amount of kaolinite.

In addition, it can be seen that as d_S is reduced, the specific surface area of the fine fraction obtained increases. This is linked to the layered structure of clay mineral particles, which explains their high specific surface area. This is not the case of the associated minerals, which have a small contribution to the total surface area of the raw clay. As the amount of clay minerals increase, so does the specific surface area.
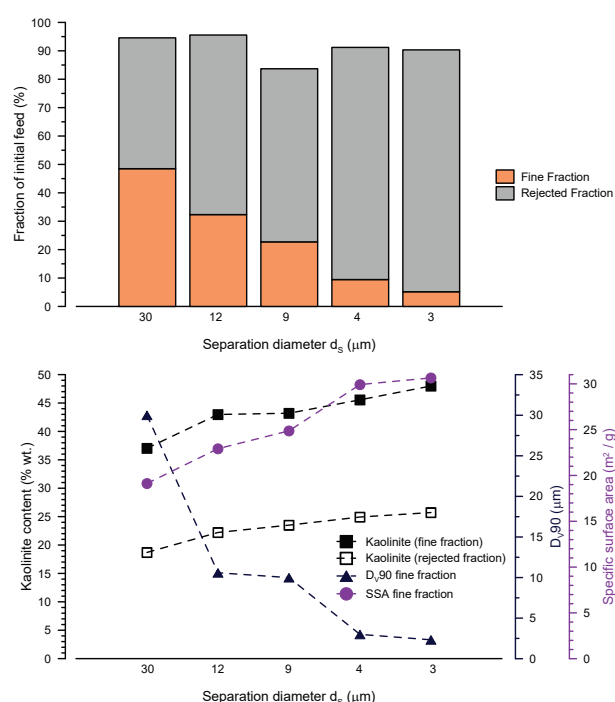
Figure 4-7: Yield of the air separation at different values of dS (top) and characterization of the fine and rejected fractions obtained (bottom).

The fine fractions obtained with the air classifier exhibit higher reactivity than the raw clay measured by the R^3 test, as seen in Figure 4-8 left. The total heat released at 24 h is doubled when comparing the raw clay (67.1 J/g solids) and the fine fraction with d_S=3 μm (139.2 J/g solids). It has been shown that the kaolinite content linearly correlates with the reactivity of calcined clays measured using the R^3 test [14], indicating that the increase in kaolinite from 30 to 48% accounts for a part of the observed reactivity rise, while the rest is associated with the increase of specific surface area (14.1 to 30.7 m^2/g for the raw clay and fine fraction, respectively). Figure 4-8 right shows the reactivity measured for each of the rejected fractions obtained. In accordance with the kaolinite content measurements (see Figure 4-7), the reactivity increases as the separation diameter is reduced. For the smaller value of d_S studied, the reactivity of the rejected fraction is similar to the one measured on the original clay.
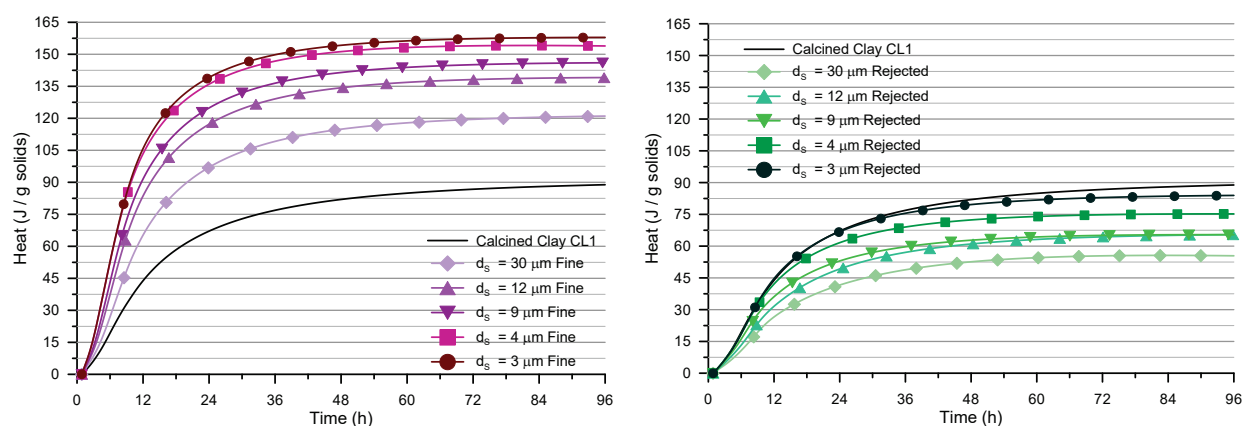
Figure 4-8: Reactivity of fine (left) and rejected (right) fractions obtained by air classification measured using the R^3 calorimetry test.

The analysis of the air classifier experiments showed that it is possible to increase the reactivity of a low grade (low kaolinite content) raw clay with a dry fractionation process. It was also observed that a significant amount of kaolinite remained in the rejected fractions. It is well known that fine kaolinite particles tend to agglomerate to form aggregates [9], and coat other associated minerals present in the raw clay [11].

To assess the possibility of reducing the amount of clay minerals collected in the rejects, the air classification process was repeated over the obtained reject fraction up to 4 times, at d_S=9 μm (12000 rpm) configuration of the classifier. The obtained results are shown in Figure 4-9. The amount of fine material collected increased slightly with each additional processing of the rejected fraction. In addition, the amount of kaolinite in the reject also slightly reduces. In general, it seems that even a high number of repetitions of the process can only slightly improve the efficiency of the separation and kaolinite concentration. This shows that the process is limited by the agglomeration degree of the clay and the efficiency of the classifier itself.
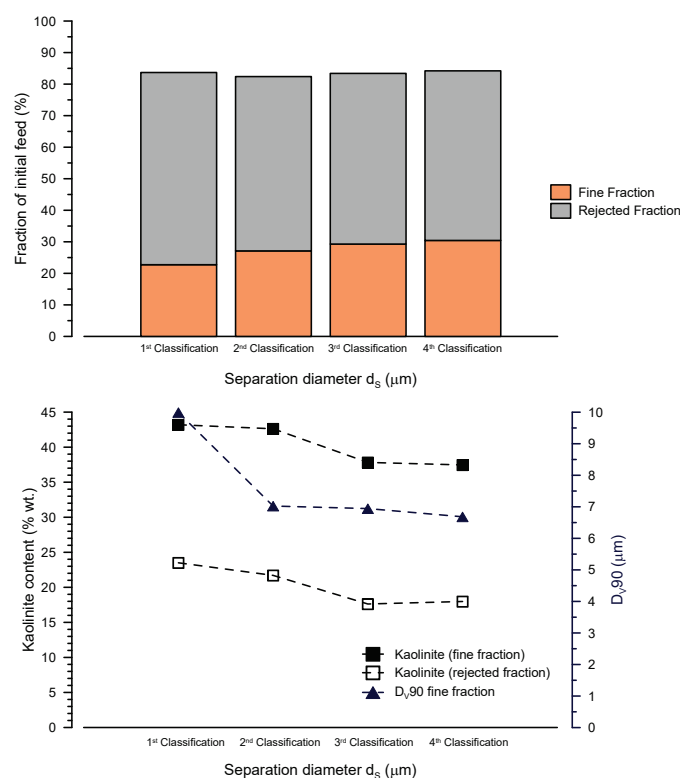
Figure 4-9: Yield of the air separation at d_S 9 μm repeated over the rejected fraction up to 4 times (top) and characterization of the fine and rejected fractions obtained (bottom).

4.3.3 The role of grinding aids on air classifier efficiency

The effect of agglomeration of the clay mineral particles on the efficiency of the separation process was further studied by using grinding aids (GAs). These organic molecules are normally used in the cement production to reduce the energy consumption and increase the yield of the grinding process [17]. They act by adsorption on the particles surface, reducing the surface energy forces.

Figure 4-10 shows the Tromp curves (grade efficiency curves) for the air separation process at dS=9 μm without the use of grinding aids and incorporating different amounts of 3 commercial products based on diethylene glycol (DEG), poly-carboxylate ether (PCE) and triethanolamine (TEA). In all cases, the bypass is reduced to less than half of the value obtained without the use of grinding aids. This provides evidence of the effective reduction in clay mineral aggregate formation, leading to an improved separation and a reduced number of fine particles being classified as rejects. The best result in this matter is obtained with the glycol-based GA. The sharpness of the separation is also increased as compared to the separation without the use of GA (an ideal separator has a sharpness of 1), and the imperfection factor is significantly reduced. The separation parameters computed from the Tromp curves are summarized in Table 4-2.
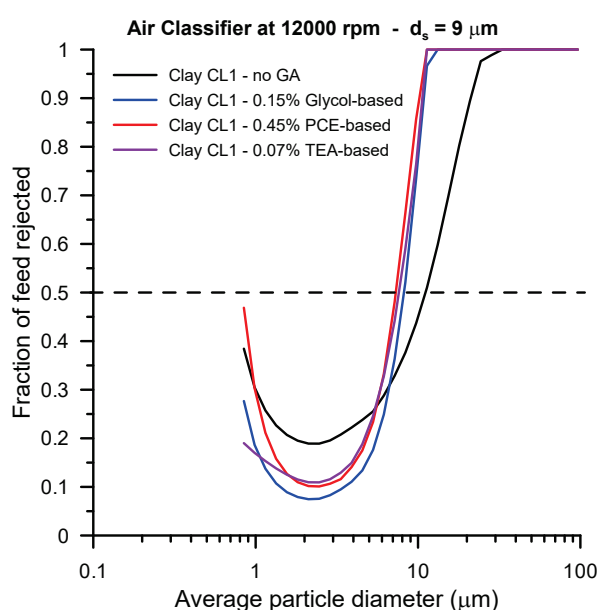
Figure 4-10: Tromp curves (grade efficiency) computed for the control case and for raw clays incorporating different commercial GAs.

Table 4-2: Summary of parameters of the separation process at dS = 9 μm.

Material	D_{Limit} (μm)	Bypass (%)	Sharpness (D_{25}/D_{75})	Imperfection factor $\left(\dfrac{D_{75} - D_{25}}{2 \cdot D_{50}}\right)$
CL1 – no GA	2.5	18.9	0.33	0.47
CL1 – 0.15% Glycol-based GA	2.1	7.5	0.63	0.22
CL1 – 0.45% PCE-based GA	2.5	10.1	0.58	0.26
CL1 – 0.07% TEA-based GA	2.5	10.9	0.54	0.29

Figure 4-11 shows the kaolinite content measured in the fine and rejected fractions in the control (no GA used) and with different molecules used. For the fine fractions, the amount of kaolinite increases, in good

agreement with the reduction in bypass shown by the Tromp curves (see Figure 4-10). Furthermore, a reduction in kaolinite in the rejects is observed. Thus, the use of GA in calcined clay production can bring benefits not only at the scale of grinding, but also if an air separation process is to be implemented to increase the kaolinite content of the final product.
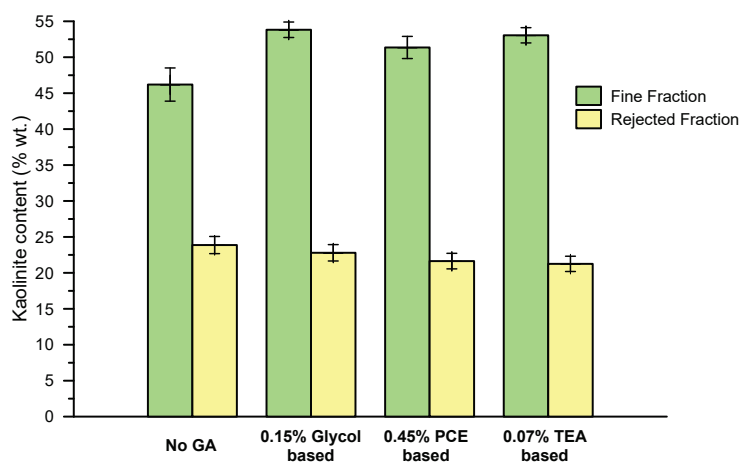
Figure 4-11: Kaolinite content of fine and rejected fraction for materials obtained with and without the incorporation of GA.

4.4   Conclusions

This study showed the feasibility of using a dry particle fractionation technique to increase the kaolinite content of low-grade clays, considerably improving their reactivity as compared to the initial material.

Based on the results presented, the following conclusions can be drawn:

1. Kaolinite in ground clays remains concentrated in the fine fraction of the particle size distribution, due to their higher grindability compared to the common associated minerals found in kaolin.

2. Particle fractionation can be used to increase the kaolinite content of clay and consequently their pozzolanic reactivity. The improvement in reactivity is explained by the increase in kaolinite content and specific surface area of the resulting material. This can make low-grade materials suitable to be used as SCM.

3. The use of grinding aids can significantly improve the efficiency of the particle selection process by reducing the agglomeration of clay minerals in ground clay, leading to a lower bypass of the air classification process and an increased kaolinite content in the fine fraction obtained.

4.5   References

[1]   M. Schneider, M. Romer, M. Tschudin, H. Bolio, Sustainable cement production—present and future, Cem. Concr. Res. 41 (2011) 642–650. doi:10.1016/j.cemconres.2011.03.019.

[2]   K.L. Scrivener, V. John, E.M. Gartner, Eco-efficient cements: potential, economically viable solutions for a low-CO2, cement-based materials industry, in: United Nations Environmental Programme (UNEP), 2016.

[3]   M. Antoni, J. Rossen, F. Martirena, K. Scrivener, Cement substitution by a combination of metakaolin and limestone, Cem. Concr. Res. 42 (2012) 1579–1589. doi:10.1016/j.cemconres.2012.09.006.

[4]   K.L. Scrivener, F. Avet, H. Maraghechi, F. Zunino, J. Ston, A. Favier, et al., Impacting factors and properties of Limestone Calcined Clay Cements (LC3), Green Mater. (2018). doi:https://doi.org/10.1680/jgrma.18.00029.

[5]   F. Avet, K. Scrivener, Investigation of the calcined kaolinite content on the hydration of Limestone Calcined Clay Cement (LC3), Cem. Concr. Res. 107 (2018) 124–135. doi:10.1016/j.cemconres.2018.02.016.

[6]   R. Fernandez, F. Martirena, K.L. Scrivener, The origin of the pozzolanic activity of calcined clay minerals: A comparison between kaolinite, illite and montmorillonite, Cem. Concr. Res. 41 (2011) 113–122. doi:10.1016/j.cemconres.2010.09.013.

[7]   S. Tsivilis, S. Tsimas, A. Moutsatsou, Contribution to the problems arising from the grinding of multicomponent cements, Cem. Concr. Res. 22 (1992) 95–102.

[8]   K. De Weerdt, Separate grinding versus intergrinding, SINTEF Rep. SBF BK A. 7022 (2007).

[9]   F. Bergaya, G. Lagaly, eds., Handbook of clay science, 2nd ed., Elsevier, Oxford, 2013.

[10]   J.C. Hathaway, Procedure for Clay Mineral Analyses used in the sedimentary petrology laboratory of the USGS, US. Geol. Surv. Methods. (1955) 8–13.

[11]   Y. Han, W. Liu, J. Zhou, J. Chen, Interactions between kaolinite Al-OH surface and sodium hexametaphosphate, Appl. Surf. Sci. 387 (2016) 759–765. doi:10.1016/j.apsusc.2016.07.002.

[12]   K. Scrivener, R. Snellings, B. Lothenbach, A practical guide to microstructural analysis of cementitious materials, (2016) 540. doi:10.7693/wl20150205.

[13]   A. Alujas, R. Fernández, R. Quintana, K.L. Scrivener, F. Martirena, Pozzolanic reactivity of low grade kaolinitic clays: Influence of calcination temperature and impact of calcination products on OPC hydration, Appl. Clay Sci. 108 (2015) 94–101. doi:10.1016/j.clay.2015.01.028.

[14]   F. Avet, R. Snellings, A. Alujas Diaz, M. Ben Haha, K. Scrivener, Development of a new rapid, relevant and reliable (R3) test method to evaluate the pozzolanic reactivity of calcined kaolinitic clays, Cem. Concr. Res. 85 (2016) 1–11. doi:10.1016/j.cemconres.2016.02.015.

[15]   A.P. Weber, K. Legenhausen, Characterization of a Classification or Separation Process, in: Ullmann's Encycl. Ind. Chem., American Cancer Society, 2014. doi:10.1002/14356007.b02_02.pub3.

[16]   B.A. Wills, J.A. Finch, Wills' Mineral Processing Technology, 8th ed., Elsevier, Waltham, 2016.

[17]   J.J. Assaad, C.A. Issa, Effect of clinker grinding aids on flow of cement-based materials, Cem. Concr. Res. 63 (2014) 1–11. doi:10.1016/j.cemconres.2014.04.006.

Chapter 5   Grinding aids in LC³ hydration

Note: This chapter is based on an article submitted to a peer reviewed journal.

Submission title: Assessing the effect of alkanolamine grinding aids in limestone calcined clay cements hydration

Franco Zunino, Karen Scrivener

Contribution of the doctoral candidate: Writing of the first manuscript draft, experimental design, conduction of the experiments.

Grinding aids are commonly used in cement manufacture to reduce electrostatic forces between powder particles and reduce agglomeration. Alkanolamines are known to also influence the hydration of the aluminate phases in cement. This study assessed the effect of TEA, TIPA and DEIPA addition on the hydration of LC³ systems. It was observed that these molecules have an enhancing effect on the aluminate reaction in LC³. They promote the hydration of ferrite and C_3A, and lead to higher amounts of hemicarboaluminate and monocarboaluminate precipitated, which contributes to porosity refinement and mechanical properties. The rate of reaction of metakaolin is not affected by the addition of TEA, independent of the iron content of the clay.

Contents

5.1   Introduction

The push to lower the carbon emissions associated with cement production is driving the industry to find solutions that are also technically and economically feasible. The only effective strategy to tackle this challenge is to reduce the clinker factor [1]. This has promoted the adoption of blended cements, which incorporate supplementary cementitious materials (SCMs) in addition to clinker and gypsum [2,3]. Today, blended cements are more common than traditional Portland cements.

Limestone calcined clay cements (LC^3) are a family of blended cements that incorporate limestone and calcined clays replacing part of the clinker [4,5]. Among all the materials that are commonly used as SCM, limestone and calcined clay are the only available in the quantities required for a reduction of the clinker factor on a global-scale [1]. Natural clays containing kaolinite are the most suitable material to make LC^3 [6]. After calcination, kaolinite transforms into metakaolin, an aluminosilicate phase that can react with portlandite to form C-A-S-H and AFm [7]. Natural clays normally contain other minerals in addition to kaolinite. These associated minerals are commonly quartz, iron oxides, feldspars and other rock forming minerals [8].

The reactivity of blended cements depends on their mineralogical composition (clinker composition, type of SCM), but also on physical characteristics of the material, especially specific surface area [9–11]. Proper grinding is crucial to ensure a good behavior of blended cements. The different grindability of the SCMs and the clinker grains makes intergrinding challenging [12]. In general, SCMs are softer than clinker and thus will tend to overgrind while the clinker grains remain coarse [13].

Grinding aids (GAs) are incorporated during comminution of clinker to reduce electrostatic forces and minimize agglomeration of clinker and SCM grains [14]. Their chemical compositions include alkanolamines such as triethanolamine (TEA), triisopropanolamine (TIPA) and diethylisopropanolamine (DEIPA), as well as glycols such as propylene glycol (PG), monoethylene glycol (MEG), and diethylene glycol (DEG). Polycarboxylate ethers (PCEs) are also commonly used as GAs. Because of their organic polar nature, GAs are preferentially adsorbed on surfaces formed by the fracture of electrovalent bonds such as Ca–O and Si–O, reducing surface energy forces [14]. This reduction leads to an increase in the fineness of the cement for a given energy consumption [14–16]. Mishra et al. showed quantitatively that the main effect of GA is the reduction of agglomeration energy [17]. Recently, it was shown that they can also improve the particle separation process of ground clays [18].

Alkanolamines are known to influence the hydration of cement in addition to improving the grinding process [19]. TEA and TIPA have been used as setting accelerators and strength enhancers [20]. Ramachadran observed that TEA could retard the hydration of the alite, but significantly accelerate the reaction of C$_3$A and the formation of ettringite [20,21]. TIPA has been observed to produce an increase in strength at later ages [22,23]. The interaction of TEA and TIPA has been associated with the formation of amine-iron complexes. Gartner and Myers proposed that the iron complex increased the solubility of iron enough to be able to coprecipitate with aluminum to form ettringite and AFm [23]. In this study, Gartner and Myers also suggest that an amine-Al complex might be formed. Recently, an atomistic model for the TEA-Al complex has been proposed by DFT calculations [24].

Despite the extensive amount of research on the effect of different alkanolamines in pure clinker phases and OPC hydration, there are no studies that address their effect in systems where additional aluminum and iron sources are introduced, such as LC^3. This paper presents a study on the effect of alkanolamine grinding aids

(TEA, TIPA and DEIPA) on the hydration kinetics and phase assemblage of LC^3. The influence of GA addition in porosity refinement and compressive strength is discussed in the light of the observed interactions of alkanolamines with iron and aluminate phases in LC^3.

5.2   Materials and methods

5.2.1   Raw materials

A commercial ordinary Portland cement (OPC) conforming to EN 197-1 as CEM I 42.5R was used in this study. Two different calcined clays were used for the preparation of LC^3 blends. First, a natural clay from Chile (Cy) with 60.3% of kaolinite as measured by TGA and a high iron content (9.44% Fe_2O_3) was selected. The clay was ground and calcined in a laboratory furnace at 800°C for 1 hour. Complete dehydroxylation of kaolinite was verified by TGA. The iron mineral after calcination corresponds to hematite. The other clay corresponds to a high purity metakaolin (MK, 95% purity from Burgess). As the content of kaolinite is higher, MK was mixed with a quartz powder (Qz) to achieve the same total kaolinite content as Cy. A commercial limestone (Omya, Durcal 5) was used.

The chemical (by XRF) and phase (by XRD / Rietveld) compositions of the raw materials are shown in Table 5-1. The particle size distribution (PSD) of these materials, measured by laser diffraction, is shown in Figure 5-1. The optical model parameters and the dispersant were selected following the recommendations given in [25].

Table 5-1: Chemical (from XRF) and phase composition (from XRD) of OPC, MK, Cy, LS and Qz.

	OPC	MK	Cy	LS	Qz
SiO_2	19.51	52.00	48.13	0.11	99.83
Al_2O_3	4.42	43.80	35.08	0.00	0.00
Fe_2O_3	3.12	0.33	9.44	0.04	0.03
CaO	63.85	0.03	0.81	54.96	0.02
Na_2O	0.19	0.14	0.20	0.06	0.00
K_2O	0.83	0.29	0.08	0.00	0.05
MnO	0.05	0.01	0.01	0.00	0.00
TiO_2	0.31	1.53	2.27	0.00	0.02
MgO	2.10	0.01	0.52	0.15	0.00
P_2O_5	0.33	0.16	0.34	0.00	0.00
SO_3	3.25	0.10	0.02	0.03	0.00
LOI	1.54	1.47	2.98	42.5	0.02
C_3S	66.5	-	-	-	-
C_2S	4.0	-	-	-	-
C_3A	4.9	-	-	-	-
C_4AF	9.6	-	-	-	-

The specific surface area (SSA) of each raw material was measured by nitrogen adsorption, using the BET model. In all cases, samples of around 1.5 g were degassed for 2 hours at 200ºC under a N_2 flux before the measurement. The specific gravity was measured using a liquid pycnometer with isopropanol as solvent. Distribution values and specific gravities are summarized in Table 5-2.
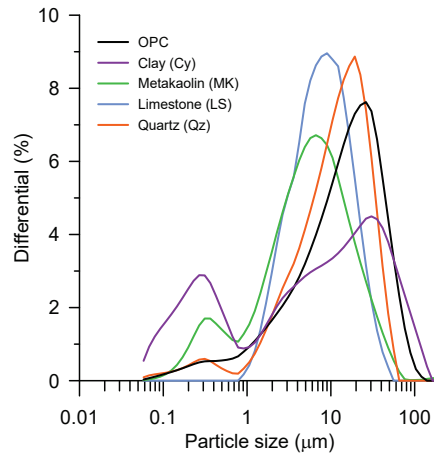
Figure 5-1: Particle size distribution of the raw materials used in this study.

Table 5-2: Distribution values, span (width), specific surface area and specific gravity of raw materials.

	OPC	MK	Cy	LS	Qz
D_V90 (μm)	41.42	20.17	56.22	19.3	11.96
D_V50 (μm)	14.22	5.13	7.72	7.71	4.56
D_V10 (μm)	1.67	0.54	0.17	2.27	0.36
Span (-)	2.80	3.83	7.26	2.21	2.54
SSA (m^2/g)	1.41	13.56	47.16	2.39	3.45
Sp. Gravity (g/cm^3)	3.09	2.20	2.61	2.71	2.65

Pure molecules of different grinding aids were used in this study. Three different alkanolamines were studied. Triethanolamine (TEA, SigmaAldrich 90279 99% purity), triisopropanolamine (TIPA, SigmaAldrich 254746 95% purity) and diethylisopropanolamine (DEIPA, SigmaAldrich 233757 93% purity) were used. In addition, the effect of alkanolamines on LC^3 hydration was compared to other families of grinding aids. Polypropylene glycol (PPG, Mn 1000, SigmaAldrich 202320), dipropylene glycol methyl ether (DPG, SigmaAldrich 484253, 99%) and polycarboxylate ether (PCE, GCP Chemicals, ADVA 955, 60% solid content) were used. In all cases, aqueous solutions at 0.5% solid content were prepared to facilitate handling, dosing and dispersion of the grinding aids.

5.2.2   Mixture design

An LC^3-50 system (50% clinker content) was used as a reference to study the effect of alkanolamine GAs on hydration and mechanical properties. The clay to limestone ratio was fixed at 2-to-1. To achieve adequate sulfate balance of the systems, 1% of gypsum was added in all cases. This leads to a mixture design composed of 54% OPC, 30% calcined clay (Cy or MK+Qz), 15% LS and 1% gypsum. A water to binder ratio (w/b) of 0.4 was used.

The addition of grinding aids to the LC^3 systems was conducted starting from the 0.5% solid content solutions prepared. The necessary amount of solution was incorporated to the mixing water before casting to achieve 100 or 200 parts per million (ppm), (0.01 and 0.02% respectively) referred to the mass of binder. These

dosages are common concentrations for this type of molecules when used as grinding aids. In the case of TEA, some experiments were conducted at higher concentrations. The water addition due to the incorporation of the GA solutions was computed and subtracted from the mixing water. LC^3 paste samples were prepared by mixing the water plus the GA with the powders using a vertical axis high shear mixer, at 1600 rpm for 2 minutes.

5.2.3   Experimental methods

The heat evolution was measured in a TAM Air isothermal calorimeter at 20ºC for up to 7 days. From the paste samples prepared, 10 g of was placed in a glass ampoule, sealed and introduced in the calorimeter.

X-ray diffraction (XRD) measurements were carried out on freshly cut slices of hardened paste at 1, 2, 3, and 7 days of hydration to follow the hydration of the clinker phases and the formation of aluminate hydrates in the systems. Rietveld refinement was conducted using the HighScore Plus v4.8 software. The slices were analyzed in a Bragg-Brentano configuration in a PANalytical X'pert pro diffractometer working at 45 kV and 40 mA with a copper source. A 1/2º soller slit was used, and scans were acquired between 7 and 70º 2θ in 14 min, equivalent to a step size of 0.0167º 2θ. The external standard method was used to compute the K-factor of the device and account for the amorphous phases present. A scan of a rutile standard was acquired in the same conditions after the experiments for this purpose.

Porosity measurements were conducted by mercury intrusion porosimetry (MIP) in paste samples at 1 and 7 days. Slices similar to the ones prepared for XRD were immersed in isopropanol for 7 days to arrest the hydration. Afterwards, they were stored in a desiccator for at least 48 hours to remove the remaining isopropanol. About 1 g of hardened paste was placed in a glass dilatometer crushed into 4 to 5 pieces. Intrusion was conducted up to a pressure of 440 MPa. A contact angle of 120° was assumed between mercury and the cement paste.

Paste samples were also used to assess compressive strength. Cubic samples of 2 cm were prepared and stored in sealed conditions until testing. Strength measurements were conducted at 1, 2, 3, 7, 14 and 28 days of hydration, using a 60 kN load cell with a 1 N resolution and a loading rate of 0.4 kN/s.

The aluminum and iron content were measured in pore solution samples collected at 1, 2, 3 and 7 days of hydration in LC^3 systems incorporating 200 and 500 ppm of TEA. The pore solution extraction was done in a cylindrical paste sample using a pore press device at 600 kN for 7 minutes. Samples were filtered using a 0.2 μm syringe filter after collection. pH was measured right after extraction. Afterwards, a 3 times dilution in 1% HNO_3 was prepared. The measurements were conducted using inductively coupled plasma optical emission spectrometry (ICP-OES).

The microstructural development was studied using scanning electron microscopy (SEM), using a FEI Quanta 200 microscope. Element distribution maps were collected from polished sections of LC^3 paste (from the same discs as for MIP measurements) embedded in resin, using an accelerating voltage of 12 kV, working distance of 12.5 mm and a spot size adjusted to obtain about 0.9 nA of current over the sample. The maps were collected at 1000x magnification in 30 cycles with a dwell time of 512 μs, resulting in a total measuring time of approximately 8 hours per map. The obtained data was then quantified using a calibration database

acquired under the same conditions. Afterwards, the *edxia* image analysis framework was used to process the hyperspectral maps and obtain phase distribution masks [26].

5.3   Results and discussion

5.3.1   The effect of TIPA, TEA and DEIPA addition in LC^3 properties

Calorimetry curves obtained for LC^3 systems with Cy (iron-rich) clay incorporating 100 and 200 ppm of alkanolamines are shown in Figure 5-2. A significant enhancement of the aluminate peak is observed, with higher maximums of the peaks for the higher dosages of GA. DEIPA exhibits the highest enhancement, followed by TEA and TIPA.

In the case of TEA (both addition levels) and DEIPA at 200 ppm a shortening of the time to reach the onset of the aluminate peak is observed. As it has been previously shown [27], the sulfate balance of blended cements is influenced by the rate of sulfate adsorption in C-A-S-H. In addition, the amount of ettringite precipitated during the alite peak can also modify the position of the aluminate peak [28]. In this case, the alite peaks appear similar in all cases, which suggests that the acceleration of the aluminate peak is linked to a higher amount of ettringite being precipitated before the onset. Ramachandran previously showed that TEA accelerates the reaction rate of C_3A [20,21] with a consequent increase in the precipitated ettringite.

Figure 5-2b shows the corresponding total heat for the different LC^3 systems studied. Despite the clear differences in the aluminate peaks observed in Figure 5-2a, the total heat curves appear similar for DEIPA, TEA and the system with 200 ppm TIPA at 48 hours. Thus, despite the clear peak shape difference, the amounts of ettringite precipitated in these systems is expected to be similar.

a)   b)
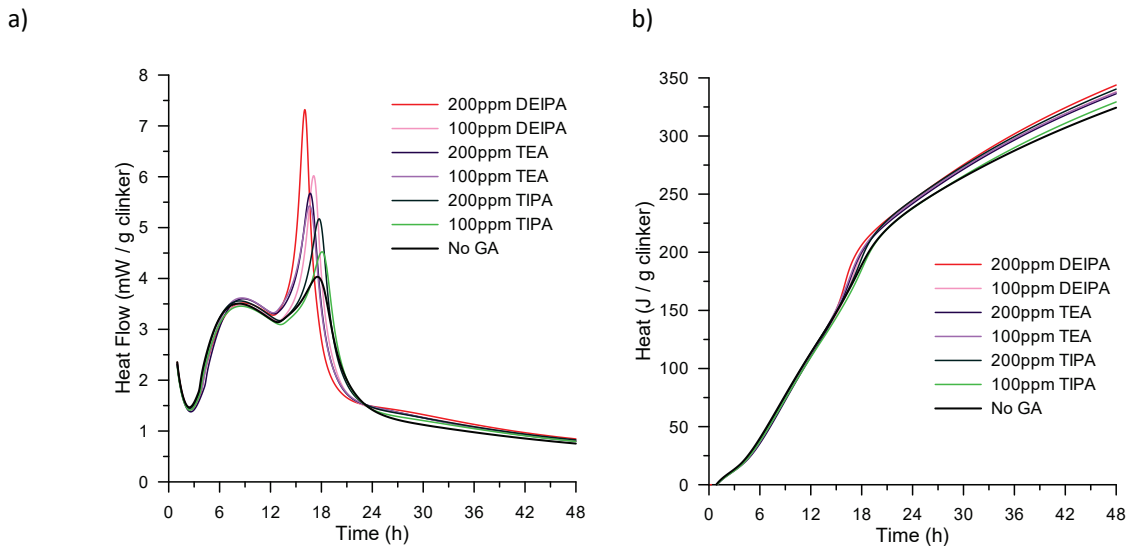
Figure 5-2: Heat flow (a) and total heat (b) curves of LC^3-50 systems with Cy clay and alkanolamine GA additions.

Calorimetry curves of LC^3 systems incorporating 100 and 200 ppm of glycol-based (PPG and DPG) and PCE-based GAs are shown in Figure 5-3. In this case, no significant effect of the grinding aids on the hydration

kinetics of LC^3 systems is observed. The total heat release is in all cases similar to the system without the addition of grinding aids. While all these molecules have proven effective in improving the grinding efficiency of calcined clays [29] and the particle classification process after grinding [18], they do not influence the hydration kinetics of LC^3-type systems at the addition levels explored.

a)

b)
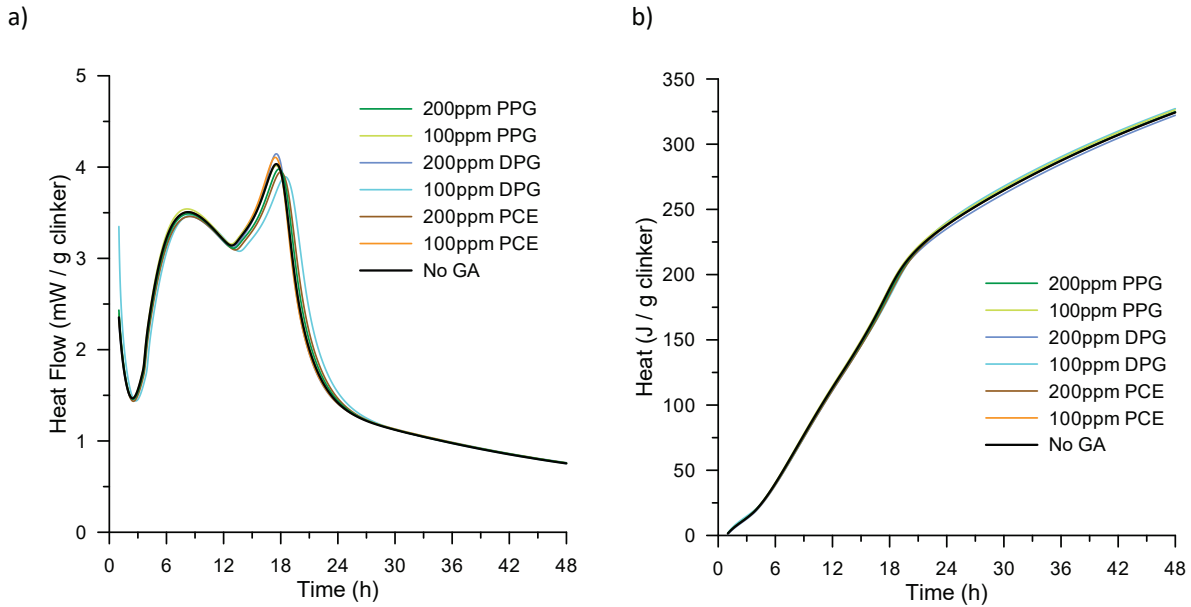
Figure 5-3: Heat flow (a) and total heat (b) curves of LC^3-50 systems with Cy clay and glycol-based/PCE GA additions.

The enhancement observed with the addition of alkanolamines in the aluminate peak of LC^3 systems show that these molecules can influence the hydration kinetics of these blended systems. To better understand the effect of alkanolamines in LC^3, experiments were conducted to assess the influence of these molecules on OPC hydration kinetics. Figure 5-4 shows a heat flow curve of plain OPC, and also with 200 ppm of addition of DEIPA and TEA, molecules that exhibited the strongest enhancement effects in the aluminate reaction of LC^3 (Figure 5-2).

A reduction of the slope of the acceleration stage of the alite peak is observed in both systems incorporating GAs. Furthermore, the height of the alite peak is reduced as compared to the plain OPC system. This could be related with a higher degree of reaction of C$_3$A/ferrite in the presence of these alkanolamines.

The reduction in slope of the acceleration period is not observed in the LC^3 systems, Figure 5-2. Moreover, the height of the alite peaks is similar among all systems with GA as compared to the control LC^3 system. It can be inferred that the addition of limestone and calcined clay in LC^3 provides sufficient enhancement of the alite reaction through filler effect to offset the negative effects observed in OPC.

Considering the position of the maximum of the alite peak in each case as a reference, the onset of the aluminate peak also occurs earlier (i.e., at a lower DoH of alite) in the OPC systems with TEA and DEIPA. This further supports the observation regarding more sulfate being consumed during the acceleration period due to an increased rate of reaction of C$_3$A and/or ferrite. The aluminate peaks also appear enhanced compared to the control OPC system.
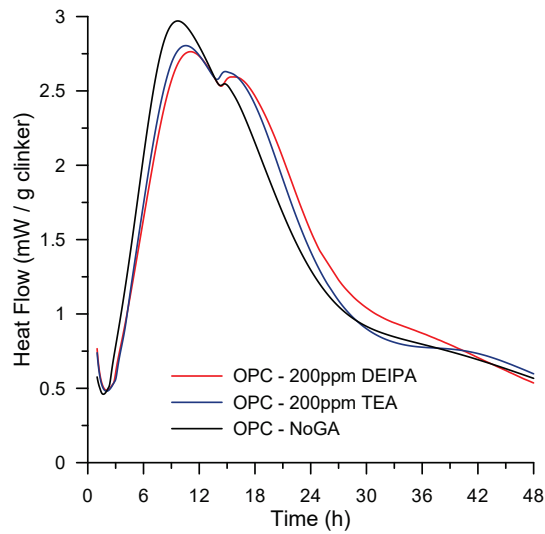
Figure 5-4: Heat flow curve of OPC with addition of 200 ppm of DEIPA and TEA.

Figure 5-5 shows the compressive strength of LC^3 systems measured in paste samples. TEA, TIPA and DEIPA have positive effects in mechanical properties but in different amounts and at different hydration times. TEA and DEIPA show increases in strength compared to the control system at early ages, TEA being significantly higher. TIPA shows similar strength at early ages, but it improves in the long term, in general agreement with previous studies [20]. Among the 3 alkanolamine molecules used, TEA appears to have the highest potential to increase the strength of LC^3-type systems.
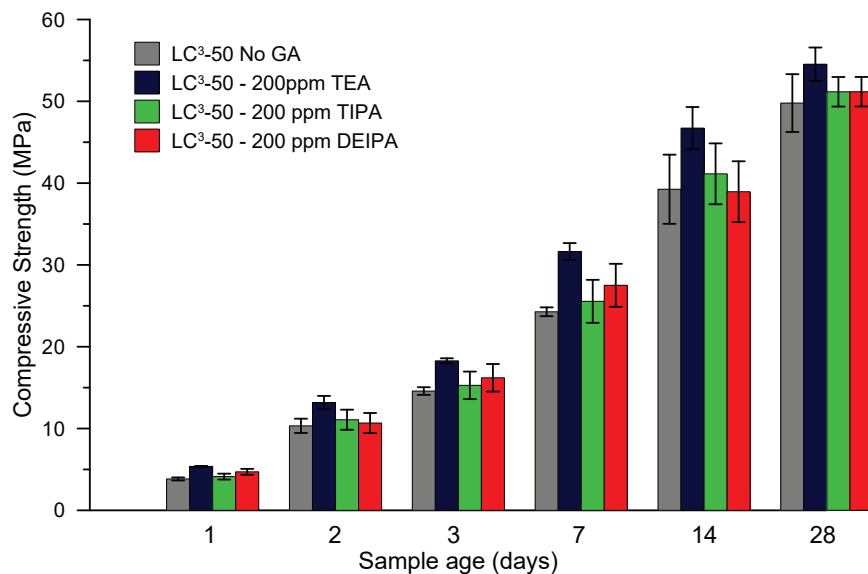
Figure 5-5: Compressive strength of LC^3-50 paste samples incorporating 200 ppm of TEA and DEIPA.

The porosity measured by MIP of the same systems shown in Figure 5-5 are presented in Figure 5-6 at 1 and 7 days of hydration. At 1 day, the system with TEA exhibits the smallest critical entry radius, while the system with DEIPA shows the lowest total porosity. DEIPA and TIPA have a similar critical entry radius to the control system. At 7 days, all the systems incorporating grinding aids have a lower critical entry radius than the control system. Therefore, the addition of alkanolamines to LC^3 in concentrations similar to the ones currently in use for cement, particularly TEA and DEIPA, can indeed have an influence on compressive strength and porosity refinement.

a)   b)
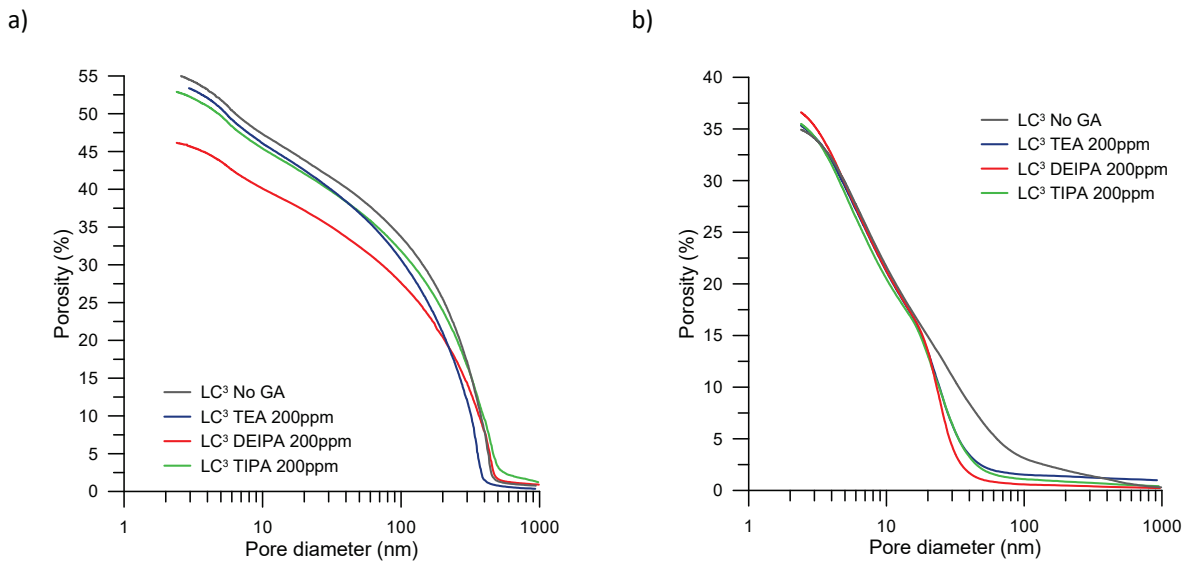
Figure 5-6: Porosity measured by MIP of LC^3-50 paste samples incorporating 200 ppm of TEA and DEIPA at 1 (a) and 7 (b) days of hydration. Contact angle assumed 120°.

To understand the origin of the refined porosity and increased strength observed in the LC^3 systems with alkanolamines, the degree of hydration of the main clinker phases and the phase assemblage was characterized by XRD. Figure 5-7 show the DoH of alite, C_3A and ferrite, and Figure 5-8Figure 5-8 the quantification of ettringite and hemicarboaluminate plus monocarboaluminate (Hc + Mc) for each system.

The DoH of alite is slightly lower in the systems incorporating GAs at 24 hours. At later ages, the differences between systems with and without alkanolamines is negligible. The DoH of C_3A is higher at 24 hours for the systems incorporating alkanolamines. Afterwards, an enhanced hydration for C_3A is observed in the systems with TEA and DEIPA. This agrees with previous observations on C_3A hydration using TEA [21]. In this study, DEIPA appears to have a similar effect, although less intense than TEA.

The DoH of ferrite (C_4AF) is significantly higher at 24 hours in all systems with GA additions. At 7 days, the system incorporating 200 ppm of TIPA depletes anhydrous ferrite, while the systems with DEIPA and TEA reach DoH values around 90% for this phase. In contrast, the control system reaches 74% DoH of ferrite at the same age. The higher DoH observed in the ferrite phase when alkanolamines are incorporated could be attributed to the formation of amine-iron and amine-aluminum complexes at high pH [23]. The increased mobility of iron and aluminum in the systems with alkanolamines might explain the higher degrees of reaction observed.

The amount of ettringite is similar among all systems, as the limiting factor is the availability of sulfate. However, the amounts of Hc and Mc precipitated are significantly higher in the systems with alkanolamines. The highest amounts are observed in the system with TEA, followed by DEIPA and TIPA. This corresponds with the trend observed in compressive strength, Figure 5-5. Recently, it has been shown that the contribution of Hc and Mc in LC^3 strength and porosity refinement is significant [30]. Thus, the enhanced precipitation of these phases could explain the increased strength observed in LC^3 systems incorporating these molecules.
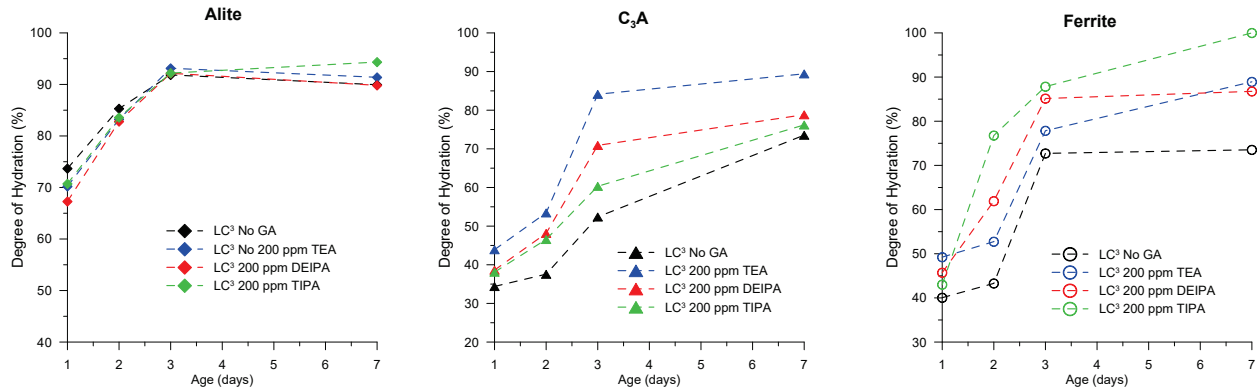
Figure 5-7: DoH of alite, C3A and ferrite in LC^3-50 systems incorporating alkanolamine GAs.
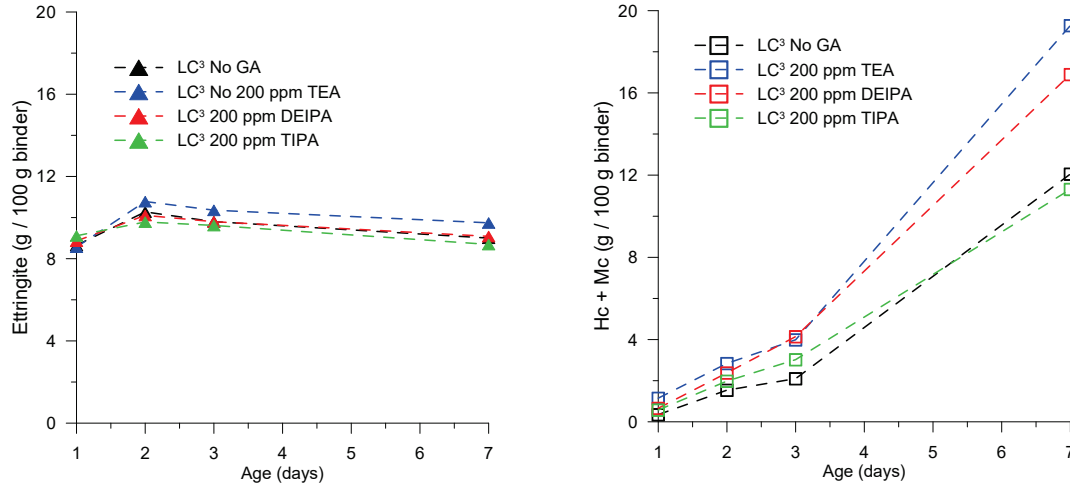
Figure 5-8: Ettringite and Hc + Mc content evolution in LC^3-50 systems incorporating alkanolamine GAs.

5.3.2   Further insights on the influence of TEA in LC^3 hydration

Since TEA was the molecule that exhibited the highest enhancement of strength in LC^3 system, the interactions of this molecule with LC^3 were studied in more detail. Figure 5-9 shows the concentration of iron and aluminum in the pore solution of an LC^3 system with 0, 200 and 500 ppm of added TEA. In this case, the MK+Qz clay (no iron) was used to study the effect of TEA addition on mobilization of iron from ferrite alone.

At 24 hours of hydration, the concentration of aluminum increase with increasing amounts of TEA. After-wards, the difference between the systems with TEA and the control system is minor. In the case of iron, it was only detected after 2 days of hydration in the system with TEA. In the control system, the measured values were always below the detection limit of 0.055 mmol/L. The content of iron in solution increases with an increase in the amount of TEA added. These observations are in good agreement with the higher degrees of reaction of ferrite measured by XRD, Figure 5-7.

The pH of the system with 500 ppm was slightly higher at 24 hours. Overall, it can be stated that TEA does not seem to accelerate the reaction of metakaolin in the same way as ferrite and possibly C_3A during the first 24 hours. In addition, as the degree of reaction of alite in the systems with TEA is expected to be slightly lower than the control (Figure 5-7), the measured pH values further confirm that metakaolin is indeed react-ing at the same rate or slightly slower in the systems with TEA.
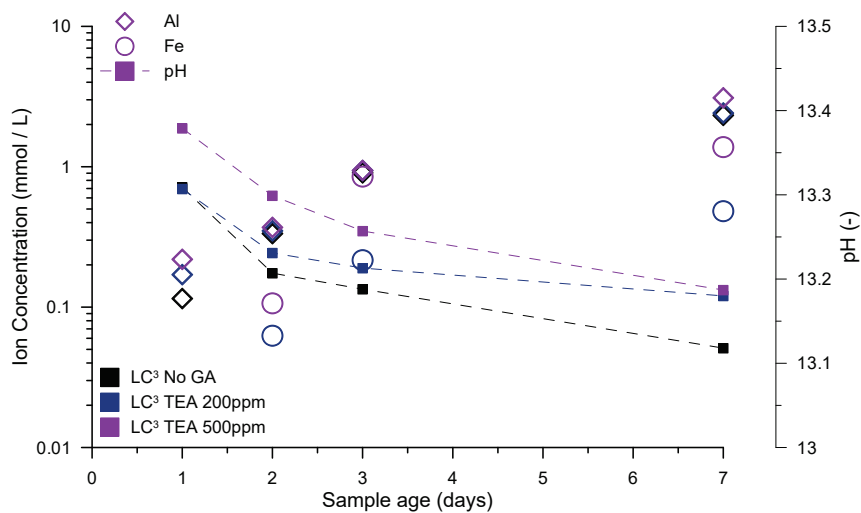
Figure 5-9: pH, aluminum and iron concentration in pore solution of LC^3-50 (MK+Qz clay) paste systems incorporating TEA.

Based on the previous results, there is a clear interaction between TEA and iron in LC^3 systems. However, there is still an open question if this interaction is limited to ferrite or also affects the iron phases present in the calcined clay fraction as part of the impurities of natural clays.

A series of isothermal calorimetry experiments were performed with the aim to clarify this question. The sources of iron from an LC^3 system were removed one by one, and the effect of TEA and DEIPA in the observed enhancement of the aluminate peak was measured. A system with Cy clay and gray cement (iron from ferrite and calcined clay), another with gray cement and MK+Qz (iron only from ferrite) and a third one with white Portland cement and MK+Qz clay (no iron in the system) were compared. The results are shown in Figure 5-10.

The enhancement of the aluminate peak observed in the systems containing gray cement and Cy clay (Figure 5-10a and Figure 5-2) is also observed in the systems with gray cement and MK+Qz clay (Figure 5-10b). This shows that the presence of iron in the calcined clay is not necessary for the enhancement to take place. This

agrees with the pore solution results, where the same synthetic clay without iron (MK+Qz) was used to pre-pare the samples and an increase in the iron concentration was observed.

However, when the iron phase from cement (ferrite) is also removed, the situation changes. As seen in Figure 5-10c, the aluminate peaks between the control system and the ones incorporating TEA and DEIPA are simi-lar, and no clear enhancement is observed. Thus, a major part of the observed enhancement of the aluminate peak in LC^3 systems incorporating alkanolamines appears to be associated with an accelerated hydration of ferrite. Nevertheless, the aluminate peaks of the systems with TEA and DEIPA in Figure 5-10c are still slightly higher than the control. This could be due to a promoted reaction of C$_3$A (still present in white cement) by the addition of TEA and DEIPA [21].

a)   b)   c)
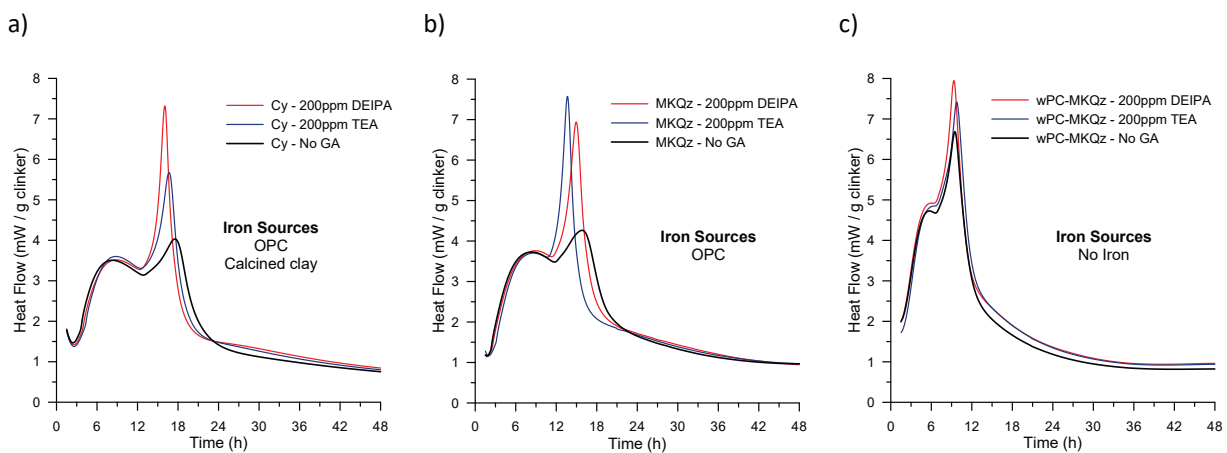
Figure 5-10: Heat flow curves of different LC^3-50 systems with additions of TEA and DEIPA and iron phases in cement and calcined clay (a), only cement (b) and neither cement or calcined clay (c).

To further explore the influence of TEA in the rate of reaction of metakaolin, the R^3 test [31] was used, as it allows to assess the intrinsic reactivity of the clay independently of the cement used. Furthermore, high cor-relation of this test with compressive strength results have been observed. Both clays, MK (no iron) and Cy (high iron content) were tested, in one case with the standard R^3 solution and in other with the addition of 500 ppm (referred to the total solids) TEA. The total heat curves obtained are shown in Figure 5-11.

The addition of TEA in the MK clay has no effect in the observed reaction kinetics. The difference with the control system is within the expected variability of this test. In the case of the high iron clay (Cy), a slight increase in the early reaction rate is observed between 12 and 30 hours in the system with 500 ppm TEA. However, the difference is small and the system without the addition of TEA reaches an equivalent degree of reaction afterwards. Both results agree with the pH values observed in Figure 5-9. Moreover, it indicates that the enhancements observed in Figure 5-10 are mainly due to the enhanced reactivity of ferrite and C$_3$A rather than metakaolin.
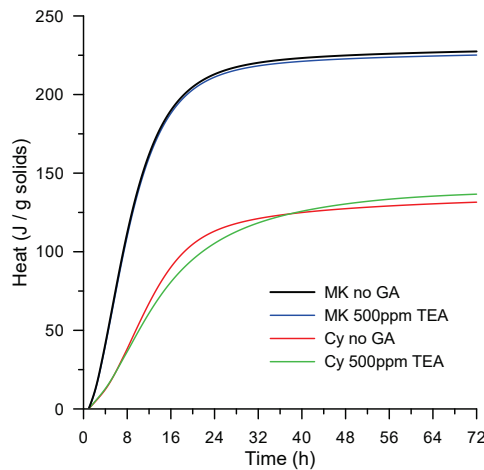
Figure 5-11: R^3 test total heat curves of Cy and MK clays with and without the addition of 500 ppm TEA.

The effect of TEA additions on the reaction of alite was further studied with higher additions of admixture. Figure 5-12 shows the heat flow curves of LC^3 systems with MK+Qz clay and additions of TEA up to 2000 ppm. Higher additions of TEA lead to more enhancement of the aluminate peak. However, the slope of the acceleration period of the alite peak decreases with increasing amounts of TEA above 200 ppm. As previously discussed, this could be explained by the increased amount of aluminum in the systems with TEA during the first hours of hydration.

Among the systems with TEA, the position of the onset of the aluminate peak appears to remain constant. As more aluminum is available in the pore solution, more ettringite is formed during the acceleration period of alite and consequently, more sulfate is consumed. On the other hand, alite reacts at a slower rate as the TEA concentration increases, and therefore the amount sulfate adsorbed into C-A-S-H decrease [27]. These two simultaneous effects seem to offset each other and overall, the onset of the aluminate reaction is not affected. However, as the slope of the acceleration period goes down the position of the alite peak also shifts right. Consequently, for the highest dosage of TEA (2000 ppm) the system appears slightly undersulfated.
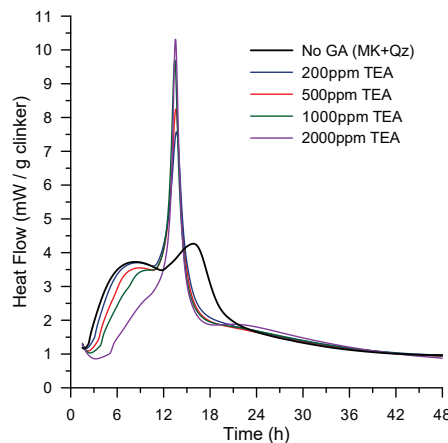
Figure 5-12: Heat flow curves of LC^3-50 systems (MK clay) with higher additions of TEA.

98

5.3.1 Microstructure of LC^3 incorporating TEA

To study the effects of the addition of TEA in the microstructure of LC^3, an hyperspectral element map of an LC^3 system with MK+Qz clay was collected for a control (No GA) and 500 ppm system at 7 days of hydration. The data obtained was analyzed with *edxia* [26], and composite micrographs were produced to assess the distribution of hydrated phases, particularly Hc and Mc. The composition of each individual point of the map is presented as scatter plots of element composition expressed as Al/Ca vs Si/Ca ratio in Figure 5-13a and Figure 5-13b for control and TEA 500 ppm systems, respectively.

In the datasets collected for the control system, iron appears distributed in the microstructure. No other iron-bearing hydrates were observed in significant quantities. The AFm points were identified and are shown as a color mask in Figure 5-14.

a)

b)
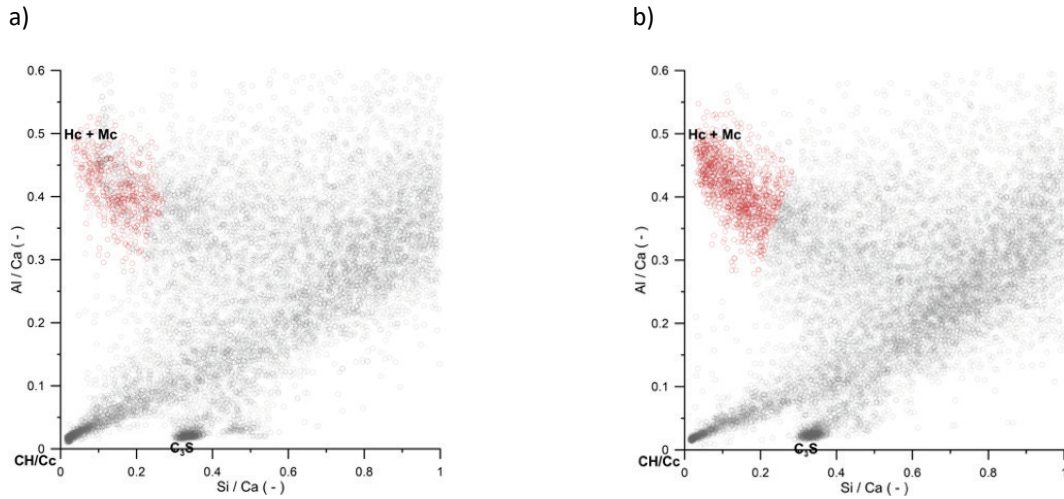
Figure 5-13: Scatter plots of elemental ratios for the map collected for LC^3 no GA (a) and TEA 500ppm (b) system at 7 days of hydration. AFm area is indicated.
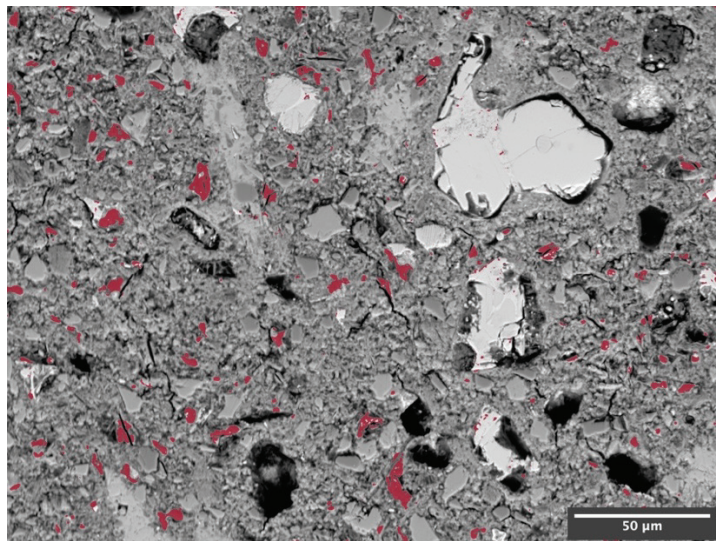
Figure 5-14: Composite micrograph of LC^3 no GA showing Hc+Mc (red). Area fraction of AFm 2.3%.

As observed in the XRD results (Figure 5-8), more Hc and Mc was observed with the addition of TEA. This is clearly observed in the composite micrograph shown in Figure 5-15 for the 500 ppm TEA system. The computed are fraction of AFm (Hc+Mc) in the No GA system was 2.3%, while in the 500 ppm one it was 6.2%. No clear iron-bearing hydrated phase is observed in this case as in the control system.
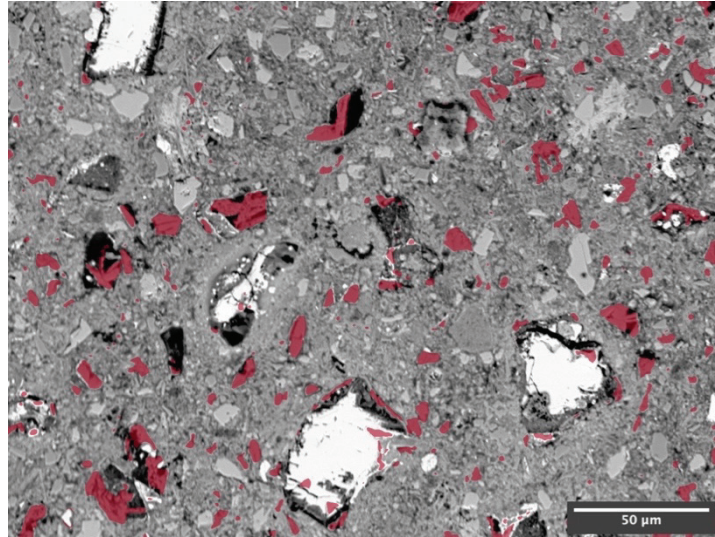
Figure 5-15: Composite micrograph of LC^3 TEA 500 ppm showing Hc+Mc (red). Area fraction of AFm 6.2%.

From a microstructural point of view, the main effect of TEA addition in LC^3 is associated with a higher precipitation of Hc and Mc, which in turn increase the mechanical properties of the material. While more iron is put into solution, it appears to remain distributed rather than precipitate in hydrated phases.

5.4   Conclusions

This study evaluated the influence of different alkanolamines on the hydration, porosity and mechanical properties of LC^3. Special attention was given to TEA, as it showed to lead to the highest increase in compressive strength.

Based on the results presented, the following conclusions can be drawn:

1. Alkanolamines have an enhancing effect on the aluminate reaction in LC^3 systems. A slight shortening of the time to reach the onset of the aluminate peak is observed for TEA and DEIPA at 200 ppm dosage due to an accelerated precipitation of ettringite. However, the amounts of ettringite observed at 24 hours are similar among all systems as it is limited by the sulfate available.

2. The addition of alkanolamines promote the hydration of ferrite and C_3A. In the case of TEA and DEIPA, an increase in the amount of Hc and Mc precipitated is observed, leading to a more refined porosity and an increase in compressive strength.

3. No decrease in the slope of the acceleration period is observed in LC^3 systems due to the addition of TEA up to 200 ppm, as the retardation effect over alite hydration is offset by the acceleration (filler) contribution of limestone and metakaolin. Higher dosages lead to decreasing rates of alite hydration. Dosages of TEA in the range of 2000 ppm may produce undersulfation of the system.

4. The addition of TEA in LC^3 leads to an increased amount of aluminum in solution at early age and a significant increase in the iron content. The interaction of TEA with iron is mainly associated with an enhanced hydration of ferrite.

5. The rate of reaction of metakaolin is not significantly affected by the addition of TEA, independently of the iron content of the clay.

5.5 References

[1]   K.L. Scrivener, V. John, E.M. Gartner, Eco-efficient cements: potential, economically viable solutions for a low-CO2, cement-based materials industry, in: United Nations Environmental Programme (UNEP), 2016.

[2]   B. Lothenbach, K. Scrivener, R.D. Hooton, Supplementary cementitious materials, Cem. Concr. Res. 41 (2011) 1244–1256. doi:10.1016/j.cemconres.2010.12.001.

[3]   M. Schneider, M. Romer, M. Tschudin, H. Bolio, Sustainable cement production—present and future, Cem. Concr. Res. 41 (2011) 642–650. doi:10.1016/j.cemconres.2011.03.019.

[4]   K. Scrivener, F. Martirena, S. Bishnoi, S. Maity, Calcined clay limestone cements (LC3), Cem. Concr. Res. (2017) 1–8. doi:10.1016/j.cemconres.2017.08.017.

[5]   K.L. Scrivener, F. Avet, H. Maraghechi, F. Zunino, J. Ston, A. Favier, et al., Impacting factors and properties of Limestone Calcined Clay Cements (LC3), Green Mater. (2018). doi:https://doi.org/10.1680/jgrma.18.00029.

[6]   R. Fernandez, F. Martirena, K.L. Scrivener, The origin of the pozzolanic activity of calcined clay minerals: A comparison between kaolinite, illite and montmorillonite, Cem. Concr. Res. 41 (2011) 113–122. doi:10.1016/j.cemconres.2010.09.013.

[7]   M. Antoni, J. Rossen, F. Martirena, K. Scrivener, Cement substitution by a combination of metakaolin and limestone, Cem. Concr. Res. 42 (2012) 1579–1589. doi:10.1016/j.cemconres.2012.09.006.

[8]   A. Alujas, R. Fernández, R. Quintana, K.L. Scrivener, F. Martirena, Pozzolanic reactivity of low grade kaolinitic clays: Influence of calcination temperature and impact of calcination products on OPC hydration, Appl. Clay Sci. 108 (2015) 94–101. doi:10.1016/j.clay.2015.01.028.

[9]   M. Cyr, P. Lawrence, E. Ringot, Efficiency of mineral admixtures in mortars: Quantification of the physical and chemical effects of fine admixtures in relation with compressive strength, Cem. Concr. Res. 36 (2006) 264–277. doi:10.1016/j.cemconres.2005.07.001.

[10]   P. Lawrence, M. Cyr, E. Ringot, Mineral admixtures in mortars effect of type, amount and fineness of fine constituents on compressive strength, Cem. Concr. Res. 35 (2005) 1092–1105. doi:10.1016/j.cemconres.2004.07.004.

[11]   F. Zunino, M. Lopez, A methodology for assessing the chemical and physical potential of industrially sourced rice husk ash on strength development and early-age hydration of cement paste, Constr. Build. Mater. 149 (2017) 869–881.

[12]   K. De Weerdt, Separate grinding versus intergrinding, SINTEF Report, 2007.

[13]   A. Pérez, A. Favier, K. Scrivener, F. Martirena, Influence Grinding Procedure, Limestone Content and PSD of Components on Properties of Clinker-Calcined Clay-Limestone Cements Produced by Intergrinding, in: Calcined Clays Sustain. Concr., Springer, 2018: pp. 358–365.

[14]   J.J. Assaad, C.A. Issa, Effect of clinker grinding aids on flow of cement-based materials, Cem. Concr. Res. 63 (2014) 1–11. doi:10.1016/j.cemconres.2014.04.006.

[15]   M. Katsioti, P.E. Tsakiridis, P. Giannatos, Z. Tsibouki, J. Marinos, Characterization of various cement grinding aids and their impact on grindability and cement performance, Constr. Build. Mater. 23 (2009) 1954–1959. doi:10.1016/j.conbuildmat.2008.09.003.

[16]   S. Sohoni, R. Sridhar, G. Mandal, The effect of grinding aids on the fine grinding of limestone, quartz and Portland cement clinker, Powder Technol. 67 (1991) 277–286. doi:10.1016/0032-5910(91)80109-V.

[17]   R.K. Mishra, D. Geissbuhler, H.A. Carmona, F.K. Wittel, M.L. Sawley, M. Weibel, et al., En route to a multi-model scheme for clinker comminution with chemical grinding aids, Adv. Appl. Ceram. 6753 (2015) 1–9. doi:10.1179/1743676115Y.0000000023.

[18]   F. Zunino, K. Scrivener, Increasing the kaolinite content of raw clays using particle classification techniques for use as supplementary cementitious materials, Constr. Build. Mater. 244 (2020). doi:10.1016/j.conbuildmat.2020.118335.

[19]   J. Cheung, A. Jeknavorian, L. Roberts, D. Silva, Impact of admixtures on the hydration kinetics of Portland cement, Cem. Concr. Res. 41 (2011) 1289–1309. doi:10.1016/j.cemconres.2011.03.005.

[20]   V.S. Ramachandran, Hydration of cement - role of triethanolamine, Cem. Concr. Res. 6 (1976) 623–631. doi:10.1016/0008-8846(76)90026-0.

[21]   V.S. Ramachandran, Action of triethanolamine on the hydration of tricalcium aluminate, Cem. Concr. Res. 3 (1973) 41–54. doi:10.1016/0008-8846(73)90060-4.

[22]   J.-P. Perez, A. Nonat, S. Pourchet, S. Garrault, M. Mosquet, C. Canevet, Why TIPA leads to an Increase in the Mechanical Properties of Mortars Whereas TEA Does Not, ACI Mater. J. 217 (2003) 583–594.

[23]   E. Gartner, D. Myers, Influence of Tertiary Alkanolamines on Portland Cement Hydration, J. Am. Ceram. Soc. 76 (1993) 1521–1530. doi:10.1111/j.1151-2916.1993.tb03934.x.

[24]   Y.L. Yaphary, Z. Yu, R.H.W. Lam, D. Lau, Effect of triethanolamine on cement hydration toward initial setting time, Constr. Build. Mater. 141 (2017) 94–103. doi:10.1016/j.conbuildmat.2017.02.072.

[25]   K. Scrivener, R. Snellings, B. Lothenbach, A Practical Guide to Microstructural Analysis of Cementitious Materials, (2016) 540. doi:10.7693/wl20150205.

[26]   F. Georget, edxia. Zenodo, (2019). doi:10.5281/zenodo.3246902.

[27]   F. Zunino, K.L. Scrivener, The influence of the filler effect in the sulfate requirement of blended cements, Cem. Concr. Res. 126 (2019). doi:10.1016/j.cemconres.2019.105918.

[28]   F. Zunino, K.L. Scrivener, Factors influencing the sulfate balance in pure phase C3S/C3A systems, Cem. Concr. Res. (n.d.). Submitted.

[29]   F. Zunino, K. Scrivener, Processing of calcined clays for applications in cementitious materials: The use of grinding aids and particle classification after grinding, in: Proc. Int. Conf. Sustain. Prod. Use Cem. Concr., Springer International Publishing, 2020. doi:10.1007/978-3-030-22034-1.

[30]   F. Zunino, K. Scrivener, The reaction between metakaolin and limestone and its effect in porosity refinement and mechanical properties, Cem. Concr. Res. (n.d.). Submitted.

[31]   F. Avet, R. Snellings, A. Alujas Diaz, M. Ben Haha, K. Scrivener, Development of a new rapid, relevant and reliable (R3) test method to evaluate the pozzolanic reactivity of calcined kaolinitic clays, Cem. Concr. Res. 85 (2016) 1–11. doi:10.1016/j.cemconres.2016.02.015.

Chapter 6   Sulfate balance in blended cements

Note: This chapter is based on an article published in a peer reviewed journal.

Submission title: The influence of the filler effect in the sulfate requirement of blended cements

Franco Zunino, Karen Scrivener

Contribution of the doctoral candidate: Writing of the first manuscript draft, experimental design, conduction of the experiments, reply to reviewers.

        In some blended cements, the optimum amount of sulfate addition differs from that observed in OPC. This study aims to understand the mechanism behind the impact of two SCMs, namely metakaolin and limestone, on the sulfate balance of blended cements. No significant impact of the aluminum content of these SCMs was observed. Instead, it is observed that the filler effect of the SCM, which accelerates the reaction of alite, is the main factor impacting the sulfate balance. As the rate of precipitation of C-S-H is increased, more sulfate is adsorbed by the C-S-H and consequently, the depletion of gypsum is reached earlier in time during the hydration process. A relationship between heat release at the onset of the aluminate peak and the gypsum content of the system was established.

Contents

6.1   Introduction

Calcium sulfate is added to clinker, during grinding, to control the reaction of the aluminate phase. This addition is usually referred to as gypsum (Calcium sulfate dihydrate, $CaSO_4 \cdot 2H_2O$) although anhydrite and hemihydrates (plaster) may also be present. The optimum sulfate addition is that which gives the greatest strength Ordinary Portland cement (OPC) (at 1 or 28 days). Nowadays, blended cements are more common than OPC. These contain supplementary cementitious materials (SCMs) such as fine limestone, granulated ground blast furnace slag, fly ash, calcined clay, natural pozzolans and silica fume, in addition to clinker and gypsum. Climate change and the push for a more sustainable concrete industry have accelerated the adoption of SCMs as a means to reduce the clinker factor and consequently, the carbon footprint of cement manufacture [1].

Limestone calcined clay cements (LC^3) are one of the promising alternatives for high performance sustainable cements [2]. LC^3 incorporates significant amounts of metakaolin, a reactive aluminosilicate phase [3]. When made in the laboratory, by mixing OPC with calcined clay and limestone, it has been observed that LC^3 requires additional gypsum on top of that contained in the OPC to obtain the highest compressive strength at 24 hours [4,5]. If the system is not adjusted for sulfate, the aluminate peak may occur before the alite peak, which consequently becomes smaller and broader. The incorporation of additional gypsum shifts the aluminate peak to later times and the alite peak recovers. The need for sulfate content adjustment has also been reported in blended mixtures with fly ash [6,7].

The main purpose of adding gypsum to OPC and blended cements is to control the reaction of C_3A and thus to prevent flash setting [8]. In the presence of gypsum, the hydration reaction of C_3A shifts from the precipitation of calcium aluminate hydrates and ettringite is formed [9]. As more gypsum is incorporated in the system, more retardation of the C_3A reaction can be achieved [10]. Usually, the adjustment of gypsum content is made based on the measurement of compressive strength at 24 hours in mortar specimens or by isothermal calorimetry [11]. However, the level of gypsum required to prevent flash setting is usually less than the content leading to the highest 24-hour strength [8].

The mechanism by which gypsum slows down the reaction of C_3A has been extensively studied, but is still a matter of debate. Originally it was suggested that a diffusion barrier is formed of ettringite or Ca-Al hydrates that retards the dissolution of C_3A [12,13], but recent work shows that there is no diffusion barrier and it is more tenable that the adsorption of sulfate (or Ca-S complexes) on C_3A active sites slows down the C_3A dissolution [14–16].

Quennoz et al. observed significant differences in the time of gypsum depletion between pure C_3A and C_3S/C_3A systems, indicating that C-S-H influences the availability of sulfate in these systems. Their results showed that the S/Ca ratio in C-S-H, measured by SEM-EDS, is considerably higher (between 0.04 to 0.1) before the aluminate peak in C_3S/C_3A mixtures. After the aluminate peak, the concentration of sulfate in C-S-H decreases to about one fourth of the value observed initially [17]. Similar observations were reported by Berodier and Scrivener in OPC blended with quartz [18], who also observed a change in C-S-H morphology due to sulfate adsorption. Both results are also in good agreement with the measurements by STEM-EDS reported by Gallucci et al. [19]. These observations show that sulfate not only interacts with C_3A during the acceleration period but also with C-S-H.

Despite the primary effect of gypsum addition being to modify the reaction of C_3A, no clear relationship between the content of aluminates phases and the gypsum requirement for proper sulfation of a system has been established. A comprehensive approach to sulfate balance that accounts for the adsorption of sulfate by C-S-H during hydration is required to better understand the hydration kinetics of blended cements. Furthermore, the contribution of the aluminate phases from SCMs themselves, such as metakaolin, to the sulfate amount required to ensure a properly sulfated system needs to be better understood. This paper looks at the effect of a variety of SCMs on the sulfate balance.

6.2 Materials and methods

6.2.1 Materials

A commercial ordinary Portland cement (OPC) conforming to EN 197-1 as CEM I 42.5R was used in this study. The chemical (by XRF) and phase (by XRD / Rietveld) composition is shown in Table 6-1. The calcined clay was a high purity metakaolin (MK, 95% purity from Burgess) to avoid side effects from secondary materials. Two limestone powders (calcite) with different particle sizes were also used in this study: the coarser material is noted as cLS and the finer one as fLS. In both cases, the content of calcium carbonate was above 98% as measured by thermogravimetric analysis (TGA). The particle size distribution (PSD) of these materials, measured by laser diffraction, is shown in Figure 6-1. The optical model parameters and the dispersant were selected following the recommendations given in [20]. Further details can be found in Table 6-2.

Table 6-1: Chemical (from XRF) and phase composition (from XRD) of OPC, metakaolin and LS.

	OPC	Metakaolin	LS
SiO_2	19.51	52.00	0.11
Al_2O_3	4.42	43.80	0.00
Fe_2O_3	3.12	0.33	0.04
CaO	63.85	0.03	54.96
Na_2O	0.19	0.14	0.06
K_2O	0.83	0.29	0.00
MnO	0.05	0.01	0.00
TiO_2	0.31	1.53	0.00
MgO	2.10	0.01	0.15
P_2O_5	0.33	0.16	0.00
SO_3	3.25	0.10	0.03
LOI	1.54	1.47	42.5
C_3S	66.5	-	-
C_2S	4.0	-	-
C_3A	4.9	-	-
C_4AF	9.6	-	-

The specific surface area (SSA) of each raw material was measured by nitrogen adsorption, using the BET method. In all cases, samples of around 1.5 g were degassed for 2 hours at 200ºC under a N_2 flux before the measurement. The specific gravity was measured using a liquid pycnometer with isopropanol as solvent.
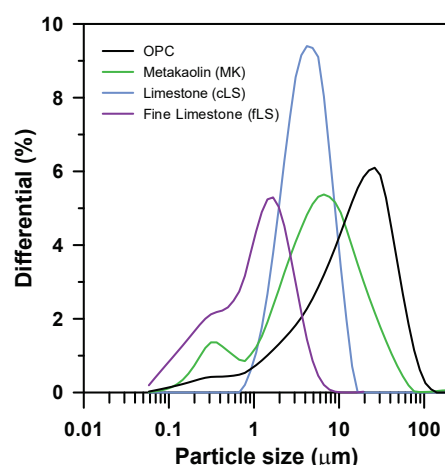
Figure 6-1: Particle size distributions of materials used in this study.

Table 6-2: Distribution values, span (width), specific surface area and specific gravity of raw materials.

	OPC	MK	cLS	fLS
D_V90 (µm)	41.42	20.17	7.93	6.72
D_V50 (µm)	14.22	5.13	3.93	1.77
D_V10 (µm)	1.67	0.54	1.80	0.24
Span (-)	2.80	3.83	1.56	3.66
SSA (m^2/g)	1.41	13.56	3.60	8.96
Sp. Gravity (g/cm^3)	3.09	2.20	2.72	2.72

6.2.2 Mixture design

The influence of the additional SSA introduced by the incorporation of SCMs (filler effect) on the sulfate balance of the system was compared to the effect of the additional aluminates sourced from the addition of metakaolin. For this purpose, OPC blends with different limestone replacements were compared to LC^3 systems that additionally incorporate metakaolin. The reference LC^3 system contained 55% OPC, 15% limestone (cLS) and 30% metakaolin (LC^3-50) on a mass basis plus different amounts of added gypsum (see Table 3). Different grades of clay (metakaolin content) were simulated by combining the 95% metakaolin material with limestone, as detailed in Table 3. Following this approach, LC^3-50 systems with clay grades ranging from 95% to 20% were prepared. From this dataset, the systems with 95%, 63% and 40% were selected for further study with different gypsum contents. Based on the computed SSA for each LC^3 system, an equivalent blend of OPC and fine limestone (fLS) was prepared, with a proportion intended to replicate the same binder surface area of each LC^3 system. As these systems do not contain any additional aluminates, the effect of the additional aluminates sourced from metakaolin can be decoupled from the contribution of the filler effect alone. The details of the mixtures are shown in Table 6-3. The water-to-binder ratio (w/b) was fixed at 0.4 by mass, for all systems.

Table 6-3: Mixture proportions of OPC, LC³-50 and OPC + fLS systems.

Mixture	OPC (%)	MK (%)	LS (%)	fLS (%)	Added Gypsum (%)	Added SO$_3$ (%)	Total SO$_3$ (%)[B]	w/c	w/b	SSA (m^2/g)
OPC	100	0.0	0.0	0.0	0.0	0.0	2.45	0.40	0.40	1.41
LC³-50 MK95	55-G	30.0	15.0	0.0	G (0 to 7)	0.0 to 3.26	1.34 to 4.43	0.73[A]	0.40	5.36
LC³-50 MK71	55-G	22.5	22.5	0.0	G (1.2)	0.56	1.87	0.73[A]	0.40	4.62
LC³-50 MK63	55-G	20.0	25.0	0.0	G (0, 0.5, 1, 1.5)	0.0 to 0.70	1.34 to 2.01	0.73[A]	0.40	4.37
LC³-50 MK47	55-G	15.0	30.0	0.0	G (0.85)	0.40	1.72	0.73[A]	0.40	3.88
LC³-50 MK40	55-G	12.6	32.4	0.0	G (0, 0.4, 0.8, 1)	0.0 to 0.47	1.34 to 1.79	0.73[A]	0.40	3.64
LC³-50 MK20	55-G	6.3	38.7	0.0	G (0.35)	0.16	1.50	0.73[A]	0.40	3.02
OPC-fLS SSA MK95	47.7	0.0	0.0	52.3	0.0	0.0	1.17	0.84	0.40	5.36
OPC-fLS SSA MK63	60.8	0.0	0.0	39.2	0.0	0.0	1.49	0.66	0.40	4.37
OPC-fLS SSA MK40	70.5	0.0	0.0	29.5	0.0	0.0	1.72	0.57	0.40	3.64

[A]: Value of w/c computed considering an OPC content of 55%. The value will vary as the concentration of added gypsum is increased.

[B]: Computed considering the SO$_3$ content of OPC measured as calcium sulfate minerals by QXRD and the OPC fractions given in this table.

6.2.3 Experimental methods

The heat evolution was measured in a TAM Air isothermal calorimeter at 20ºC for up to 7 days. Paste samples were mixed with a high shear mixer at 1600 rpm for two minutes, 10 g of paste was placed in a glass ampoule, sealed and introduced in the calorimeter. The onset of the aluminate peak was identified using the heat flow derivative, as shown in Figure 6-2 left.

To separate the heat flow from the aluminate reaction, the heat evolution from the same systems were measured, but with an extra 5% of gypsum to retard the aluminate peak and give the full shape of the alite peak, which was then subtracted from the overall curves, as shown in Figure 6-2 right for an LC³ system. The area associated with the aluminate peak was computed as the difference in total heat of the original mixture and that of the over sulfated system, between the maximum of the alite peak and 24 hours, as this was the time when the ettringite content was measured by XRD. Furthermore, in-situ XRD measurements showed that in all cases, the maximum amount of ettringite formed was reached before this time.

X-ray diffraction (XRD) measurements were carried out on freshly cut slices of hardened paste at 24 hours of hydration to determine the amounts of ettringite and AFm formed after the aluminate peak. Rietveld refinement was conducted using the HighScore Plus v4.8 software. The slices were analyzed in a Bragg-Brentano configuration in a PANalytical X'pert pro diffractometer working at 45 kV and 40 mA with a copper source. A 1/2º soller slit was used, and scans were acquired between 7 and 70º 2θ in 14 min, equivalent to a step size of 0.0167º 2θ. The external standard method was used to compute the K-factor of the device and account for the amorphous phases present [21]. A scan of a rutile standard was acquired in the same conditions after the experiments for this purpose.
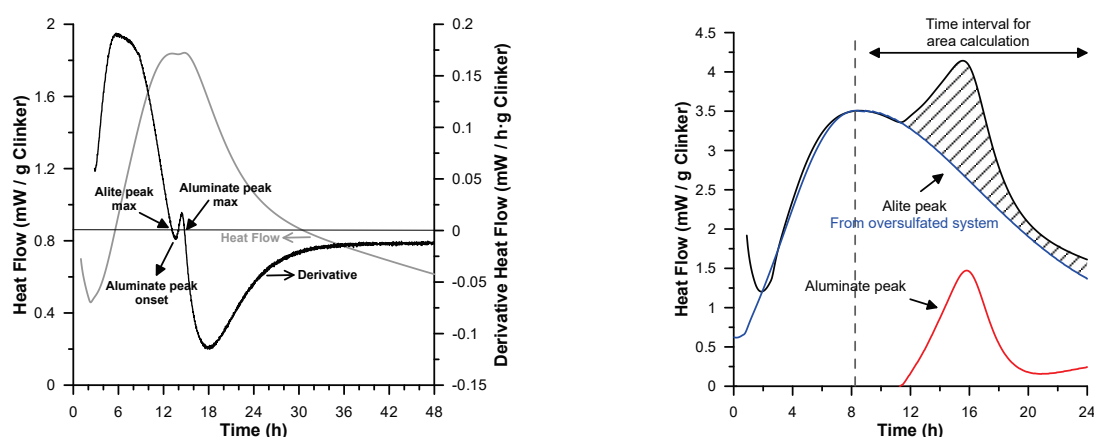
Figure 6-2: Identification of the aluminate peak onset using the derivative of the heat flow (left) and decoupling procedure applied to compute the aluminate peak area, shown as an example in the case of LC^3-50 MK95 (right).

For in-situ XRD experiments, paste specimens were prepared in the same manner as the isothermal calorimetry samples. In this case, a 1º soller slit was used. The 14 min scans were collected every 30 min up to 48 hours of hydration. The paste samples were mounted on a disc-shaped sample holder, and covered with a 12.7 µm thick Kapton film that was secured on top with a ring. The temperature was controlled at the base of the sample holder with a Peltier stage and kept constant at 20ºC.

6.3   Results and discussion

6.3.1   Early hydration of Portland cement

The heat flow curve for the OPC used in this study is shown in Figure 6-3. The main kinetic events related to the alite and aluminate reactions are highlighted. Previous studies have shown that C_3S dissolves quickly during the acceleration period of the alite reaction. In parallel, during the alite peak, ettringite is precipitated continuously and consequently the gypsum content decreases. In addition, sulfate becomes adsorbed on C-S-H [17]. When the solid gypsum is depleted from the system, there is an increase in slope of the heat evolution. This leads to the second (aluminate) peak, which is linked to an accelerated formation of ettringite during this period (second ettringite formation as described in [17,22]), associated with a higher rate of C_3A dissolution.
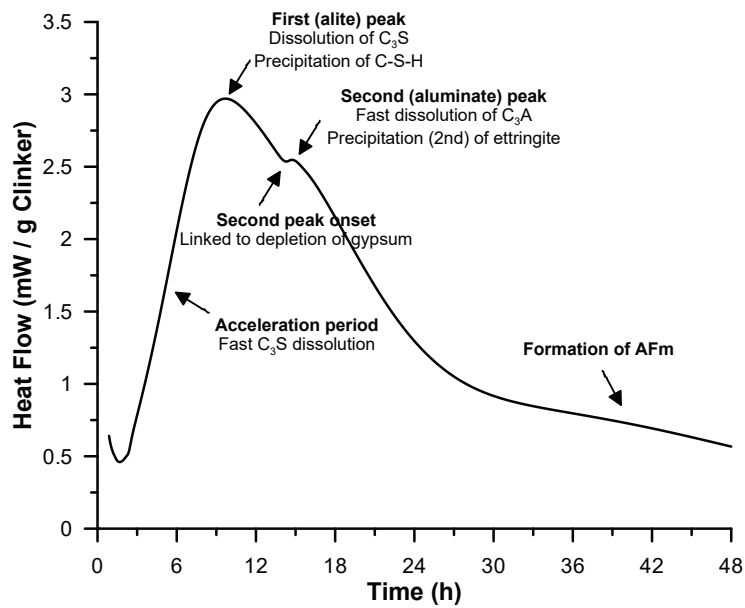
Figure 6-3: Heat flow curve of OPC highlighting the main hydration events during the first 24 hours.

6.3.2 Early hydration in LC³ systems

Figure 6-4 shows the calorimetry results for LC³-50 MK95 systems compared to OPC, normalized per gram of clinker. A significant acceleration (time shift) and enhancement (height) of the aluminate reaction is observed in all LC³ systems as compared to the reference OPC. For the system without additional gypsum added (LC³-50 0% Add. Gypsum), it is observed that the enhanced aluminate peak is almost super imposed on the alite peak, leading to a situation close to undersulfation.

The addition of 1 to 2 percent of additional gypsum leads to a situation where the aluminate peak is delayed and the alite and aluminate peaks are separated similar to the pattern observed in OPC. As the aluminate peak shifts to the right, it becomes lower and broader.

In addition, a strong acceleration and enhancement of the alite (first) peak is also observed in all LC³ systems, which is linked to the increased shear rate between particles and the surface provided by the addition of limestone and metakaolin [18]. The filler contribution of limestone and metakaolin in LC³ appears to be in-dependent of the gypsum addition. Other LC³ systems studied exhibit the same behavior as the LC³-50 MK95 systems shown in Figure 4.

The incorporation of metakaolin provides another source of aluminum to the system in addition to C_3A. In previous studies, it has been suggested that the intensity of the aluminate peak in LC³ is linked to the amount of metakaolin in the system [23]. However, this correlation is not systematic as seen in Figure 6-5. The calo-rimetry curves for LC³ systems with pure (95%) metakaolin and a calcined clay with only 50% metakaolin content are compared. By deconvoluting the calorimetry curves, it was seen that the total heat associated with the aluminate peak differs by less than 5% between the two systems, and is actually slightly higher in the system with lower metakaolin content. This further indicates that aluminate from the metakaolin does not explain the observed changes in the aluminate peak.
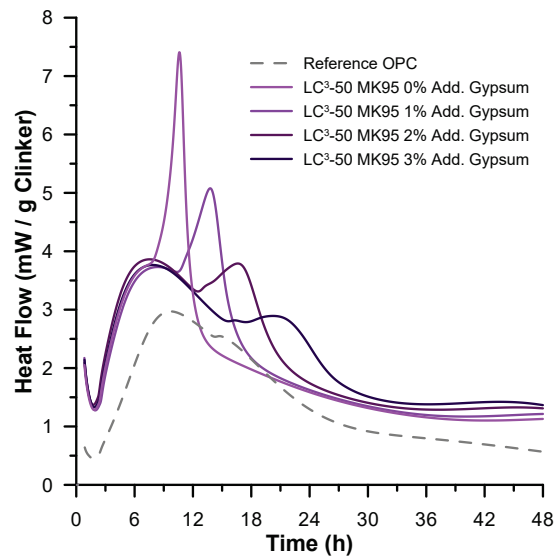
Figure 6-4: Heat flow of LC³-50 MK95 systems with different amounts of gypsum addition.

The system which has the higher SSA clay (50% metakaolin content) shows more acceleration and enhancement of the alite peak, related to an increased filler effect of the clay fraction. Simultaneously, this system exhibits more acceleration of the aluminate reaction. This suggests that the filler effect in LC³ due to the incorporation of fine clay leading to the acceleration of the C_3S reaction, might be linked to the acceleration of the aluminate peak (i.e., gypsum depletion). Furthermore, this suggests that the degree of reaction of C_3S (and consequently, of C-S-H precipitation) and the onset time of the aluminate peak are related.
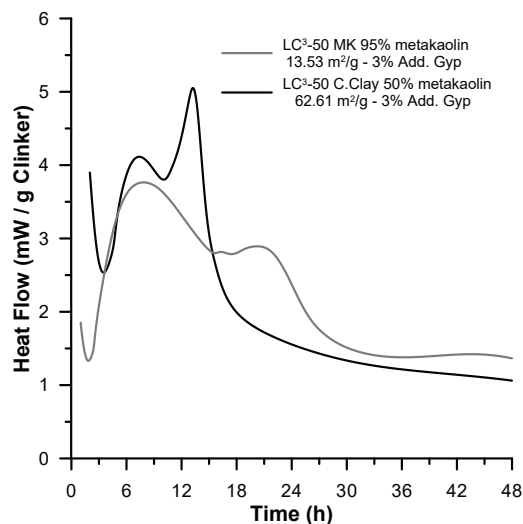
Figure 6-5: Heat flow of LC³-50 blends incorporating fine calcined clay with 50% metakaolin and the MK material (95% metakaolin).

6.3.3 Early hydration in OPC + limestone systems

To decouple the possible contribution of the additional aluminates phases from the filler effect, additional experiments were carried out in systems of OPC with fine limestone. In these cases, there are no additional aluminate phases in the system. As shown in Table 6-3, the SSA of these systems was matched to each of the reference LC^3-50 systems by varying the OPC and fLS proportions. The isothermal calorimetry results are shown in Figure 6-6. As observed, the same acceleration and enhancement of the aluminate peak seen in LC^3 is observed in these systems. Moreover, the degree of acceleration of the aluminate reaction is related to the observed enhancement of the alite peak, in agreement with the results on LC^3-50 blends shown in Figure 6-5.

The effect on the aluminate peak has been observed in OPC + limestone and OPC + quartz systems [24] and those with silica fume [25]. Thus, the acceleration of the aluminate peak appears to be linked to the amount of surface area supplied to the system, rather than the aluminum content of the added material.
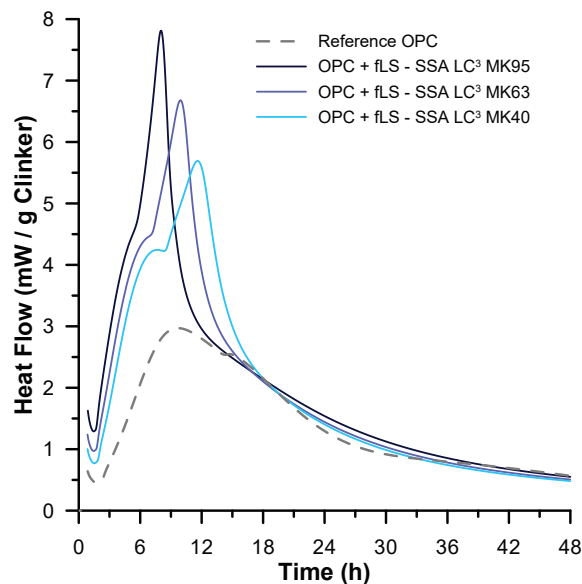
Figure 6-6: Heat flow of OPC + fLS systems with matched SSA to the different LC^3-50 blends studied.

6.3.4 Mechanism relating the rate of C_3S reaction and the occurrence of the aluminate peak

The results indicate that the effects of SCMs on the aluminate peak are mostly explained by the specific surface area of the material, as seen in the results for OPC+fLS, rather than its chemical composition (aluminum content). As the filler effect influences hydration by enhancing/accelerating the hydration of C_3S and consequently, the rate of C-S-H precipitation [18], a relationship between C-S-H precipitation rate and sulfate depletion can be inferred.

The adsorption of sulfate by C-S-H is proportional to the sulfate concentration in solution [26]; up to the depletion of solid gypsum in the system this is high. Quennoz [17] and Berodier [27] showed that a significant amount of sulfate can be detected by microanalysis in the C-S-H. They reported S/Ca ratios ranging from 0.04 to 0.1 prior to the aluminate peak. While neither of these studies was able to measure the sulfate content in C-S-H before 10 hours due to the low quantity of hydration products available, both clearly show that the S/Ca ratio of C-S-H remains high until the onset of the aluminate peak.

The acceleration of the silicate reaction leads to a faster precipitation of C-S-H, more C-S-H formation implies more sulfate adsorbed, and therefore, the earlier the gypsum depletion point will be reached. The aluminate peak is triggered by the depletion of sulfate from the solution, which drops quickly (by about 20 times) after the solid gypsum is consumed. Before gypsum depletion, the sulfate concertation is determined by the gypsum solubility, while after no gypsum or other sulfate sources are available, the sulfate concentration is limited by its equilibrium with ettringite [28].

The drop in the sulfate concentration in solution causes an acceleration of the C_3A dissolution while simultaneously sulfate ions are desorbed from the C-S-H, becoming available to react during a second formation of ettringite (aluminate peak).

The total heat released during the acceleration period, before gypsum depletion, can be used as an estimate of the amount of C-S-H precipitated. Figure 6-7 shows the relationship between heat release at the time of the aluminate peak onset and the SO_3 content for all the systems studied; this shows a clear linear relationship as expected.

Another aspect to notice is that the regression shown in Figure 6-7 crosses the SO_3 axis at a positive value. This indicates that there is some SO_3 consumption, in addition to the sorption on the C-S-H. This can be attributed to the sulfate associated with the ettringite precipitation before the aluminate peak, as observed in the in-situ XRD experiments. The total heat shown in Figure 6-7 also includes this heat associated with ettringite precipitation before the aluminate peak. This amount is similar among the different types of systems studied.

Figure 6-7: Heat released at the aluminate peak (A.P.) onset versus gypsum content of the system. P-value of regression $5.89 \cdot 10^{-14}$.
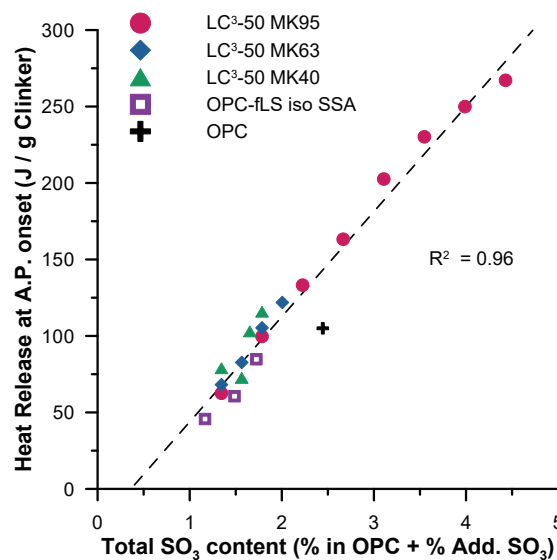
6.3.5 Hydration products of the aluminate reaction in LC³

The in-situ XRD measurements, Figure 6-8 for the LC³-50 MK-95 system, indicate that the main phase formed during the aluminate peak is ettringite, in agreement with previous studies on OPC [18,29]. It can be observed that ettringite is detected from the beginning of the reaction. It has been previously observed that the amount of metakaolin does not influence the ettringite content in LC³ systems, being rather determined by the added sulfate content [23]. After the maximum amount of ettringite is reached, hemicarboaluminate (Hc) is formed.
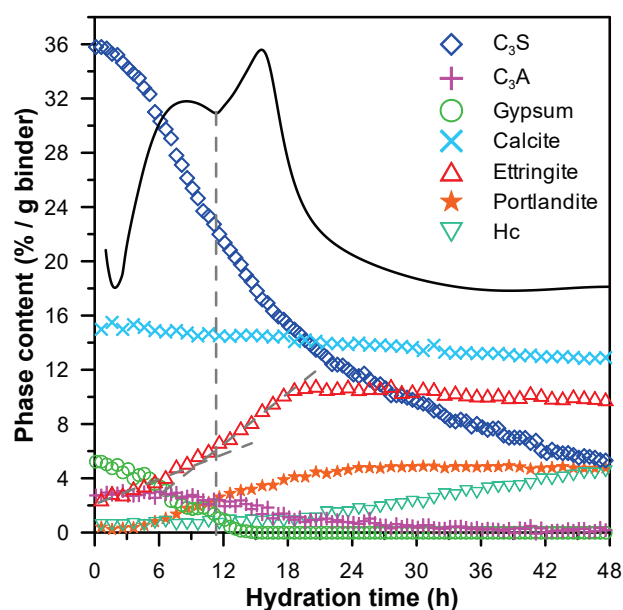
Figure 6-8: In-situ XRD results showing the content of the main phases participating in the reaction during the first 48 hours of hydration for LC³-50 MK-95.

Solid line indicates the associated heat flow curve, and dashed lines indicate the aluminate peak onset and provide an eye-guide for the change in ettringite precipitation rate.

The deconvolution of the calorimetry curves was done in all systems in order to compare the computed heat release associated with the aluminate peak with the amount of ettringite (and AFm phases) formed at 24 hours measured on fresh slices by XRD (Figure 6-9). In the case of blended cements, the precipitation of an AFm phase (hemicarboaluminate) was observed before 24 hours. As it was not possible to isolate the heat release associated to the formation of ettringite and AFm during this period, they were considered together.

The heat evolved in the aluminate peak is directly related to the amounts of aluminate phases formed, Figure 6-10. Here, the ettringite precipitated during the alite peak is also included, but it is not accounted for in the heat released during the aluminate peak. As the in-situ XRD results show, this amount is similar among the different system studied, and thus the heat release during the aluminate peak can still be related to the overall ettringite precipitated.
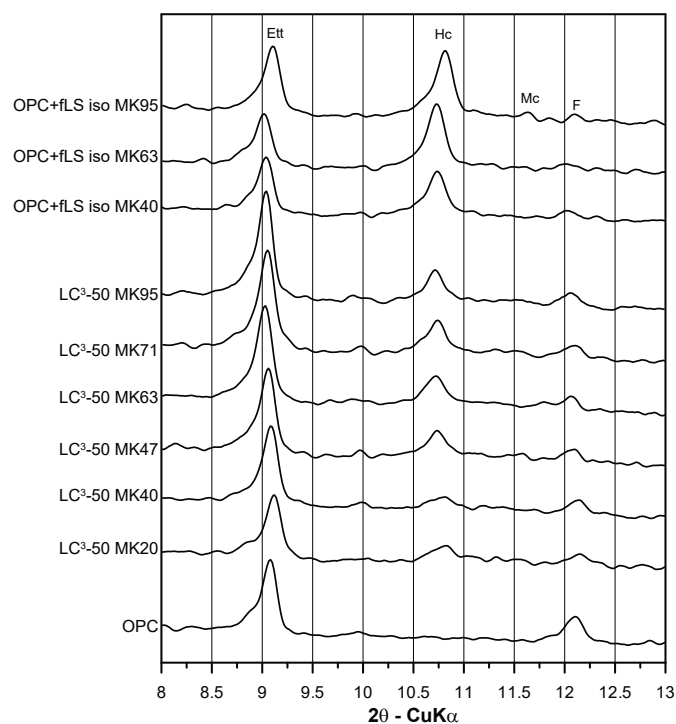
Figure 6-9: XRD patterns at 24 hours of hydration collected from fresh slices.

Ett = ettringite; Hc = hemicarboaluminate; Mc = monocarboaluminate; F = ferrite.
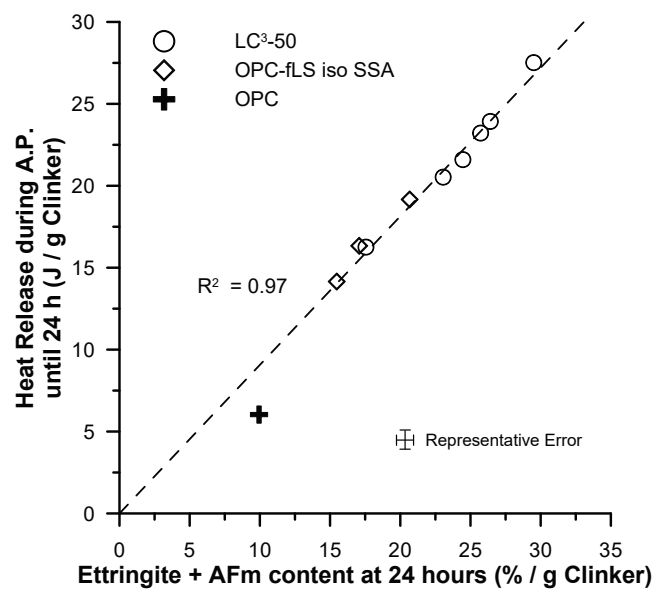
Figure 6-10: Ettringite (AFt) and AFm (Hc + Mc) content measured at 24 hours versus computed heat associated to the aluminate peak (A.P.). P-value of regression $8.67 \cdot 10^{-8}$.

Although the peak is enhanced even in the systems with only limestone, where all the alumina must come from the clinker component, the heats for the systems with metakaolin are generally higher indicating some contribution from the MK reaction to this peak. By comparison of Figure 6-4 and Figure 6-6, it can be seen that more acceleration of the aluminate peak can be achieved with the incorporation of limestone alone as compared to LC^3 for the same amount of surface area added. This could be explained by limestone being a better surface for C-S-H nucleation [18], in agreement with the enhancements observed in the alite peaks in both systems. On the other hand, more ettringite is formed in the LC^3 system, even considering that the second formation of ettringite occurs later. In addition, the replacement level of OPC by fLS are lower compared to LC^3-50, thus, more C_3A is available. As aluminates are required to form ettringite, these can be partially sourced from metakaolin. Further experiments on LC^3 with high gypsum contents showed that the precipitation of ettringite can be sustained by the aluminates from metakaolin well beyond the maximum availability of C_3A.

Figure 6-11 shows schematically the mechanisms behind the sulfate balance in OPC and blended cements, considering the contribution of the filler effect and the adsorption of sulfate into C-S-H.
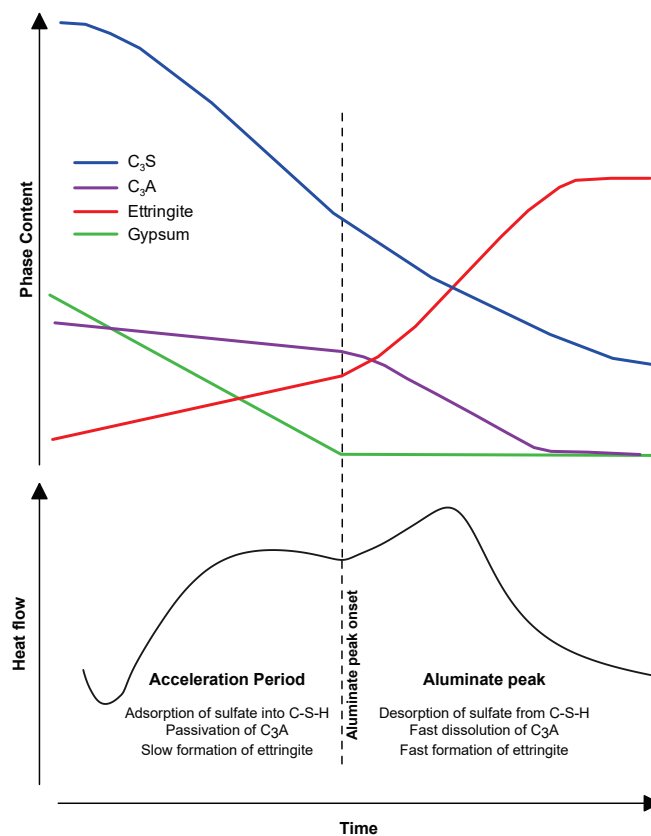
Figure 6-11: Diagram of proposed mechanism involving sulfate adsorption on C-S-H during the acceleration period. Expected phase assemblage (top) and heat flow profile (bottom).

6.4   Conclusions

The results presented here relate the filler effects of SCMs to the calcium sulfate addition required for proper sulfation. The adsorption of sulfate by C-S-H is the important factor linking these two things.

Based on the results presented, the following conclusions can be drawn:

1. Supplementary cementitious materials can have a significant impact on the sulfate balance of blended cements due to their filler effect. The impact is related to additional surface area, rather than the chemical composition of the material. In particular, the aluminate content of calcined clay does not influence the sulfate requirement for proper sulfation.

2. Sulfate ions are adsorbed in the C-S-H precipitated due to the ongoing hydration of C_3S. The increase in the rate of reaction of C_3S due to the filler effect accelerates the precipitation rate of C-S-H, increasing the amount of sulfate adsorbed. The depletion of gypsum occurs earlier and consequently the aluminate peak shifts left.

3. The amount of heat released at the onset of the aluminate peak is linearly correlated with the sulfate content of the system for a given binder composition. This means that the amount of C-S-H required to deplete sulfate linearly increases with the initial sulfate content of the system.

4. After gypsum is depleted, sulfate is desorbed from C-S-H following the decrease in the concentration in the pore solution, and becomes available to precipitate additional ettringite. The heat release during the aluminate peak can be solely explained by the precipitation of ettringite and AFm.

6.5   References

[1]   B. Lothenbach, K. Scrivener, R.D. Hooton, Supplementary cementitious materials, Cem. Concr. Res. 41 (2011) 1244–1256. doi:10.1016/j.cemconres.2010.12.001.

[2]   K. Scrivener, F. Martirena, S. Bishnoi, S. Maity, Calcined clay limestone cements (LC3), Cem. Concr. Res. (2017) 1–8. doi:10.1016/j.cemconres.2017.08.017.

[3]   M. Antoni, Investigation of cement substitution by combined addition of calcined clays and limestone, École Polytechnique Fédérale de Lausanne, 2011.

[4]   K.L. Scrivener, F. Avet, H. Maraghechi, F. Zunino, J. Ston, A. Favier, et al., Impacting factors and properties of Limestone Calcined Clay Cements (LC3), Green Mater. (2018). doi:https://doi.org/10.1680/jgrma.18.00029.

[5]   M. Antoni, J. Rossen, F. Martirena, K. Scrivener, Cement substitution by a combination of metakaolin and limestone, Cem. Concr. Res. 42 (2012) 1579–1589. doi:10.1016/j.cemconres.2012.09.006.

[6]   I. De la Varga, J. Castro, D.P. Bentz, F. Zunino, J. Weiss, Evaluating the hydration of high volume fly ash mixtures using chemically inert fillers, Constr. Build. Mater. 161 (2018) 221–228. doi:10.1016/j.conbuildmat.2017.11.132.

[7]   M.D. Niemuth, L. Barcelo, J. Weiss, Effect of Fly Ash on Optimum Sulfate Levels Measured Using Heat and Strength at Early Ages, Adv. Civ. Eng. Mater. 1 (2012) 20120012. doi:10.1520/acem20120012.

[8]   W. Lerch, The influence of gypsum on the hydration and properties of portland cement pastes, Am. Soc. Test. Mater. J. (1946).

[9]   RILEM T.C., The hydration of tricalcium aluminate and tetracalcium aluminoferrite in the presence of calcium sulfate, Mater. Struct. 19 (1986) 137–147. doi:10.1007/BF02481758.

[10]   A. Quennoz, K.L. Scrivener, Hydration of C3A–gypsum systems, Cem. Concr. Res. 42 (2012) 1032–1041. doi:10.1016/j.cemconres.2012.04.005.

[11]   ASTM C563, Standard Guide for Approximation of Optimum SO3 in Hydraulic Cement, 2018. doi:10.1520/C0563-18.2.

[12]   W. Corstanje, H.N. Stevels, J.M. Stevels, Hydration reactions in pastes C3S+C3A+CaSO4 2aq + water at 25°C, Cem. Concr. Res. 4 (1974) 417–431.

[13]   M. Collepardi, G. Baldini, M. Pauri, Tricalcium aluminate hydration in the presence of lime, gypsum or sodium sulfate, Cem. Concr. Res. 8 (1978) 571–580.

[14]   H. Minard, S. Garrault, L. Regnaud, A. Nonat, Mechanisms and parameters controlling the tricalcium aluminate reactivity in the presence of gypsum, Cem. Concr. Res. 37 (2007) 1418–1426. doi:10.1016/j.cemconres.2007.06.001.

[15]   R.J. Myers, G. Geng, J. Li, E.D. Rodríguez, J. Ha, P. Kidkhunthod, et al., Role of adsorption phenomena in cubic tricalcium aluminate dissolution, Langmuir. 33 (2016) 45–55. doi:10.1021/acs.langmuir.6b03474.

[16]   G. Geng, R.J. Myers, Y.-S. Yu, D.A. Shapiro, R. Winarski, P.E. Levitz, et al., Synchrotron X-ray nanotomographic and spectromicroscopic study of the tricalcium aluminate hydration in the presence of gypsum, Cem. Concr. Res. 111 (2018) 130–137. doi:10.1016/j.cemconres.2018.06.002.

[17]   A. Quennoz, K.L. Scrivener, Interactions between alite and C3A-gypsum hydrations in model cements, Cem. Concr. Res. 44 (2013) 46–54. doi:10.1016/j.cemconres.2012.10.018.

[18]   E. Berodier, K. Scrivener, Understanding the filler effect on the nucleation and growth of C-S-H, J. Am. Ceram. Soc. 97 (2014) 3764–3773. doi:10.1111/jace.13177.

[19]   E. Gallucci, P. Mathur, K. Scrivener, Microstructural development of early age hydration shells around cement grains, Cem. Concr. Res. 40 (2010) 4–13. doi:10.1016/j.cemconres.2009.09.015.

[20]   K. Scrivener, R. Snellings, B. Lothenbach, A Practical Guide to Microstructural Analysis of Cementitious Materials, (2016) 540. doi:10.7693/wl20150205.

[21]   B.H. O'Connor, M.D. Raven, Application of the Rietveld Refinement Procedure in Assaying Powdered Mixtures, Powder Diffr. 3 (1988) 2–6. doi:10.1017/S0885715600013026.

[22]   K.L. Scrivener, Development of the microstructure during the hydration of Portland cement, University of London, 1984.

[23]   F. Avet, K. Scrivener, Investigation of the calcined kaolinite content on the hydration of Limestone Calcined Clay Cement (LC3), Cem. Concr. Res. 107 (2018) 124–135. doi:10.1016/j.cemconres.2018.02.016.

[24]   D.P. Bentz, C.F. Ferraris, S.Z. Jones, D. Lootens, F. Zunino, Limestone and Silica Powder Replacements for Cement: Early-Age Performance, Cem. Concr. Compos. 78 (2017) 43–56. doi:10.1016/j.cemconcomp.2017.01.001.

[25]   F. Lavergne, R. Belhadi, J. Carriat, A. Ben Fraj, Effect of nano-silica particles on the hydration, the rheology and the strength development of a blended cement paste, Cem. Concr. Compos. 95 (2019) 42–55. doi:10.1016/j.cemconcomp.2018.10.007.

[26]   R. Barbarulo, H. Peycelon, S. Leclercq, Chemical equilibria between C-S-H and ettringite, at 20 and 85 °C, Cem. Concr. Res. 37 (2007) 1176–1181. doi:10.1016/j.cemconres.2007.04.013.

[27]   E. Berodier, Impact of the supplementary cementitious materials on the kinetics and microstructural development of

cement hydration, EPFL Thesis 6417, 2015.

[28]   A. Vollpracht, B. Lothenbach, R. Snellings, J. Haufe, The pore solution of blended cements: a review, Mater. Struct. Constr. 49 (2016) 3341–3367. doi:10.1617/s11527-015-0724-1.

[29]   A. Quennoz, Hydration of C3A with Calcium Sulfate Alone and in the Presence of Calcium Silicate, EPFL Thesis 5035, 2011.

Chapter 7   Sulfate balance in C_3S/C_3A systems

Note: This chapter is based on an article published in a peer reviewed journal.

Franco Zunino, Karen Scrivener

Contribution of the doctoral candidate: Writing of the first manuscript draft, experimental design, conduction of the experiments.

Understanding the sulfate balance mechanism of cement is needed for an effective use of sustainable blended cements. Pure phase systems allow to study the interaction between sulfate and each of the phases involved in early age hydration separately. This paper explores the effect of different factors on sulfate requirement in C_3S/C_3A systems. It was observed that reaction rates of both C_3S and C_3A have an influence on the overall sulfate balance, as they affect the amount of sulfate adsorbed on C-S-H and the amount of ettringite formed, respectively. Furthermore, the type of sulfate source used (gypsum or hemihydrate) can also significantly change the position of the aluminate peak for the same total sulfate in the system.

Contents

7.1 Introduction

Calcium sulfate is added to clinker during grinding in order to control the reaction of tricalcium aluminate (C_3A) and prevent flash setting [1]. In the presence of gypsum, the hydration reaction of C_3A shifts from the precipitation of platey calcium aluminate hydrates and ettringite is formed [2]. As more gypsum is incorporated in the system, more retardation of the C_3A reaction can be achieved [3]. If the level of sulfate addition is insufficient, the aluminate peak may occur before the tricalcium silicate (C_3S) peak and the later becomes smaller and broader with lower degrees of hydration and strength at early ages [4,5]. The optimum amount of sulfate required is usually determined on the basis of compressive strength tests at 1 or 28 days.

The widespread adoption of blended cements necessitates better understanding of the sulfate requirement for these systems. Recently, we showed that the surface area provided by the addition of supplementary cementitious materials (SCMs), rather than the amount of alumina in the anhydrous blend, explains the increased sulfate requirement of limestone calcined clay cement (LC^3) [6]. Sulfate is adsorbed in C-S-H during the acceleration part of the C_3S peak. A faster rate of C-S-H precipitation due to the "filler effect" consequently leads to an earlier depletion of solid gypsum. After this point, sulfate is desorbed from C-S-H and is available to react with aluminates to form ettringite. A linear relationship was found between the SO_3 content of the system and the heat released until the onset of the aluminate peak.

Model mixtures of pure C_3S and C_3A powders allow the effects of the finenesses of the different phases to be studied. By adjusting the fineness of each pure phase independently, the effect of the rate of reaction of C_3S and C_3A on the sulfate balance of the overall system can be studied. In addition, C_3S/C_3A systems behave similarly to OPC in terms of sulfate balance. More gypsum leads to a retardation of the onset of the aluminate peak, and C-S-H precipitation influences the balance. Quennoz et al. [7] observed significant differences in the time of gypsum depletion between pure C_3A and C_3S/C_3A systems showing that C-S-H also participates in the sulfate balance of these systems, as in the case of OPC and blended cements [8].

The mechanism by which gypsum slows down the reaction of C_3A has been extensively studied, but is still a matter of debate. Recent studies support the idea of adsorption of sulfate or sulfate complexes in C_3A surface as the most tenable mechanism explaining the observed retardation [9–11]. The common textbook view that ettringite forms a diffusion barrier is not supported by the evidence [12,13].

In addition to the well known effect of sulfate on C_3A, an enhancement effect of gypsum over alite hydration has also been reported [5,14]. Mota et al. proposed that sulfate adsorbed in the C-S-H needles can modify the growth process by promoting repulsion between the growing needles [14]. Gunay et al. also concluded that the adsorption of calcium sulfate on C-S-H modifies the nucleation and growth process [15], in agreement with previous findings of Bentur [16] that showed an increase in the amount of C-S-H formed.

In this study, C_3S/C_3A pure phase systems are used to assess the influence of different mixture design and kinetic factors on the sulfate balance of the system. In particular, the influence of the C_3A and C_3S rate of reaction are explored, along with the dissolution rate of the sulfate source used. The heat release at the onset of the aluminate peak versus the SO_3 content of the system is revisited, and an explanation of this trend based on measurable properties of the system is given.

7.2 Materials and methods

7.2.1 Synthesis of pure phases

The synthesis of pure tricalcium silicate (C_3S) and tricalcium aluminate (C_3A) was conducted following the procedure described in [17] for the production of large amounts of material. For the synthesis of C_3S, calcium carbonate (VWR) and fumed silica (0.2 μm, Sigma-Aldrich) were used. The sintering temperature was maintained at 1600ºC for 4 hours, and the samples were air quenched subsequently. The result was triclinic (T_1) C_3S with a free lime content below 0.5% in all batches, as quantified by Rietveld refinement.

For the synthesis of C_3A, the same calcium carbonate as for C_3S was combined with aluminum oxide (Al_2O_3, Merck), keeping the CaO content of the raw mix fixed at 62.5% (slightly above the stoichiometric amount) to prevent the formation of mayenite ($C_{12}A_7$). The sintering temperature was maintained at 1450ºC for 4 hours, and the samples were air quenched subsequently. As a result, cubic C_3A was obtained, with free lime content of 0.4-0.7% measured by Rietveld refinement in the different batches. A representative diffractogram of both materials is shown in Figure 7-1.
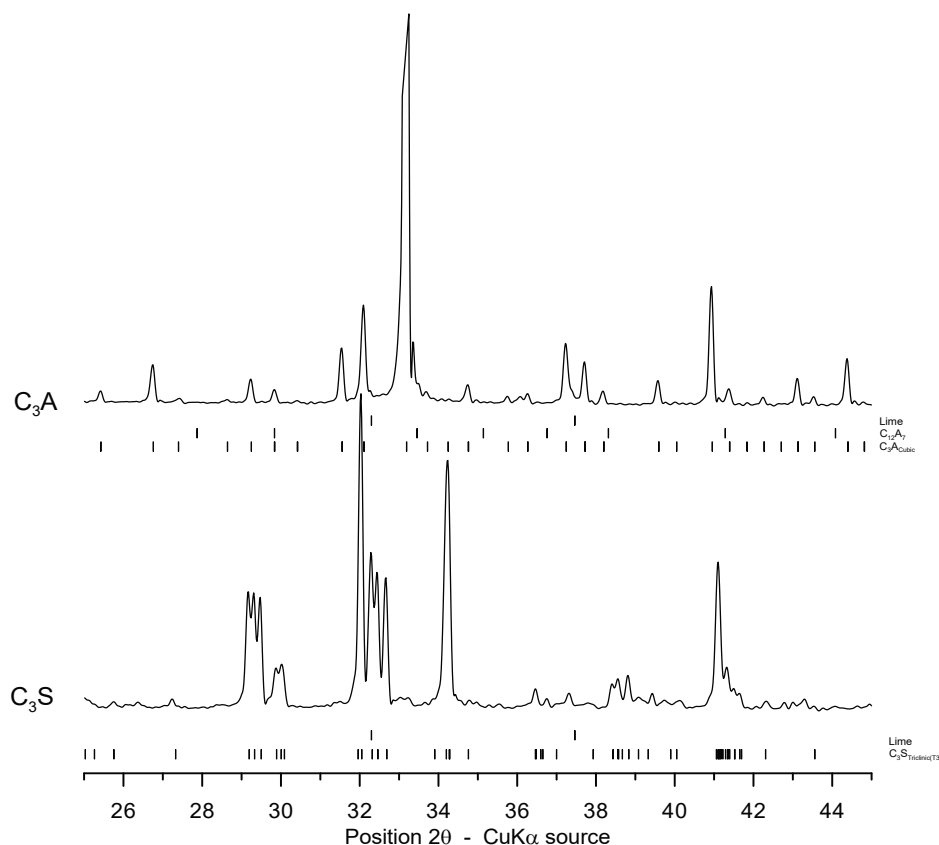
Figure 7-1: Diffractograms of the pure triclinic C_3S and cubic C_3A synthetized in this study.

7.2.2 Raw material characterization

After synthesis, the pure phases were ground in a concentric disc mill in batches of 100 g. For the production of coarse C_3S and C_3A, 30 seconds of grinding was applied twice. The grinding rounds were kept short to

prevent excessive heating of the material. In the case of fine C_3S and C_3A, the process of grinding for 30 seconds was repeated 6 times. Subsequently, particle size distribution was measured by laser diffraction using isopropanol as dispersant, Figure 7-2.
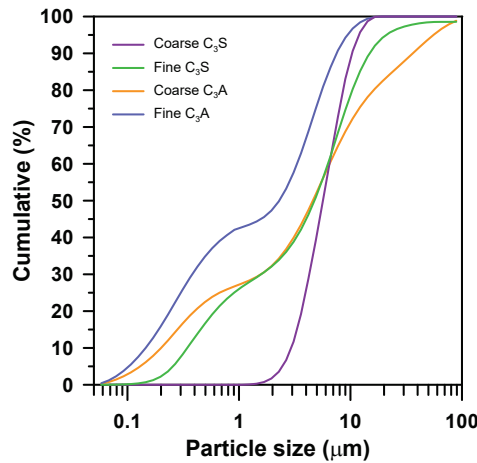
Figure 7-2: Particle size distribution of the pure phase materials used in this study.

The specific surface area (SSA) of each raw material was measured by nitrogen adsorption, using the BET method. In all cases, samples of around 1.5 g were degassed for 2 hours at 200ºC under a N_2 flux before the measurement. The specific gravity was measured using a helium pycnometer. The measured values of the raw powders are summarized in Table 7-1.

Table 7-1: Distribution values, span (width), specific surface area and specific gravity of raw materials.

	Coarse C_3S	Coarse C_3A	Fine C_3S	Fine C_3A
D_V90 (μm)	10.5	35.6	14.5	7.7
D_V50 (μm)	5.7	4.9	4.9	2.3
D_V10 (μm)	2.9	0.2	0.4	0.2
Span (-)	1.33	7.22	2.88	3.26
SSA (m^2/g)	1.09	1.03	2.87	4.53
Sp. Gravity (g/cm^3)	3.15	3.05	3.15	3.07

7.2.3 Mixture design and experimental methods

The base mixture was a pure C_3S system with a water to binder ratio of 0.5 by mass (1.570 w/s ratio by volume). From this reference, all other mixtures were prepared keeping constant the volumetric w/s ratio. For the C_3S/C_3A systems, a ratio of 92/8 by mass was selected, which is similar to the ratio found in many Portland cement clinkers. Mixtures were prepared by combining C_3S and C_3A and different amounts of gypsum ($CaSO_4 \cdot 2H_2O$, Merck precipitated 99% purity) or hemihydrate ($2CaSO_4 \cdot H_2O$, Acros 97% purity) as sources of sulfate. The sulfate source was incorporated by replacing part of the C_3S/C_3A mixture.

The heat evolution was measured in a TAM Air isothermal calorimeter at 20ºC for up to 6 days. Paste samples were mixed with a high shear mixer at 1600 rpm for two minutes, 10 g of paste was placed in a glass ampoule, sealed and introduced in the calorimeter.

For in-situ XRD experiments, paste specimens were prepared in the same manner as the isothermal calorimetry samples. The paste samples were mounted on a disc shaped sample holder, and covered with a 12.7 μm thick Kapton film which was secured on top with a ring. The temperature was controlled at the base of the sample holder with a Peltier stage and kept constant at 20ºC. The samples were analyzed in a Bragg-Brentano configuration in a PANalytical X'pert pro diffractometer working at 45 kV and 40 mA with a copper source. A 1º soller slit was used, and scans were acquired between 7 and 70º 2θ in 14 min, equivalent to a step size of 0.0167º 2θ. The external standard method was used to compute the K-factor of the device and account for the amorphous phases present. The scans were collected every 30 min up to 24 hours of hydration. Rietveld refinement was conducted using the HighScore Plus v4.8 software.

7.3 Results and discussion

7.3.1 The effect of gypsum addition on C_3A and C_3S hydration

The influence on hydration kinetics of different additions of gypsum on the two C_3As studied (fine and coarse) are shown in Figure 7-3. As seen, the duration of the first stage of hydration (before the main peak), corresponding to the precipitation of ettringite, depends on the amount of gypsum added for the same C_3A, but also on the fineness of the material, in good agreement with previous studies [3]. In pure C_3A-gypsum systems, the observed peak corresponds to the transformation of ettringite to AFm, and is triggered by gypsum depletion from the system [7]. In the results presented, 30% gypsum addition to fine C_3A leads to a similar retardation of the peak as 20% addition to coarse C_3A. Finer C_3A is able to react faster with gypsum and therefore, there is an earlier depletion.

a)   b)
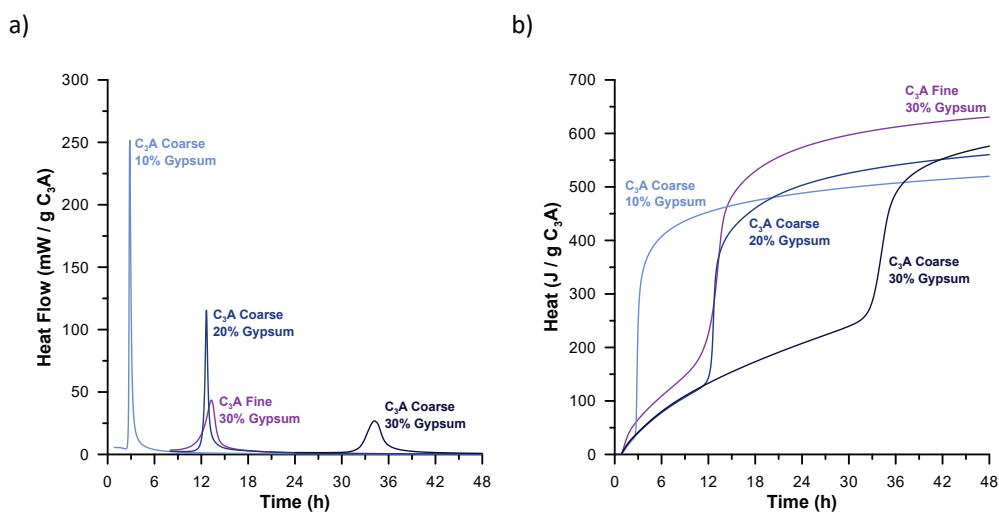
Figure 7-3: Heat flow (a) and total heat (b) of pure fine and coarse C_3A systems with different gypsum additions.

The effect of different gypsum additions on pure triclinic C_3S (fine and coarse) are shown in Figure 7-4. In this case, the amounts of gypsum added are much lower than the ones used in pure C_3A systems. It is observed that the induction period is slightly longer in the systems with gypsum as compared to pure C_3S. In addition, gypsum leads to an enhancement of the main peak of hydration for both particle sizes studied. These effects are observed even at low gypsum additions. After around 6 hours of hydration, the degree of hydration (DoH) of C_3S with gypsum addition is significantly higher than plain C_3S. Further discussion on the effect of gypsum addition on C_3S hydration is presented in section 7.3.9.
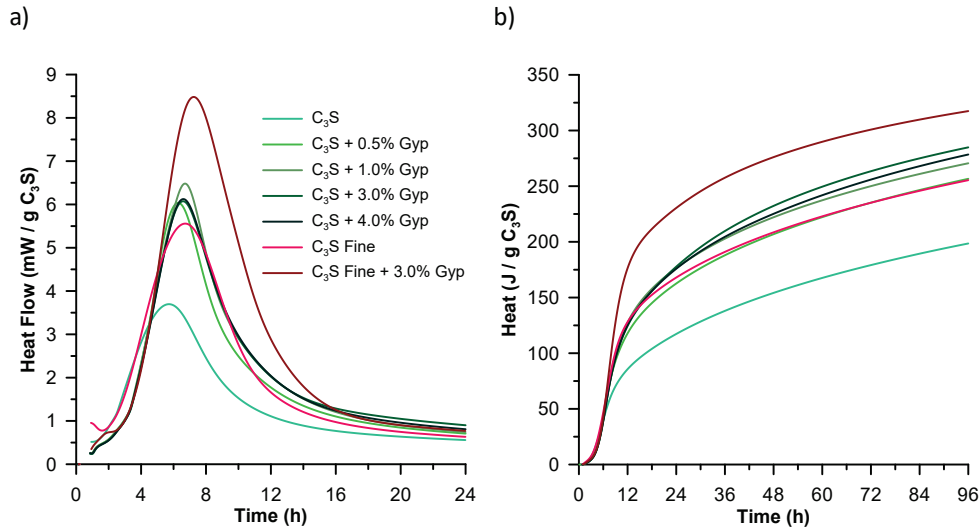
Figure 7-4: Heat flow (a) and total heat (b) of pure fine and coarse C_3S systems with different gypsum additions.

7.3.2 The effect of C_3A fineness on C_3S/C_3A systems

The influence of the C_3A fineness on the sulfate balance of C_3S/C_3A systems was studied by comparing the calorimetry curves of systems combining fine C_3S with either coarse or fine C_3A, and different levels of gypsum addition. As in the case of pure C_3A, the aluminate peak occurs after solid gypsum is depleted from the system. However, in this case it is associated with a second formation of ettringite, similar to that observed in OPC [5]. Figure 7-5 shows the heat flow and heat curves for fine C_3S mixed with coarse C_3A, while Figure 7-6 contains the results for fine C_3S mixed with fine C_3A systems.

In general, two main cases can be distinguished regarding the sulfate balance of the C_3S/C_3A systems: one where the aluminate peak occurs before the C_3S peak (undersulfated), characterized by a lower and broader C_3S peak following the aluminate peak, and others where the aluminate peak occurs after the C_3S one (properly sulfated), characterized by a higher and narrower C_3S peak preceding the aluminate one.

As in the case of pure C_3A systems (Figure 7-3) more gypsum is required to retard the aluminate peak in the systems with fine C_3A (Figure 7-6) as compared to coarse C_3A (Figure 7-5). In all cases, the C_3S peak is similar, thus the contribution of sulfate adsorption on C-S-H to gypsum depletion can be considered similar in systems with an aluminate peak occurring at a relatively similar hydration time (for example, $C_3S_{Fine}C_3A$ 3.0% gypsum compared to $C_3S_{Fine}C_3A_{Fine}$ 4.0% gypsum). This suggest that, in addition to sulfate adsorption on C-S-H, there

is another factor linked to the rate of reaction of C_3A itself that should be considered in the sulfate balance of the system.
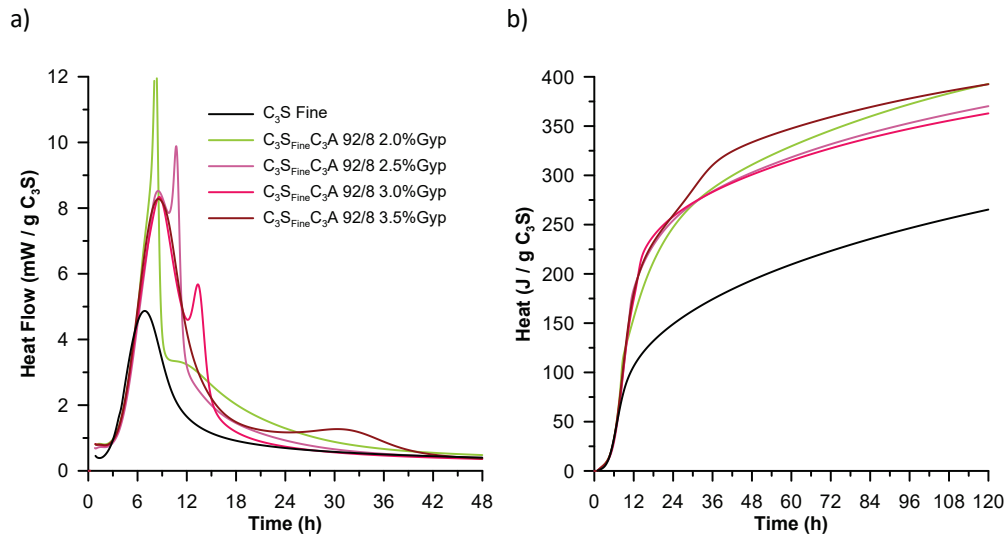
Figure 7-5: Heat flow (a) and total heat (b) of C_3S/C_3A systems 92/8 with coarse C_3A and different gypsum additions.
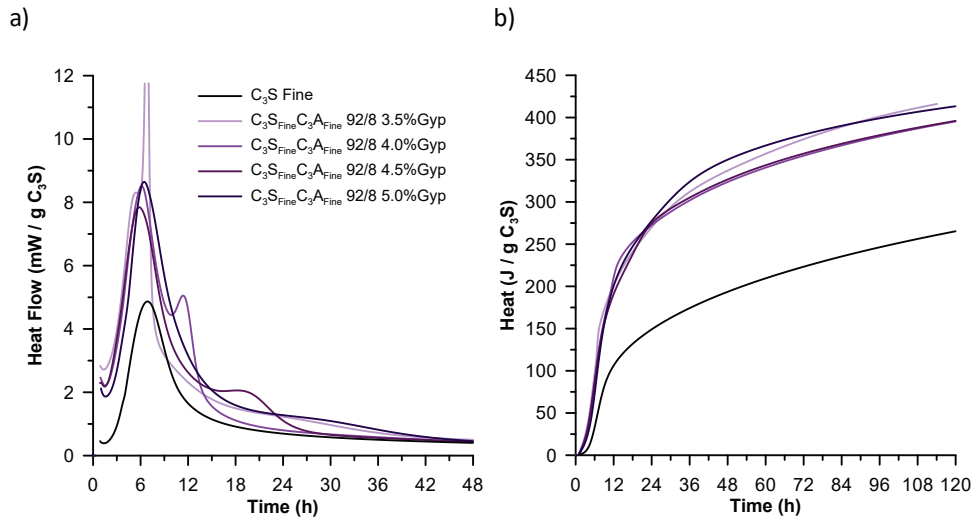
Figure 7-6: Heat flow (a) and total heat (b) of C_3S/C_3A systems 92/8 with fine C_3A and different gypsum additions.

7.3.3   The effect of C_3S fineness on C_3S/C_3A systems

The influence of the C_3S fineness on the sulfate balance of C_3S/C_3A systems was studied by comparing the calorimetry curves of systems combining fine and coarse C_3S with coarse C_3A (Figure 7-5 and Figure 7-7 respectively), and different amounts of gypsum. As observed, more retardation of the aluminate peak is observed in the systems with coarse C_3S for the same gypsum addition. As an example, the system with 3.0% gypsum has the maximum of the aluminate peak at around 14 hours in the fine C_3S system and 31 hours in

the coarse C$_3$S one. Similarly, 2.0% gypsum addition leads to an undersulfated system in the system with fine C$_3$S, while it is properly sulfated in the case of coarse C$_3$S. These differences are linked to the amount of sulfate that is adsorbed on C-S-H before the aluminate peak. Finer C$_3$S reacts faster, and therefore more C-S-H is precipitated before this point, increasing the amount of sulfate adsorbed and triggering and earlier depletion of solid gypsum.
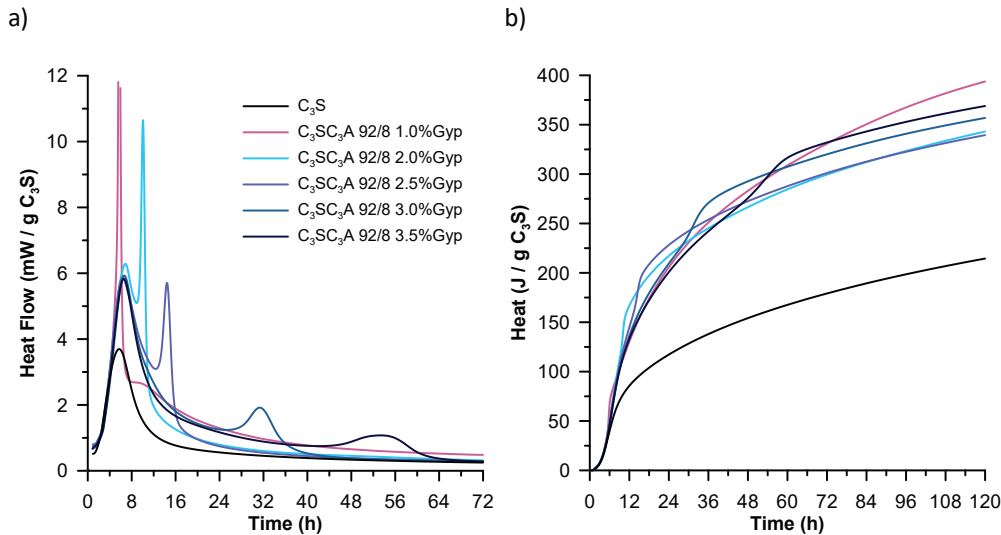
Figure 7-7: Heat flow (a) and total heat (b) of C$_3$S/C$_3$A systems 92/8 with coarse C$_3$S and C$_3$A, and different gypsum additions.

7.3.4   Heat release versus SO$_3$ content

Quennoz and Scrivener [5] showed that sulfate adsorption on C-S-H plays a major role in the sulfate balance of C$_3$S/C$_3$A systems. Recently, Zunino and Scrivener [6] showed that the sulfate balance can be affected by the incorporation of SCMs due to the increase in the rate of C-S-H precipitation by the filler. A linear correlation between the total SO$_3$ content of the system and the heat release up to the onset of the aluminate peak, taken as an indication of the amount of C-S-H formed, was found. In this study, the same correlation was obtained for the different C$_3$S/C$_3$A systems, as shown in Figure 7-8.

Two linear trends were found in this case: one grouping the systems with coarse C$_3$A, and one for the systems with fine C$_3$A. An important observation is that the slope of both linear trends is almost the same, and they just differ on the intercept with the SO$_3$ axis.

The fineness of C$_3$S leads to an enhancement of the C$_3$S peak (see Figure 7-4), which can be considered an analogue effect to the addition of SCMs. In Figure 7-8, it can be seen that this effect does not change the heat-SO$_3$ correlation between the systems if the C$_3$A fineness and quantity remains the same. This is in good agreement with the results shown in [6], as in that case all the systems were prepared with the same OPC (i.e., same C$_3$A) and at relatively similar levels of OPC replacement.

In [6], it was suggested that the intercept with the SO$_3$ axis represented the amount of sulfate consumed before the aluminate peak due to the precipitation of ettringite. In pure phase systems, this hypothesis can be verified experimentally, and it will be discussed in subsection 7.3.5. Even considering that the C$_3$A fineness shifts the linear trend obtained, the slope remains constant, suggesting that the slope of the regression could

be related to another property of the system that remains constant among the different systems. This will be addressed in subsection 7.3.6.

Figure 7-8: Heat release at the aluminate peak (A.P.) onset vs total SO_3 content for all the C_3S/C_3A 92/8 systems with different gypsum additions studied.

7.3.5 Intercept with SO_3 axis: link with the amount of ettringite formed before the aluminate peak

As seen in Figure 7-8, an increase in the fineness of C_3A leads to a shift to the right of the regression line obtained. Based on the observation of pure C_3A and C_3S/C_3A systems with fine and coarse C_3A, it is inferred that the difference might be associated to the amount of ettringite formed before the onset of the aluminate peak (gypsum depletion point). To study the relationship between the amount of ettringite formed before the onset and the intercept of the regression lines with the SO_3 axis, in-situ XRD experiments were conducted on a system with fine and coarse C_3A. The gypsum content was adjusted in each case so that the aluminate peak occurs between 12 and 18 hours. This led to a mixture design with 2.5% gypsum in the coarse C_3A system, and 3.75% gypsum in the fine C_3A one. In both cases fine C_3S was used.

Figure 7-9 shows the phase assemblage of the coarse (a) and fine (b) C_3A system. The amount of ettringite formed before the onset of the aluminate peak is significantly higher in the fine C_3A system. The amounts of ettringite measured at the onset of the aluminate peak for each system are shown in Table 2. Even considering the inherent error associated with this type of measurements, these figures provide at least an idea of the order of magnitude of the ettringite content. Stoichiometrically, 3 moles of SO_3 are required to form 1 mol of ettringite, leading to a mass ratio of 0.191 g SO_3/g ettringite formed. This value can be used to compute the amount of SO_3 required to form the ettringite measured by in-situ XRD, which are summarized in Table 7-2, along with the intercepts computed from the regression lines shown in Figure 7-8.

Table 7-2: Ettringite formed before the aluminate peak measured by in-situ XRD, computed SO$_3$ required and intercept of the Heat-SO$_3$ regression with the SO$_3$ axis.

System	Ettringite at A.P. onset (% C$_3$S+C$_3$A)	SO$_3$ required (% C$_3$S+C$_3$A)	Intercept Heat-SO$_3$ with SO$_3$ axis (% C$_3$S+C$_3$A)	Variation (%)
C$_3$S+C$_3$A 92/8 Coarse C$_3$A	1.1	0.211	0.22	4.1
C$_3$S+C$_3$A 92/8 Fine C$_3$A	4.5	0.852	0.87	2.1
C$_3$S+C$_3$A 92/8 Fine C$_3$A Hemi	9.5	1.820	1.99	8.5

The computed SO$_3$ required to form the observed ettringite are in within 10% variation of the intercept of the corresponding regression lines in Figure 7-8 for both systems. Thus, the intercept is indeed linked to the amount of ettringite formed before the occurrence of the aluminate peak, and a shift right can be triggered by an increase of this amount (finer C$_3$A and/or higher C$_3$A content).

The heat associated with the formation of ettringite before the aluminate peak is included in the values shown in Figure 7-8. A variation of the actual correlation obtained could be presumed. However, the amount of ettringite formed before the aluminate peak onset is similar for systems with the same C$_3$A fineness. This was also observed in OPC-based blended systems [6]. The high correlation coefficients obtained in Figure 7-8 indicate that systems with the same C$_3$A share the same intercept despite their different SO$_3$ content, and consequently the ettringite content formed before the aluminate peak (see Table 7-2). If the amount of sulfate added is beyond the amount that is able to be adsorbed in C-S-H and consumed by ettringite precipitation, gypsum depletion would not be reached (i.e. the aluminate peak is not visible) and thus, the parameters for determining a point in Figure 7-8 cannot be obtained.

a)

b)
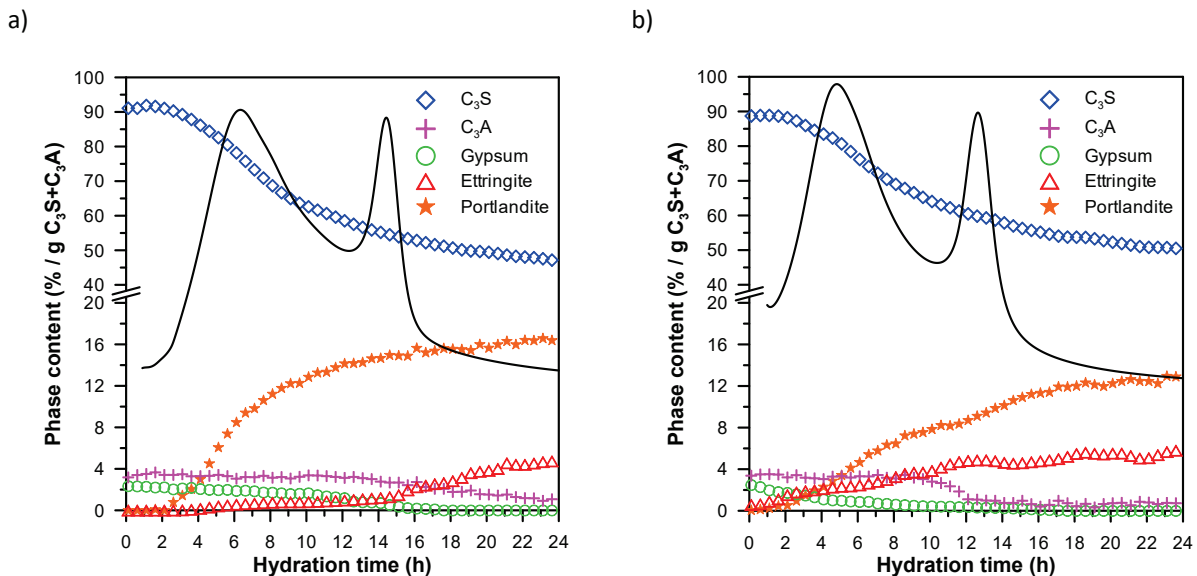
Figure 7-9: Initial phase assemblage measured by in-situ XRD of C$_3$S/C$_3$A 92/8 systems with coarse (a) and fine (b) C$_3$A.

7.3.6 Slope: relation to $/Ca ratio of C-S-H

Previous studies have reported values for the sulfur-to-calcium ($/Ca) ratio of C-S-H before the aluminate peak for C_3S/C_3A systems [5] and also in blended OPC [8]. These datasets were acquired using SEM/EDS. The values reported for the $/Ca ratio of C-S-H before the aluminate peak vary from 0.04 to 0.06. Another study measured by STEM/EDS the $/Ca ratio evolution of cement at early ages, reporting values over the same range during the first hours of hydration [18].

As it was shown in Figure 7-8, while the different systems have different heat-SO_3 relationships depending on the amount of ettringite formed before the aluminate peak, the slope remains constant. The amount of C-S-H formed was computed at a DoH equivalent to the heat release of the slope, assuming an enthalpy of reaction of 524 J/g C_3S [19]. The sulfur content equivalent to the addition of 1% SO_3 (per gram of C_3S+C_3A) to this obtained amount of C-S-H was used to compute the theoretical $/Ca ratio. As there might exist uncertainty of the value of the slope obtained by regression of the heat-SO_3 correlation, a sensitivity analysis of the $/Ca ratio was made for different values of the slope, Figure 7-10. Furthermore, the value $/Ca ratio was computed for a variety of Ca/Si ratio values of C-S-H. As seen, the computed $/Ca are in good agreement with the measured values of $/Ca found in the literature [5,8,18] for typical values of Ca/Si during this period of hydration. Thus, the slope of the heat-SO_3 correlation is linked to the sulfur amount adsorbed into C-S-H before the aluminate peak.
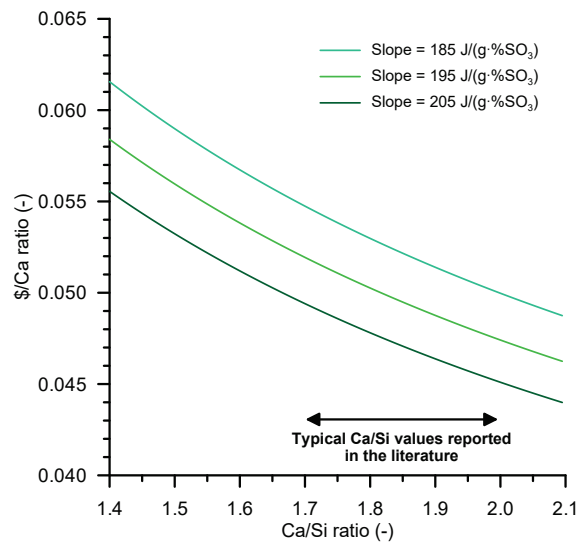
Figure 7-10: $/Ca as a function of Ca/Si ratio of C-S-H for different slope values of the heat-SO_3 regression trendline.

7.3.7 Sulfate adsorption in C-S-H and initial amount of ettringite influence the sulfate balance

The results presented indicate that the overall sulfate balance of these systems is controlled by two factors: first, the adsorption of sulfate on C-S-H and second, the rate of precipitation of ettringite before the aluminate peak.

The contribution of both factors to the sulfate balance of the system should be considered simultaneously. This can be concluded based on the calorimetry results shown in Figure 7-11. In these systems, the gypsum/C_3A and gypsum/C_3S ratios were adjusted by varying the gypsum content in system with C_3S/C_3A ratios of 94/6, 92/8 and 90/10. Figure 7-11a shows that the gypsum/C_3A ratio cannot be solely used to predict the sulfate demand, as the position of the aluminate peak in all cases is different. In this case, the differences are explained by the reduction in the amount of C-S-H formed (due to a lower content of C_3S as the amount of C_3A increase) and the consequent lower adsorption of sulfate. In fact, the systems with more C_3A (less C_3S) exhibit a more retarded aluminate peak. This agrees with the experiment of Quennoz and Scrivener on alite [5].

Figure 7-11b shows systems where the gypsum/C_3S ratio was fixed. As seen, the position of the aluminate peak is different in all the systems, showing that adsorption of sulfate on C-S-H neither can solely explain the position of the aluminate peak. In this case, the systems with less C_3A exhibit a more retarded aluminate peak, as the amount of ettringite that is formed is lower. In the 94/6 system, the aluminate peak is not seen even after 6 days, indicating that the amount of C_3A and the adsorption on C-S-H were not able to deplete solid gypsum from the system.
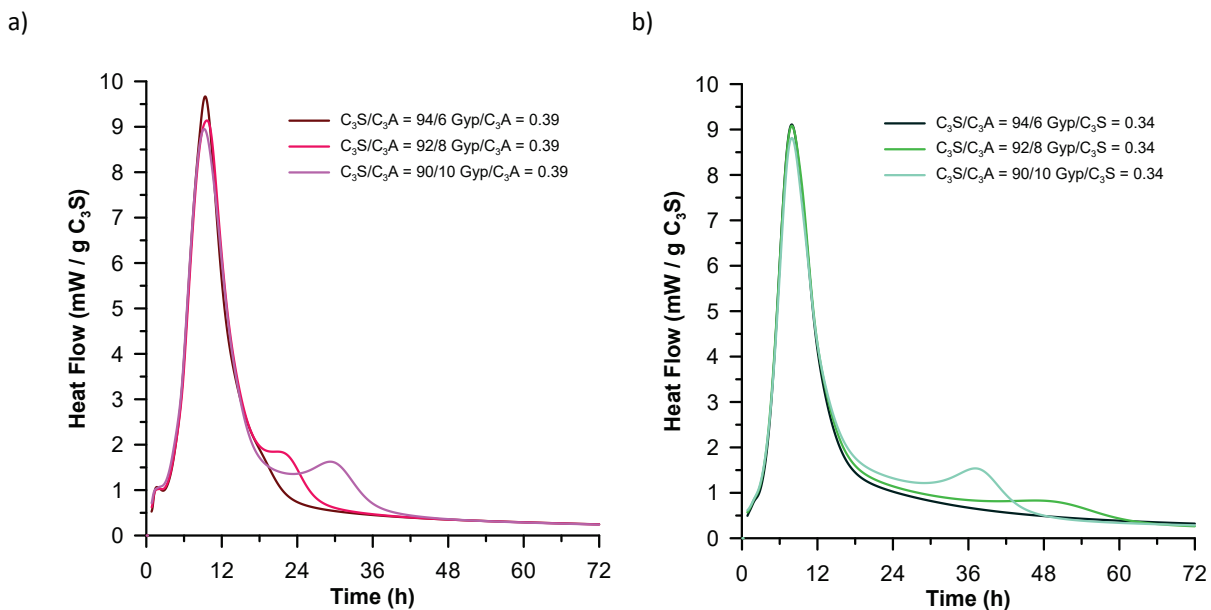
Figure 7-11: Heat flow curves of C_3S/C_3A systems with fine C_3S and coarse C_3A, with varying Gypsum/C_3A (a) and Gypsum/C_3S (b) ratios.

7.3.8 The effect of the sulfate source on the sulfate balance of C_3S/C_3A systems

The amount of ettringite that is formed before the onset of the aluminate peak is one of the factors that explains the sulfate balance of C_3S/C_3A systems. More ettringite can be precipitated during this period by increasing the fineness of C_3A and/or the amount of C_3A. In addition, it has been shown in previous studies that the source of sulfate can also influence the initial reactivity of C_3A. Hemihydrate has a faster rate dissolution compared to gypsum [20].

To study the influence of the dissolution rate of the sulfate source, some replicates of the systems containing fine C_3S and fine C_3A were prepared using hemihydrate instead of gypsum. As the SO_3 content of these compounds is different (SO_{3Gyp}/SO_{3Hemi} = 0.84) the content of hemihydrate was adjusted to match the SO_3 content of the gypsum (noted as $GypSO_{3EQ}$), Figure 7-12. An addition of 4.0% $GypSO_{3EQ}$ leads to an undersulfated system, which is not the case for the same SO_3 content if the sulfate source is gypsum (see Figure 7-6). As the observed ability to retard the aluminate peak was lower as compared to gypsum at the same sulfate addition, higher SO_3 contents were also prepared (5.5% and 6.0% $GypSO_{3EQ}$). These results also show that the retardation of the C_3A reaction by the addition of gypsum or hemihydrate depends on the type of sulfate source used for the same added SO_3 content. Therefore, the dissolution rate of the sulfate source is another factor to be accounted for to determine the position of the aluminate peak.

a)   b)
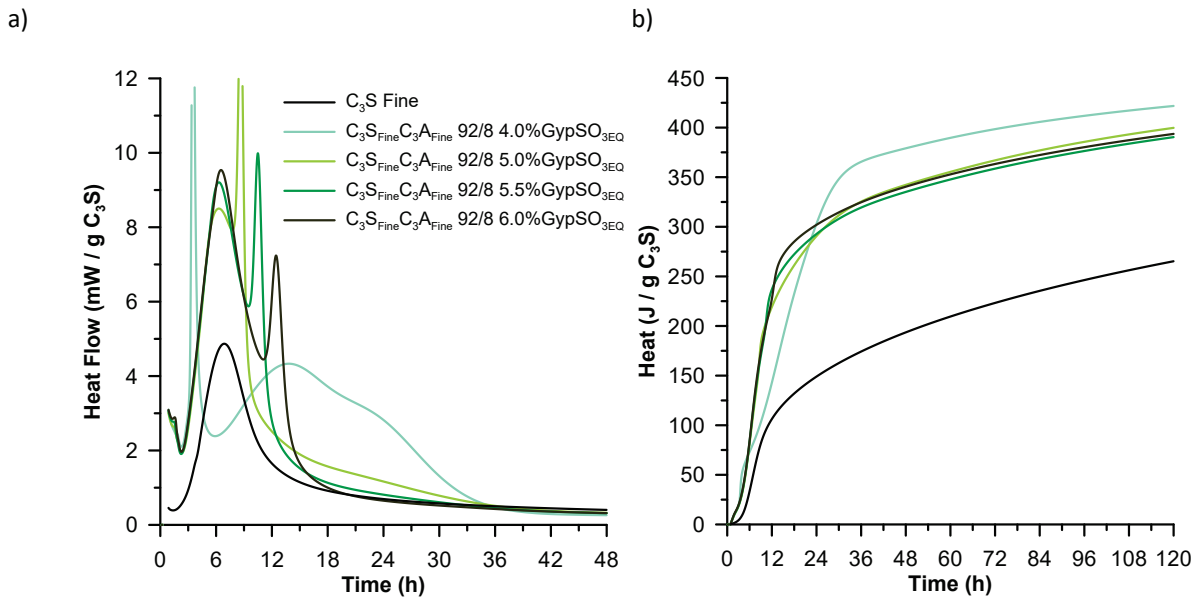
Figure 7-12: Heat flow (a) and total heat (b) of C_3S/C_3A systems 92/8 with fine C_3A and different hemihydrate additions.

Since the C_3S used for the systems shown in Figure 7-6 and Figure 7-12 is the same and the observed C_3S peaks are similar, the difference in the retardation of the aluminate peak observed is attributed to the early formation of ettringite before the onset of the aluminate peak. The heat-SO_3 regression was also performed and compared to the gypsum systems prepared with the same pure phases, Figure 7-13. As observed, the systems containing hemihydrate as sulfate source fall in a different line shifted right respect to the mixtures with gypsum.

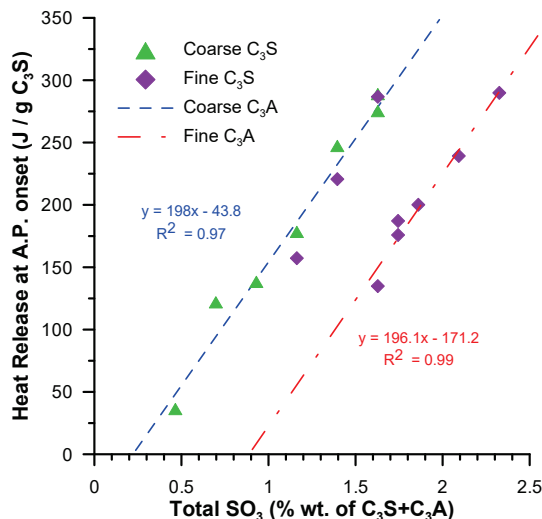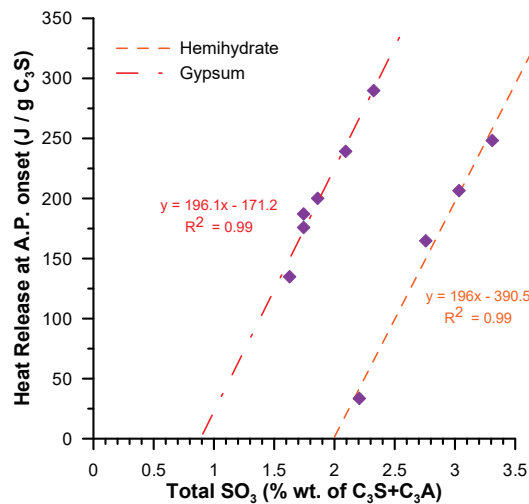Figure 7-13: Heat release at the aluminate peak (A.P.) onset vs total SO₃ content for C₃S/C₃A 92/8 systems with fine pure phases and different gypsum or hemihydrate additions.

The initial ettringite content was verified by an in-situ XRD measurement on the system containing 6.0% hemihydrate, Figure 7-14. Hemihydrate turns to into gypsum during the first hours of hydration. The initial amount of ettringite is significantly higher as compared to the gypsum system (Figure 7-9b). The first point is acquired between 6 and 10 minutes after initial contact of the materials with water, and the difference shows that indeed hemihydrate is able to provide more sulfate ions in solution, which react quickly with C₃A to form ettringite, before the slowing down of the C₃A reaction. Afterwards, the rate of ettringite precipitation is controlled by the rate of reaction of C₃A which is similar among systems with the same C₃A fineness, in agreement with the similar slope observed for ettringite content over time in Figure 7-9b for the system with gypsum and Figure 7-14 for the system with hemihydrate.

The slope of the heat-SO₃ regression remains the same as for gypsum, Figure 7-8. Thus, the $/Ca ratio of C-S-H is not significantly affected by a change in the sulfate source of the system, but rather the initial ettringite content increases. The intercept for the regression of the systems with hemihydrate was also compared with the theoretical SO₃ required to form the ettringite measured by in-situ XRD, being is also within 10% variation of the computed intercept, Table 7-2.
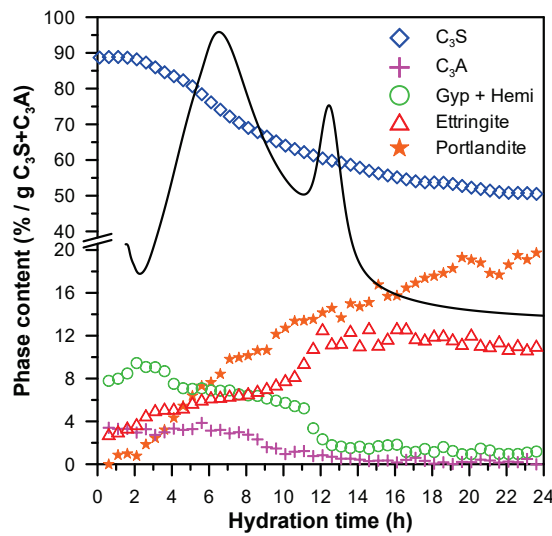
Figure 7-14: Initial phase assemblage measured by in-situ XRD of C_3S/C_3A 92/8 system with fine pure phases and 6.0% hemihydrate addition.

7.3.9   Further insights on the effect of gypsum addition on C_3S hydration

As it was shown in section 7.3.2, in undersulfated systems where the aluminate peak precedes the C_3S one, a lower and broader C_3S peak is observed. Several hypotheses have been formulated to explain this observation. Quennoz and Scrivener [5] suggested that the re-acceleration of the alite reaction was slowed down due to the presence of aluminum in the pore solution of undersulfated system. Bergold et al. [4] proposed that the aluminate reaction interfered with C-S-H precipitation due to interactions with AFm.

While the actual mechanism explaining the change in the kinetics of the C_3S reaction in undersulfated systems is still unclear, some insights can be gathered from the results of this study. It was shown that gypsum addition can have an enhancement effect on pure triclinic C_3S (see Figure 7-4). Figure 7-15 shows two C_3S/C_3A systems, one undersulfated (1.0% gypsum) and one properly sulfated (2.0% gypsum), and also the curves for the corresponding C_3S and C_3S+gypsum with the same sulfate content as the properly sulfated C_3S/C_3A system.

The DoH of C_3S in C_3S/C_3A properly sulfated is significantly higher to the one of pure C_3S. On the other hand, the peak of the C_3S+gypsum system matches the one of the properly sulfated C_3S/C_3A system. Therefore, a big part of the difference between the peaks of C_3S alone and in the C_3S/C_3A system with 2.0% gypsum can be explained by the enhancement effect of sulfate on C_3S hydration.

In the undersulfated C_3S/C_3A system, the C_3S peak is lower and broader compared to the properly sulfated case. To compare the DoH of C_3S in both C_3S/C_3A systems, the calorimetry curves were decoupled. The aluminate peak was then integrated, and the total heat associated with it is shown as vertical arrow markers in Figure 7-15b. This shows that after 48 hours of hydration, the DoH of C_3S in properly and undersulfated systems is similar, despite the significantly different kinetics during the first hours of hydration. This agrees with data from Bergold et al. [4], where virtually the same DoH of C_3S was computed from in-situ XRD data of under and properly sulfate systems after 46.5 hours.

The difference of heat release associated with the aluminate reaction between the properly and under sulfated system can be explained by the different types of phases precipitated during the aluminate peak in undersulfated (precipitation of AFm) and properly sulfated (second formation of ettringite) systems [5].
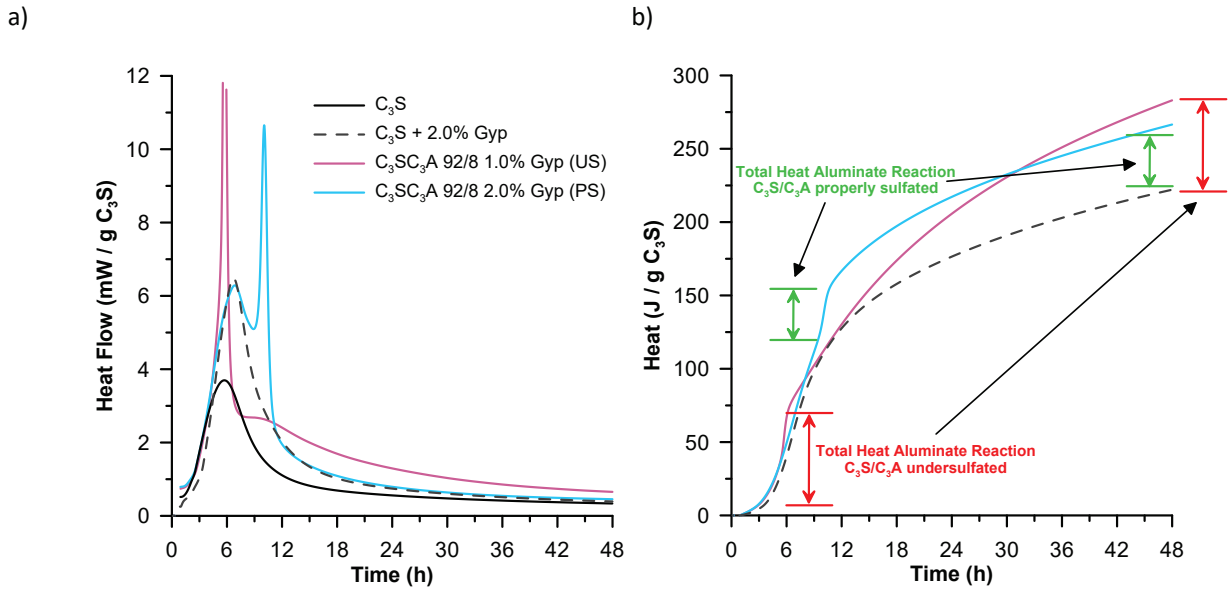
Figure 7-15: Heat flow (a) and total heat (b) of under and properly sulfated C_3S/C_3A systems, in addition to pure C_3S and sulfated C_3S.

The results of this study showed that an enhancement of the C_3S peak is observed with gypsum additions, leading to an increased DoH. Quennoz and Scrivener [5] observed the same effect on alite (C_3S with additions of alumina and magnesium oxide) with similar levels of gypsum addition. However, they did not observe the same effect on their pure C_3S material. It should be noted that the height of the peak of pure C_3S reported in their study is close to 11 mW/g C_3S, much higher than even the fine C_3S with 3% gypsum system reported here. This indicates that their material was very fine, and therefore the overall enhancement effect of gypsum is less significant in such fast reacting material. An analogue observation was made on a fine alite from a commercial OPC by Adu-Amankwah et al. [21].

Several hypotheses have been proposed to explain the observed enhancement of gypsum on C_3S/alite. Bergold et al. [4] proposed a seeding effect of (nano-)ettringite to explain the higher DoH measured in alite systems with gypsum addition. In light of the results of this study, this hypothesis is unlikely, as the enhancement of the peak is observed as well in pure C_3S system, where no aluminates (and consequently, ettringite) are present. This suggests that the cause of the enhancement of C_3S hydration by gypsum is an interaction exclusively between this phase and C_3S (and/or C-S-H), rather than one that involves the aluminates. Further research is required to clarify the mechanism behind this interaction.

7.4   Conclusions

This study compared the effect of different factors that affect the rate of sulfate consumption during the early stages of hydration of C_3S/C_3A systems, modifying their sulfate balance. As it was shown, the interaction between C_3S, C_3A and sulfate is complex and therefore the sulfate balance cannot be explained by a single factor.

Based on the results presented, the following conclusions can be drawn:

1. Two main factors explain the sulfate balance of C_3S/C_3A systems: first, the amount of ettringite precipitated before the onset of the aluminate peak and second, the adsorption of sulfate into C-S-H.

2. The fineness of C_3A modifies the amount of ettringite precipitated before the aluminate peak, while the fineness of C_3S affects the rate of C-S-H precipitation. Both factors can consequently play a role in the final position of the aluminate peak in C_3S/C_3A systems.

3. The intercept with the SO_3 axis of the heat-SO_3 curve is linked to the amount of ettringite precipitated before the onset, while the slope is driven by the \$/Ca ratio of C-S-H during this period. The intercept can be modified by changing the kinetics of reaction of C_3A or the type of sulfate source.

4. The addition of sulfate enhances the hydration of C_3S. The DoH of C_3S in C_3S/C_3A systems is higher as compared to pure C_3S. This can be explained by the enhancement of C_3S hydration by the addition of gypsum.

5. Undersulfated C_3S/C_3A systems exhibit a lower and broader C_3S peak as compared to properly sulfated systems. At 48 hours, the DoH of C_3S in under and properly sulfated system is the same, thus, the effect of the different kinetics of C_3S reaction on the overall DoH is constrained to the first two days of hydration.

7.5 References

[1]   W. Lerch, The influence of gypsum on the hydration and properties of portland cement pastes, Am. Soc. Test. Mater. J. 12 (1946) 1–41.

[2]   RILEM T.C., The hydration of tricalcium aluminate and tetracalcium aluminoferrite in the presence of calcium sulfate, Mater. Struct. 19 (1986) 137–147. doi:10.1007/BF02481758.

[3]   A. Quennoz, K.L. Scrivener, Hydration of C3A–gypsum systems, Cem. Concr. Res. 42 (2012) 1032–1041. doi:10.1016/j.cemconres.2012.04.005.

[4]   S.T. Bergold, F. Goetz-Neunhoeffer, J. Neubauer, Interaction of silicate and aluminate reaction in a synthetic cement system: Implications for the process of alite hydration, Cem. Concr. Res. 93 (2017) 32–44. doi:10.1016/j.cemconres.2016.12.006.

[5]   A. Quennoz, K.L. Scrivener, Interactions between alite and C3A-gypsum hydrations in model cements, Cem. Concr. Res. 44 (2013) 46–54. doi:10.1016/j.cemconres.2012.10.018.

[6]   F. Zunino, K.L. Scrivener, The influence of the filler effect in the sulfate requirement of blended cements, Cem. Concr. Res. 126 (2019). doi:10.1016/j.cemconres.2019.105918.

[7]   A. Quennoz, Hydration of C3A with Calcium Sulfate Alone and in the Presence of Calcium Silicate, EPFL Thesis 5035, 2011.

[8]   E. Berodier, Impact of the supplementary cementitious materials on the kinetics and microstructural development of cement hydration, EPFL Thesis 6417, 2015.

[9]   H. Minard, S. Garrault, L. Regnaud, A. Nonat, Mechanisms and parameters controlling the tricalcium aluminate reactivity in the presence of gypsum, Cem. Concr. Res. 37 (2007) 1418–1426. doi:10.1016/j.cemconres.2007.06.001.

[10]   R.J. Myers, G. Geng, J. Li, E.D. Rodríguez, J. Ha, P. Kidkhunthod, et al., Role of adsorption phenomena in cubic tricalcium aluminate dissolution, Langmuir. 33 (2016) 45–55. doi:10.1021/acs.langmuir.6b03474.

[11]   G. Geng, R.J. Myers, Y.-S. Yu, D.A. Shapiro, R. Winarski, P.E. Levitz, et al., Synchrotron X-ray nanotomographic and spectromicroscopic study of the tricalcium aluminate hydration in the presence of gypsum, Cem. Concr. Res. 111 (2018) 130–137. doi:10.1016/j.cemconres.2018.06.002.

[12]   W. Corstanje, H.N. Stevels, J.M. Stevels, Hydration reactions in pastes C3S+C3A+CaSO4 2aq + water at 25°C, Cem. Concr. Res. 4 (1974) 417–431.

[13]   M. Collepardi, G. Baldini, M. Pauri, Tricalcium aluminate hydration in the presence of lime, gypsum or sodium sulfate, Cem. Concr. Res. 8 (1978) 571–580.

[14]   B. Mota, T. Matschei, K. Scrivener, The influence of sodium salts and gypsum on alite hydration, Cem. Concr. Res. 75 (2015) 53–65. doi:10.1016/j.cemconres.2015.04.015.

[15]   S. Gunay, S. Garrault, A. Nonat, P. Termkhajornkit, Influence of calcium sulphate on hydration and mechanical strength of tricalcium silicate, in: Internnatinal Congr. Chem. Cem., Madrid, Spain, 2011: pp. 3–8.

[16]   A. Bentur, Effect of Gypsum on the Hydration and Strength of C3S Pastes, J. Am. Ceram. Soc. 59 (1976) 210–213. doi:10.1111/j.1151-2916.1976.tb10935.x.

[17]   X. Li, A. Ouzia, K. Scrivener, Laboratory synthesis of C3S on the kilogram scale, Cem. Concr. Res. 108 (2018) 201–207. doi:10.1016/j.cemconres.2018.03.019.

[18]   E. Gallucci, P. Mathur, K. Scrivener, Microstructural development of early age hydration shells around cement grains, Cem. Concr. Res. 40 (2010) 4–13. doi:10.1016/j.cemconres.2009.09.015.

[19]   K. Fujii, W. Kondo, Estimation of Thermochemical Data for Calcium Silicate Hydrate (C-S-H), J. Am. Ceram. Soc. 66 (1983) C-220-C-221. doi:10.1111/j.1151-2916.1983.tb11011.x.

[20]   S. Pourchet, L. Regnaud, J.P. Perez, A. Nonat, Early C3A hydration in the presence of different kinds of calcium sulfate, Cem. Concr. Res. 39 (2009) 989–996. doi:10.1016/j.cemconres.2009.07.019.

[21]   S. Adu-Amankwah, L. Black, J. Skocek, M. Ben Haha, M. Zajac, Effect of sulfate additions on hydration and performance of ternary slag-limestone composite cements, Constr. Build. Mater. 164 (2018) 451–462. doi:10.1016/j.conbuildmat.2017.12.165.

Chapter 8   Precipitation of Hc and Mc in LC³

Note: This chapter is based on an article in final preparation for submission to a peer reviewed journal.

Submission title: The reaction between metakaolin and limestone and its effect in porosity refinement and mechanical properties

Franco Zunino, Karen Scrivener

Contribution of the doctoral candidate: Writing of the first manuscript draft, experimental design, conduction of the experiments.

In limestone calcined clay cements (LC³), more hemicarboaluminate and hemicarboaluminate is observed as compared to other blended cements. In this study, the factors that influence reaction between metakaolin and limestone were assessed. It was found that the third peak of hydration observed in LC³ systems corresponds to a precipitation of these phases. Metakaolin content and sulfation level can influence the position and magnitude of this peak. It was observed that aluminates from metakaolin can also participate in the precipitation of ettringite if sulfate is available. The precipitation of hemi and monocarboaluminate have a significant effect on porosity refinement and strength.

Contents

8.1   Introduction

Sustainability in the cement industry is a major concern [1]. The most effective strategy to tackle this challenge at a worldwide scale is to reduce the clinker factor in cements based on Portland cement clinker [2]. This has accelerated the adoption of blended cements that incorporate supplementary cementitious materials (SCMs) replacing part of the Portland cement (OPC) fraction. Among commonly used SCMs are fine limestone, granulated blast furnace slag and fly ash [3]. Fly ash and slag are together available in amounts close to 15% of cement production [4]. This means that we need to look for other materials to further reduce clinker factor, such as calcined clays.

Limestone calcined clay cements (LC^3) are one of the promising alternatives for high performance sustainable cements [5]. LC^3 incorporates significant amounts of metakaolin, a reactive aluminosilicate phase [6] formed after calcination of kaolinitic clays, and ground limestone (CaCO$_3$). Both materials are widely available and therefore are suitable to face the current shortage of SCMs [2]. In addition to metakaolin and limestone, an additional amount of gypsum is normally required to achieve proper sulfate balance and maximize the performance of LC^3. This addition of sulfate compensates the filler effect contribution of metakaolin and limestone in the sulfate depletion. The optimization of the sulfate addition in LC^3 blends was studied in [7,8].

LC^3 can achieve equivalent strength to OPC at 7 days with a clinker factor of 50% if the kaolinite content of the calcined clay used is above 40% [9–11]. The high reactivity of metakaolin contributes to achieve a dense microstructure in LC^3 systems at early ages [9], making LC^3 a particularly good cement in terms of durability [12]. Higher amounts of AFm are observed in LC^3 systems due to the reaction between metakaolin and limestone [6,9].

The C-A-S-H of LC^3 systems shows some differences in chemical composition as compared to OPC [13]. Particularly, the amount of aluminum in C-A-S-H is significantly higher due to the higher concentration of this element in the pore solution [9,14]. Nevertheless, the morphology of C-A-S-H is not significantly affected by the addition of limestone and calcined clay as compared to OPC [13].

8.1.1   Reactions occurring in LC^3 cements

Metakaolin (AS$_2$) can react with portlandite (CH) produced during cement hydration to form C–A–S–H [9,11], thus contributing to strength by space filling (Eq. 8-1).

When limestone (Cc) is added to an OPC system, calcium monocarboaluminate (C$_4$AcH$_{11}$, Mc) and hemicarboaluminate (C$_4$Ac$_{0.5}$H$_{12}$, Hc) are formed [15,16] instead of monosulphoaluminate (C$_4$A\$H$_{12}$) as AFm phases, which leaves more sulfates available to form ettringite (Eq. 8-2). The formation of the CO$_3$-AFm phases has been found to be related to the bulk molar CO$_2$/Al$_2$O$_3$ and SO$_3$/Al$_2$O$_3$ ratios of the system by thermodynamic modelling [17].

In systems incorporating an additional source of amorphous alumina such as metakaolin, higher amounts of Hc and Mc are observed. This is due to the reaction of aluminates from metakaolin with calcium carbonate from limestone, leading to the formation of additional hemicarboaluminate.

145

$$AS_2 + 3CH + 6H \longrightarrow C-A-S-H + C_2ASH_8 \qquad (8\text{-}1)$$

$$C_3A + 0.5Cc + 0.5CH + 11.5H \longrightarrow C_4Ac_{0.5}H_{12} \qquad (8\text{-}2)$$

$$AS_2 + 0.5Cc + 3.5CH + 8.5H \longrightarrow C_4Ac_{0.5}H_{12} \qquad (8\text{-}3)$$
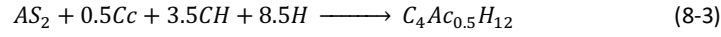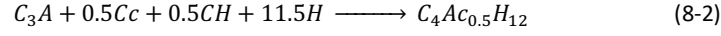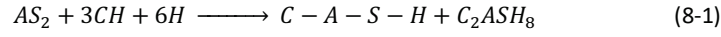
While is it clear that the additional precipitation of CO_3-AFm contributes to space filling, the impact of this on mechanical properties and the kinetics of this reaction have not been explored in detail. This paper studies the role of the additional formation of hemicarboaluminate and monocarboaluminate from the reaction of metakaolin and limestone on mechanical properties and space filling of LC^3 systems. In addition, the kinetics of this reaction are studied, and the effect of different factors that can influence this reaction are presented.

8.2   Materials and methods

8.2.1   Materials

A commercial ordinary Portland cement (OPC) conforming to EN 197-1 as CEM I 42.5R was used in this study. The chemical (by XRF) and phase (by XRD / Rietveld) composition are shown in Table 8-1. The calcined clay was a high purity metakaolin (MK, 95% purity from Burgess) to avoid side effects from secondary materials. A limestone powder with a content of calcium carbonate above 98% as measured by thermogravimetric analysis (TGA) was selected to prepare the LC^3 blends.

To decouple the effect of the aluminum contribution from Portland cement (C_3A phase) and metakaolin, some systems were prepared using pure C_3S + LC^2 (combination of limestone, calcined clay and gypsum). The synthesis of pure tricalcium silicate (C_3S) was conducted following the procedure described in [18]. Calcium carbonate (VWR) and fumed silica (0.2 μm, Sigma-Aldrich) were used. The sintering temperature was maintained at 1600ºC for 4 hours, and the samples were air quenched subsequently. The result was triclinic (T_1) C_3S with a free lime content below 0.5% in all batches, as quantified by Rietveld refinement. After synthesis, the C_3S was ground in a concentric disc mill in batches of 100 g for 30 seconds in six repetitions.

The particle size distribution (PSD) of these materials, measured by laser diffraction, is shown in Figure 8-1. The optical model parameters and the dispersant were selected following the recommendations given in [19].
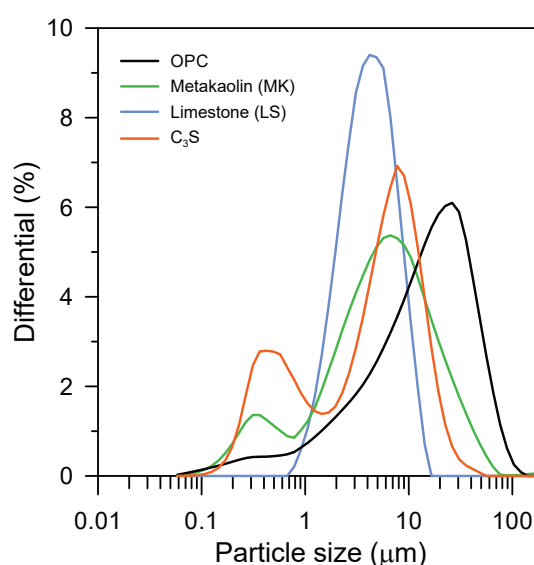
Figure 8-1: Particle size distributions of materials used in this study.

Table 8-1: Chemical (from XRF) and phase composition (from XRD) of OPC, metakaolin, LS and C_3S.

	OPC	Metakaolin (MK)	LS	C_3S
SiO_2	19.51	52.00	0.11	24.11
Al_2O_3	4.42	43.80	0.00	0.00
Fe_2O_3	3.12	0.33	0.04	0.07
CaO	63.85	0.03	54.96	74.57
Na_2O	0.19	0.14	0.06	0.00
K_2O	0.83	0.29	0.00	0.00
MnO	0.05	0.01	0.00	0.00
TiO_2	0.31	1.53	0.00	0.00
MgO	2.10	0.01	0.15	0.15
P_2O_5	0.33	0.16	0.00	0.00
SO_3	3.25	0.10	0.03	0.00
LOI	1.54	1.47	42.5	1.05
C_3S	66.5	-	-	99.5
C_2S	4.0	-	-	-
C_3A	4.9	-	-	-
C_4AF	9.6	-	-	-

The specific surface area (SSA) of each raw material was measured by nitrogen adsorption, using the BET model. In all cases, samples of around 1.5 g were degassed for 2 hours at 200ºC under a N_2 flux before the measurement. The specific gravity was measured using a liquid pycnometer with isopropanol as solvent except in the case of C_3S where a helium pycnometer was used instead. Values are shown in Table 8-2.

Table 8-2: Distribution values, span (width), specific surface area and specific gravity of raw materials.

	OPC	MK	LS	C_3S
D_V90 (μm)	41.42	20.17	7.93	14.5
D_V50 (μm)	14.22	5.13	3.93	4.9
D_V10 (μm)	1.67	0.54	1.80	0.4
Span (-)	2.80	3.83	1.56	2.88
SSA (m^2/g)	1.41	13.56	3.60	2.87
Sp. Gravity (g/cm^3)	3.09	2.20	2.72	3.15

8.2.2 Mixture design

The contribution of the different sources of aluminates on the precipitation of hemicarboaluminate and monocarboaluminate was studied comparing LC^3 systems with equivalent mixtures where the OPC is replaced by C_3S. The reference LC^3 system contained 55% OPC, 15% limestone and 30% calcined clay (LC^3-50) on a mass basis plus an additional amount of gypsum (0 or an optimum content determined by calorimetry in preliminary trials), as shown in Table 8-3. The calcined clay fraction in LC^3-50 was varied between materials of different grade (metakaolin content). These synthetic clays were prepared by mixing pure MK (95% metakaolin) with limestone, as detailed in Table 8-3. Following this approach, LC^3 systems with calcined clay MK content ranging from 95% to 20% were prepared. The LC^3 system with 95% metakaolin was studied at a variety of gypsum contents in addition to 0 and the optimum (1.6%). The water-to-binder ratio (w/b) was fixed at 0.4 by mass in all cases.

The synthetic calcined clays with 95, 63 and 40% of metakaolin were selected to further study the formation of hemicarboaluminate and monocarboaluminate in $C_3S + LC^2$ systems. For these mixtures, a w/b ratio of 0.5 by mass was used to achieve sufficient workability with a comparable plasticizer dosage as the OPC-based systems (0.75 to 1.5% by mass of solids). Gypsum was added to the systems in the same proportion as in the equivalent LC^3 mixtures, in order to keep constant as many factors as possible and isolate the contribution of C_3A. The mixture design of these systems is also shown in Table 8-3.

Table 8-3: Mixture proportions of OPC, LC^3 and $C_3S + LC^2$ systems.

Mixture	OPC (%)	C_3S (%)	MK (%)	LS (%)	Added Gypsum (%)	w/c	w/b	SSA (m^2/g)
OPC	100	0.0	0.0	0.0	0.0	0.40	0.40	1.41
LC^3 MK95	55-G	0.0	30.0	15.0	G (0 to 12)	0.73[A]	0.40	5.36
LC^3 MK63	55-G	0.0	20.0	25.0	G (0 and 1)	0.73[A]	0.40	4.37
LC^3 MK47	55-G	0.0	15.0	30.0	G (0 and 0.85)	0.73[A]	0.40	3.88
LC^3 MK40	55-G	0.0	12.6	32.4	G (0, and 0.7)	0.73[A]	0.40	3.64
LC^3 MK20	55-G	0.0	6.3	38.7	G (0 and 0.35)	0.73[A]	0.40	3.02
C_3S	0.0	100	0.0	0.0	0.0	0.50	0.50	2.87
$C_3S + LC^2$ MK95	0.0	53.4	30.0	15.0	1.6	0.94	0.50	6.14
$C_3S + LC^2$ MK63	0.0	54.0	20.0	25.0	1.0	0.93	0.50	5.16
$C_3S + LC^2$ MK40	0.0	54.3	12.6	32.4	0.7	0.92	0.50	4.43

[A]: Value of w/c computed considering an OPC content of 55%. The value will vary as the concentration of added gypsum is increased.

8.2.1 Experimental methods

The heat evolution was measured in a TAM Air isothermal calorimeter at 20ºC for up to 7 days. Paste samples were mixed with a high shear mixer at 1600 rpm for two minutes, 10 g of paste was placed in a glass ampoule, sealed and introduced in the calorimeter.

X-ray diffraction (XRD) measurements were carried out on freshly cut slices of hardened paste at 1, 2, 3, 7, 28 and 90 days of hydration to determine the amounts of ettringite, portlandite and AFm formed. Rietveld refinement was conducted using the HighScore Plus v4.8 software. In the case of $C_3S + LC^2$ systems, TGA (30 to 1000°C with a heating ramp of 10°C/min under N_2) was also conducted on the same samples to obtain a second measurement of CH content. The slices were analyzed in a Bragg-Brentano configuration in a PANalytical X'pert pro diffractometer working at 45 kV and 40 mA with a copper source. A 1/2º soller slit was used,

and scans were acquired between 7 and 70º 2θ in 14 min, equivalent to a step size of 0.0167º 2θ. The external standard method was used to compute the K-factor of the device and account for the amorphous phases present. A scan of a rutile standard was acquired in the same conditions after the experiments for this purpose.

Porosity measurements were conducted by mercury intrusion porosimetry (MIP) in paste samples at 1, 2, 3 and 7 days. Slices similar to the ones prepared for XRD were immersed in isopropanol for 7 days to arrest the hydration. Afterwards, they were stored in a desiccator for at least 48 hours to remove the remaining isopropanol. About 1 g of hardened paste was placed in a glass dilatometer crushed into 4 to 5 pieces. Intrusion was done up to a pressure of 440 MPa. A contact angle of 120° was assumed between mercury and the cement paste.

In-situ measurements of porosity refinement were conducted using ultrasonic pulse velocity measurements (Ultratest IP-8 device). Fresh paste samples of LC^3 MK95 and MK40 were placed in a ring device mounted over a vibration reducing table. Two high resolution (0.05 μs) ultrasonic cells were placed in opposite sides of the cell, and the pulse velocity was recorded up to 120 hours of hydration at 23°C.

Mortar samples were prepared following EN 196-1 standard to determine the compressive strength of the LC^3 systems. The binder design was the same as shown in Table 3, and they were combined with standardized sand in a sand-to-binder ratio of 3 by mass. Sealed-curing conditions at 20°C was applied to the samples until the time of testing. Tests were performed at 1, 2, 3, 7, 28 and 90 days.

The microstructural development was studied using scanning electron microscopy (SEM), using a FEI Quanta 200 microscope. Element distribution maps were collected from polished sections of LC^3 paste (from the same discs as for MIP measurements) embedded in resin, using an accelerating voltage of 12 kV, working distance of 12.5 mm and a spot size adjusted to obtain about 0.9 nA of current over the sample. The maps were collected at 1000x magnification in 30 scans with a dwell time of 512 μs, resulting in a total measuring time of approximately 8 hours per map. The data obtained was then quantified using a calibration database acquired under the same conditions. Afterwards, the *edxia* image analysis framework was used to process the hyperspectral maps and obtain phase distribution masks [20].

To further explore the influence of metakaolin content and sulfate addition on the phase assemblage of LC^3 systems, thermodynamic modeling was conducted using the Gibbs energy minimization method (GEMS). For this purpose, GEMS version 3 Software was employed [21], coupled with the CEMDATA18 thermodynamic database [22]. The phase composition of the OPC used was considered, and the addition of metakaolin was controlled to emulate different grades of clay. The incorporation of aluminum into C-A-S-H was also accounted for, using as input the Al/Ca ratios measured by SEM.

8.3 Results and discussion

8.3.1 The third peak of hydration in LC^3 cements

A typical heat flow curve observed in LC^3 systems is compared to an OPC system in Figure 8-2. The first alite peak occurs after the end of the induction period, it is associated with a fast dissolution of C$_3$S and precipitation of C-(A)-S-H. Ettringite is also continuously precipitated during this time, and sulfate is adsorbed in C-(A)-S-H [23]. The alite peak of LC^3 appears enhanced as compared to OPC due to the filler contributions of limestone and metakaolin. It has been shown that this enhancement also influences the sulfate balance of LC^3 systems [7]. If the LC^3 systems are properly sulfated, the aluminate peak occurs after the alite peak when solid gypsum is depleted, triggering the desorption of sulfate from C-(A)-S-H. This aluminate peak corresponds to a fast dissolution of C$_3$A, leading to the (second) precipitation of ettringite [23,24]. A third hydration peak is observed in LC^3 systems, with a maximum between 48 and 72 hours of hydration. This hydration peak is significantly larger than the one observed in OPC following the aluminate peak, which is normally associated with formation of AFm.
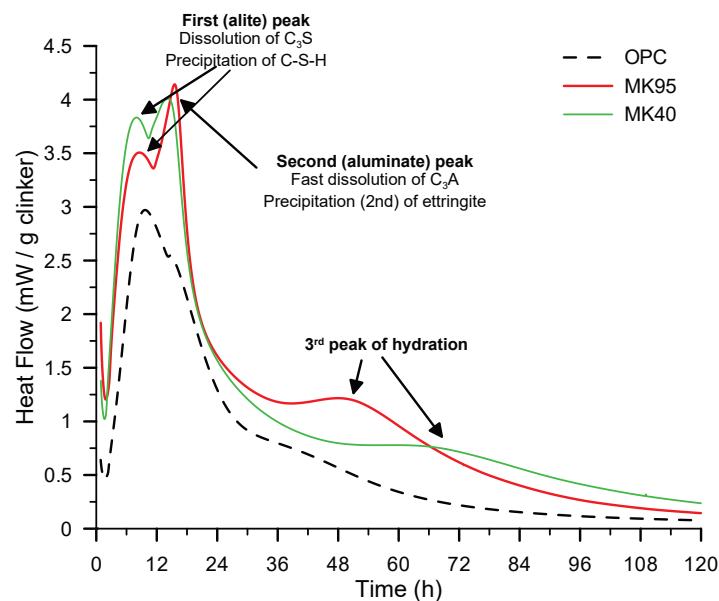
Figure 8-2: Calorimetry curve of OPC and LC^3 MK95 and MK40 systems showing the main hydration peaks and the third hydration peak observed in LC^3 between 36 and 84 hours.

Figure 8-3 shows the XRD patterns of OPC, LC^3 MK95 and MK40. Hc and Mc are observed in very small quantities in the LC^3 systems at 24 hours, while in OPC the peaks are not clearly observed until 7 days of hydration. Both LC^3 and OPC form Hc and Mc as AFm phases, as OPC contains about 3% limestone. Between 2 and 3 days, the amounts of Hc and Mc increase significantly in the LC^3 systems. On the other hand, the ettringite peaks remain constant over the same period of time. At 28 days, OPC and LC^3 systems both show Hc and Mc peaks, these are significantly higher in LC^3. The diffractograms at 90 days show some additional consumption of CH in LC^3 systems.

These observations raise the question about the source of aluminum that sustain the intense Hc and Mc formation observed in LC^3 at early age, but not observed in the OPC system. As the amount of ettringite remains fairly constant up to 90 days, the only possibilities are unreacted C_3A and/or metakaolin.

a)
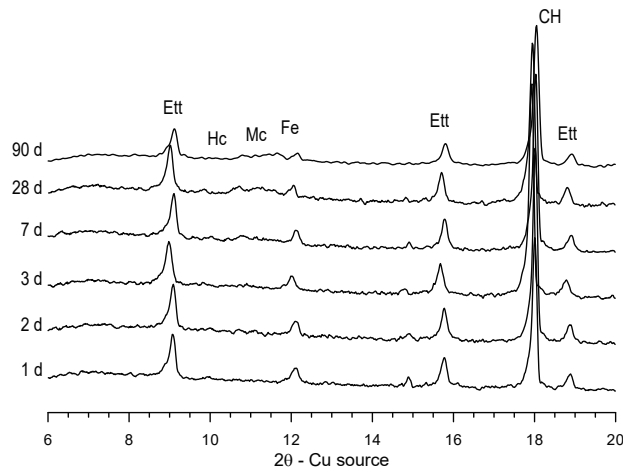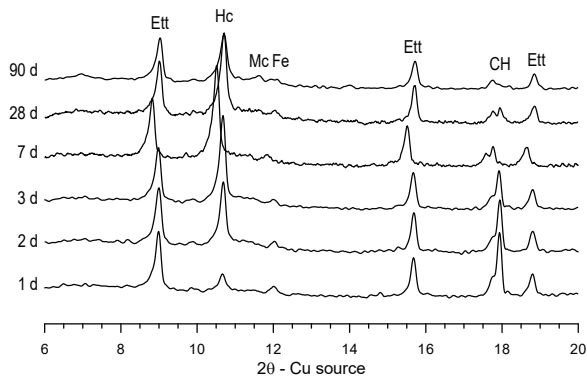
b)   c)
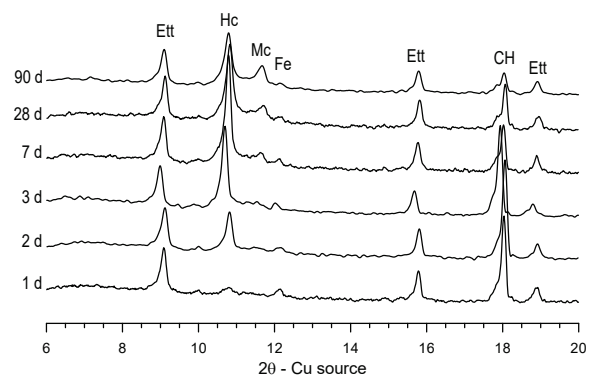
Figure 8-3: XRD patterns of hydrated paste from OPC (a), LC^3 MK95 (b) and LC^3 MK40 (c).

8.3.2   The third peak of hydration in $C_3S + LC^2$ cements

The aluminate contribution of C_3A and metakaolin to the enhanced formation of Hc and Mc observed in LC^3 were decoupled using the $C_3S + LC^2$ systems. In these materials, aluminium can only come from metakaolin. In Figure 8-4, the heat flow curves of $C_3S + LC^2$ with MK95, MK63 and MK40 are shown and compared to pure C_3S and $C_3S + 1\%$ gypsum. The enhancement of the main hydration peak seen in the $C_3S + LC^2$ systems is a combination of the effects of gypsum enhancement on C_3S hydration [8] and the filler effect contribution of limestone and metakaolin.

A peak with maximum between 48 and 72 hours is observed in all the C_3S + LC^2 systems. The intensity and the position of the maximum heat flow is dependent on the clay grade as in the OPC-based LC^3 systems (Figure 8-2). To study the phase assemblage of the systems during this peak, XRD analysis and Rietveld refinement up to 7 days of hydration was conducted for both C_3S + LC^2 MK95 and MK40. Figure 8-5 shows the computed amounts of ettringite, Hc + Mc and CH. Measurements of CH by TGA are also presented, along with a theoretical computation of the CH produced by the system based on the DoH of C_3S (assuming Ca/Si ratio of C-S-H equal to 1.7).
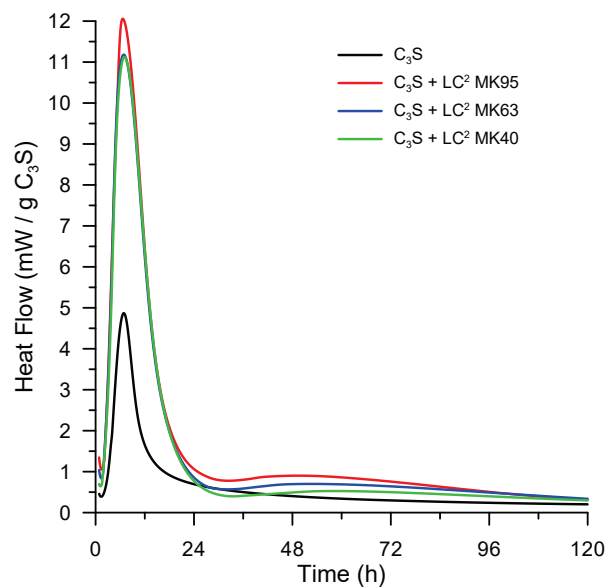
Figure 8-4: Heat flow curves of C_3S + LC^2 systems with MK95, MK63 and MK40 clay grades.

The measured CH values by both techniques are similar and follow the same trend. The difference between the CH produced by C_3S hydration and the measured ones indicates that as early as 24 hours there is some pozzolanic reaction taking place. The extent of CH consumption is related to the metakaolin content of the system during the first 7 days of hydration.

Hc/Mc is not detected at 24 hours in either C_3S + LC^2 systems. In the system with higher MK content (MK95) Hc is detected at 2 days of hydration, while it is not observed in the system with lower metakaolin content (MK40). At 3 days, Hc is detected in both systems. This trend follows the corresponding positions of the peaks shown in Figure 8-4 for these systems.

In the LC^3 systems, Hc is observed after 24 hours of hydration (Figure 8-3). This suggest that in LC^3 systems some aluminates from C_3A can participate in the precipitation of AFm after depletion of solid gypsum, and later on (during the third peak) the additional aluminates from metakaolin will contribute the aluminium required for this reaction. This is not the case in C_3S + LC^2 systems where C_3A is not present, and thus AFm phases are not detected at 24 hours. More Mc is observed in C_3S + LC^2 systems relative to Hc as compared to the corresponding LC^3 systems at later ages. This suggests that the pH of the pore solution might play a role

in the formation of one or another type of CO_3-AFm phases. In OPC-based systems, pH will be slightly higher due to the presence of minor amounts of alkalis.

As observed in Figure 8-5, ettringite is detected in both cases after 1 day of hydration. This indicates that during the first 24 hours of hydration, the dissolved aluminates from MK are available to form ettringite if sulfate ions are also available. This could explain why LC^3 systems precipitate more ettringite per gram of OPC as compared to other blended cements, as shown in [7]. Furthermore, this suggests that it is more difficult to reach a point of oversulfation (i.e., where the aluminate peak is no longer observed due to depletion of aluminates before sulfate) in LC^3 systems as compared to OPC or other blended cements. This subject is further discussed in subsection 8.3.4.

The ettringite content is higher in the system with MK95 grade clay as a higher amount of sulfate was added to this system. Hc + Mc content at 7 days is also higher in the system with MK95 clay as compared to MK40. After two days of hydration, the ettringite content stabilizes in both systems when solid gypsum is depleted from the system.
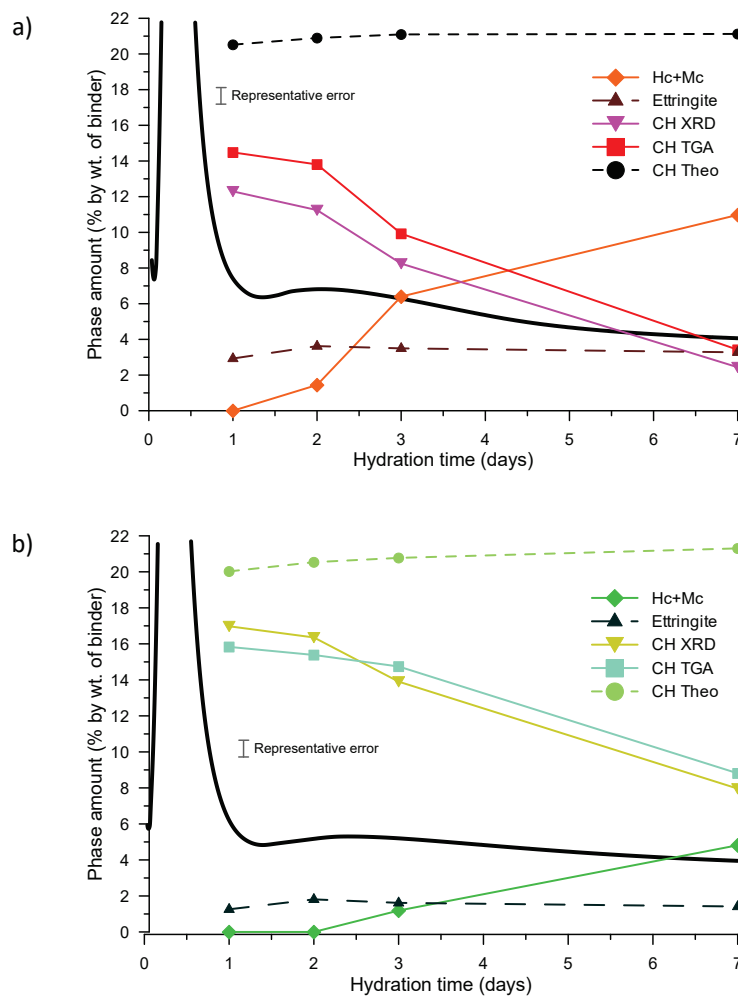
Figure 8-5: Evolution of ettringite, portlandite and Hc + Mc precipitation in C_3S + LC^2 systems with MK95 (a) and MK40 (b) clay grades.

8.3.3   Factors influencing the reaction of MK and LS: metakaolin content

The two LC^3 systems shown in Figure 8-2 suggest that the magnitude and position of the third peak depends on the total metakaolin content of the system. In Figure 8-6, a larger dataset of heat flow curves is presented, but in this case for LC^3 systems with 0% addition of gypsum. This is intended to decouple the contribution of metakaolin content and sulfate content (discussed in the next section) on the position and intensity of the third hydration peak. Metakaolin content has a strong effect in the position and intensity at the maximum of the third hydration peak. For the MK95 system, the peak reaches its maximum at about 54 hours, while for the MK20 system this occurs after 86 hours of hydration.
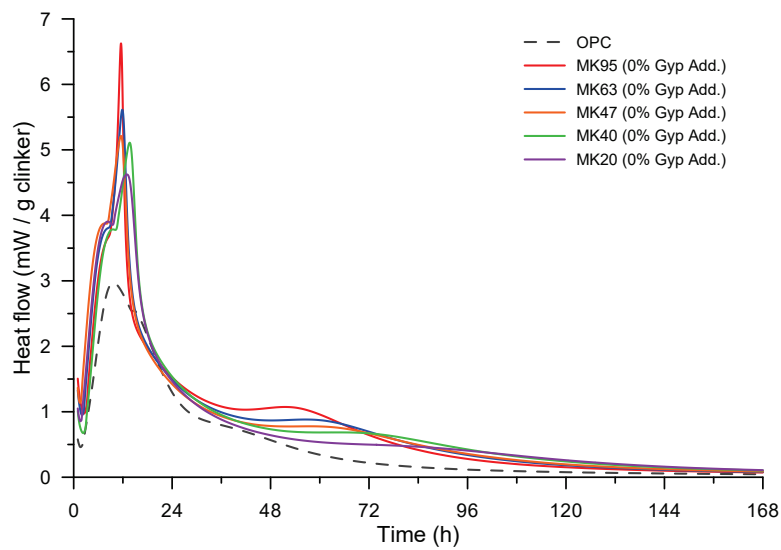
Figure 8-6: Heat flow curves of LC^3 systems with different grades of clay, with no additional gypsum incorporated to the system.

The observations made based on the calorimetry results shown in Figure 8-6 would suggests that more CO_3-AFm will be precipitated in LC^3 as the metakaolin content increases. However, the quantification of these phases by XRD (Figure 8-7) show that this is only the case at very early age, before 7 days of hydration. Afterwards, the highest amount of Hc and Mc is observed in the MK40 system, with decreasing amounts of CO_3-AFm measured as the metakaolin content increase. For the system with MK20, the Hc + Mc content is significantly lower at all ages. A previous study shows that this trend in Hc + Mc formation is also the case at later ages [9]. In the referenced study, it is proposed that the precipitation of Hc and Mc is limited in the high-grade systems due to the lack of capillary pores above a critical size. In this case, precipitation becomes more difficult due to the higher supersaturation level required.

Lower amounts of CO_3-AFm for high metakaolin (MK95) systems is not observed at 7 days in the $C_3S + LC^2$ systems shown in Figure 8-5. This is likely due to the higher w/b ratio used in these systems (0.5, as opposed to 0.4 in all OPC-based materials). This difference supports the hypothesis of a space limitation being the reason of the lower amounts of Hc and Mc phases observed in higher grade systems at later ages.
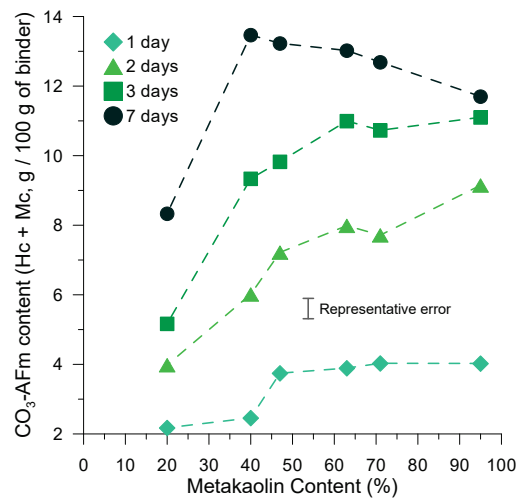
Figure 8-7: Evolution of Hc + Mc precipitation in LC^3 systems with different grades of clay.

Figure 8-8 presents the expected phase assemblage obtained by thermodynamic modelling. The system considered for the model consists of 54% OPC, 30% calcined clay, 15% limestone and 1% gypsum, at w/b 0.4. The phase assemblage was computed for different amounts of metakaolin reacted in the system. These values are also shown in separate axes as equivalent clay grades of in LC^3-50 at four different degrees of reaction of metakaolin to make easier comparisons with the experimental data.

In thermodynamic modelling, normally only Mc is observed, as Hc is assumed as a metastable phase [17]. The Mc content increases up until about 12% per mass of binder of metakaolin reacted and then decrease as strätlingite starts to precipitate. The lower Hc + Mc content measured for LC^3 MK20 (Figure 8-7) can be interpreted from the modeling results, as even at 100% degree of reaction (DoR) of metakaolin, the content of Mc precipitated is limited by the amount of metakaolin available. Ettringite content remains stable over the whole range simulated (for a constant gypsum content), in agreement with the experimental results.

Differences are observed between phase assemblage predicted by thermodynamic modelling for LC^3 systems and the measured ones over real samples. In the XRD patterns shown in Figure 8-3, CH is observed even at later ages for both LC^3 systems shown (MK95 and MK40). Furthermore, strätlingite is not clearly observed in LC^3 systems up to 90 days of hydration. Based on the modelling results, the lack of strätlingite suggests that the degree of reaction of metakaolin in the MK95 system is low. A previous study reported 30% DoR at 90 days for a system analogue to MK95 [25]. Higher DoR values were measured for lower grade clays.

Porosity refinement and lack of capillary pores are not accounted for in the modelling results presented, where a theoretical thermodynamic equilibrium condition is used to compute the phase assemblage. The influence of space filling could explain the observed differences between the modelling results and the experimental data. However, there is still an open question regarding if the lack of space establishes an actual limit for the reaction of metakaolin, or the differences between the model and experimental results are also related to a kinetic effect.
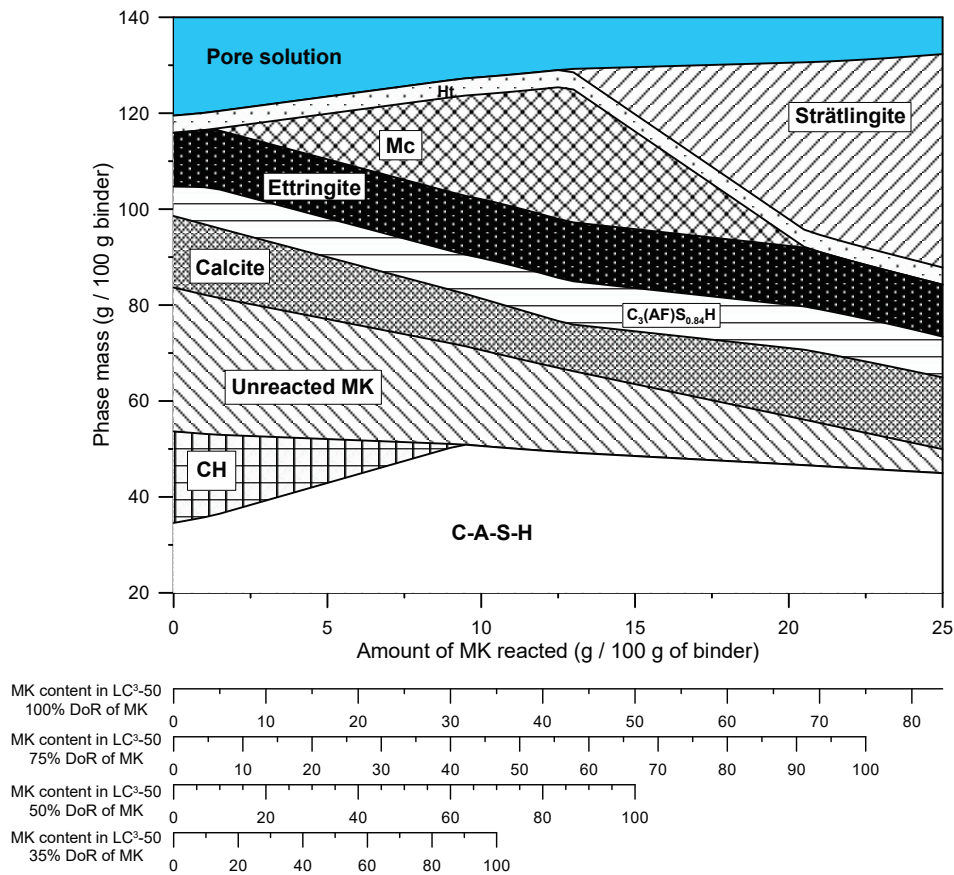
Figure 8-8: Phase assemblage of LC^3 with different clay grades, computed at equilibrium by thermodynamic modeling.

To explore further the influence of pore refinement on the limitation of metakaolin reaction observed in high grade LC^3 systems, the phase assemblage of LC^3 MK95, MK63, MK40 and MK20 was measured by XRD on a sealed sample stored for 2.5 years at 20°C. The measured diffractograms are shown in Figure 8-9. CH is depleted in the MK95 and MK63 systems (the content after Rietveld refinement in MK63 was negligible, although a small peak is still visible at 18° 2θ). This indicates that the reaction of metakaolin continues after 90 days in these systems, as CH was observed at 90 days. The degree of reaction of metakaolin can be estimated using the auxiliary axes in Figure 8-8. The MK40 and MK20 system still exhibit some remaining CH. This shows that the DoR of metakaolin in MK40 increased but it is not 100%, as this system should be able to deplete CH according to thermodynamic modelling. In the case of MK20, CH remains present even at 100% DoR in an LC^3 blend with 20% metakaolin content.

Strätlingite is observed in the MK95 and in lower amounts in the MK63 system. Based on the thermodynamic modeling results, strätlingite is not expected in the MK40/MK20 system even at 100% DoR, in agreement with the experimental results. The presence of strätlingite in MK95 and MK63 systems further supports the observation that metakaolin reaction still occur after 90 days at a slower rate. As seen in Figure 8-8, a DoR of metakaolin above 50% would be required to precipitate this phase in MK95 and about 75% for MK63. This is well beyond the values previously reported for LC^3-50 systems with similar clay grades at 90 days [25]. Therefore, metakaolin reaction in LC^3 appears to be slowed down, but not limited, by the reduction in space

available for precipitation. The reaction continues until depletion of CH if the metakaolin content of the system is sufficiently high (around 30% for the LC^3-50 systems studied).

The relative amount of Mc with respect to Hc also increased in the long term. In contrast with the patterns shown in Figure 8-3 where a small and broad Mc peak is observed, the older samples of the same systems exhibit a higher and sharper peak, comparable or higher to the one of Hc. While more CO$_3$-AFm precipitated during this period after 90 days, the magnitude of the variation in the Hc/Mc ratio suggests that some Hc might have transformed into Mc, although Hc is still clearly present in the samples. Two points should be made in this regard. The relative amount of Mc increases in the long term, approaching the phase assemblage predicted by thermodynamic modeling. Nevertheless, Hc remains present and thus possess some degree of long-term stability, rather than being a metastable phase, in systems beyond the compositional boundaries usually described for its formation [17].
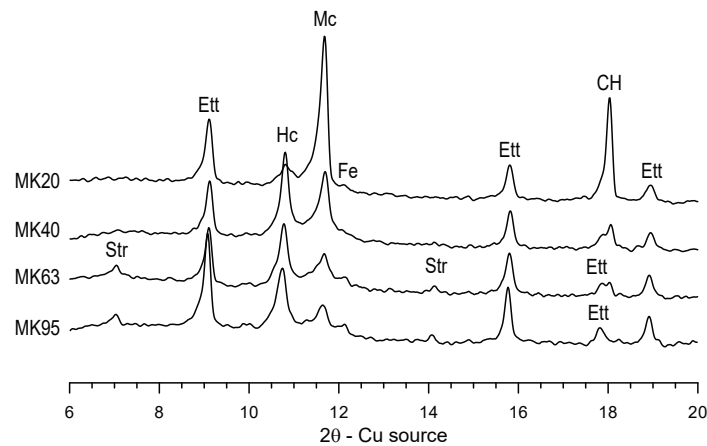
Figure 8-9: XRD patterns of LC^3 systems measured after 2.5 years of hydration in sealed conditions.

8.3.4   Factors influencing the reaction of MK and LS: sulfate content

The effect of the sulfate content on the reaction of metakaolin and limestone in LC^3 was studied in the LC^3 MK95 system, with added gypsum contents varying from 0 to 12% by mass of binder. The heat flow curves of these systems are shown in Figure 8-10. An enhanced aluminate peak is seen in all cases. As the amount of gypsum added increases, the onset of the aluminate peak shifts right. In all the systems the aluminate peak is clearly observed, indicating that the point of depletion of solid gypsum is reached. Regarding the peak associated with the reaction of metakaolin and limestone, an acceleration is observed with an increasing amount of gypsum addition. At contents of 7 and 12% of added gypsum, the second and third peaks seem to overlap partially.

XRD analysis was conducted in these systems to observe possible changes in the phase assemblage due to the addition of larger amounts of sulfate. Phase quantification obtained by Rietveld refinement for ettringite, Hc + Mc and CH contents are shown in Figure 8-11 a, b and c respectively. In the case of ettringite, a theoretical computation was conducted based on the total SO$_3$ available in the system.
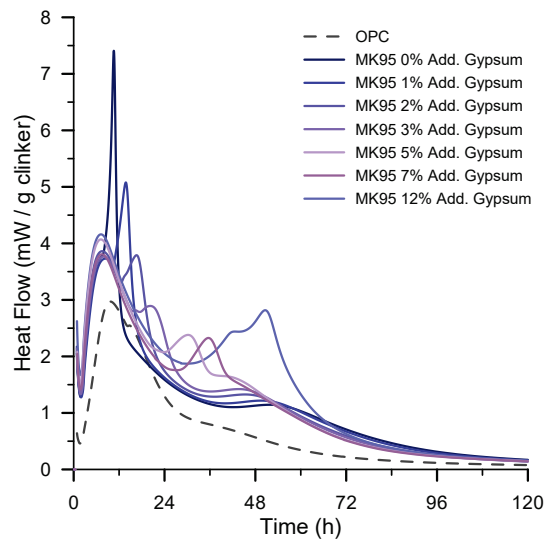
Figure 8-10: Heat flow curves of LC³ MK95 with different amounts of gypsum additions.
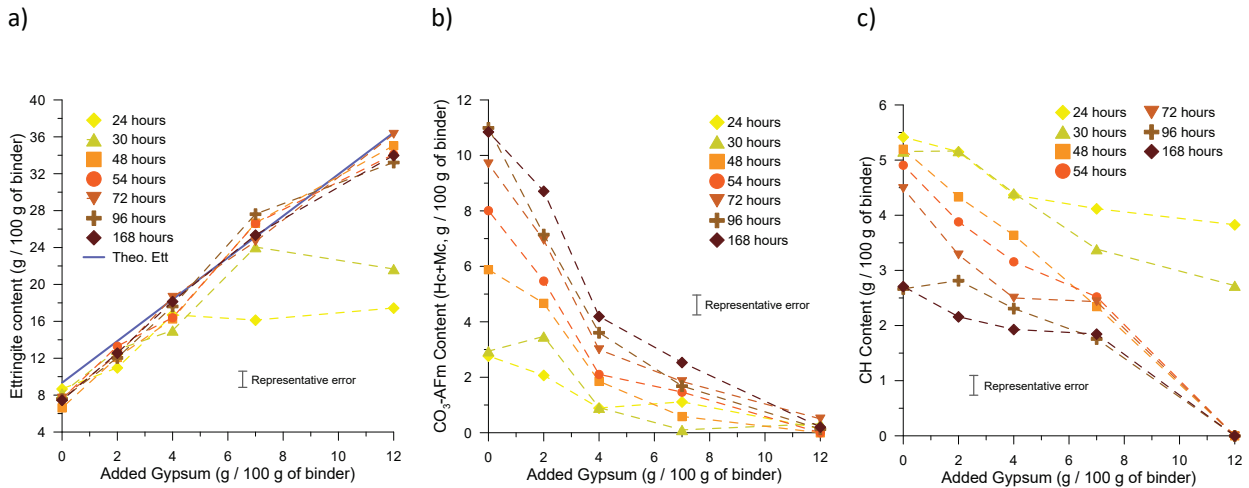
Figure 8-11: Ettringite (a), Hc+Mc (b) and portlandite (c) content of LC³ MK95 system in time with different amounts of gypsum additions.

The ettringite content increases steadily with the increase in gypsum content of the system. This indicates that the aluminates from metakaolin participate in the formation of additional ettringite until gypsum is depleted, as the amounts are well above the potential formation with aluminates from C₃A only. The amounts observed are in close correlation with the computed theoretical contents for each system. Furthermore, the increase in ettringite content is accompanied by a decrease in the Hc + Mc content, Figure 8-11b. Therefore, it can be inferred that the aluminates available from metakaolin dissolution will participate in the precipitation of ettringite as long as the concentration of sulfate in the pore solution is high.

In normal OPC systems, aluminates from C_3A reacts with sulfate to form ettringite during the first hours of hydration. From a stoichiometry point of view, C_3A and gypsum also provide enough calcium to sustain this ettringite formation. In the case of ettringite formed by the reaction of aluminates from metakaolin and gypsum the situation is different, as metakaolin does not contain calcium. However, ettringite still forms as seen in Figure 8-11a, indicating that calcium comes from the alite hydration via the pore solution. Figure 8-11c shows that the amount of CH decreases significantly as the amount of gypsum is increased in the system, reaching even complete depletion at 7 days for a 12% gypsum addition.

Thermodynamic modelling was carried out for a system analogue to the one shown in Figure 8-8, but with just 7% metakaolin reacted (24.5% DoR of MK95 system) to emulate the conditions at early age before CH depletion. Different gypsum additions were introduced from 0 to 12%. These additions correspond to the amount of sulfate added on top of the sulfate contained in the OPC fraction, as in the studied mixtures.

The results shown in Figure 8-12 are in general agreement with the experimental observations by XRD. As the amount of added gypsum increase, the amount of Mc and CH reduces due to an increased precipitation of ettringite that consumes the aluminates from metakaolin. For 12% of added gypsum content, no CH is observed and the content of Mc is also close to zero, as seen in the experimental results at 7 days.
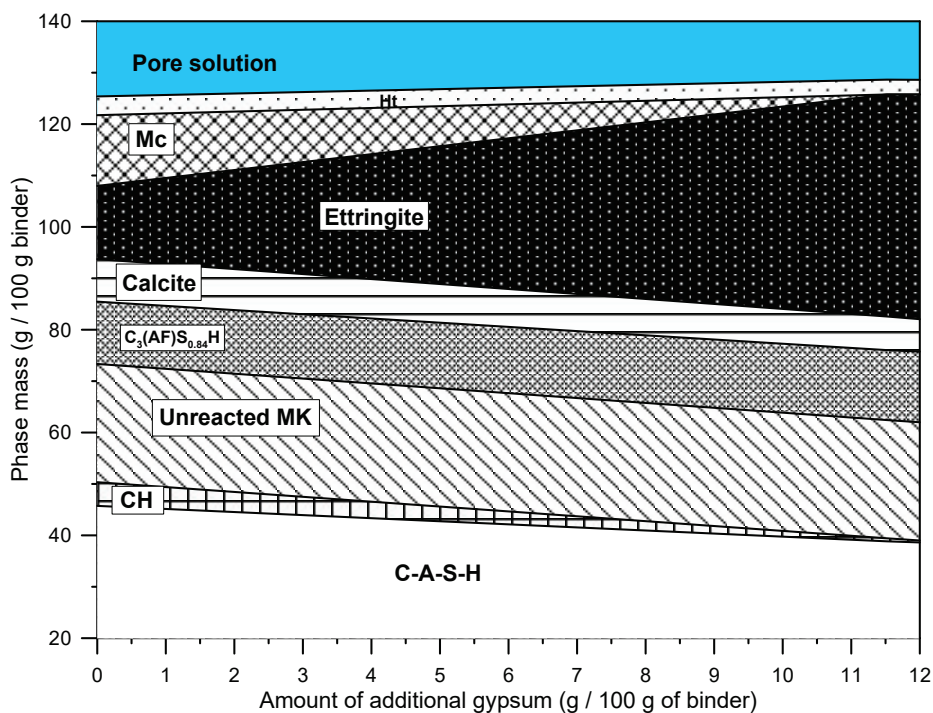
Figure 8-12: Phase assemblage of LC^3 gypsum additions between 0 and 12%, computed at equilibrium by thermodynamic modeling.

8.3.5   Factors influencing the reaction of MK and LS: w/b ratio

As discussed in the previous sections, porosity refinement has an effect on the reaction kinetics of metakaolin. The effect of initial space was studied by increasing the w/b ratio of MK95 and MK40 systems to

0.8. It should be noted that no bleeding was observed in the high w/b systems. The heat flow and total heat curves are shown in Figure 8-13.

The aluminate peak of both LC^3 systems appears enhanced in the w/b 0.8 systems as compared to w/b 0.4. However, the position of the onset of the peaks is slightly retarded in the high w/b systems, which can be explained by the lower alite peak observed [7]. The corresponding third peaks appear retarded in the w/b 0.8 systems.

The total heat curves shown in Figure 8-13b present some additional insights regarding the hydration of LC^3 systems. Up to about 48 hours for MK95 and 80 hours for MK40, the systems at high and low w/b follow equal hydration rates. At this point, a split occurs between the corresponding high and low w/b systems. The low w/b system slows down while the high w/b ratio systems continue at a high rate of reaction for a longer period of time. The time when the curve splitting occurs matches relatively well with the position of the maximum of the third peak of hydration in the low w/b systems. As it will be shown in the next section, at this time the corresponding systems reach a high degree of porosity refinement due to the precipitation of CO$_3$-AFm. The origin of the refinement that leads to a slowdown in the reaction is then linked to the formation of Hc and Mc, as evidenced by the match between the third peak of hydration in LC^3 and the split point of the curves with high and low w/b.

a)   b)
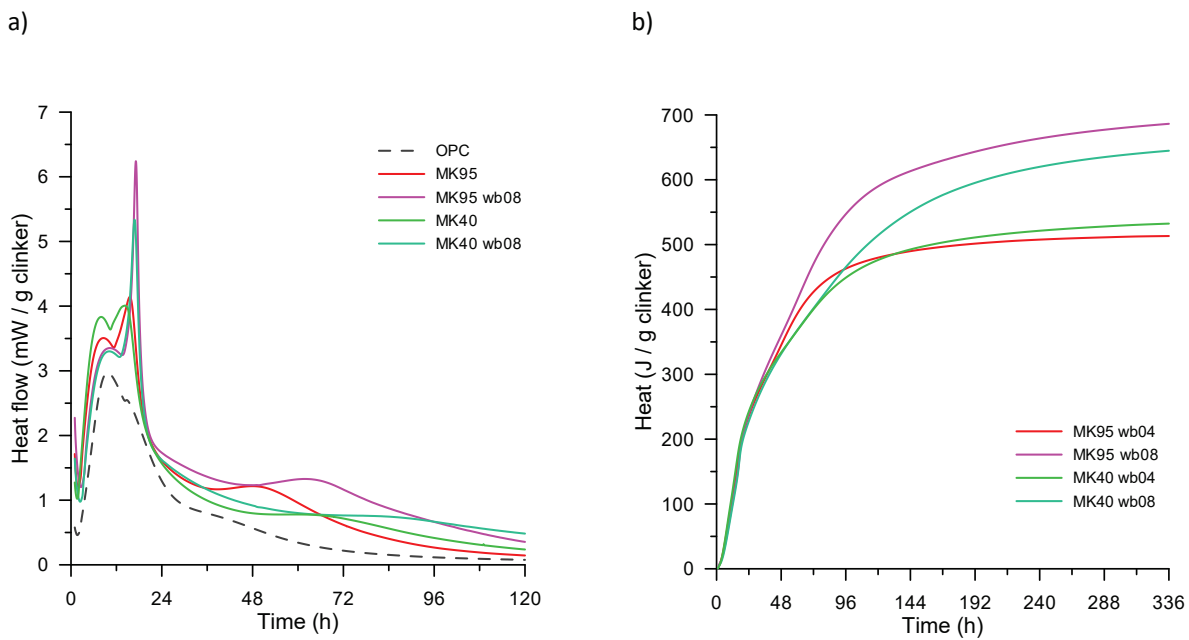
Figure 8-13: Heat flow (a) and total heat (b) of LC^3 MK 95 and MK40 with w/b ratio of 0.4 and 0.8.

8.3.6   Microstructural development of LC^3

SEM-EDS analysis was used to study the microstructural development in LC^3 pastes in relation to the precipitation of Hc and Mc. The systems MK95 and MK40 were selected as the difference in the position of the third peak between them is sufficiently large to be able to track the effect of this reaction in the microstructure. Elemental composition maps were collected for samples hydrated for 1, 3 and 7 days for both systems.

Processing of the data was conducted using *edxia* to obtain the data points in an Al/Ca versus Si/Ca diagram, as shown in Figure 8-14a. In the plot, the points corresponding to Hc/Mc have been highlighted along with CH/Calcite and anhydrous cement grains. Points close to ettringite composition were not observed indicating that it is intimately mixed with C-A-S-H. Several points corresponding to intermix of metakaolin and AFm are observed. The histogram of the BSE dataset was used to clearly identify points corresponding to anhydrous C_3A and C_4AF, as they appear intercalated with AFm points. *Edxia* also allows to create masks from clusters of points that are identified to correspond to a certain phase, as shown in Figure 8-14b.

a)
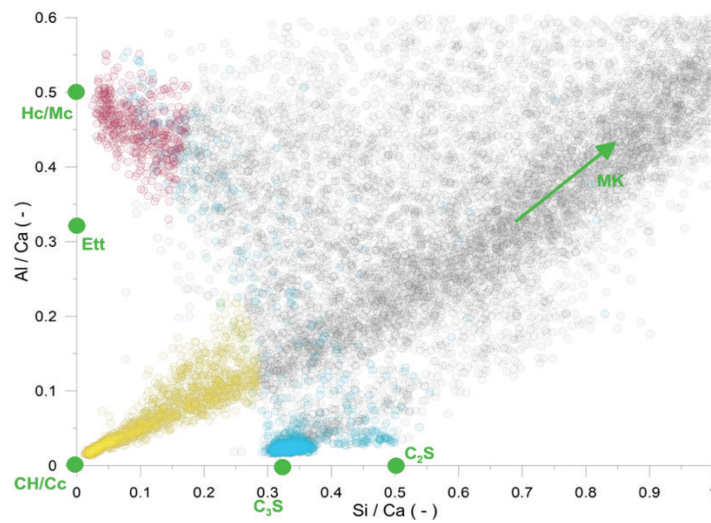
b)
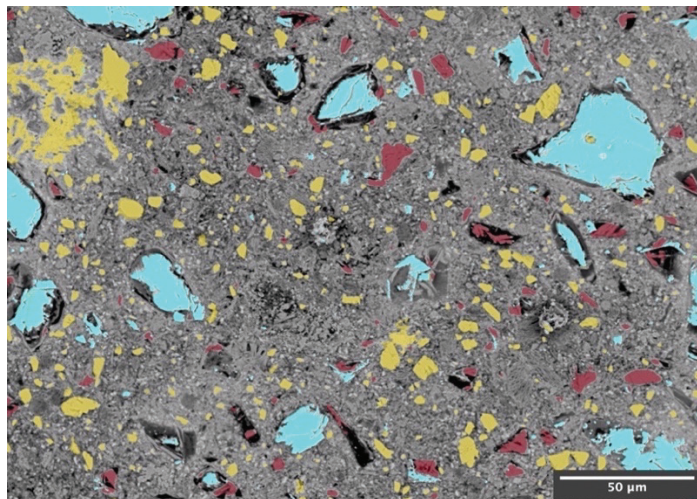
Figure 8-14: Al/Ca vs Si/Ca diagram obtained from EDS data collected from the sample of the LC³ MK95 system at 3 days (a) and masks of CH/Cc, AFm and anhydrous clusters shown overlapped to the BSE micrograph (b).

Portlandite + limestone in yellow, Hc + Mc in red, anhydrous cement grains in cyan.

Masks for Hc/Mc were created for each map, and superimposed to the BSE image. The micrographs with highlighted CO_3-AFm clusters are shown in Figure 8-15. Precipitation of CO_3-AFm takes place in large pores that remain after OPC hydration. At 1 and 3 days, the area coverage of AFm clusters is very similar between MK95 and MK40 systems. However, at 7 days more AFm is observed in the MK40 sample, in good agreement with XRD results (Figure 8-7). The microstructure of MK95 appears more compact and the porosity more refined at this age. Surface area fractions of the AFm clusters were computed in each case based on the masks generated and are shown alongside each micrograph.

LC^3-50 MK40   LC^3-50 MK95

1d

AFm area: 0.87%   AFm area: 0.79%

3d

AFm area: 2.16%   AFm area: 2.42%

162

7d

AFm area: 6.41%   AFm area: 5.44%
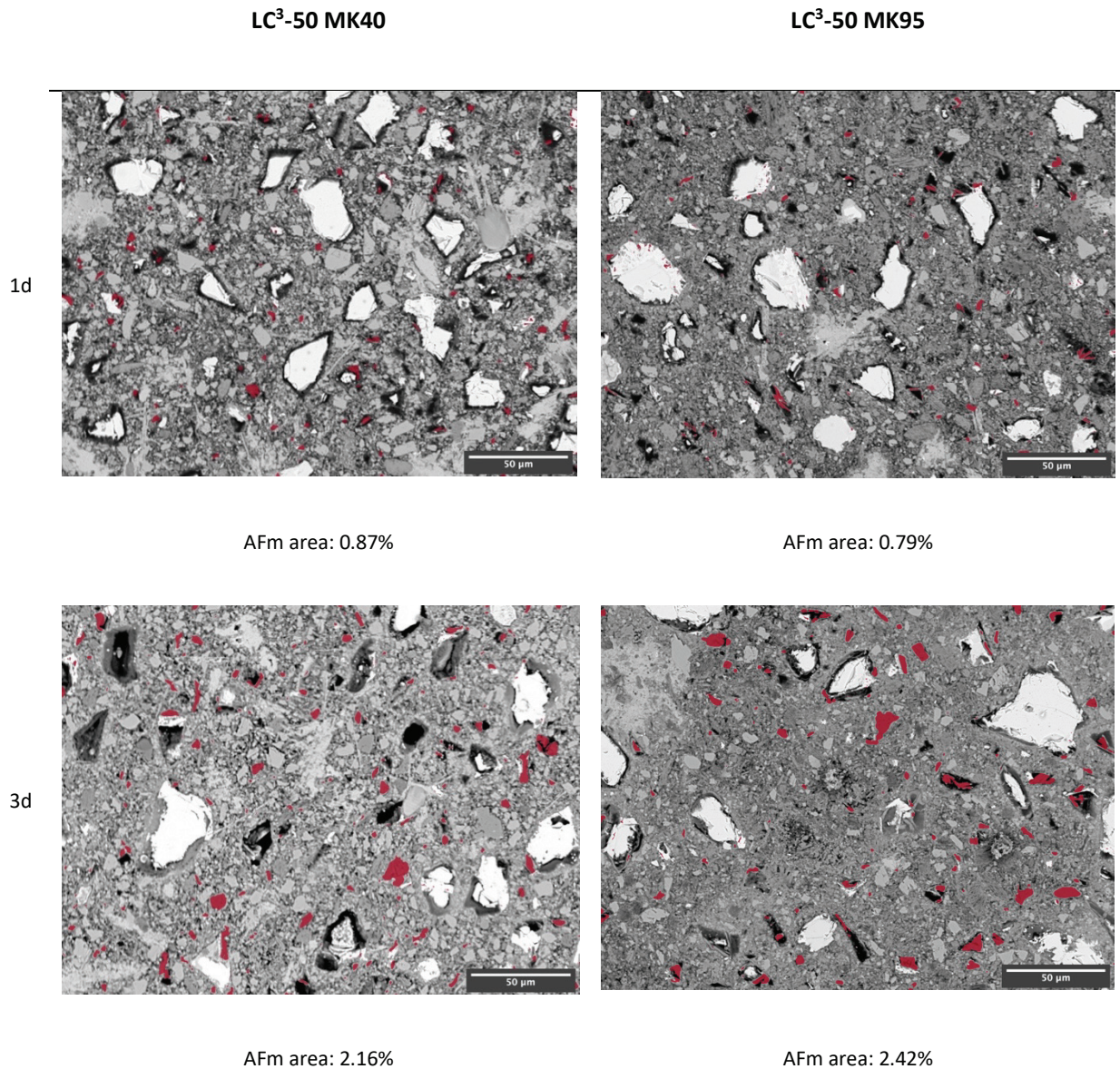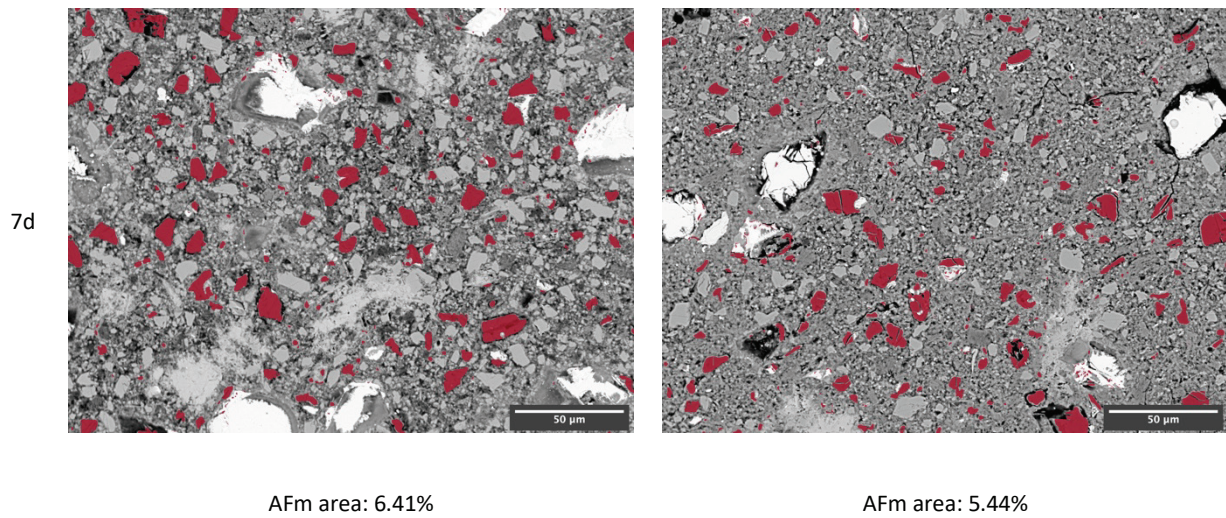
Figure 8-15: BSE maps of MK95 and MK40 systems at 1, 3 and 7 days with CO_3-AFm phase highlighted in red.

Higher resolution micrographs show the Hc/Mc grains blend with the surrounding C-A-S-H (Figure 8-16). Ettringite is observed highly intermixed with C-A-S-H. This explains the absences of points around the ettringite composition in Figure 8-14a due to volume of interaction effects. Unreacted metakaolin particles are also highly intermixed/integrated with the C-A-S-H matrix, explaining the high degree of scatter observed in the point representation for Al/Ca above 0.3.
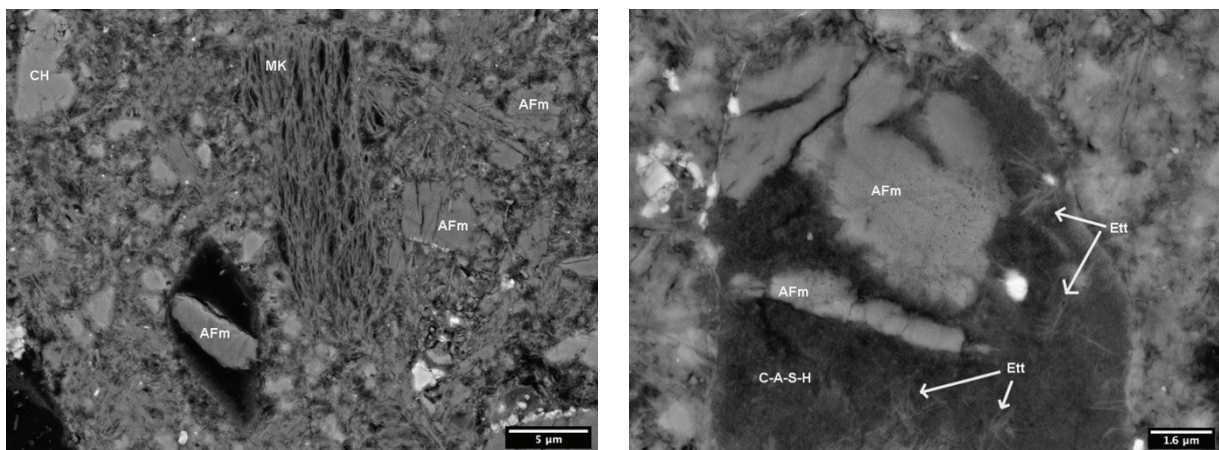
Figure 8-16: BSE micrographs of LC³ MK95 hydrated for 3 days, showing grains of AFm blending with the surrounding C-A-S-H matrix.

163

8.3.7 The effect of Hc and Mc in porosity refinement and mechanical properties

Compressive strength results of mortar tests are presented in Figure 8-17. At 1 day, strength is lower than plain OPC, and relatively similar among LC^3 systems with different grades. Strength depends mainly on OPC hydration at this point, and the differences can be attributed to different kinetics of alite hydration as the surface of the binder increases (see Table 3). At 2 and 3 days, a clear dependence of compressive strength and the metakaolin content of the system is observed. This agrees with a previous study that stablished metakaolin content as the main parameter controlling LC^3 strength [9]. From 7 days onwards, the situation changes, and the relationship between metakaolin content and strength is less obvious, especially in systems with higher grade clays where similar strengths are observed. This observation was also made in [9], where a loss of linearity in the strength-metakaolin content correlation was observed at later ages.

As it was discussed in section 8.3.3, metakaolin content has an effect in the kinetics of the reaction of metakaolin and limestone (third peak). In addition, this reaction occurs mainly between 2 and 4 days of hydration, depending on the grade of the clay (earlier for higher metakaolin content). This suggests that the precipitation of Hc and Mc associated with the third peak observed in LC^3 systems is responsible for the strength increase observed at these ages in the mortars. Hc and Mc have then a direct influence in the compressive strength of LC^3 systems. At 7 days, the peak already occurred in all systems, and as a consequence the strengths become more similar between different grades of clay. The MK20 system remains lower since the reaction is limited by metakaolin availability.
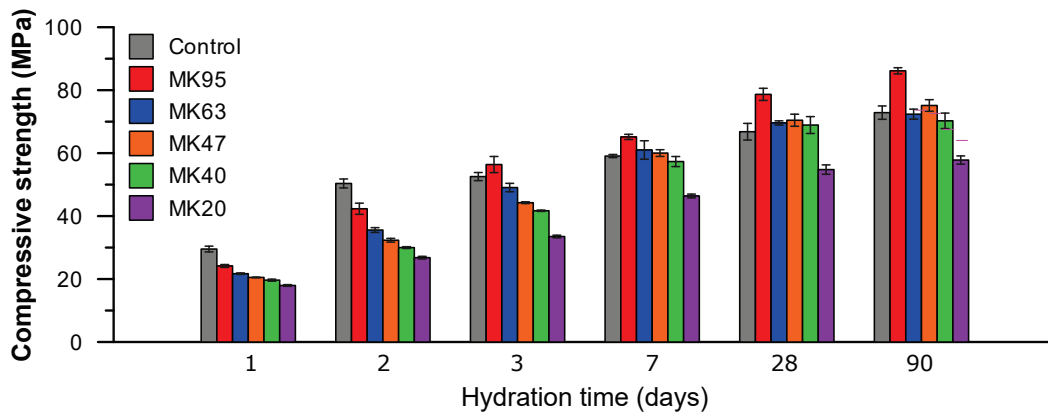
Figure 8-17: Compressive strength of LC^3 systems with different grades of clay.

To further explore this hypothesis, an in-situ measurement of ultrasonic pulse velocity was performed in the MK95 and MK40 systems. An increase in pulse velocity is normally associated with a reduction of the pore volume. As seen in Figure 8-18, a clear split between the two systems occurs at the time of the third peak of the MK95 system, indicated that precipitation of CO_3-AFm indeed leads to a measurable reduction in porosity and to the observed increase in strength. Later on, the third peak of the MK40 system takes place, and catches up with the MK95 system, as also observed in the calorimetry measurements. Thus, when the pore structure becomes refined, the reaction slows down, in agreement with previous studies [9].
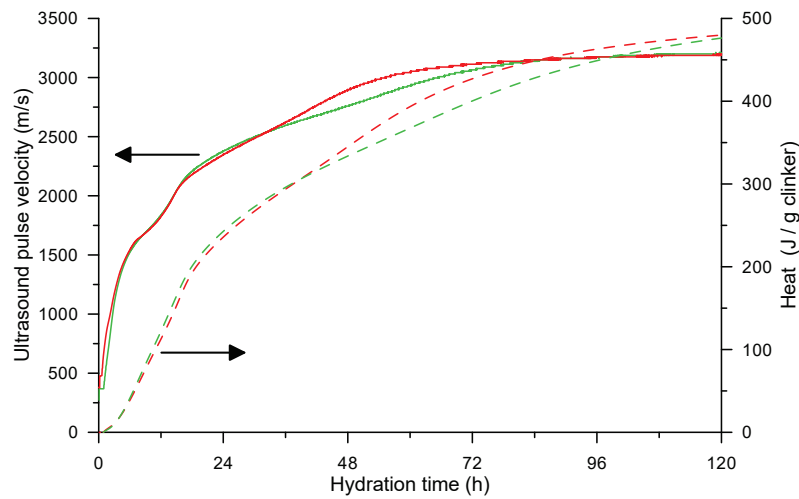
Figure 8-18: In-situ ultrasound pulse velocity measured on LC³ MK95 and MK40 systems at 23°C.

Calorimetry curves (at 20°C) of the same systems included for comparison.

Figure 8-19 shows the total porosity measured by MIP for different LC³ systems at 1, 2, 3 and 7 days. At 1 day (Figure 8-19a), the critical entry radius of LC³ system is similar among the different systems, and significantly larger than OPC. At 2 days (Figure 8-19b), MK95 refines significantly, due to an earlier formation of Hc and Mc in this system. At 3 days (Figure 8-19c), the critical entry radius of MK95 and MK63 is smaller than OPC, while MK40 and MK20 further refine and start to approach it. Finally, at 7 days (Figure 8-19d) all systems exhibit smaller critical entry radiuses as compared to OPC. The refinement of MK95 is marginal between 3 and 7 days, while the other systems evolve significantly.

a)

b)

c)

d)
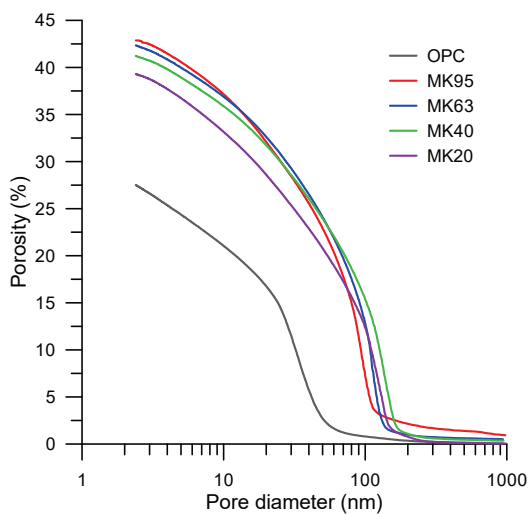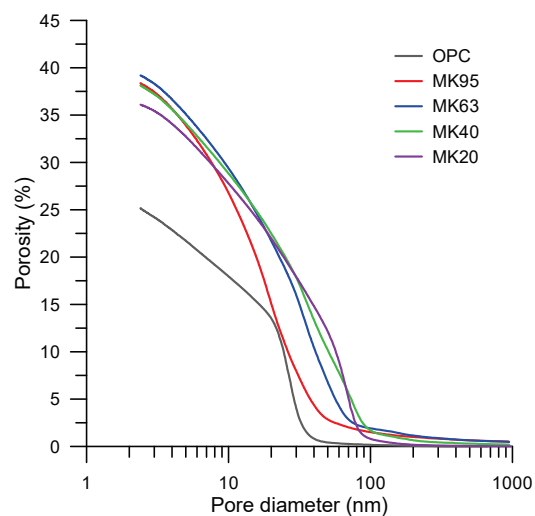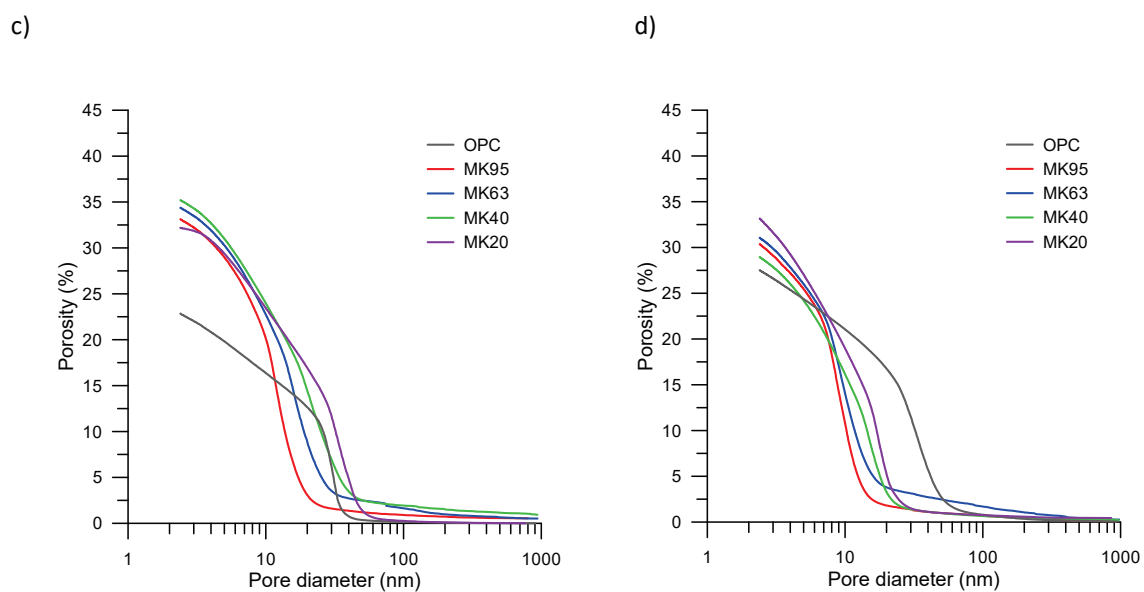
Figure 8-19: Total porosity measured by MIP on OPC and LC³ systems with different grades of clay after 1 (a), 2 (b), 3 (c) and 7 (d) days of hydration.

8.4   Conclusions

In this paper, the reaction of metakaolin and limestone was studied and its effects on porosity refinement and mechanical properties were assessed. As in LC^3-type cements the content of aluminates is significantly higher as in a conventional OPC, aluminate hydrates play an important role in the hydration and properties of this systems.

Based on the results presented, the following conclusions can be drawn:

1. The third peak of hydration observed in LC^3 cements corresponds to a precipitation of hemicarboaluminate and monocarboaluminate from the reaction of metakaolin and calcined clay, which takes place between 2 and 4 days of hydration.

2. Metakaolin and sulfate content both affect the position of the third peak of hydration. These factors lead to an earlier occurrence of the peak. An increase in the water to binder ratio of the system leads to a slight retardation of the third peak. However, as more space is available for precipitation of hydrates, the slowdown of the reaction occurs later and higher heat release per gram of OPC are observed at early ages.

3. The aluminates from metakaolin can participate in the formation of ettringite until depletion of solid gypsum in the system. This reaction occurs instead of CO_3-AFm precipitation until gypsum is depleted, leading to a reduction in the amounts of Hc and Mc. This precipitation of ettringite requires additional calcium from the system. Thus, this reaction also leads to a reduction in CH content.

4. Hemicarboaluminate and monocarboaluminate precipitate in pores left behind by clinker hydration. The clusters of CO_3-AFm integrate to the surrounding C-A-S-H matrix, effectively contributing to porosity refinement and strength development. The precipitation of Hc and Mc is responsible for the rapid porosity refinement observed in LC^3 at early ages that leads to a slowdown of the reaction rate of metakaolin.

5. Metakaolin reaction is slowed down, but not limited, by the lack of space available for precipitation. However, the reaction keeps going at a slow rate and ultimately, CH is depleted from the system. The observed phase assemblage in long term samples approaches the one computed by thermodynamic modelling at equilibrium.

8.5   References

[1]   M. Schneider, M. Romer, M. Tschudin, H. Bolio, Sustainable cement production—present and future, Cem. Concr. Res. 41 (2011) 642–650. doi:10.1016/j.cemconres.2011.03.019.

[2]   K.L. Scrivener, V. John, E.M. Gartner, Eco-efficient cements: potential, economically viable solutions for a low-CO2, cement-based materials industry, in: United Nations Environmental Programme (UNEP), 2016.

[3]   B. Lothenbach, K. Scrivener, R.D. Hooton, Supplementary cementitious materials, Cem. Concr. Res. 41 (2011) 1244–1256. doi:10.1016/j.cemconres.2010.12.001.

[4]   IEA, CSI, Technology Roadmap: Low-Carbon transition in the Cement Industry, 2018. doi:10.1007/springerreference_7300.

[5]   K. Scrivener, F. Martirena, S. Bishnoi, S. Maity, Calcined clay limestone cements (LC3), Cem. Concr. Res. (2017) 1–8. doi:10.1016/j.cemconres.2017.08.017.

[6]   M. Antoni, Investigation of cement substitution by combined addition of calcined clays and limestone, École Polytechnique Fédérale de Lausanne, 2011.

[7]   F. Zunino, K.L. Scrivener, The influence of the filler effect in the sulfate requirement of blended cements, Cem. Concr. Res. 126 (2019). doi:10.1016/j.cemconres.2019.105918.

[8]   F. Zunino, K.L. Scrivener, Factors influencing the sulfate balance in pure phase C3S/C3A systems, Cem. Concr. Res. (n.d.). Submitted.

[9]   F. Avet, K. Scrivener, Investigation of the calcined kaolinite content on the hydration of Limestone Calcined Clay Cement (LC3), Cem. Concr. Res. 107 (2018) 124–135. doi:10.1016/j.cemconres.2018.02.016.

[10]   K.L. Scrivener, F. Avet, H. Maraghechi, F. Zunino, J. Ston, A. Favier, et al., Impacting factors and properties of Limestone Calcined Clay Cements (LC3), Green Mater. (2018). doi:https://doi.org/10.1680/jgrma.18.00029.

[11]   M. Antoni, J. Rossen, F. Martirena, K. Scrivener, Cement substitution by a combination of metakaolin and limestone, Cem. Concr. Res. 42 (2012) 1579–1589. doi:10.1016/j.cemconres.2012.09.006.

[12]   S. Sui, W. Wilson, F. Georget, H. Maraghechi, H. Kazemi-Kamyab, W. Sun, et al., Quantification methods for chloride binding in Portland cement and limestone systems, Cem. Concr. Res. 125 (2019). doi:10.1016/j.cemconres.2019.105864.

[13]   F. Avet, E. Boehm-Courjault, K. Scrivener, Investigation of C-A-S-H composition, morphology and density in Limestone Calcined Clay Cement (LC3), Cem. Concr. Res. 115 (2019) 70–79. doi:10.1016/j.cemconres.2018.10.011.

[14]   E. L'Hôpital, B. Lothenbach, G. Le Saout, D. Kulik, K. Scrivener, Incorporation of aluminium in calcium-silicate-hydrates, Cem. Concr. Res. 75 (2015) 91–103. doi:10.1016/j.cemconres.2015.04.007.

[15]   D.P. Bentz, P.E. Stutzman, F. Zunino, Low-temperature curing strength enhancement in cement-based materials containing limestone powder, Mater. Struct. Constr. 50 (2017). doi:10.1617/s11527-017-1042-6.

[16]   O. Chowaniec, Limestone Addition in Cement, 2012. https://infoscience.epfl.ch/record/174700.

[17]   T. Matschei, B. Lothenbach, F.P. Glasser, The role of calcium carbonate in cement hydration, Cem. Concr. Res. 37 (2007) 551–558. doi:10.1016/j.cemconres.2006.10.013.

[18]   X. Li, A. Ouzia, K. Scrivener, Laboratory synthesis of C3S on the kilogram scale, Cem. Concr. Res. 108 (2018) 201–207. doi:10.1016/j.cemconres.2018.03.019.

[19]   K. Scrivener, R. Snellings, B. Lothenbach, A Practical Guide to Microstructural Analysis of Cementitious Materials, (2016) 540. doi:10.7693/wl20150205.

[20]   F. Georget, edxia. Zenodo, (2019). doi:10.5281/zenodo.3246902.

[21]   D.A. Kulik, T. Wagner, S. V. Dmytrieva, G. Kosakowski, F.F. Hingerl, K. V. Chudnenko, et al., GEM-Selektor geochemical modeling package: Revised algorithm and GEMS3K numerical kernel for coupled simulation codes, Comput. Geosci. 17 (2013) 1–24. doi:10.1007/s10596-012-9310-6.

[22]   B. Lothenbach, D.A. Kulik, T. Matschei, M. Balonis, L. Baquerizo, B. Dilnesa, et al., Cemdata18: A chemical thermodynamic database for hydrated Portland cements and alkali-activated materials, Cem. Concr. Res. 115 (2019) 472–506. doi:10.1016/j.cemconres.2018.04.018.

[23]   A. Quennoz, K.L. Scrivener, Interactions between alite and C3A-gypsum hydrations in model cements, Cem. Concr. Res. 44 (2013) 46–54. doi:10.1016/j.cemconres.2012.10.018.

[24]   K.L. Scrivener, Development of the microstructure during the hydration of Portland cement, University of London, 1984.

[25]   F. Avet, X. Li, K. Scrivener, Determination of the amount of reacted metakaolin in calcined clay blends, Cem. Concr. Res. 106 (2018) 40–48. doi:10.1016/j.cemconres.2018.01.009.

Chapter 9   Conclusions

Contents

This research project studied various aspects related to the extension and improvement of the use of natural clays in LC^3. The main conclusions of this project are presented according to the main thematic areas covered in this thesis. In addition, the main contributions to cement science, concrete and the LC^3 technology are highlighted at the end of each subsection, along with perspectives for the application of the findings in the field.

9.1 The effect of calcite impurities in kaolinitic clays (*Chapter 3*)

The effect of calcite impurities, which are present in some natural clay deposits, was studied in terms of reactivity and properties of the calcined product. The main findings of this study are:

- o Calcite impurities can lead to a reduction in reactivity of calcined clays. However, this reduction is minor and can be offset by reducing the calcination temperature to 700°C and extending the residence time to allow full dehydroxylation of kaolinite.

- o A granular deposit was found partially covering the metakaolin particles after calcination of clays with calcite impurities. This deposit corresponds to a new amorphous phase formed by the interaction of calcite and kaolinite particles, with Al/Si ratio about 0.75-0.88 and Ca/Si 0.86-1.65.

9.1.1 Practical perspectives

This study showed that natural clays with up to 10% calcite can be used as SCM without compromising reactivity. A reduction of maximum calcination temperature to 700°C and extending the residence time to ensure complete dehydroxylation of kaolinite are proposed as guidelines for effectively processing these materials in the field. This study enables the use of natural resources in regions where clays are often found intermixed with calcite, as it is the case of Cuba, Switzerland and some regions of Africa.

9.2 The use of grinding aids in LC^3 cements (*Chapter 4* and *5*)

The effect of mineral admixtures typically used during production (grinding) of Portland cement when used on LC^3 cements was described. The benefits of using grinding aids in LC^3 are not limited to an increase in yield during production due to a reduction in agglomeration, but they can also influence the phase assemblage and increase mechanical properties in the case of alkanolamines. The main conclusions of these studies are:

- It was shown that particle classification can be used to increase the kaolinite content of clays in cases where only low-grade material is available. Under the experimental conditions of this study, it was possible to double the kaolinite content of the raw clay.

- Alkanolamines enhance the hydration kinetics of LC^3. It was observed that alkanolamines increase the DoH of C_3A and ferrite in LC^3 systems, leading to an increased precipitation of Hc and Mc compared to the control system. More Hc and Mc further refine the pore structure of LC^3 at early age, increasing compressive strength.

- TEA does not have a major influence in the reaction kinetics of calcined clay, independent of the iron content of the clay.

9.2.1   Practical perspectives

Grinding aids have great potential to improve the production of calcined clay and to enhance performance of LC^3. Beyond the improvement in the grinding stage, the use of grinding aids is effective to deagglomerate ground clay and significantly increased the efficiency of a dry particle separation process, even at lower surface coverage compared to cement. In addition, the hydration enhancement provided by the addition of alkanolamines could enable and improvement of mechanical properties at early ages, which is more critical in blended cements, without much additional cost.

These findings are relevant for the industrial application of LC^3 technology, where grinding aids are used on a daily basis. Furthermore, the advantages shown in these studies could be extended to co-grinding situations, reducing equipment and production cost.

9.3   Sulfate balance of LC^3 and other blended cements (*Chapter 6* and *7*)

A mechanism to explain the sulfate balance of LC^3 and other blended cements was described in this study. The new insights presented explain the origin of the increased sulfate demand observed in LC^3. Furthermore, the mechanism proposed can be generalized to any cementitious system containing aluminates. The main conclusions of this study are:

- Supplementary cementitious materials can influence the sulfate balance of a blended cement. However, this influence is not related with their aluminum content, but rather to their fineness (filler effect contribution).

- The mechanism that relates the filler effect and sulfate balance is the adsorption of sulfate in C-(A)-S-H during the alite peak. Fine mineral additions increase the precipitation rate of C-(A)-S-H and consequently, the amount of sulfate adsorbed. An earlier depletion of solid gypsum is reached and as a consequence the aluminate peak occurs earlier.

- The amount of ettringite formed before the aluminate peak also affects the sulfate demand.

o Other factors can influence the sulfate balance of a system by influencing either C-(A)-S-H precipitation or ettringite formation (for example, the dissolution rate of the sulfate source). Other factors not directly studied in this project but known for influencing either C-(A)-S-H precipitation or ettringite (for example, chemical accelerators, seeds, other sulfate sources) are expected to influence the sulfate balance accordingly.

o The higher DoH of C_3S (and/or alite) observed in multiphase systems (and/or OPC) as compared to pure phase systems is most likely due to the enhancement of alite reaction by the addition of gypsum. The enhancement effect is observed in both alite and pure C_3S. While this study does not describe the mechanism, it establishes that it is not related to aluminate phases.

9.3.1 Practical perspectives

A mechanism to explain the sulfate balance in a cementitious system was proposed. Furthermore, a close relationship between the alite and aluminate reaction kinetics was established. These findings provide the initial input required to extend current models for alite hydration to incorporate the aluminate reaction. This would enable a more comprehensive understanding of the hydration process of systems closer to real Portland cements.

The mechanism for sulfate balance proposed is shown schematically in Figure 9-1, where the calorimetry profile of an LC^3 cement is divided in two stages, indicating the main reactions taking place in each of them.
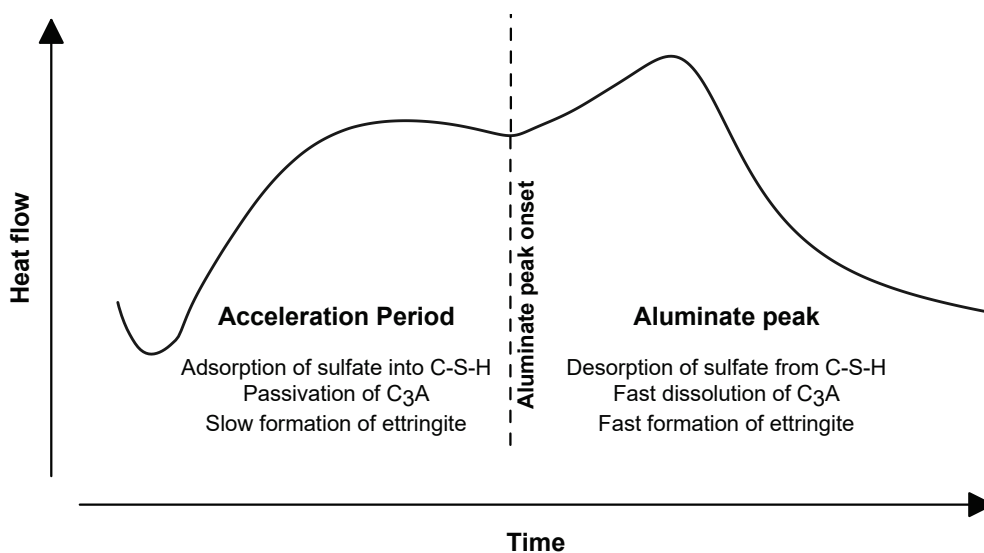
Figure 9-1: Scheme of the mechanism proposed for the sulfate balance of blended cements.

A relationship between the two main factors that influence the sulfate balance was found, namely the linear correlation of the total heat to onset of the aluminate peak (proportional to the amount of C-(A)-S-H) and the SO3 content of the system found for a variety of systems are schematically shown in Figure 9-2.

As it was discussed in *Chapter 7*, the intercept and the slope of the curve are related to measurable system properties (amount of ettringite precipitated before the onset of the aluminate peak and \$/Ca ratio of C-(A)-S-H, respectively). These associations are crucial for a successful implementation of this mechanism in hydration models based in measurable properties of the system, rather than fitting parameters.
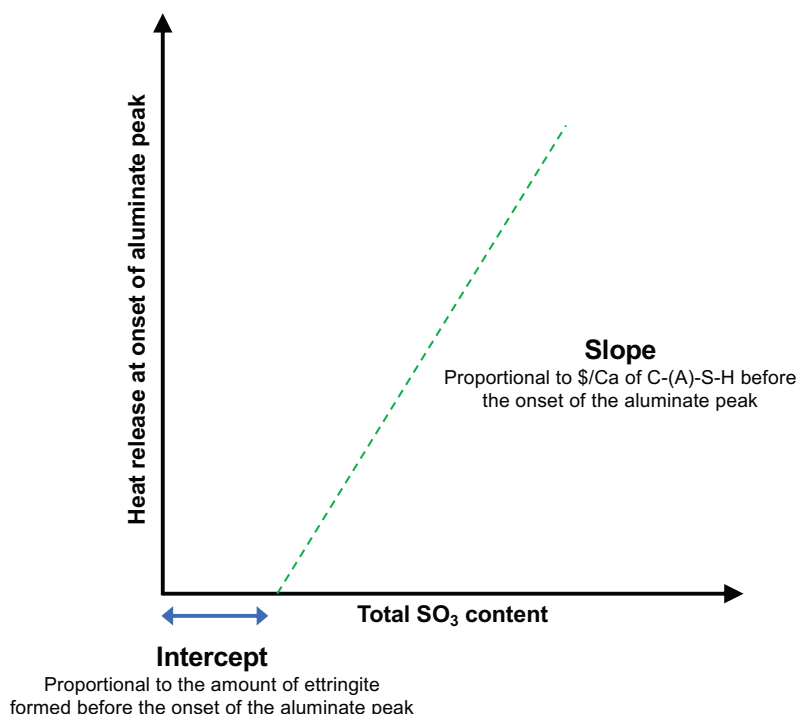
Figure 9-2: Representation of the Heat-SO$_3$ relationship presented in the study.

In addition, a method to decouple the hydration peaks of cementitious systems was proposed, based on the use of over sulfated systems to subtract the alite peak. This method is simple, but effective and extensible to a variety of different system compositions and characteristics. In this study, this method enabled to associated the heat released during the aluminate peak with ettringite formation. As it was shown in *Chapter 5*, the aluminate peak can change significantly in height but not necessarily in total area. This analytical approach will enable to effectively assess these variations in future work.

9.4 Precipitation of hemicarboaluminate and monocarboaluminate in LC^3 (*Chapter 8*)

The influence of hemicarboaluminate and monocarboaluminate on mechanical properties was studied. The main conclusions of this study are:

- o The precipitation of hemicarboaluminate and monocarboaluminate in LC^3 cements leads to a significant refinement of the porosity and increase in compressive strength.

o   A third peak of hydration is observed in LC^3, corresponding to the formation of Hc and Mc from the reaction of metakaolin and limestone. The position of this peak depends on the metakaolin and sulfate content of the system.

o   Aluminates from metakaolin participate in the precipitation of ettringite as long as sulfate is available in the system. The calcium for this reaction comes from portlandite.

o   In the long term, the reaction of metakaolin and clinker is slowed down due to the high degree of porosity refinement achieved by LC^3 systems. However, the reaction of metakaolin does not stop and continues at a slow rate over the long term. Strätlingite is observed in high metakaolin content samples hydrated for 3 years.

9.4.1   Practical perspectives

This study shows that precipitation of Hc and Mc in LC^3 influences mechanical properties. Thus, any strategy leading to an increase in the amount of these phases precipitated (for example, the addition of alkanolamines shown in *Chapter 5*) has the potential to increase compressive strength of the system. This knowledge can be used to design new admixtures and technological solutions to improve the mechanical behavior of LC^3 formulations at early ages.

In addition, the participation of aluminates in other chemical reactions, such as the formation of ettringite, was clearly established. The findings on the interaction of the different hydration reactions occurring simultaneously at early age could then be used to improve modeling tools, allowing a more accurate prediction of phase assemblage of LC^3 systems.

9.5   Future work and open questions

This research project provides new knowledge on the hydration mechanisms of LC^3 and processing techniques to make better use of natural clay resources to produce LC^3. Some aspects remain open after this study, and further research is required to provide a definite answer to them. A selection of open questions is presented in this section as perspectives for future work in the area.

9.5.1   Grinding aids in LC^3

Does the difference in molar weight of TEA, TIPA and DEIPA explains part of the differences in the behavior observed in LC^3 systems?

TEA was observed to lead to the highest increase in compressive strength of LC^3 systems. TEA has a lower molar weight (149.2 g/mol) compared to DEIPA (163.2 g/mol) and TIPA (191.3 g/mol). As the dosing was conducted on a mass basis, more molecules were added in the case of TEA as compared to DEIPA and TIPA. Experiments conducted at equal molecular dosage should be conducted and compared to the dataset presented in this study to clarify if this effect is significant.

Can we further enhance the strength increase with high dosages of alkanolamines if the sulfate dosage is further adjusted?

Chapter 6 and *chapter 7* established the mechanism behind the additional sulfate demand observed in LC^3 systems. In *chapter 5*, it was observed that alkanolamines increased the amount of Hc and Mc formed, improving strength. However, at high dosages, a decrease in the intensity of the alite peak was observed, similar to undersulfation. An interesting outlook would be to explore the feasibility of using high dosages of alkanolamines to further increase strength, compensating the reduction of the alite peak by the addition of sulfate.

Can grinding aids provide an enhancement of workability of LC^3 systems?

An aspect not explored in this study is the effect grinding aids molecules in LC^3 workability. This could be of interest for industrial applications, as it would consequently reduce the superplasticizer demand to achieve a certain slump. Most likely, PCE-based grinding aids will improve the flowability of LC^3 pastes. However, other formulations such as glycol-based grinding aids have shown a promising potential in preliminary trials. As these molecules are in general cheaper than PCE, their use could lead to an overall cost reduction of LC^3 concrete.

9.5.2   Effect of sulfate on the hydration of alite and blended cements

What is the mechanism that explains the morphological and growth changes in C-S-H in the presence of sulfate?

It was observed that the addition of gypsum enhanced the hydration of pure C$_3$S, and that this enhancement explains the observed differences in DoH in pure C$_3$S and C$_3$S/C$_3$A systems. A significant difference in the morphology of the C-S-H formed in the presence of gypsum was also observed. However, the mechanism behind this difference is unclear. The interaction of sulfate with C-S-H needs to be described in detail at an atomistic and experimental level to clarify the effect on sulfates on morphology and the nucleation and/or growth process of C-S-H. Some preliminary results in this matter are shown in Appendix 3.

What explains the variation of shape in the aluminate peak of different blended cements?

This thesis described a mechanism that explains the position of the aluminate peak in a blended cement. However, the observed changes in the shape of the peak (sharpening/broadening) remains as an open question. In some cases, as when alkanolamines are added to LC^3 systems, a significant change in shape is observed without a major variation in total heat (peak area).

Does the fineness of the metakaolin in calcined clay influence the amount of ettringite formed during the alite peak?

This study established that aluminates from calcined clay can participate in the precipitation of ettringite, as long as sulfate is available. As it was also shown, finer metakaolin leads to an acceleration of the aluminate

peak due to an increased filler effect over alite hydration. However, finer metakaolin could also lead to higher amounts of ettringite formed during the alite peak, further influencing the position of the aluminate peak.

9.5.3 Hydration and mechanical properties of LC^3

Is it possible to increase the water-to-binder ratio in LC^3 systems without a major compromise in strength?

It is well known that an increase in water-to-cement ratio leads to a decrease in strength in Portland cement systems. However, in LC^3 other factors need to be considered, such as an early refinement of the capillary pores that slows down the reaction of metakaolin. In this study, it was observed that an increase of water-to-binder ratio of 0.4 to 0.8 led to a significant increase in total heat release in the later system. The influence of these coupled effects in strength of LC^3 systems need to be understood to improve mixture design of LC^3 formulations, increasing the flowability at the same time.

What is the extent of metakaolin reaction in the long term?

It was observed that metakaolin reacts, at a slow rate, at later ages in LC^3 systems. While porosity refinement seems to influence the kinetics of this reaction, it does not limit the reaction. Furthermore, the thermodynamic modelling and experimental results at later age of LC^3 shown in this study suggests that the reaction continues even after depletion of portlandite. Additional experiments are required to determine the extent of metakaolin reaction in the long term. As portlandite is depleted in some of these systems, previous approaches based on portlandite consumption to assess the metakaolin degree of reaction are not suitable.

Appendices

Appendix 1 – The influence of grinding aids on limestone and calcined clay grinding

Note: This appendix contains some sections of the conference paper entitled "Improving the behaviour of calcined clay as supplementary cementitious material by a combination of controlled grinding and particle selection", by F. Zunino and K. Scrivener, published in the proceedings of the 3rd International conference on calcined clays for sustainable concrete, held in 2019 in Delhi, India. Some of the experiments were conducted by R. de Ribains as a semester project under the supervision of F. Zunino and K. Scrivener.

Grinding aids (GAs) are incorporated during comminution of clinker to reduce electrostatic forces and minimize agglomeration of clinker and SCM grains [1]. Such additions are commonly used to increase cement fineness and compressive strength for given specific energy consumption (Ec) of the grinding mill [1–3]. After the grinding process, GAs may not preserve their original molecule structures. However, they do remain adsorbed onto the cement particles to entail variations of cement properties whether in the fresh or hardened state [1].

The effect of grinding aids on the agglomeration of calcined clay during grinding was studied using unground calcined clay passing #8 sieve (2.4 mm), and a lab scale rotary jar mill. The clay had a calcined kaolinite content of 62%. The grinding was performed in controlled conditions of time and load of the mill, incorporating different dosages of commercial grinding aids based on poly carboxylate ether (PCE), glycol or amines. 1 kilogram of material was loaded in the mill each time. The grinding aid was applied by spraying the surface of the powder to emulate addition procedures used in the field.

Effect of the incorporation of grinding aids in the agglomeration of clay during grinding

Calcined clay was ground in the conditions described above for 60 min in order to observe the effects of grinding aids incorporation on the strong agglomeration observed in clays without the addition of these molecules. The three commercial grinding aids were included in the dosages recommended by the manufacturer (0.45% PCE-based, 0.13% amine-based, 0.12% glycol-based, all percentages by mass).

As observed in Figure A1-1, all of the products used showed a strong effect on reducing the clay covering layer of the mill walls and grinding media, which impacts the efficiency of the process. Particle size distribution of samples collected every 15 minutes during the grinding process allowed to observe that fine clay is obtained faster with the use of grinding aids. However, the ultimate fineness is similar as this is mainly controlled by the mill geometry and the grinding media load.

The effect of grinding aid dosage was also explored for the PCE-based formulation. In this case, the dosage added was 0.15%, 0.75% and 1.5% by mass. Pictures of the mill after 60 minutes of grinding are shown in Figure A1-2. In all cases the grinding media and the jar mill walls appear free of agglomerated material. However, from a qualitative point of view the increase in dosage does not yield a significant improvement.
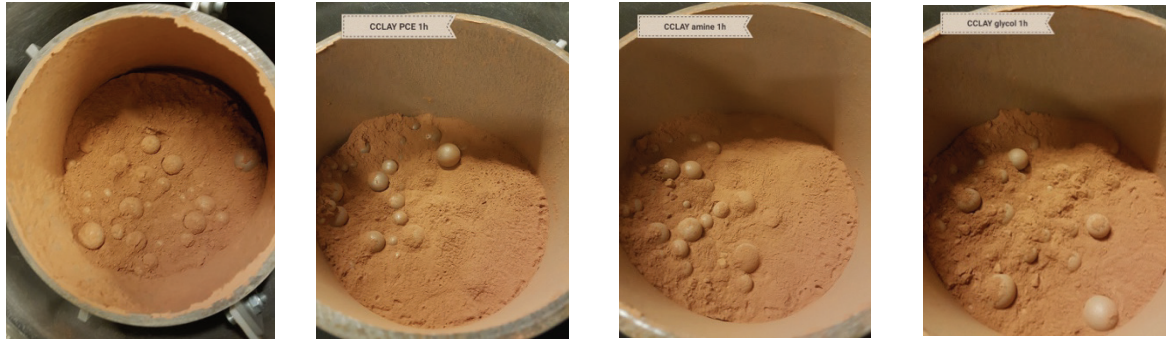
Figure A1-1: Photographs of ground clay after 60 min incorporating (from left to right) no GA, PCE based GA, Amine based GA and Glycol based GA.
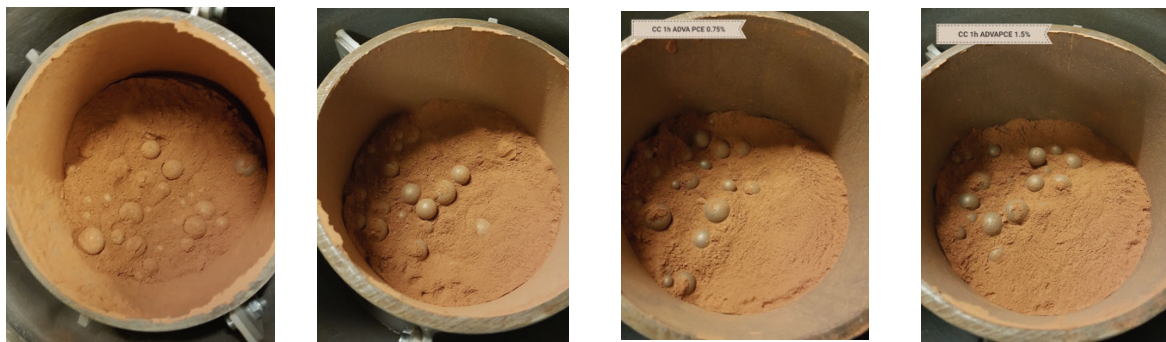
Figure A1-2: Photographs of ground clay after 60 min incorporating (from left to right) no GA and PCE-based grinding aid at 0.15%, 0.75% and 1.5% addition by mass of powder.

Particle size distribution and specific surface area measurements of the samples collected every 15 minutes were conducted. It was observed that the increase in the surface area as a function of particle size is almost negligible (2% increase of surface area, for a D_{V50} reduction from 50 to 10 μm, as shown in Figure A1-3), in contrast to what is normally observed in cement and other SCMs. This is explained as the main source of surface area from clays is their internal porosity, which is independent of the particle size over the range explored in this study. After 60 minutes of grinding, no further refinement of the powder was observed. It can be seen that the reduction in D_{V50} occurs faster in the systems with GA as compared to the control.
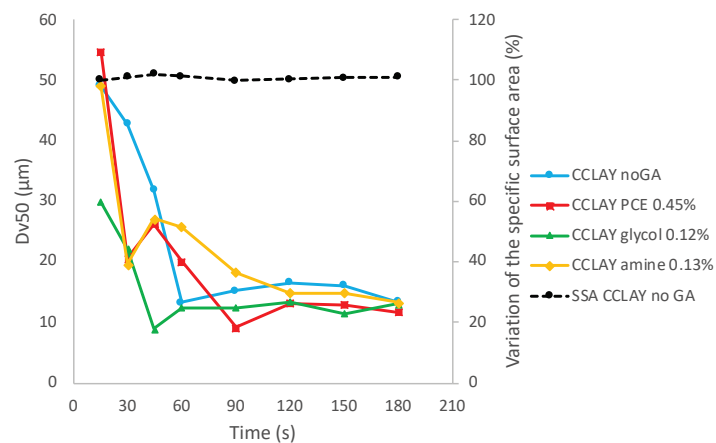
Figure A1-3: Evolution of D_{V50} and SSA for increasing grinding times and using different grinding aids over calcined clay.

The effect of grinding aids on grinding efficiency was also studied for limestone. In this case, a calcareous aggregate (98% $CaCO_3$ measured by TGA) was used. A pre-sieving analogue to the calcined clay was conducted, and the ball mill was loaded in the same conditions. It was observed that higher grinding times were required to achieve fine material. The PCE based was used at 0.45% and the glycol-based GA was used at 0.12% and 0.33% dosages. Pictures of the ball mill after 2 hours of grinding are shown in Figure A1-4. As observed, agglomeration is also observed as in the case of calcined clay. The best results among the tests conducted are obtained with the high dosage of glycol-based GA.

Figure A1-4: Photographs of limestone after 120 min incorporating (from left to right) no GA, PCE-based GA at 0.45%, glycol-based GA at 0.12% and 0.33%.

Particle size distribution and specific surface area measurements of the samples collected every 15 minutes were conducted as in the case of calcined clay. In this case, the specific surface area increases as the D_{V50} values decrease, which is the behaviour expected for powders without internal porosity, Figure A1-5.
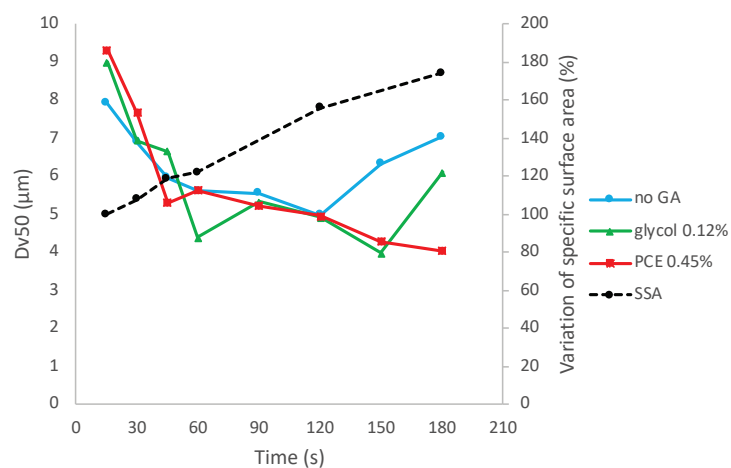
Figure A1-5: Evolution of D_{V50} and SSA for increasing grinding times and using different grinding aids over limestone.

Concluding Remarks

Grinding aids reduce the agglomeration of calcined clay and limestone during the grinding process. This de-agglomeration translates into a faster refinement of the powder under the same energy input. This, the use of grinding aids has the potential to increase the yield of a grinding process of calcined clay and limestone in industrial conditions.

References

[1]		J.J. Assaad, C.A. Issa, Effect of clinker grinding aids on flow of cement-based materials, Cem. Concr. Res. 63 (2014) 1–11. doi:10.1016/j.cemconres.2014.04.006.

[2]		M. Katsioti, P.E. Tsakiridis, P. Giannatos, Z. Tsibouki, J. Marinos, Characterization of various cement grinding aids and their impact on grindability and cement performance, Constr. Build. Mater. 23 (2009) 1954–1959. doi:10.1016/j.conbuildmat.2008.09.003.

[3]		S. Sohoni, R. Sridhar, G. Mandal, The effect of grinding aids on the fine grinding of limestone, quartz and Portland cement clinker, Powder Technol. 67 (1991) 277–286. doi:10.1016/0032-5910(91)80109-V.

Appendix 2 – Influence of metakaolin content, limestone size and mixture design on LC^3 properties

Note: This appendix is based on the conference paper entitled "Influence of kaolinite content, limestone particle size and mixture design on early-age properties of limestone calcined clay cements (LC^3)", by F. Zunino and K. Scrivener, published in the proceedings of the 3rd International conference on calcined clays for sustainable concrete, held in 2019 in Delhi, India.

This study explores the effect of kaolinite content from 20 to 95% on porosity refinement and mechanical properties of LC^3-50 and LC^3-65 (50% and 65% clinker factor respectively) systems by dilution of pure metakaolin. The effect of metakaolin dilution was coupled with other factors that were observed to have a significant impact on hydration kinetics and strength. A detailed comparison between LC^3-50 and LC^3-65, currently allowed in the European standard, is provided showing that the main difference in mechanical properties occurs at 1 d for an equivalent kaolinite content. Finally, guidelines for an effective and optimized utilization of clays of different grades (kaolinite contents) in LC^3 systems are given.

Materials and methods

Portland cement classified as CEMI 42.5R was used for the preparation of blended cement pastes. The limestone powders were supplied from commercial manufacturers and were used as received. For the base mixtures of this study, a limestone with D_{V50} = 4.1 μm was used. A pure metakaolin (95% purity) was used in this study as calcined clay. Lower grades of clay were achieved by dilution of the pure metakaolin with limestone. A base mixture design of LC^3-50 with clay-to-limestone ratio of 2:1 was used (50% clinker, 30% calcined clay, 15% limestone and 5% gypsum). From there, different levels of dilution were explored by combining pure metakaolin and additional limestone in the 30% clay fraction of the binder, ranging from 95% metakaolin content (30% calcined clay and 15% limestone) down to 20% metakaolin (6.3% calcined clay and 38.7% limestone) content.

The LC^3-65 systems were designed by increasing the clinker factor up to 65% and keeping the relative proportions between limestone and clay constant in the remaining fraction for comparison with LC^3-50.

A constant w/b ratio of 0.4 by mass was used for all mixtures. Compressive strength was measured in mortar samples in conformity with EN 196-1 standard procedure. For the limestone particle size study, mortar samples were cast at w/b 0.4 in the same way as the base mixtures. Two additional limestone sizes were used: D15 (coarse limestone, with D_{V50} = 17.5 μm) and BUG (fine limestone, with D_{V50} = 1.8 μm). The coarse and fine limestone replaced the limestone used to dilute down the 95% metakaolin down to the desired values (therefore, an increased amount of fine or coarse limestone is added as the metakaolin content goes down), while the initial 15% base limestone content of the LC^3-50 with clay-to-limestone ratio of 2:1 system was always kept constant with the D_{V50} = 4.1 μm limestone. For the mixtures where the alkali content was adjusted, KOH was used to achieve a total alkali content, expressed as percentage of Na$_2$O$_{EQ}$ of the total binder, of 0.8% and 1.0%. The particle size distribution of the raw materials used are shown in Figure A2-1, measured by laser diffractometry.
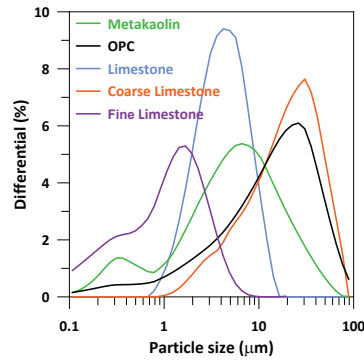
Figure A2-1: Particle size distribution of the raw materials used in this study.

Mercury intrusion porosimetry (MIP) was conducted on paste samples cast with analogous compositions to the mortar mixtures in selected systems. The aim of these experiments was to compare the effect of coarse and fine limestone inclusions in the porosity refinement profile. In addition, isothermal calorimetry at 20ºC was conducted to assess the hydration kinetics of the systems. Furthermore, it was used to study the effect of raw materials properties in the aluminate reaction of LC^3.

Results and Discussion

Effect of calcined clay grade (metakaolin content) and clinker factor on compressive strength

Results for compressive strength of mortar with 50% and 65% clinker factors are presented on Figure A2-2. In in general, LC^3-65 exhibits a higher strength at 1 day as compared to LC^3-50. This is attributed to the higher clinker content. At this age, the hydration of clinker dominates the production of hydrates. However, this difference starts to disappear already at 2 days, starting from the systems with higher metakaolin content. At 7 days, the difference is negligible across the whole range explored. LC^3-65 formulations are currently allowed in the European EN 197 standard as CEMII/B-Q-L, but not the LC^3-50 based formulations. From a strength point of view, it appears that the difference between both clinker factors is restricted to the very early stage of hydration. Furthermore, as it will be shown in the next section, this difference can be shortened even further by the refinement of the limestone fraction of the adjustment of the alkali content.
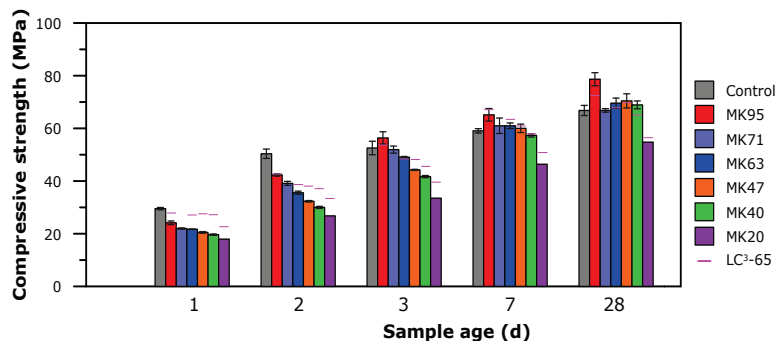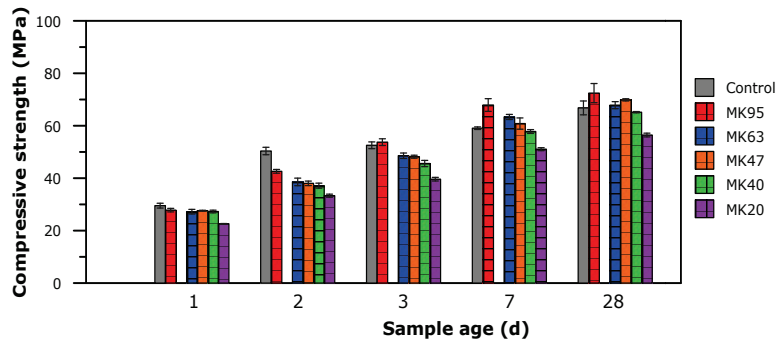
Figure A2-2: Compressive strength of LC³-50 (top) and LC³-65 (bottom) mortar mixtures with different amounts of metakaolin. Eye guides are included in the top figure referring to the LC³-65 strength at each metakaolin level.

Effect of limestone particle size compressive strength of LC³-50 formulations

Results of LC³-50 mixtures where coarse (D15) or fine (BUG) limestone is incorporated are shown in Figure A2-3. It can be observed that for the same metakaolin content, the surface area of limestone has a significant effect on compressive strength, specially at early age. In fact, at 1, 2 and 3 days the effect of limestone refinement on strength is higher for a given mixture than the observed variation for a reduction in metakaolin content. Thus, limestone particle size is a relevant factor that influence the strength of LC³ at early age, and could be used to increase the performance of binders in scenarios where only low-grade clays are available. Furthermore, the use of fine limestone allows to approach to the strength level of LC³-65 formulations at 1 day.
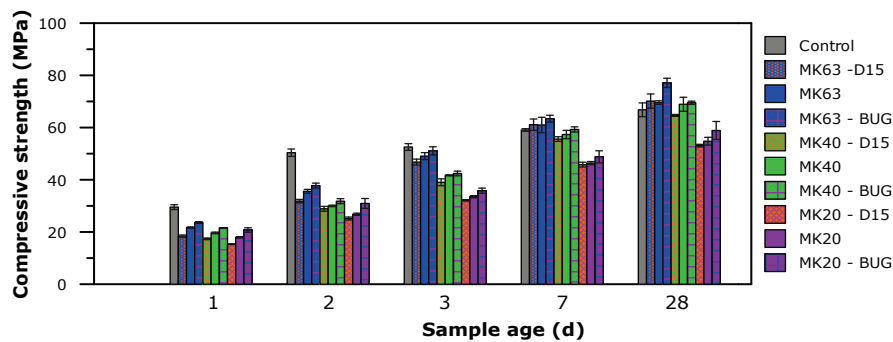
Figure A2-3: Compressive strength of LC³-50 mortar with coarse (D15) and fine (BUG) limestone.

Figure A2-4 shows the porosity profiles obtained after 7 days of hydration by MIP of a group of LC³-50 systems with normal size and coarse limestone. As observed, the incorporation of coarse limestone leads to a higher total porosity in both cases (MK63 and MK40). However, in the case of MK63 the difference is smaller and the critical entry radius with coarse limestone is slightly lower than the reference system, which could explain the similar result in strength at this age between the D15 and the reference system, as opposed to MK40.
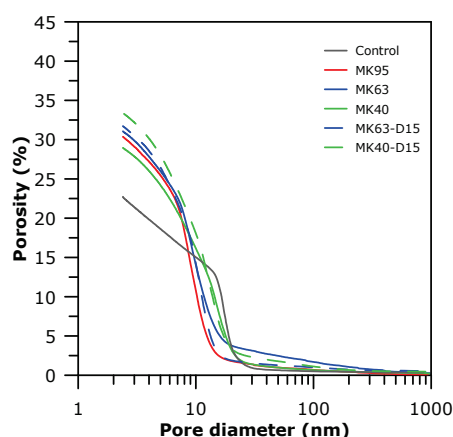
Figure A2-4: Porosity profiles of LC^3-50 systems at 7 days measured by MIP (contact angle 120º).

Physical (fine limestone) and chemical (alkali content) strategies to increase strength

To explore the possibilities to increase early age strength of LC^3-50 systems using chemical strategies, alkali adjustment was used. Figure A2-5 shows the studied mixtures with 63 and 40% metakaolin content, with adjusted alkali content, fine limestone (BUG) addition or a combination of both. In addition, the reference values for the MK63 and MK40 with the reference limestone are also included for comparison. As seen, for the two metakaolin contents studied, the mixtures with an increased alkali content up to 1% Na$_2$O$_{EQ}$ shown higher strength at early ages. A decrease of strength is observed at 7 and 28 days as compared to the reference system, but within the error of the experiment. The combination of fine limestone and alkali adjustment exhibited an even higher increase of strength at 1, 2 and 3 days.
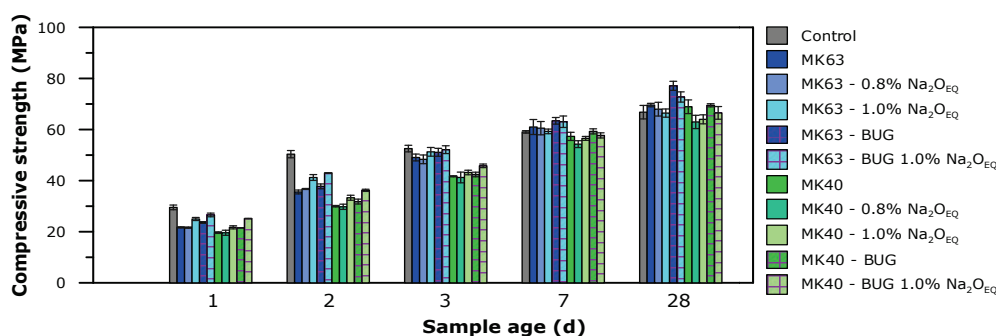
Figure A2-5: Compressive strength of LC^3-50 mortar mixtures that incorporate different strategies to increase early age strength (alkali adjustment, limestone refinement or a combination of both).

Concluding remarks

Calcined kaolinite content is linked with compressive strength of LC^3 systems. However, other design parameters such as limestone fineness shown a strong influence in strength and therefore, can be managed to achieve the desired performance of the mixture.

The inclusion of fine limestone in LC^3-50 mixtures proved to be an effective way to increase early-age strength to levels comparable to LC^3-65 formulations.

Further increase can be achieved adjusting the alkali content of the binder, with no negative impact observed at later age strength at the amounts below 1% Na$_2$O$_{EQ}$.

Appendix 3 – Effect of sulfate on nucleation and growth of C-S-H

The results shown in *Chapter 7* showed that an enhancement of the C_3S peak is observed with gypsum additions, leading to an increased DoH.

Several hypotheses have been proposed to explain the observed enhancement of gypsum on C_3S/alite. Bergold et al. [1] proposed a seeding effect of (nano-)ettringite to explain the higher DoH measured in alite systems with gypsum addition. In light of the results of this study, this hypothesis is unlikely, as the enhancement of the peak is observed as well in pure C_3S system, where no aluminates (and consequently, ettringite) are present. This suggests that the cause of the enhancement of C_3S hydration by gypsum is an interaction exclusively between this phase and C_3S (and/or C-S-H), rather than one that involves the aluminates. Moreover, this shows that the hypothesis of sulfate modifying the growth of C-S-H proposed by Mota et al. [2] is still plausible.

The needle length was measured during the hydration of plain C_3S and C_3S with 3% addition of gypsum, before (4 h), during (7 h) and after (24 h) the peak. As seen in Figure A3-1a, the average needle length is larger in the system with gypsum during the acceleration period, indicating a modification of the C-S-H growth process. At 24 hours, the needle length of the system with and without gypsum addition is the same. As at this time the difference in DoH between the systems is significant (Figure A3-1b). This rather suggest a difference in the nucleation density (more C-S-H needles. The specific surface area of the material is higher in the sample with 3% gypsum, following a trend similar to the measured total heat (Figure A3-1b).

a)   b)
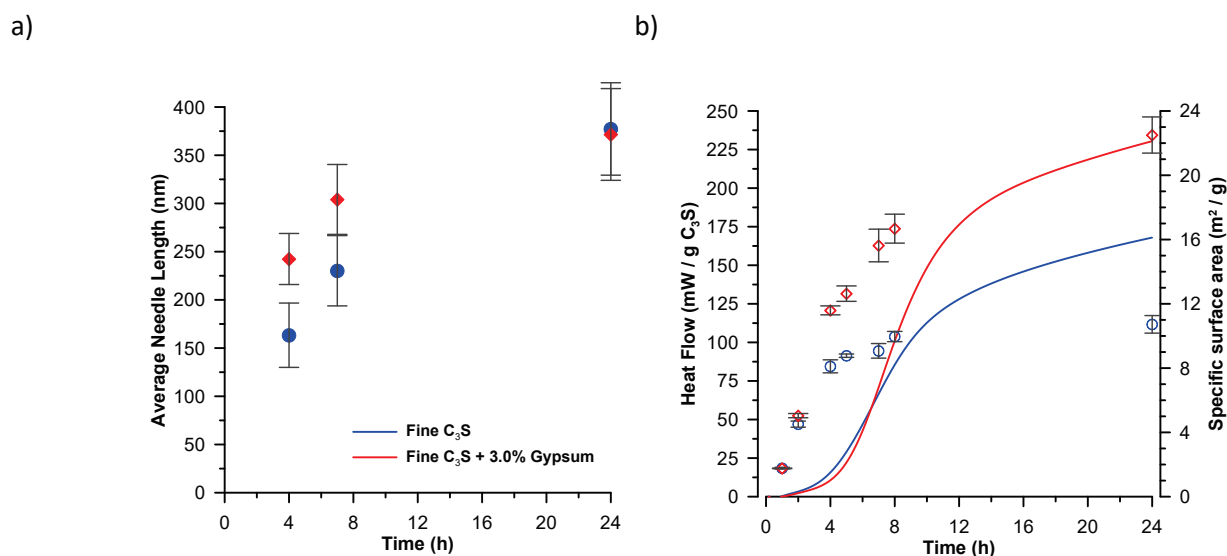
Figure A3-1: Average needle length at 4, 7 and 24 hours (a) and SSA and total heat (b) of C_3S and C_3S+3% gypsum.

The morphology of C-S-H needles precipitating on the surface of C_3S with and without the addition of gypsum is shown in Figure A3-2 for different hydration times. At 2 hours (start of the acceleration period), the surface of C_3S appears irregular and covered of irregular needles. They also seem to be, in general, not oriented relative to the surface of the grain. On the contrary, the needles seen on the system with 3% gypsum appear more defined and longer. Furthermore, clusters of needles are clearly visible, with more needles

perpendicularly oriented respect to the grain surface. At 4 hours (acceleration period) the samples without gypsum addition shows thick needles, poorly defined and oriented. Large portions of the C_3S surface are still visible. In the case of C_3S with 3% gypsum longer needles are seen, grouped in clusters and growing outwards the surface. Significantly less free surface is observed in this case. At 7 hours (peak time of C_3S + 3% gypsum sample, slightly after the peak for plain C_3S) the situations remain similar as at 4 hours. Needles keep growing in both samples, but in the one containing gypsum the orientation remains preferentially perpendicular to the grain. In the system without gypsum, the surface of the grain is still visible. At 24 hours the difference between both systems is clear. While some needles appear to have grown perpendicular to the surface in the plain C_3S system, in the 3% gypsum system the number of needles is clearly higher and the orientation of the needles is mainly perpendicular. The morphology of the system with 3% gypsum appears more similar to other observations made on OPC grains [3,4] rather than pure C_3S [5].
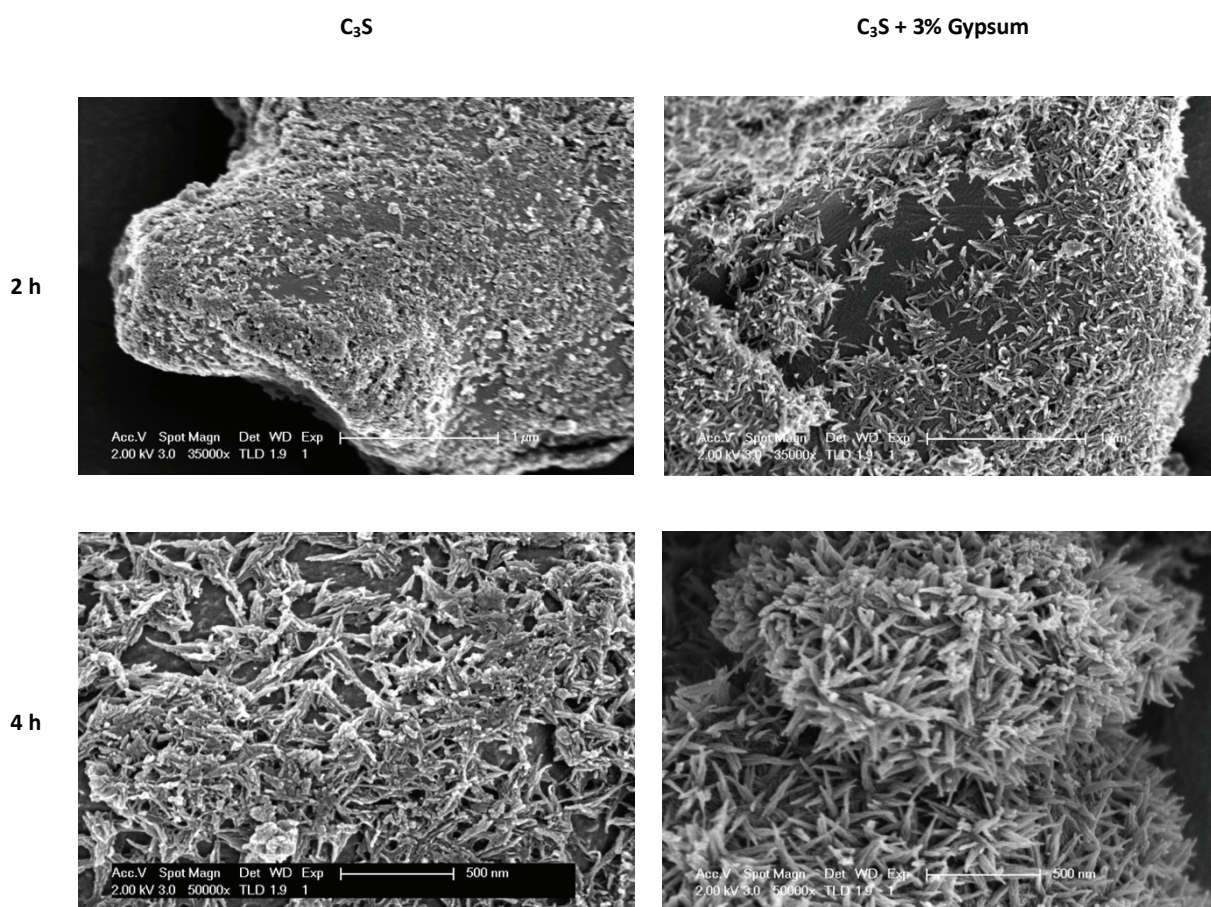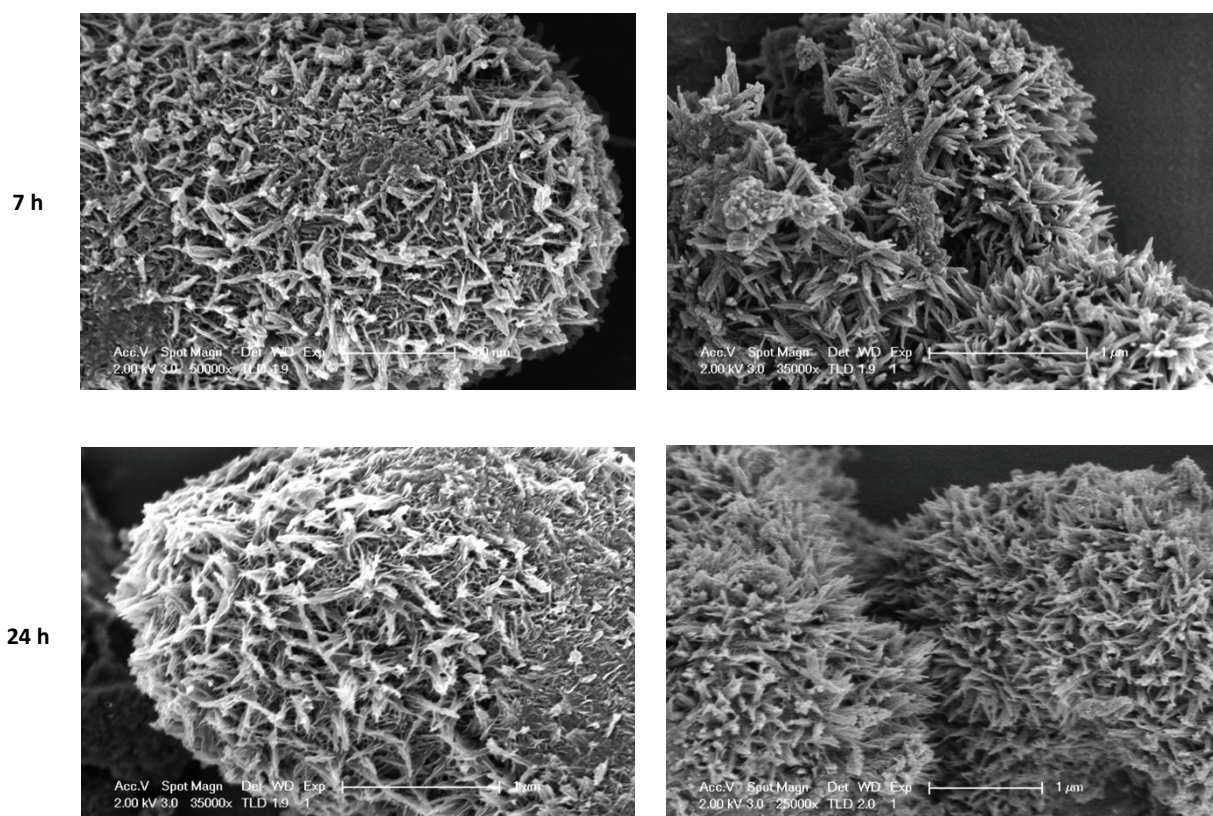
C_3S　　　　　　　　　　　　　　　　　　　**C_3S + 3% Gypsum**

Figure A3-2: HR-SEM micrographs of C$_3$S grains at different hydration times for plain C$_3$S and C$_3$S + 3% gypsum.

Concluding remarks

The addition of sulfate enhances the hydration of C$_3$S. This effect is not linked to the presence of aluminate phases, and is rather associated to a modification in the growth process of C-S-H during the first 24 hours. In the sulfate C$_3$S system, divergent needles are observed.

References

[1]   S.T. Bergold, F. Goetz-Neunhoeffer, J. Neubauer, Interaction of silicate and aluminate reaction in a synthetic cement system: Implications for the process of alite hydration, Cem. Concr. Res. 93 (2017) 32–44. doi:10.1016/j.cemconres.2016.12.006.

[2]   B. Mota, T. Matschei, K. Scrivener, The influence of sodium salts and gypsum on alite hydration, Cem. Concr. Res. 75 (2015) 53–65. doi:10.1016/j.cemconres.2015.04.015.

[3]   K.L. Scrivener, Development of the microstructure during the hydration of Portland cement, University of London, 1984.

[4]   E. Berodier, K. Scrivener, Understanding the filler effect on the nucleation and growth of C-S-H, J. Am. Ceram. Soc. 97 (2014) 3764–3773. doi:10.1111/jace.13177.

[5]   A. Bazzoni, M. Cantoni, K.L. Scrivener, Impact of annealing on the early hydration of tricalcium silicate, J. Am. Ceram. Soc. 97 (2014) 584–591. doi:10.1111/jace.12691.

Appendix 4 – Particle packing optimization of LC^3 formulations

Note: This appendix is based on and article entitled "Enhancing workability and early-age strength of limestone calcined clay cements by particle packing optimization", by F. Zunino, A. Favier, I. Katrantzis and K. Scrivener.

Introduction

Workability, critical for a successful field implementation of cement-based materials, depends strongly on mixture proportions and the characteristics of the mixture constituents [1]. Previous research found that limestone has an increased ability to reduce the yield stress compared to quartz of similar particle size distribution and specific surface area [2]. In the case of clays, their addition has a negative impact on yield stress and viscosity due to their high specific surface area and the decrease of the particle packing of the system [3]. The general approach to overcome this effect has been to use chemical admixtures such as superplasticizers to improve the workability of the material. However, it has been observed that higher dosages are required to achieve the same level of flowability compared to normal Portland cement systems, as a sacrificial volume is retained inside the clay structure, avoiding the interaction of the plasticizer with cement grains [4].

A second strategy to improve the workability of cement pastes is to increase the packing density of the solid fraction [5,6]. Several models have been formulated to represent the space filling capacity of spherical particles [7], and the potential of this approach for cement-based materials has been addressed [8]. This approach could offer a technical and economically feasible strategy to offset the increased water demand observed in LC^3 systems.

In this study, particle packing optimization of LC^3 systems will be performed by adjustment of the limestone fraction using commercially available products. The effect of the increased maximum packing fraction on compressive strength, hydration kinetics and workability is discussed. Finally, recommendations are given to apply the packing model in LC^3 blends.

Materials and methods

Application of the solid particle packing model

The model of Andreasen and Andersen [7,9] was used to establish the mixture design used in this study. This model describes the optimal particle size distribution (PSD) based on a continuous geometric packing model, that can be achieved by combining materials with different continuous PSDs. On the other hand, it considers the finite character of the different PSDs, by assuming a maximum and minimum particle diameter (d_{max} and d_{min}, respectively) associated with the mixture of powders.

The function for the particle size distribution with the highest solid packing fraction according to the model ($F_{th}(d)$) is shown in Eq. (1):

$$F_{th}(d) = \frac{d^\alpha - d_{min}^\alpha}{d_{max}^\alpha - d_{min}^\alpha} \ for \ \alpha \neq 0 \qquad (1)$$

where α corresponds to the distribution modulus, which for discrete particle size distributions takes positive values, typically $0<\alpha<0.37$ [7]. Brouwers also reported that the highest packing density can be obtained when $\alpha=0$. In this case, Eq. (1) can be simplified to Eq. (2):

$$F_{th}(d) = \frac{\ln d - \ln d_{min}}{\ln d_{max} - \ln d_{min}} \; for \; \alpha = 0 \qquad (2)$$

This theoretical distribution was compared to the distribution $F_{ex}(d)$, defined from the particle size distributions of raw materials $F_{i,ex}$ and described by Eq. (3).

$$F_{ex}(d) = \sum_i c_i . F_{i,ex} \qquad (3)$$

where c_i corresponds to the volume fraction of the constituent i in the LC^3 blend, and $F_{i,ex}$ is the cumulative PSD experimentally measured for the same constituent.

In this study, only the limestone (LS) fraction of the LC^3 blends was adjusted to increase the particle packing of the system. This decision was taken to replicate possible realistic scenarios of application, as a wide range of limestone powders with different particle sizes are commercially available. Furthermore, it is unlikely to have cement and/or clays with different PSDs to combine them as means of a particle packing optimization process. The c_i of the different limestone powders used in each blend were allowed vary to get the best fit between $F_{ex}(d)$ and $F_{th}(d)$. This was achieved by minimizing the computed residual sum of squares (Σ) between the two PSD functions, using a least-square optimization algorithm. Thus, the lowest the value Σ, the higher the particle packing of the system according to the model, which is shown graphically on Figure A4-1a. For the optimization process, the discretization of the PSD functions was done on a logarithmic size scale.

As an initial approach to design the mixture proportions, a value of $\alpha=0$ was assumed for the computation of $F_{th}(d)$, which mathematically describes the maximum achievable packing of the system as a linear function of the cumulative PSD versus d in log-scale [7] (Figure A4-1b). As a very large amount of powders with different PSDs are required to be blended to achieve the quasi-linear PSD distribution described by the model, this assumption is generally considered unrealistic. The consequences will be discussed in the results section of this paper, and more realistic values of α derived from experimental measurements over the blended powders will be presented.
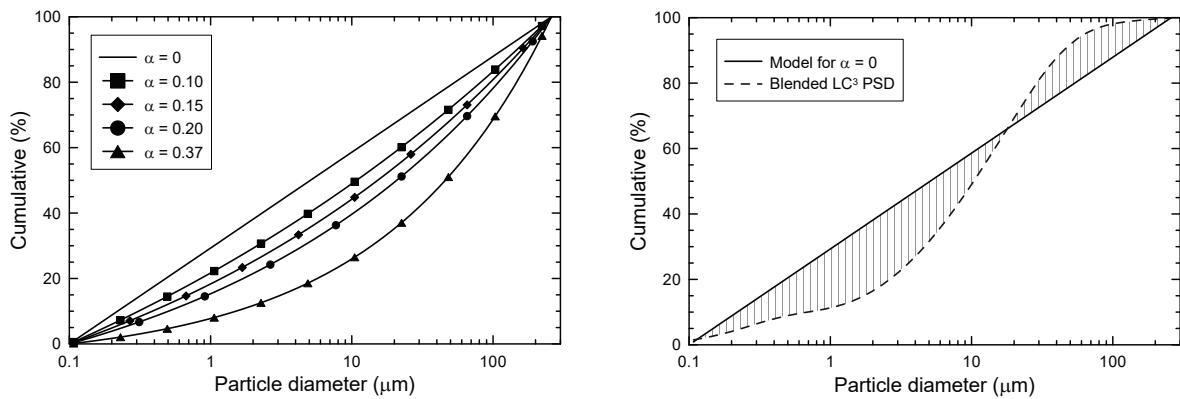
Figure A4-1: Effect of α on the shape of the cumulative distribution predicted for maximum packing by the model (left) and model versus experimental LC^3 PSD, graphically showing the residual sum of squares used as packing parameter (right).

To provide a comparison to Σ as a particle packing estimation parameter, the maximum packing density (ϕ_c) was also measured experimentally based on centrifuge determinations of extractable water [2,8]. The parameter was computed from Eq. (4), measuring the non-extractable pore solution volume (V_{liquid}) after two rounds of centrifugation at 6000 rpm during 20 minutes. A dispersion of each of the LC³ blends with a dispersant-to-solids ratio of 3 (by mass) was used to perform the measurements. The initial volume of solids (V_{solids}) was computed using density measurements of each of the LC³ blend constituents according to ASTM C188 method (see Table A4-1). A solution of 0.01% sodium metaphosphate was selected as dispersant, since it prevents the agglomeration of clay mineral particles [10].

$$\phi_c = \frac{V_{solids}}{V_{solids} + V_{liquid}}$$

(4)

Raw materials

A commercial ordinary Portland cement (OPC, CEMI 42.5R conforming to EN 197-1) was used in this study. Two different calcined clays were used. The first one (CC-1) had a calcined kaolinite content of 50%, while the second (CC-2) had a calcined kaolinite content of 62%, both measured by thermogravimetric analysis (TGA) using the weight loss between 400ºC and 600ºC. In the case of CC-1, it was industrially produced and after preliminary testing, it was found that it was not completely calcined.

A total of six LS powders available in the market with different PSD were selected and used to prepare the different LC³ blends. The LS were grouped according to the source from where they were sourced. The first group (Group 1) was composed of three LS, code named D5, D65 and D130. The second group (Group 2) was composed of two LS, code named J15 and J130. Finally, a sixth fine limestone powder (code named LSF) was selected due to its fineness and unimodal PSD. In the case of LSF powder, it was grouped along with D130 (Group 3) to have one fine (LSF) and coarse (D130) PSD available for the optimization. In all cases, the powders correspond to grounded limestone (non-precipitated). The mineralogical composition was checked by X-ray diffraction (XRD), corresponding to calcite in all of them. The calcium carbonate content was verified to be above 95% in all samples by thermogravimetric analysis (TGA).

The raw materials were characterized by X-ray fluorescence (XRF) analysis, using the fusion beads sample preparation method with lithium tetraborate ($Li_2B_4O_7$) as the fluxing agent. The phase composition of OPC was determined by quantitative XRD analysis. Only one set of values is presented for the LS powders, as it represents on average the chemical composition of the whole range of LS used.

Table A4-1: Chemical composition of OPC, calcined clay and limestone samples (mass %).

	OPC	CC-1	CC-2	LS
SiO_2	19.51	56.06	48.13	0.11
Al_2O_3	4.42	36.80	35.08	0.00
Fe_2O_3	3.12	3.43	9.44	0.04
CaO	63.85	0.20	0.81	54.96
Na_2O	0.19	0.22	0.20	0.06
K_2O	0.83	0.23	0.08	0.01
MnO	0.05	0.00	0.01	0.00
TiO_2	0.31	2.35	2.27	0.01
MgO	2.10	0.41	0.52	0.15
P_2O_5	0.33	0.10	0.34	0.00
SO_3	3.25	0.05	0.01	0.03
LOI	1.54	0.36	2.98	42.5
C_3S	66.50	-	-	-
C_2S	4.00	-	-	-
C_3A	4.90	-	-	-
C_4AF	9.60	-	-	-
Sp. gravity (g/cm³)	3.086	2.509	2.605	2.718

Mixture design

In order to assess the effect of packing optimization under realistic conditions, some compositions boundaries were defined. This study focused on LC^3-50 (50% clinker factor) and LC^3-65 (65% clinker factor) as base composition for the blended mixture design. The amount of OPC was fixed in all cases depending on the selected LC^3 base system type, and the ratios between calcined clay-to-limestone (c/l) were chosen to be 2:1, 1:1 and 1:2 (by mass). The gypsum content was adjusted in all of the systems to account for the additional aluminates introduced by the calcined clay.

The PSDs of a given LS group, combined with one of the calcined clays and OPC were used to apply the packing model as detailed in the previous section. In order to assess more accurately the effect of particle packing on the properties of the different systems, the worst (lower) packing case scenario was also considered in some of the systems as mean of comparison with the optimized cases. This was achieved by maximization of Σ, in contraposition to the maximization required to maximize the particle packing.

The amount of OPC plus additional gypsum required was kept at a constant level equal to clinker factor plus 5% by mass for each system (i.e. 55% for LC^3-50 and 70% for LC^3-65). In two experimental points, the calcined clay-to-limestone ratio was allowed to vary as well during the optimization, with a maximum allowed calcined clay content based on the portlandite (CH) generation capacity of the system at full hydration (3 and 1 moles of CH produced per mole of C_3S and C_2S reacted, respectively [11]) and the molar ratio of CH consumption during metakaolin (MK) pozzolanic reaction (3 moles of CH consumed per mole of MK reacted). For an LC^3-50 system, this limit was found to be around 40% for CC-1 and 36.5% (both by mass) for CC-2. This approach does not assure the full reaction of the MK supplied to the system, as it neglects other required conditions such as water and space availability. Nevertheless, it is a useful and simple computation to establish an upper-limit for the optimization process.

A control (100% OPC) system with a water-to-cement (w/c) ratio of 0.5 by mass was used (water-to-solids volume ratio (w/s$_V$) of 1.54). For all the LC^3 blends, the volume of solids was adjusted after the mixture design to keep w/s$_V$ constant at 1.54. The mixture design, along with the corresponding computed Σ values are summarized on Table A4-2.

Table A4-2: Mixture design based on the selected particle packing optimization model, grouped by LC^3 system type and LS group.

	Design / clay	c/l	O/W[a]	OPC (%)	CC (%)	D5 (%)	D65 (%)	D130 (%)	J15 (%)	J130 (%)	LSF (%)	Gyp[b] (%)	Σ	w/b[c]	w/s$_V$
GROUP 1	Control*	-	-	100	-	-	-	-	-	-	-	-	-	0.50	1.54
	LC^3-50 / CC-1*	2:1	O	54.00	30.0	12.1	0.0	2.9	-	-	-	1.00	11625	0.55	1.54
	LC^3-50 / CC-1	1:1	O	54.25	22.5	17.3	0.0	5.2	-	-	-	0.75	13161	0.54	1.54
	LC^3-50 / CC-1	1:1	W	54.25	22.5	0.0	22.5	0.0	-	-	-	0.75	15417	0.54	1.54
	LC^3-50 / CC-1*	1:2	O	54.50	15.0	22.6	0.0	7.4	-	-	-	0.50	13994	0.54	1.54
	LC^3-50 / CC-2	2:1	O	54.00	30.0	15.0	0.0	0.0	-	-	-	1.00	11186	0.54	1.54
GROUP 2	LC^3-50 / CC-1*	2:1	O	54.00	30.0	-	-	-	15	0	-	1.00	11163	0.55	1.54
	LC^3-50 / CC-1	1:1	O	54.25	22.5	-	-	-	22.5	0	-	0.75	12444	0.54	1.54
	LC^3-50 / CC-1	1:1	W	54.25	22.5	-	-	-	0	22.5	-	0.75	13430	0.54	1.54
	LC^3-50 / CC-1	1:2	O	54.50	15.0	-	-	-	30	0	-	0.50	13855	0.54	1.54
	LC^3-50 / CC-2	1:2	O	54.50	15.0	-	-	-	30	0	-	0.50	13627	0.54	1.54
GR	LC^3-50 / CC-1*	2:1	O	54.00	30.0	-	-	0.0	-	-	15.0	1.00	10451	0.55	1.54

	LC³-50 / CC-1	2:1	W	54.00	30.0	-	-	15.0	-	-	0.0	1.00	12553	0.55	1.54
	LC³-50 / CC-1*	1:1	O	54.25	22.5	-	-	3.0	-	-	19.5	0.75	11489	0.54	1.54
	LC³-50 / CC-1*	1:2	O	54.50	15.0	-	-	6.7	-	-	23.3	0.50	12656	0.54	1.54
	LC³-50 / CC-1	free	O	53.70	40.0	-	-	-	-	-	5.0	1.30	9359	0.55	1.54
	LC³-50 / CC-2	free	O	53.80	36.5	-	-	-	-	-	8.53	1.20	9078	0.54	1.54
G1	LC³-65 / CC-1	2:1	O	69.35	20.0	10.0	0.0	0.0	-	-	-	0.65	13692	0.53	1.54
	LC³-65 / CC-1	1:1	O	69.50	15.0	14.0	0.0	1.0	-	-	-	0.50	14813	0.53	1.54
	LC³-65 / CC-1	1:2	O	69.70	10.0	18.0	0.0	2.0	-	-	-	0.30	16001	0.53	1.54
G3	LC³-65 / CC-1	2:1	O	69.35	20.0	-	-	0.0	-	-	10.0	0.65	12616	0.53	1.54
	LC³-65 / CC-1	1:2	O	69.70	10.0	-	-	0.0	-	-	20.0	0.30	13994	0.53	1.54

[a]: O = optimum case from packing model   W = worst case from packing model
[b]: Additional gypsum, not including the gypsum originally contained in the commercial OPC used
[c]: water-to-binder ratio by mass, considering as binder OPC, calcined clay, LS and additional gypsum
* indicates that this system was also cast as standard mortar, keeping the same paste composition
All % values correspond to mass % over the solid fraction

In order to assess the representability of the results in materials involving the presence of aggregates, standard mortars conforming to EN 196-1 standard were cast for some of the systems (noted on Table 2). The same paste composition was kept as indicated on Table 2, and standard sand was introduced in the quantities and size fractions described in the standard.

Experimental methods

Particle size distribution (PSD) of the calcined clays, limestone powders, and OPC were measured using a Malvern Mastersizer laser diffractometer. The PSD was measured 4 times in three different samplings per material, while stirring at 2200 rpm. Isopropanol (refractive index 1.378) was used as a dispersant in the case of OPC, and an aqueous solution of 0.01% poly acrylic acid (PAA) was selected as dispersant of the limestone powders. In the case of calcined clays, an aqueous solution of 0.01% of sodium metaphosphate was selected [12]. For PSD calculations, 1.529/0.01, 1.596/0.001 and 1.700/0.1 were used as refractive index/extinction coefficient (real/imaginary) of the calcined clay, LS powders, and OPC, respectively.

Isothermal calorimetry measurements were conducted using a TAM Air isothermal calorimeter at 20 °C to study the hydration kinetics of the different mixtures. Tests were conducted on cement paste samples from the same batches as the samples used in compressive strength and workability tests. 10 g of samples were placed in a glass ampoule after casting, and the heat flow was monitored up to 7 d of hydration.

XRD was used to characterize the crystalline phase composition of raw materials (powders) and LC³ systems during hydration, allowing the computation of the degree of hydration of clinker at the ages where compressive strength was also measured. For powders, XRD analysis was performed on back-mounted sample holders, which reduce the effects of preferred orientation. For hydrated samples, XRD measurements were carried out on freshly cut paste slices at 2 d, 7 d and 28 d.

Samples were mounted on a XRD sample holder and measured in Bragg–Brentano configuration using a X'Pert PANalytical diffractometer equipped with a CuKα source (wavelength 1.5406 Å), operated at 45 kV and 40 mA. Samples were scanned from 7º to 70º 2θ with a step size of 0.0167º 2θ using a X'Celerator detector, resulting in an equivalent time per step of 60 s and 30 s for powders and hydrated samples, respectively. For the analysis of the collected patterns, HighScore Plus version 4.6 was used coupled with the PDF2 crystallographic database.

The **workability** of paste was assessed using a mini-slump cone on paste samples. The mini-slump cone has a bottom diameter of 38 mm, a top diameter of 19 mm, and a height of 57 mm. The mini-slump cone was filled with paste after casting in two layers, with care of filling the entire inner volume. The cone was lifted in 5 seconds, and 4 diameter measurements were taken with a caliper with a precision of ±0.01 mm.

For the mortar mixtures that were cast, the flow table test was performed in conformity with EN 1015-3 standard.

To monitor **compressive strength** development, 20 mm cubic specimens of paste were used. Specimens were removed from their molds after one day of curing and stored in sealed bags in a chamber at 20 °C ± 3 °C and 95 % relative humidity (RH) until the time of testing. Compressive strength tests were conducted at 1 d, 7 d and 28 d on 3 specimens at each age, with a constant 0.4 kN/s loading rate being employed in all cases.

For the mortar specimens, the EN 196-1 standard testing procedure was applied, testing two 40x40x160 mm prism at 2 d, 7 d and 28 d. Compressive strength was measured on the two halves of the prism (split in flexural test according to the standard) at a constant loading rate of 2.4 kN/s.

Results and discussion

PSD, hydration and strength

The PSD of OPC and calcined clays used in this study are graphically presented in Figure 2. It can be observed on the differential plot (Figure A4-2a) that calcined clays exhibit a clear bimodal distribution. The first particle population as a modal particle size around 0.25 μm, while the second group of coarser particles is more heterogeneous and the sizes range from 1 μm to 100 μm.

a)   b)
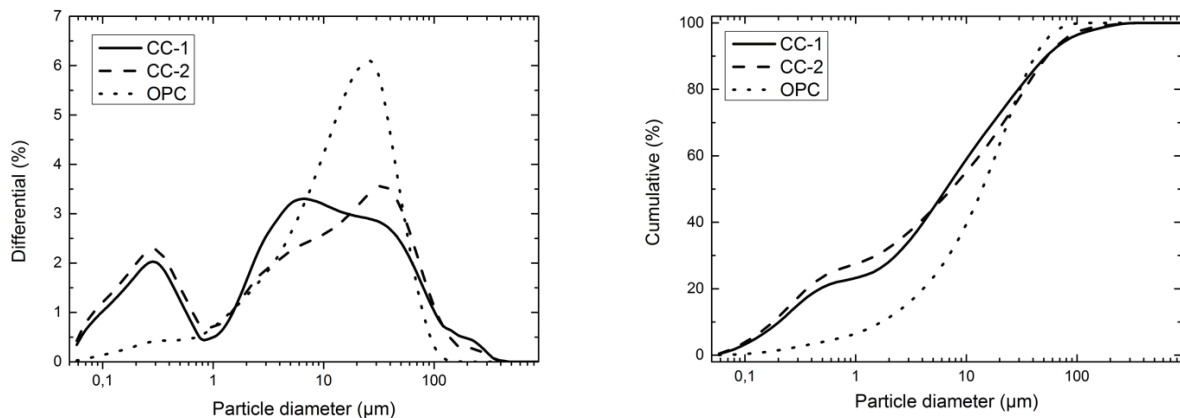
Figure A4-2: Particle size distribution of OPC and calcined clays CC-1 and CC-2, a) differential plot and b) cumulative distribution.

For the LS powders, the PSD are presented in Figure A4-3. It can be seen that the LS corresponding to the Group 1 (D5, D65 and D130) have narrower distributions compared to the Group 2 (J15 and J130) ones. In the case of J130, it exhibits a bimodal distribution with populations around 4 μm and 50 μm. LSF has the narrower distribution of all the LS studied, with a span of 1.5. The specific surface area (SSA) was also

measured by nitrogen adsorption and computed by the BET method using 10 points. The percentile particle sizes, distribution spans and SSA are summarized for all the raw materials on Table A4-3.
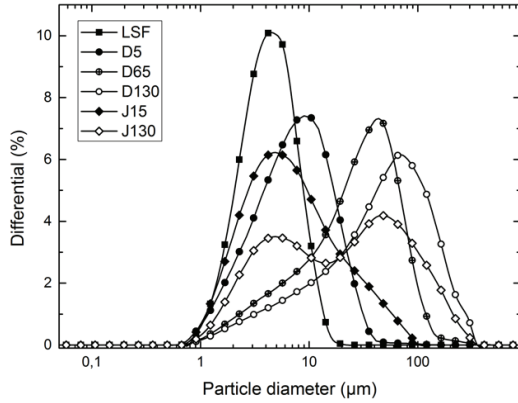
a)   b)
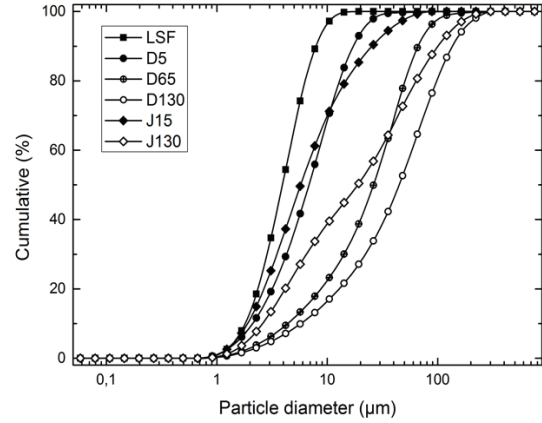
Figure A4-3: Particle size distribution of LS powders used in this study, a) differential plot and b) cumulative distribution.

Table A4-3: Summary of particle size and surface area of OPC, calcined clays and LS powders used in this study.

	D_V10 (µm)	D_V50 (µm)	D_V90 (µm)	Span $(D_V90- D_V10)/D_V50$	SSA (m^2/g)
OPC	1.7	14.2	41.4	2.8	1.41
CC-1	0.2	6.6	56.2	8.5	8.18
CC-2	0.2	7.7	56.1	7.3	46.87
D5	2.2	6.9	16.9	2.1	2.39
D65	4.2	26.2	65.5	2.3	0.62
D130	5.7	48.3	140.6	2.8	0.37
J15	2.0	5.7	26.2	4.3	2.28
J130	2.7	19.3	103.6	5.2	1.93
LSF	1.7	4.1	7.7	1.5	3.60

Figure A4-4 shows the effect of packing optimization by adjustment of the LS fraction, quantified using the Σ parameter, on heat release measured by isothermal calorimetry. LC^3-50 / CC-1 with c/l 2:1, O and W systems from Group 3 (optimized and worst packing conditions achievable by application of the model, respectively) are shown as examples, as the same trends were observed from other LS groups when comparing similar cases. It can be observed that regardless of the coarsening of the LS fraction in the W case, where only D130 was used compared to O where only LSF was selected, there is no significant retardation of the silicate (first) peak of hydration. However, there is a substantial difference in the aluminate (second) hydration peak between both systems. The optimized (O) system shows a more prominent peak, associated to a higher rate of reaction of the dissolved aluminates at this stage. As both systems have the same calcined clay and gypsum contents, the difference is mainly attributed to the increased specific surface area of the LS fraction (3.60 vs 0.37 m^2/g for the O and W system respectively) which promotes the reaction of the aluminate phases. Despite the observed difference in the second peak, the total heat release (Figure A4-4b) of the mixtures remains almost identical until approximately 48 h of hydration. This is consistent with the observed compressive strength (Table A4-5) of the systems at this age, where no significant difference is observed.
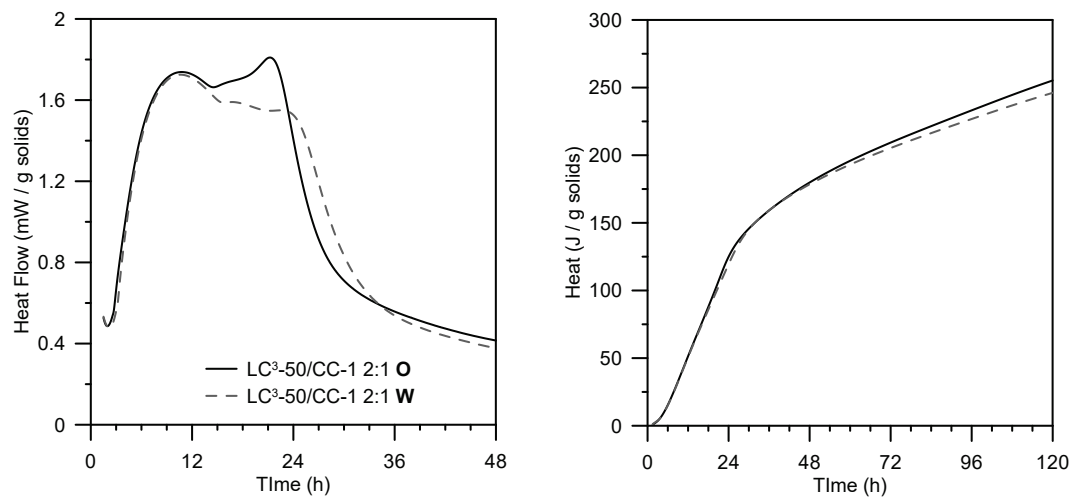
Figure A4-4: Heat flow (left) and total heat (right) measured by isothermal calorimetry over optimized (O) and worst case (W) LC³-50 system.

Figure A4-5 shows the XRD patterns collected over hydrated samples of the same two systems. It can be observed that both Hc and Mc peaks are higher in the optimized system. At 48 h of hydration, the amount of Hc quantified by Rietveld refinement is 1.2% and 0.6% in the O and W systems, respectively. At 28 d, the sum of Hc and Mc adds to 5.3% and 4.6% in the O and W systems. The degree of hydration (DoH) of clinker and the measured compressive strength for each of the samples is indicated in Figure A4-5 as well. It can be observed that the O system has a higher DoH at 2 d and 7 d, which is consistent with an increased rate of reaction of clinker due to the addition of a finer LS powder. However, this difference is small at early-age and among the experimental error at 28 d. Thus, hydration kinetics differences are unlikely to explain by themselves the observed differences in compressive strength observed for the same system under different packing conditions.
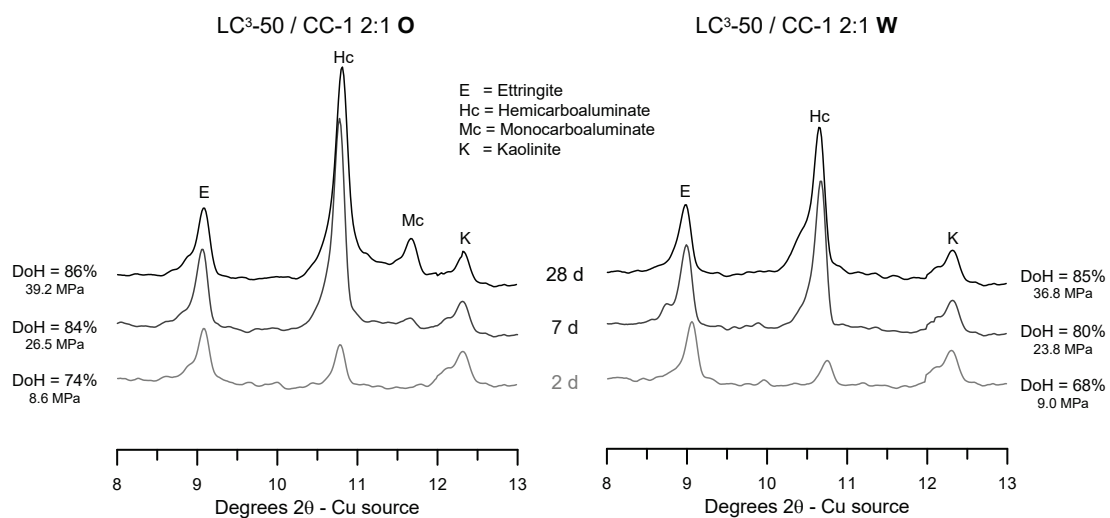
Figure A4-5: XRD patterns at 2 d, 7 d and 28 d for LC³-50 / CC-1 with c/l 2:1, O and W systems. The computed DoH of clinker is indicated for each pattern.

Figure A4-6 shows compressive strength results of all systems studied at 2 d, 7 d and 28 d versus Σ, which indicates the agreement of the PSD of the binder as compared to the optimal packing distribution of the model used. As all the systems are grouped together, the observed scatter from the regression lines is attributed to other effects influencing compressive strength different from the solid particle packing of the system, such as the DoH of clinker and calcined clay as it was discussed previously in light of the XRD results. Nevertheless, in general higher strength can be attributed to systems with smaller values of Σ, both on LC^3-50 and LC^3-65 systems.

Table A4-4: Regression parameters for compressive strength of LC^3 versus Σ.

Regression	Figure	p-value	Standard error
LC^3-50 Strength vs Σ, 2 d	6 left	6.81·10^{-3}	1.03 MPa
LC^3-50 Strength vs Σ, 7 d	6 left	2.35·10^{-5}	2.10 MPa
LC^3-50 Strength vs Σ, 28 d	6 left	6.92·10^{-4}	3.51 MPa
LC^3-65 Strength vs Σ, 2 d	6 right	7.78·10^{-2}	1.63 MPa
LC^3-65 Strength vs Σ, 7 d	6 right	4.15·10^{-2}	1.43 MPa
LC^3-65 Strength vs Σ, 28 d	6 right	3.37·10^{-2}	1.90 MPa

The computed p-values and standard errors for the regression are given in Table A4-4. As seen, the correlations are significant in all but one (LC^3-65 at 2 d) cases under 95% confidence criteria (p-value < 5.00·10^{-2}). Furthermore, the strength differences observed over the explored Σ range is well above the computed standard error. In general, p-values at 2 d are higher as compared to 7 d and 28 d. This could be attributed to the stronger effect of kinetics at 2 d due to the refinement of the LS fraction, as it was discussed previously, which could offset any improvement gained by packing optimization. In the case of LC^3-65, the proportion of LS is smaller than LC^3-50, explaining the observed trend towards higher p-values.
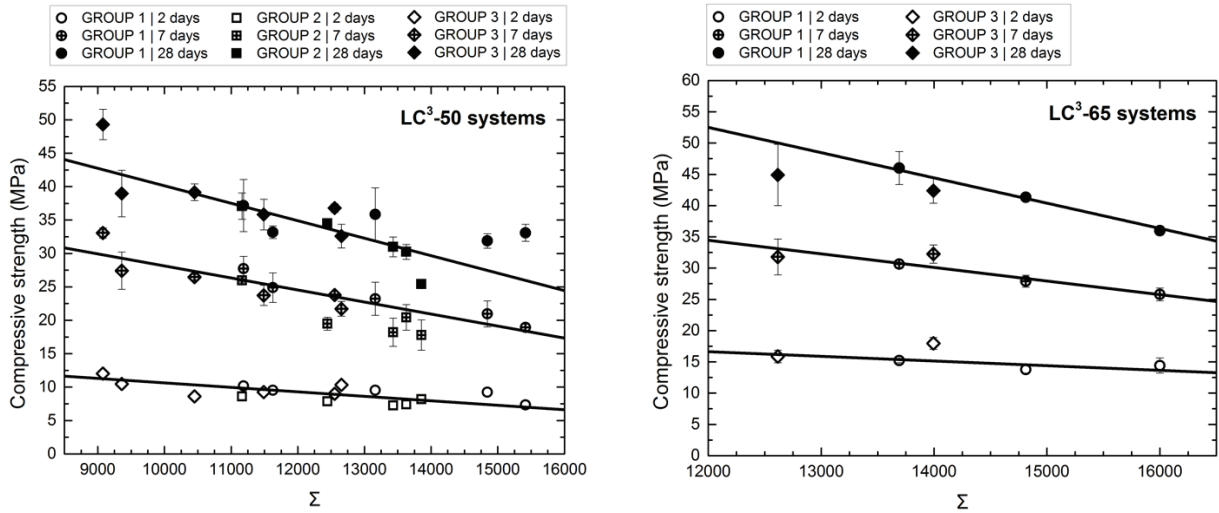
Figure A4-6: Compressive strength of cement paste samples at 2 d, 7 d and 28 d versus Σ for LC^3-50 (left) and LC^3-65 (right) systems.

A summary of the values measured for compressive strength of all systems can be found on Table A4-5. In the case of the mortar mixtures, the correlation between packing of the binder and compressive strength is less clear. This is attributed to two different effects. First, the paste (binder + water) proportion in the EN 196-1 standard mortar mixture design is 35.4% by volume (26.7% by mass of the total material) assuming the average density of the blended LC^3 binders used in this study and therefore, it represents a small proportion compared to the sand fraction. The packing of the sand fraction is constant among all systems and already optimized as prescribed in EN 196-1. In addition, only the LS fraction of the binder is optimized and thus, the

difference between optimized and non-optimized systems is a small part of the binder fraction. In other words, the margin for improvement of Σ by optimization of the LS fraction is limited. For these reasons, it is expected to see a dilution of the positive effects of packing optimization on strength, observed at the cement paste scale, in the mortar mixtures. However, as it will be discussed in the next section, the effects on workability can be clearly observed at the mortar scale.

Workability

The interest of particle packing optimization in cement-based materials is twofold. In addition to an increase in the compressive strength of a particular mixture, particle packing optimization is also expected to reduce the amount of water required for lubrication of particles, if the volume fraction of solids (ϕ) remains constant. In other words, the flow of the mixture will increase under the same w/s_v conditions. This is explained by an increase in the maximum packing density (ϕ_c) of the system, leading to a reduction in the apparent viscosity of the system for a fixed value of ϕ given by w/s_v. Several models have been proposed to relate the viscosity and the solid volume fraction of suspensions, such as the Einstein's equation [13], the Krieger-Dougherty's [14] model and parametric models such as Liu's [5].

Figure A4-7 shows that there is a strong correlation between the measured ϕ_c values and the calcined clay content (p-value $6.54 \cdot 10^{-9}$), which is responsible for the reduction in free water available for lubrication. By inspection of Eq. (4), it can be seen that if V_{liquid} is increased due to a higher amount of water entrapped in the clay porosity, the computed value of ϕ_c will decrease. In fact, the value of ϕ_c determined for a suspension of pure CC-1 is 38.5%, which contrast with the value of 57% obtained for a quartz powder with similar PSD measured under the same conditions. The advantage of ϕ_c compared to Σ as packing estimation parameters is that it can also accounts by the water entrapped inside the porosity of clay, which is responsible for a significant proportion of the workability reduction in LC^3 systems.

As the Andreasen and Andersen model assumes closed-surface (non-porous) particles where only the diameter is considered in the packing optimization, the effect of in-particle water retention is neglected. On the other hand, as the measurement of ϕ_c relies on a water extraction procedure, this effect has a strong impact on the measured values. Therefore, it is expected that ϕ_c exhibits better correlation with slump results.
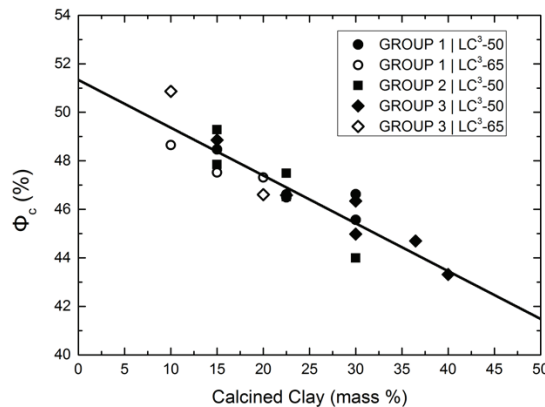
Figure A4-7: Correlation between experimentally estimated ϕ_c versus calcined clay content.

Figure A4-8 left shows that ϕ_c shows high correlation with the workability of pastes as measured by the mini-cone slump, further reinforcing the relevance of water retention for flowability. The correlation can also be translated in terms of calcined clay content (Figure A4-8 right), showing that this mixture design parameter is the overwhelming factor controlling the workability of LC^3 systems. Two main trends are observed in both cases, the lower workability one corresponding to all of the studied systems except from Group 3, which exhibit a much higher slump for a given value of ϕ_c, even higher than the value measured for a pure OPC mixture in some cases. Group 3 is constituted of D130 and LSF materials. As D130 is also considered as part of Group 1, the attention was turned to the LSF powder being responsible of this abnormal behavior.

LSF is the finest of the materials considered in this study, thus the presence of organic residues used during the manufacturing process as grinding aids was suspected. It has been reported that some grinding aid molecules adsorbed into cement grain surfaces can behave as water reducing admixtures [15]. To probe this hypothesis, 200 g of LSF material were subjected to calcination at 500ºC for 1 h. This temperature was selected as it lies below the lower limit of the $CaCO_3$ decomposition, as it was confirmed by XRD analysis of the resulting material, where no traces of free lime were detected. PSD of the thermally treated LSF was also verified to be the same as the original material. Afterwards, two replicates of the LC^3-50 with c/l ratio 1:1 and 1:2 from Group 3 were re-cast using the thermally treated material. As seen in Figure 8a and 8b, the slump of the systems is significantly reduced, and both systems with treated LSF appear to fall in the same trend as the other systems. No significant differences in hydration kinetics between the systems containing thermally treated LSF and the original material were observed.

The computed p-values for the regression of Group 1 and Group 2 slump values versus ϕ_c and calcined clay content were $1.50 \cdot 10^{-2}$ and $2.14 \cdot 10^{-3}$ respectively (standard errors of 11.9 and 10.2 mm), while the corresponding p-values for the Group 3 slump versus ϕ_c and calcined clay content (dashed lines) were $4.73 \cdot 10^{-3}$ and $1.54 \cdot 10^{-3}$ (standard errors of 30.1 and 25.1 mm respectively).
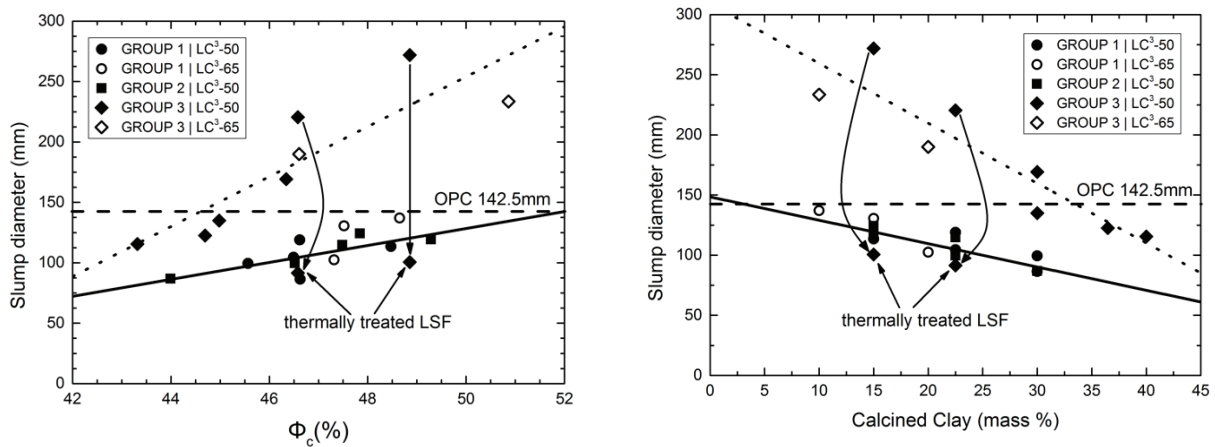
Figure A4-8: Slump values, measured by mini-cone test, versus a) maximum packing density (ϕ_c) and b) calcined clay content.

Values for slump and ϕ_c are summarized on Table A4-5. It can be noted that the measured value of slump for the worst-case systems (W) from Group 1 and Group 2 are higher to their corresponding optimized counterparts (O). This is explained as the result of the computation of the highest Σ achievable (lowest particle

packing) value led to the inclusion of a much larger amount of coarse limestone particles. This results in an increase of the particle spacing at a fixed replacement ratio, leading to a reduction in the ability of the mixture to resist shear (i.e. a decrease of the yield stress). This is in good agreement with rheological measurements performed in a previous study on systems with similar composition [6]. The only exception is the O-W pair of systems corresponding to the LS Group 3. In this case, while more coarse particles are indeed incorporated in the W system, the effect is offset by the lack of LSF which, as discussed before, dramatically increases flowability by the inclusion of other organic compounds. Thus, while the application of the Andreasen and Andersen lead to an increment in compressive strength, it appears to fail to provide the best formulation to optimize workability. A possible explanation is that workability is highly affected by several factors completely neglected by the model, such as particle porosity (absorption capacity), spacing and in the case of LC^3, calcined clay content.

Table A4-5: Summary of compressive strength, slump, flow table values and ϕ_c measured in paste and mortar samples.

				COMPRESSIVE STRENGTH						WORKABILITY		
	Design / clay	c/l	O/W	2 d (MPa)	STD (MPa)	7 d (MPa)	STD (MPa)	28 d (MPa)	STD (MPa)	Slump (mm)	Flow Table (%)	ϕ_c (%)
LC³ CEMENT PASTE GROUP 1	Control	-	-	22.26	0.58	40.33	0.48	51.66	1.92	142.50	-	-
	LC³-50 / CC-1	2:1	O	9.54	0.02	24.90	2.21	33.19	0.93	99.50	-	45.57
	LC³-50 / CC-1	1:1	O	9.52	0.42	23.22	2.48	35.84	3.98	104.50	-	46.49
	LC³-50 / CC-1	1:1	W	8.34	0.16	18.94	0.48	33.09	1.28	118.94	-	46.62
	LC³-50 / CC-1	1:2	O	9.23	0.36	20.96	1.95	31.87	1.08	113.50	-	48.47
	LC³-50 / CC-2	2:1	O	10.16	0.38	27.75	1.82	37.18	3.89	86.50	-	46.63
GROUP 2	LC³-50 / CC-1	2:1	O	8.60	0.28	25.96	0.25	37.07	1.97	86.85	-	43.99
	LC³-50 / CC-1	1:1	O	7.85	0.20	19.48	0.96	34.51	0.71	99.55	-	46.52
	LC³-50 / CC-1	1:1	W	7.24	0.60	18.21	1.12	30.99	1.47	114.78	-	47.49
	LC³-50 / CC-1	1:2	O	8.17	0.10	17.79	2.28	25.43	0.56	124.20	-	47.86
	LC³-50 / CC-2	1:2	O	7.39	0.34	20.44	1.93	30.24	1.11	119.26	-	49.29
GROUP 3	LC³-50 / CC-1	2:1	O	8.62	0.21	26.47	0.40	39.17	1.26	169.25	-	46.34
	LC³-50 / CC-1	2:1	W	8.99	0.18	23.78	0.20	36.79	0.66	135.00	-	44.98
	LC³-50 / CC-1	1:1	O	9.25	0.42	23.73	1.52	35.83	2.29	220.50	-	46.58
	LC³-50 / CC-1	1:2	O	10.35	0.32	21.72	1.12	32.61	1.77	272.00	-	48.86
	LC³-50 / CC-1	free	O	10.47	0.22	27.43	2.79	38.99	3.48	115.50	-	43.32
	LC³-50 / CC-2	free	O	12.02	0.10	33.07	0.75	49.30	2.28	122.50	-	44.70
G1	LC³-65 / CC-1	2:1	O	15.21	0.36	30.63	0.64	45.99	2.63	102.50	-	47.32
	LC³-65 / CC-1	1:1	O	13.78	0.58	27.89	0.94	41.34	0.38	130.50	-	47.52
	LC³-65 / CC-1	1:2	O	14.42	1.21	25.80	1.03	36.00	0.71	137.00	-	48.65
G3	LC³-65 / CC-1	2:1	O	15.87	1.01	31.78	2.88	44.90	4.89	190.00	-	46.61
	LC³-65 / CC-1	1:2	O	17.96	0.94	32.24	1.47	42.40	2.03	233.50	-	50.86
MORTAR G1	Control	-	-	29.92	2.80	43.32	1.35	49.16	0.76	-	87.99	-
	LC³-50 / CC-1	2:1	O	16.27	0.33	36.99	0.70	45.21	2.10	-	60.43	-
	LC³-50 / CC-1	1:2	O	13.44	0.80	27.66	0.46	34.11	0.74	-	82.09	-
G2	LC³-50 / CC-1	2:1	O	16.73	0.35	35.52	1.73	43.32	0.48	-	59.94	-
G3	LC³-50 / CC-1	2:1	O	15.64	0.35	35.15	0.73	42.60	1.10	-	115.31	-
	LC³-50 / CC-1	1:1	O	13.94	0.44	27.43	0.88	37.63	0.94	-	148.52	-
	LC³-50 / CC-1	1:2	O	12.94	0.85	25.55	0.38	32.33	0.36	-	163.29	-

A good correlation (p-value 4.38·10⁻⁵, standard error 12.4 mm) is observed between slump values on LC^3 paste samples and flow table results measured on standard mortars, as seen in Figure A4-9. Despite the relative lower fraction of binder in the mortars, it is in fact the phase that provides the lubrication to the particles (powders and sand) in the fresh state.
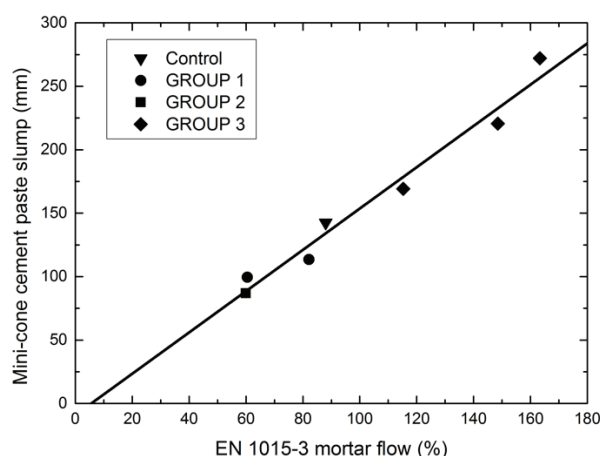
Figure A4-9: Slump values, measured by the mini-cone test on paste, versus flow table values measured according to EN 1015-3 on mortars.

Revisiting the distribution modulus (α) for LC^3 blended systems

Even considering that strength improvements were achieved by the optimization of the solid particle packing using the model with α equal to 0, some issues arise from this assumption which justify revisiting the influence of this parameter. Despite that it can be mathematically shown that this value leads to the maximum particle packing [7], the obtained model distribution (see Figure A4-1) is far from the normal shape from real OPC and SCMs in general. A PSD with a straight-line shape will only be approached by the combination of several powders with different sizes and relatively unimodal distributions. With calcined clays this is never the case. In addition, as discussed in the previous section, the model fails to produce mixture designs with improved workability. While this can be attributed in part to the water retention in clay particles, in systems with the same calcined clay content the difference should be still noticeable.

Two LC^3-50 blends optimized using α equal to 0, incorporating CC-1, c/l 1:1, with limestones from Group 1 and 2 respectively were measured for PSD using laser diffraction as a whole binder. As in this case the system contains a mixture of powders, the refractive index was adjusted by weighting the pure constituent (OPC, LS and CC) values using the volume fraction of the different constituents, obtaining a value of 1.632/0.01 for the real/imaginary component. In both cases, good agreement was found between the theoretical (computed using Eq. (3)) and the measured PSDs. As both systems corresponded to optimized systems, the Andreasen and Andersen was re-fitted to the curves leaving as free variable the value of α. This was done to achieve a value of the distribution modulus which described more accurately the shape of the experimentally observed PSDs. The average between both computed values was 0.18, lying between the 0<α<0.37 range normally described for packing optimization. The optimization of the systems was re-computed using α values in the vicinity of 0.18 starting again from the raw materials, and compared to the initial mixture design. Results are summarized on Table A4-5.

Table A4-5: Mixture design for different values of the distribution modulus (α), obtained by fitting the Andreasen and Andersen model.

	Design / clay	c/l	α	D5 (%)	D65 (%)	D130 (%)	J15 (%)	J130 (%)	Σ
GROUP 1	LC³-50 / CC-1	1:1	0.00	17.30	0.00	5.20	-	-	13161
	LC³-50 / CC-1	1:1	0.10	7.43	0.00	15.07	-	-	7040
	LC³-50 / CC-1	1:1	0.15	0.66	0.00	21.84	-	-	5117
	LC³-50 / CC-1	1:1	0.20	0.00	0.00	22.50	-	-	4562
	LC³-50 / CC-1	1:1	0.25	0.00	0.00	22.50	-	-	5444
GROUP 2	LC³-50 / CC-1	1:1	0.00	-	-	-	22.50	0.00	12444
	LC³-50 / CC-1	1:1	0.10	-	-	-	4.60	17.90	6953
	LC³-50 / CC-1	1:1	0.15	-	-	-	0.00	22.50	5738
	LC³-50 / CC-1	1:1	0.20	-	-	-	0.00	22.50	6183
	LC³-50 / CC-1	1:1	0.25	-	-	-	0.00	22.50	8011

The first thing to notice is that in both cases, as the value of α used increases the proportion of coarse LS (either D130 or J130) suggested by the model increases. This is in fact the same trend observed in the W systems designed with α equal to 0, which as seen in Table A4-5 exhibited higher slump compared to the O systems with the same OPC/CC composition. In addition, the quality of the fitting between real and model PSDs improves, as evidenced by the significant decrease of the value of Σ as compared to the α=0 case. As observed in Figure A4-1a, an increase in the value of α can be interpreted as a coarsening of the model's PSD. Figure A4-10 shows two model microstructures with ϕ = 0.3 and a PSD corresponding to the model theoretical function for two values of α. As observed, even considering that the volume of solids is the same in both cases, the microstructure computed with the distribution of higher α appears less blocked in terms of free space, due to the reduction of fine particles and the increase in the inter-particle spacing [16]. In addition, the total particle quantity decreases due to the addition of coarser LS particles.
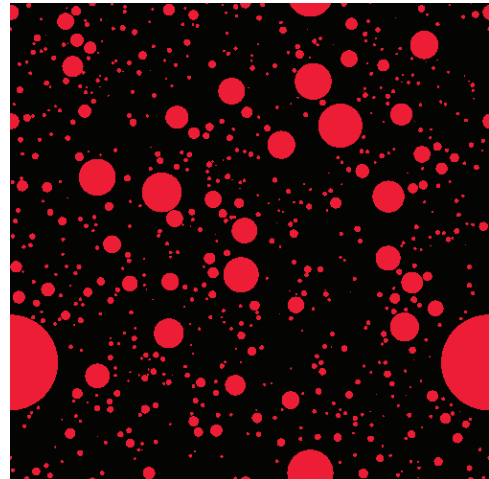
a)
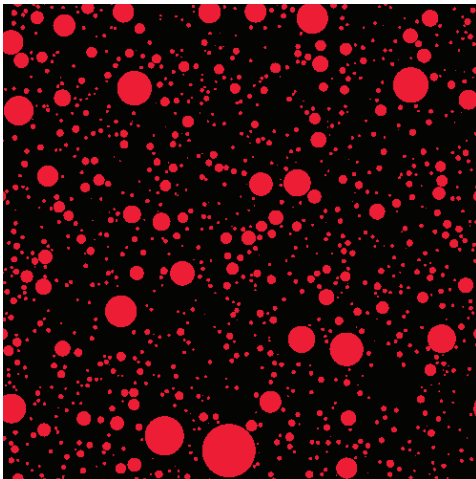
b)

Figure A4-10: Model microstructures using PSD from the Andreasen and Andersen packing model considering α equal a) 0 and b) 0.25.

Increasing of the packing density of the LS fraction in LC^3 binders can increase compressive strength at some extent. However, the magnitude of the effect is limited due to the small proportion of the LS fraction in the binder, and the constant w/s_V ratio approach adopted in this study for mixture design. Thus, even if the maximum packing density is increased, the total solids and the initial water volume, which can be understood as the initial porosity of the system, are constant. The inclusion of coarse particles in the LS fraction lead to improvements in the workability of the systems at constant w/s_V. However, this requires an adjustment of the distribution modulus in order to get this indication from the packing model used in this study. If the increased flow obtained is translated into a reduction of the water content in the mixture to the extent of constant slump, a much significant increase of strength would be expected if the comparison basis between optimized and non-optimized mixtures is constant flow rather than w/s_V.

Conclusions

In this study, particle packing optimization of the LS fraction of different formulations of LC^3 binders was performed as a mean of increasing compressive strength and improving workability. Based on the results obtained, the following conclusions can be drawn:

1. While compressive strength showed to be correlated with the packing parameter associated with the model (Σ), the effect of calcined clay content on workability is predominant. It was observed that the model is unable to predict workability changes, as it neglects the microstructure of calcined clay particles that increase water demand.

2. The maximum packing density (ϕ_c) determined by centrifugation showed to be a reliable parameter to correlate with slump tests, as it accounts for the water retained inside calcined clay particles. Good correlation between the mini-cone slump test and the standard flow table test results was observed.

3. For a given addition of calcined clay to an LC^3 system, the inclusion of coarse limestone particles appears to improve the flow of the mixture, which is explained by a reduction in the number of particles in the LS fraction and a consequent decrease in the overall specific surface area. On the other hand, fine limestone showed to be beneficial for early-age strength.

References

[1]   D.P. Bentz, C.F. Ferraris, Rheology and setting of high volume fly ash mixtures, Cem. Concr. Compos. 32 (2010) 265–270. doi:10.1016/j.cemconcomp.2010.01.008.

[2]   D.P. Bentz, C.F. Ferraris, S.Z. Jones, D. Lootens, F. Zunino, Limestone and Silica Powder Replacements for Cement: Early-Age Performance, Cem. Concr. Compos. 78 (2017) 43–56. doi:10.1016/j.cemconcomp.2017.01.001.

[3]   N. a. Tregger, M.E. Pakula, S.P. Shah, Influence of clays on the rheology of cement pastes, Cem. Concr. Res. 40 (2010) 384–391. doi:10.1016/j.cemconres.2009.11.001.

[4]   O. Akhlaghi, T. Aytas, B. Tatli, D. Sezer, A. Hodaei, A. Favier, et al., Modified poly(carboxylate ether)-based superplasticizer for enhanced flowability of calcined clay-limestone-gypsum blended Portland cement, Cem. Concr. Res. 101 (2017) 114–122. doi:10.1016/j.cemconres.2017.08.028.

[5]   D.M. Liu, Particle packing and rheological property of highly-concentrated ceramic suspensions: ϕm determination and viscosity prediction, J. Mater. Sci. 35 (2000) 5503–5507. doi:10.1023/A:1004885432221.

[6]   K. Vance, A. Kumar, G. Sant, N. Neithalath, The rheological properties of ternary binders containing Portland cement , limestone , and metakaolin or fly ash, Cem. Concr. Res. 52 (2013) 196–207. doi:10.1016/j.cemconres.2013.07.007.

[7]   H.J.H. Brouwers, Particle-size distribution and packing fraction of geometric random packings, Phys. Rev. E. 74 (2006) 031309. doi:10.1103/PhysRevE.74.031309.

[8]   D.P. Bentz, S.Z. Jones, D. Lootens, Minimizing Paste Content in Concrete Using Limestone Powders - Demonstration Mixtures, (2016). doi:10.6028/NIST.TN.1906.

[9]   A.H.M. Andreasen, Ueber die Beziehung zwischen Kornabstufung und Zwischenraum in Produkten aus losen Körnern (mit einigen Experimenten), Kolloid-Zeitschrift. 50 (1930) 217–228. doi:10.1007/BF01422986.

[10]   Y. Han, W. Liu, J. Zhou, J. Chen, Interactions between kaolinite Al-OH surface and sodium hexametaphosphate, Appl. Surf. Sci. 387 (2016) 759–765. doi:10.1016/j.apsusc.2016.07.002.

[11]   P. Mehta, P. Monteiro, Concrete: Microstructure, Properties, and Materials, 3rd ed., McGraw-Hill Professional, New York, 2005.

[12]   K. Scrivener, R. Snellings, B. Lothenbach, eds., A Practical Guide to Microstructural Analysis of Cementitious Materials, CRC Press, 2016. doi:10.7693/wl20150205.

[13]   K. Asaga, D.M. Roy, Rheological properties of cement mixes: IV. Effects of superplasticizers on viscosity and yield stress, Cem. Concr. Res. 10 (1980) 287–295.

[14]   I.M. Krieger, T.J. Dougherty, A Mechanism for Non-Newtonian Flow in Suspensions of Rigid Spheres, Trans. Soc. Rheol. 3 (1959) 137–152. doi:10.1122/1.548848.

[15]   J.J. Assaad, C.A. Issa, Effect of clinker grinding aids on flow of cement-based materials, Cem. Concr. Res. 63 (2014) 1–11. doi:10.1016/j.cemconres.2014.04.006.

[16]   E. Berodier, K. Scrivener, Understanding the filler effect on the nucleation and growth of C-S-H, J. Am. Ceram. Soc. 97 (2014) 3764–3773. doi:10.1111/jace.13177.

Appendix 5 – LC^3 performance at low temperature

Note: This appendix contains some results published in the conference paper "Reactivity and performance of limestone calcined-clay cements (LC^3) cured at low temperature", by F. Zunino and K. Scrivener, published in the Proceedings of the International conference on advances in construction materials and systems, ICAMS 2017.

The combination of metakaolin and limestone in OPC-based systems can achieve synergetic benefits from both well-known systems. The additional reactive aluminum supplied by metakaolin can enhance limestone reaction and allow higher replacement levels with improved performance. For this reason, LC^3 have become of great interest. This study focuses on understanding the effect of lower curing temperature on the hydration and strength development of LC^3 systems. In particular, the effect of the increased solubility of limestone in the presence of aluminates from clay is explored.

Materials and methods

Portland cement classified as CEMI 42.5R from Holcim was used in the study for the preparation of blended cement paste. A kaolinitic clay from Chile with 60.3% kaolinite content as quantified by thermogravimetric analysis (TGA) was also used. Ground clay was calcined in alumina crucibles at 800ºC for 1 h in a high temperature furnace. After calcination, the complete dehydroxylation of kaolinite was confirmed by TGA. As for the limestone fraction, Durcal 5 from OMYA (D_{50} = 5 μm) was used. The mineralogical composition of the limestone was confirmed to be completely calcite by X-ray diffraction (XRD) analysis.

Blended LC^3 cement samples were prepared with different clay-to-limestone rations (c/l), in order to assess the effect on hydration of increased amounts of limestone at low temperature. A volumetric water-to-solids ratio (w/s) of 1.234 was used for all of the mixtures. The volumetric approach was intended to provide a fair comparison basis with different blending proportions, by keeping the initial porosity (i.e. water volume) constant. The powder materials were blended for 30 minutes using a Turbula blender. Water and raw materials were preconditioned at the curing temperature (10 or 20°C) 24 h prior to mixing. Mixing was performed on plastic containers using a high shear mixer operating at 1600 rpm for 2 minutes. The detailed mixture design can be found on Table A5-1.

Table A5-1: Mixture proportioning for LC^3 systems.

Mixture ID	Clinker + Gypsum (% wt. binder)	Limestone (% wt. binder)	Calcined Clay (% wt. binder)	c/l ratio	w/b
Control	100	0	0	-	0.40
LS225	77.5	22.5	0	-	0.41
LC^{3}50 − 2/1	55	15	30	2	0.43
LC^{3}50 − 1/1	55	22.5	22.5	1	0.43
LC^3 50 − 1/2	55	30	15	0.5	0.43
LC^3 65 − 2/1	70	20	10	2	0.42

Compressive strength was measured in mortar samples in conformity with EN 196-1 standard procedure. XRD of fresh slices was conducted following the procedure described in *Chapter 6.* In addition, MIP measurements were conducted following the procedure shown in *Chapter 8*.

Results and discussion

Compressive strength of mortars cured at 10 or 20°C are shown in Figure A5-1. Until 7 days of hydration, the strength of the LC^3 systems cured at low temperature is lower than their 20°C counterparts. Between 1 and 7 days, the system diluted with limestone only (LS225) exhibits higher strength than any LC^3-50 system at 10°C, but it is lower at 7 days at normal curing conditions.

It is observed that at low temperature, the difference between the systems with different clay to limestone ratio is negligible, while at 20°C the system with more clay exhibits higher strength. This is associated with a significant reduction of the rate of reaction of metakaolin at low temperature. At 28 days, the strength of LC^3-65 cured at low temperature is similar to the 20°C systems, and catches up with OPC strength. At 90 days, the strength of LC^3-50 systems at low temperature approaches the values observed under normal curing conditions. Thus, the same level of porosity refinement is achievable at both curing conditions, but at 10°C the time required is significantly longer.
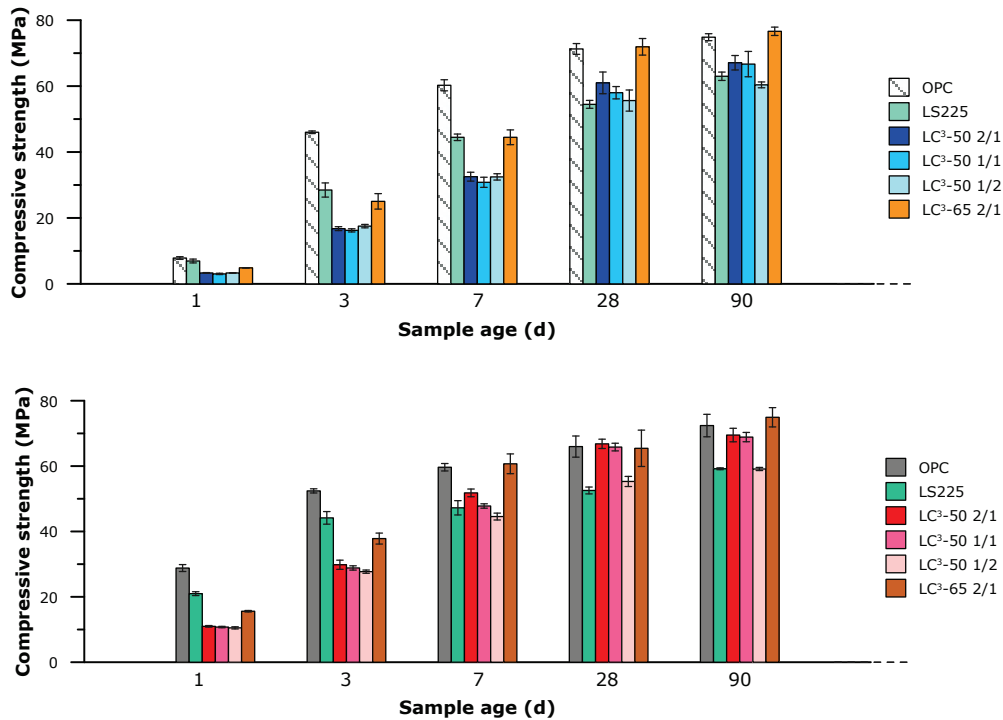

Figure A5-1: Compressive strength of mortars cured at 10°C (top) and 20°C (bottom).

The DoH of clinker was computed for all systems at 1, 7 and 28 days from the XRD patterns collected. Results are presented in Figure A5-2. As observed, at 1 days there is a significant difference between both curing conditions. Thus, part of the difference in strength observed can be attributed to a slower reaction of the clinker fraction. However, at 7 and 28 days the values measured at 10°C and 20°C are similar, in agreement with the similar strengths observed for the OPC systems at these ages between both curing temperatures. As at the same ages, there is a considerable strength gap between both curing temperatures for LC^3 systems, this difference can be associated with a slower reaction of metakaolin at 10°C and a consequent smaller contribution to porosity refinement.
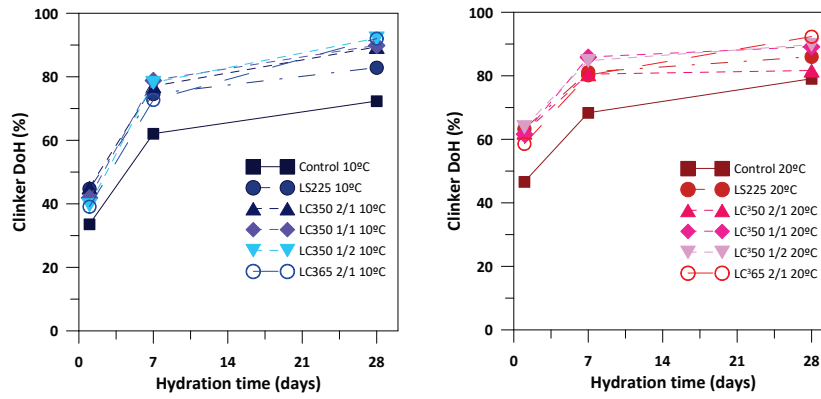
Figure A5-2: DoH of clinker of systems cured at 10°C (left) and 20°C (right).

When comparing the compressive strength results at 1, 7 and 28 days with the heat release per mL of water, a linear correlation is observed (Figure A5-3). It is observed that the trend points to higher strength levels for the low curing temperature systems for the same amount of heat release, suggesting that the nature and quality of the hydration products changed compared to normal (20°C) curing conditions.
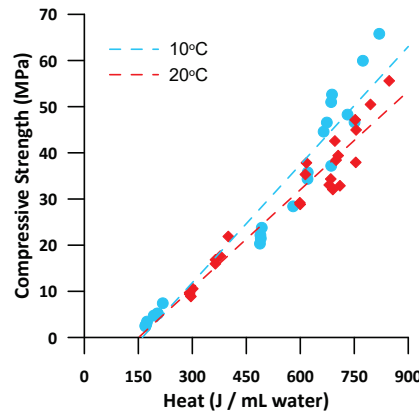
Figure A5-3: Heat released versus compressive strength of systems cured at 10 and 20°C.

Figure A5-4 shows the diffractograms of LC^3-50 2/1 system at 1, 7 and 28 days. The formation of Hc and Mc occurs slower at 10°C due to the reduced reactivity of metakaolin. At 28 days the amount of Hc and Mc observed at 10°C and 20°C is similar, in agreement with compressive strength observations.

Figure A5-4: Diffractograms of LC^3-50 2/1 system cured at 10 and 20°C.

Figure A5-5 shows the total porosity curves and the evolution of the critical entry diameter for the LC^3-50 2/1 system. At 1 and 7 days, the porosity is coarser in the low temperatures systems. However, from 28 days onwards the total porosity profile and the critical entry diameter appears similar between both curing temperatures.
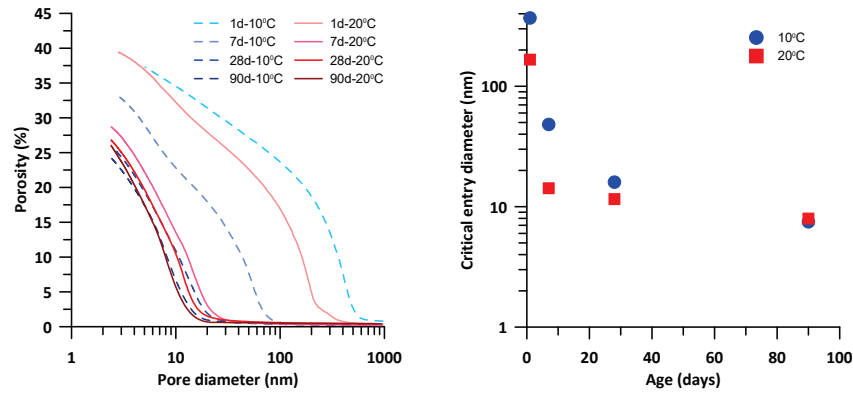
Figure A5-5: Total porosity (left) and critical entry diameter (right) of LC^3-50 2/1 system cured at 10 and 20°C.

Concluding remarks

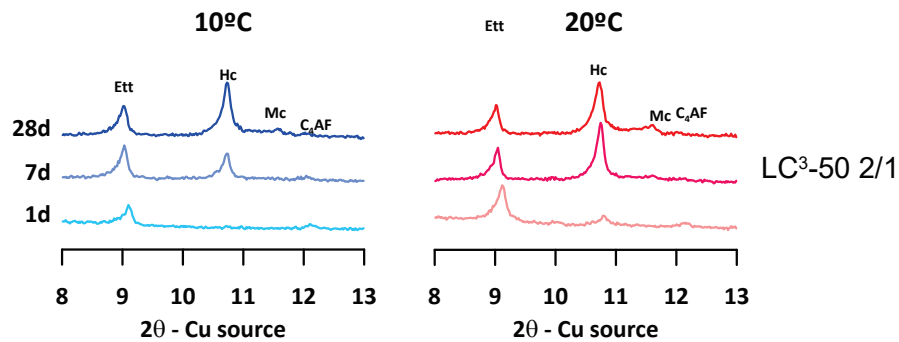From the results presented in this study, it is observed that the LC^3 system can take advantages of the enhanced limestone reaction in low temperature curing conditions, achieving similar properties to their 20°C counterparts in the long term. However, the reactivity of clay is also significantly reduced and consequently the strength at early ages is lower. At 28 days, the strength of the LC^3 systems cured at low temperature is slightly lower but comparable to the systems at 20ºC. In particular, the LC^3-65 formulation appears to be more robust for low temperature applications. In addition, higher amounts of limestone can be used at low temperature without a major effect in strength, as the reactivity of calcined clay is significantly reduced.

Curriculum Vitae

FRANCO ALBERTO ZUNINO SOMMARIVA

franco.zunino@epfl.ch / francozunino@gmail.com
M.Sc. - Ph.D.
École Polytechnique Fédérale de Lausanne (EPFL)
Switzerland

PERSONAL INFORMATION

Date of Birth	29-04-1989
Nationality	Chilean
Address	Rue de Verdeaux 10B, 1020 Renens, Vaud, Switzerland
Phone	+41 (0)78 679 19 65
Languages	Spanish (native speaker)
	English (advanced user)
	French (proficient user, B2)
	Italian (basic knowledge)
	German (basic knowledge)

EDUCATION

2016 – 2020	Doctor of Science (Ph.D.)
	ÉCOLE POLYTECHNIQUE FÉDÉRALE DE LAUSANNE (EPFL)
	Construction Materials Laboratory (LMC)
	Thesis nominated for EPFL distinction
2013 – 2014	Master of Science in Engineering (M.Sc.)
	PONTIFICIA UNIVERSIDAD CATÓLICA DE CHILE
	Degree obtained on July 25th 2014 with Maximum Distinction
2008 – 2014	Civil Engineer, Building Design and Construction
	Approved with Maximum Distinction
	PONTIFICIA UNIVERSIDAD CATÓLICA DE CHILE
1998 – 2007	COLEGIO CALASANZ
	Primary and Secondary School

EMPLOYMENT HISTORY

2015 – 2016	School of Engineering
	PONTIFICIA UNIVERSIDAD CATÓLICA DE CHILE (PUC)
	Position: Instructor Associate Lecturer
2014 – 2016	PONTIFICIA UNIVERSIDAD CATÓLICA DE CHILE (PUC)
	Research Associate – Department of Construction Engineering and Management
2014 – 2015	PONTIFICIA UNIVERSIDAD CATÓLICA DE CHILE (PUC)
	Research Manager – PROJECT FONDEF D10I1086
2014	PONTIFICIA UNIVERSIDAD CATÓLICA DE CHILE (PUC)
	Instructor Teaching Assistant ICE2833 – Reinforced Concrete Structures Design Workshop

2014	VMB INGENIERÍA ESTRUCTURAL LTDA.
	Structural Engineering Department
	Position: Professional intern

AWARDS AND GRANTS

| 2019 | BEST PRESENTATION (1st PLACE) |
| | Young Researcher Competition – 3rd ICCCSC – New Delhi, INDIA |

| 2018 | BEST PRESENTATION (1st PLACE) |
| | Young Researcher Competition on LC³ – Beijing, CHINA |

| 2018 | BEST PRESENTATION (1st PLACE) |
| | Young Researchers Forum IV – U. New Castle, UK |

| 2016 | CHILEAN GOVERNMENT Ph.D. SCHOLARSHIP (BECA CHILE) |
| | 2016 Academic year – Offer declined by applicant |

| 2016 | SWISS GOVERNMENT EXCELLENCE SCHOLARSHIP |
| | 2016-2017 Academic year |

| 2014 | COMMENCEMENT INVITED SPEAKER |
| | 2014 Annual Graduation Ceremony, School of Engineering, PUC |

2014	BEST GRADUATED STUDENT
	2014 Annual Graduation Ceremony
	Department of Construction Engineering and Management, School of Engineering, PUC

| 2013 | SIKA AWARDS CHILE 2013 |
| | Sika Chile S.A. |

2008 – 2012	MONSEÑOR JOAQUÍN LARRAÍN GANDARILLAS AWARD
	Pontificia Universidad Católica de Chile
	Awarded to the best 10 students average results on admission tests nationwide

PUBLICATIONS

PUBLISHED PEER-REVIEWED JOURNAL PAPERS

| 2020 | **F. Zunino**, K.L. Scrivener, Factors influencing the sulfate balance in pure phase C3S/C3A systems, Cem. Concr. Res. 133 (2020). doi:10.1016/j.cemconres.2020.106085. |

| 2020 | **F. Zunino**, E. Boehm-Courjault, K. Scrivener, The impact of calcite impurities in clays containing kaolinite on their reactivity in cement after calcination, Mater. Struct. 9 (2020). doi:10.1617/s11527-020-01478-9. |

| 2020 | **F. Zunino**, K.L. Scrivener, Increasing the kaolininte content of raw clays using particle classification techniques for use as supplementary cementitious materials, Constr. Build. Mater. 244 (2020). doi:10.1016/j.conbuildmat.2020.118335. |

| 2019 | **F. Zunino**, K.L. Scrivener, The influence of the filler effect in the sulfate requirement of OPC and blended cements, Cem. Concr. Res. 126 (2019). doi:10.1016/j.cemconres.2019.105918. |

2018   K.L. Scrivener, F. Avet, H. Maraghechi, **F. Zunino**, J. Ston, A. Favier, et al., Impacting factors and properties of Limestone Calcined Clay Cements (LC3), Green Mater. (2018). doi:https://doi.org/10.1680/jgrma.18.00029.

2018   **F. Zunino,** D. Bentz, J. Castro, Reducing setting time of blended cement paste containing high-SO_3 fly ash (HSFA) using chemical/physical accelerators and by fly ash pre-washing, Cem. Concr. Compos. 90 (2018) 14-26 doi:10.1016/j.cemenconcomp.2018.03.018

2018   I. De la Varga, J. Castro, D.P. Bentz, **F. Zunino**, J. Weiss, Evaluating the hydration of high volume fly ash mixtures using chemically inert fillers, Constr. Build. Mater. 161 (2018) 221–228. doi:10.1016/j.conbuildmat.2017.11.132.

2017   **F. Zunino**, M. Lopez, A methodology for assessing the chemical and physical potential of industrially sourced rice husk ash on strength development and early-age hydration of cement paste, Constr. Build. Mater. 149 (2017) 869–881.

2017   D.P. Bentz, P.E. Stutzman, **F. Zunino**, Low-Temperature Curing Strength Enhancement in Cement-Based Materials Containing Limestone Powder, Mater. Struct. 50 (2017).

2017   R. Serpell, **F. Zunino**, Recycling of hydrated cement pastes by synthesis of α'H-C_2S, Cem. Concr. Res. 100 (2017) 398–412. doi:10.1016/j.cemconres.2017.08.001.

2017   D.P. Bentz, C.F. Ferraris, S.Z. Jones, D. Lootens, **F. Zunino**, Limestone and Silica Powder Replacements for Cement: Early-Age Performance, Cem. Concr. Compos. 78 (2017) 43–56. doi:10.1016/j.cemconcomp.2017.01.001.

2016   P. Martinez, M. Soto, **F. Zunino**, C. Stuckrath, M. Lopez, Effectiveness of tetra-ethyl-ortho-silicate (TEOS) consolidation of fired-clay bricks manufactured with different calcination temperatures, Constr. Build. Mater. 106 (2016) 209–217. doi:10.1016/j.conbuildmat.2015.12.116.

2016   D.P. Bentz, **F. Zunino**, D. Lootens, Chemical versus Physical Acceleration of Cement Hydration, Concr. Int. 38 (2016) 37–44.

2016   **F. Zunino**, M. Lopez, Decoupling the physical and chemical effects of supplementary cementitious materials on strength and permeability: a multi-level approach, Cem. Concr. Compos. 65 (2016) 19-28.

2016   M. Soto, P. Martinez, C. Stuckrath, **F. Zunino**, M. Lopez, Assessing the efectiveness of ethyl-silicate consolitaion of fired-clay bricks manufactured with different calcination temperatures, Constr. Build. Mater. 106 (2016) 209-217.

2015   **F. Zunino**, J. Castro, M. Lopez, Thermo-mechanical assessment of concrete microcracking damage due to early-age temperature rise, Constr. Build. Mater. 81 (2015) 140-153.

2014   D. Moreno, **F. Zunino**, Á. Paul, M. Lopez, High strength lightweight concrete (HSLC): Challenges when moving from the laboratory to the field, Constr. Build. Mater. 56 (2014) 44–52.

PUBLISHED PEER-REVIEWED CONFERENCE PAPERS

2019   **F. Zunino**, K. Scrivener, Improving the behaviour of calcined clay as supplementary cementitious materials by a combination of controlled grinding and particle selection, 3rd International conference on calcined clays for sustainable concrete, New Delhi – INDIA.

2019   **F. Zunino**, K. Scrivener, Influence of kaolinite content, limestone particle size and mixture design on early-age properties on limestone calcined clay cements (LC3), 3rd International conference on calcined clays for sustainable concrete, New Delhi – INDIA.

| 2019 | **F. Zunino**, K. Scrivener, The origin of the increased sulfate demand of blended cements incorporating aluminium-rich supplementary cementitious materials, 3rd International conference on calcined clays for sustainable concrete, New Delhi – INDIA. |

| 2019 | **F. Zunino**, K. Scrivener, The effect of calcite and gibbsite impurities in calcined clay on its reactivity, 3rd International conference on calcined clays for sustainable concrete, New Delhi – INDIA. |

| 2019 | **F. Zunino**, K. Scrivener, Improving the behaviour of calcined clay as supplementary cementitious materials by a combination of controlled grinding and particle selection, International conference for sustainable production and use of cement and concrete, Santa Clara – CUBA. |

| 2018 | **F. Zunino**, K. Scrivener, Effects of grinding aids on limestone calcined clay cements (LC^3) workability, 12th International conference on superplasticizers and other chemical admixtures in concrete, Beijing – CHINA. |

| 2017 | **F. Zunino**, K. Scrivener, Reactivity and performance of limestone calcined-clay cements (LC^3) cured at low temperature, 2nd International conference on calcined clays for sustainable concrete, La Havana – CUBA. |

| 2017 | **F. Zunino**, K. Scrivener, Assessing the effect of calcite impurities in clay on optimal dehydroxylation parameters for enhanced reactivity, 2nd International conference on calcined clays for sustainable concrete, La Havana – CUBA. |

| 2017 | **F. Zunino**, K. Scrivener, Hydration of limestone calcined-clay cements (LC^3) cured at low temperature, 37th cement and concrete science conference, London – UK. |

| 2017 | **F. Zunino**, K. Scrivener, Reactivity and performance of limestone calcined-clay cements (LC^3) cured at low temperature, International conference on advances in construction material and systems ICACMS, Chennai – INDIA. |

| 2017 | **F. Zunino**, K. Scrivener, Morphological Characterization of calcite-contaminated calcined clays using high resolution scanning electron microscopy, Euroseminar on microscopy applied to building materials EMABM, Les Diablerets – SWITZERLAND. |